

# **Caged luciferin probes for the bioluminescence imaging of nitroreductase and hydrogen sulfide in living animals**

THÈSE N° 7313 (2016)

PRÉSENTÉE LE 12 OCTOBRE 2016

À LA FACULTÉ DES SCIENCES DE BASE

LABORATOIRE DE CHIMIE BIO-ORGANIQUE ET D'IMAGERIE MOLÉCULAIRE

PROGRAMME DOCTORAL EN CHIMIE ET GÉNIE CHIMIQUE

ÉCOLE POLYTECHNIQUE FÉDÉRALE DE LAUSANNE

POUR L'OBTENTION DU GRADE DE DOCTEUR ÈS SCIENCES

PAR

**Anzhelika VOROBYEVA**

acceptée sur proposition du jury:

Dr R. Hovius, président du jury  
Prof. E. Dubikovskaya, directrice de thèse  
Dr S. Parkinson, rapporteur  
Dr C. Gahan, rapporteur  
Prof. C. Heinis, rapporteur



ÉCOLE POLYTECHNIQUE  
FÉDÉRALE DE LAUSANNE

Suisse  
2016



# Acknowledgements

I would like to sincerely thank Professor Elena A. Dubikovskaya for giving me the opportunity to work on these exciting projects and to learn my way through the PhD studies. I truly appreciate all your advice and support that provoked the creative thinking and the development of new ideas into productive research. It has always been inspiring and motivational to work by your side.

I am especially grateful to all past and present members of the group for the great atmosphere and collaborative spirit. It has been a pleasure to work with everyone, to solve every day research puzzles and to learn from the best. I am particularly thankful to the post-docs, Dr. Riccardo Sinisi, Dr. Ghyslain Budin and Dr. Jens Frigell for teaching, supervising and showing me the right way. I would also like to thank everyone who helped and contributed to the experimental part of my projects, Grigory Karateev and Dr. Pavlo Khodakivskyi for help and supervision of the synthesis, Aurélien Godinat for helping with the animal work and everything around it, Dr. James Collins for helping with bacterial experiments, Dr. Georgy Mikhaylov for helping with mice studies and Tamara Maric for helping with cell work.

I would also like to thank all external collaborators, Dr. David Hacker at PECT, EPFL for teaching me the molecular biology techniques and providing support when needed. I thank Dr. Elizabeth Allen and Ehud Drori from the Hanahan lab at EPFL for letting me use their facilities and helping with the animal studies. Big thanks to Dr. Mark Tangney and Mike Stanton in UCC, Ireland for welcoming me in their lab for two weeks. I really appreciate your interest in my project and incredible productivity that resulted in a great collaboration. I am thankful to Prof. Emmet Mc Cormack and Kjetil Lund for welcoming me in their lab in the University of Bergen, Norway and running the experiments. I really appreciate all the scientific advice and discussions with Dr. Chieh Jason Chou about my projects.

I am very thankful to Dr. Christophe Roussel and Dr. Samuel Terrettaz for helping with the teaching assistant duties.

I would like to thank Dr. Jens Frigell, Dr. Hacer Karatas, Dr. Riccardo Sinisi and Dr. Kaycie Deyle for proof-reading the thesis and providing your input and comments that have been of a great help to me.

I am thankful to the members of my thesis jury, Prof. Christian Heinis, Dr. Scott Parkinson and Dr. Cormac Gahan for taking their time and effort to evaluate my work and to Dr. Rudolf Hovius for chairing the committee.

I am thankful to my friends that became a part of my life here, the people who kept me out of the lab and enjoyed my company and the good moments shared together. I cannot express enough gratitude to my family who always believed in me and supported me no matter the distance between us. Finally, my heartfelt gratitude goes to Jens. Thank you for being by my side, for the continuous encouragement, support and advice that was always deeply appreciated.

Lausanne, the 18<sup>th</sup> of August 2016





# Abstract

Molecular imaging advances our understanding of cellular and molecular functions within complex biological systems. The development of novel imaging probes that can be applied to answer fundamental biological questions, diagnose and monitor disease progression and the efficacy of therapy *in vivo* is essential to the field of molecular imaging.

Bioluminescence imaging is a powerful technique that allows to study and follow biological processes of interest non-invasively in real-time in living animals. Activatable bioluminescent probes can be designed according to the target of interest and can provide imaging signal in response to the specific stimuli. A strategy called "caged luciferin" can be used to design new bioluminescent probes for imaging of enzymatic activity, the presence of small molecules or metabolite uptake *in vivo*.

In Chapter 1 we present an overview of bioluminescence imaging, with a focus on firefly luciferase-luciferin system. The caged luciferin approach is discussed and examples of existing caged luciferin probes are presented.

In Chapter 2 we describe the development of a bioluminescent probe for imaging of bacterial nitroreductase activity and show the potential for its application in different areas of research. Bacterial nitroreductases have been widely utilized in the gene-directed enzyme prodrug therapy (GDEPT) approach for cancer therapy that reached clinical trials. However, both preclinical and clinical development of NTR-based GDEPT systems has been hampered by the lack of imaging tools that allow *in vivo* evaluation of transgene expression. We developed the NTR caged luciferin (NCL) probe and demonstrated its application for sensitive bioluminescence imaging of NTR *in vitro*, in bacteria and cancer cells, as well as *in vivo* in mouse models of bacterial infection and NTR-expressing tumor xenografts. We anticipate that this probe would significantly accelerate the development of cancer therapy approaches based on GDEPT and other fields where evaluation of NTR expression is important.

In Chapter 3 we describe the development of a bioluminescent probe for imaging of hydrogen sulfide (H<sub>2</sub>S) using the caged luciferin approach. The objective of the research was to develop a probe that can detect endogenously produced H<sub>2</sub>S noninvasively in real-time in living animals. We present a series of caged luciferin probes that were evaluated on their ability to rapidly and selectively detect H<sub>2</sub>S in *in vitro* assays, in cells and in bacterial culture. The two selected probes were applied for imaging of exogenous H<sub>2</sub>S in the gastrointestinal tract in living mice. We anticipate further applications of the best performing probe for imaging of H<sub>2</sub>S production by gut microbiota in mice.

In Chapter 4 we present the overall conclusion followed by the outlook and future perspectives.

## Keywords

*In vivo* imaging; bioluminescence; luciferin; caged luciferin probe; bioluminescent probe; nitroreductase; hydrogen sulfide.

# Résumé

L'imagerie moléculaire a fait progresser notre compréhension des fonctions cellulaires et moléculaires dans des systèmes biologiques complexes. Le développement de nouvelles sondes d'imagerie qui peuvent être utilisées pour répondre à des questions biologiques fondamentales, à des fins de diagnostic ainsi qu'au suivi de la progression de maladies et de l'efficacité d'un traitement *in vivo* est essentiel dans le domaine de l'imagerie moléculaire.

L'imagerie par bioluminescence est une technique puissante qui permet d'étudier et de suivre des processus biologiques d'intérêt de façon non-invasive, en temps réel et sur des animaux vivants. Les sondes bioluminescentes activables peuvent être conçues en fonction de la cible d'intérêt et peuvent fournir des signaux lumineux en réponse à certains stimuli spécifiques. Une stratégie appelée "caged luciferin" peut être utilisée pour concevoir de nouvelles sondes bioluminescentes pour l'imagerie d'activités enzymatiques, de la présence de petites molécules ou de l'absorption de métabolites *in vivo*.

Dans le chapitre 1, nous présentons un aperçu de l'imagerie par bioluminescence, en mettant l'accent sur le système de luciférase-luciférine de luciole (firefly). L'approche de "caged luciferin" est discutée et des exemples de ce type de sondes existantes sont présentés.

Dans le chapitre 2, nous décrivons le développement d'une sonde bioluminescente pour l'imagerie de l'activité de nitroréductase bactérienne et nous montrons son potentiel d'application dans différents domaines de recherche. Les nitroréductases bactériennes ont été largement utilisées dans l'approche de thérapie à pro-médicament enzymatique dirigée par les gènes (gene-directed enzyme prodrug therapy, GDEPT) pour le traitement du cancer qui a atteint les essais cliniques. Cependant, à la fois le développement préclinique et clinique de systèmes GDEPT basés sur les NTR ont été entravés par le manque d'outils d'imagerie qui permettent l'évaluation *in vivo* de l'expression du transgène. Nous avons développé une luciférine masquée comme sonde pour les NTR (NTR caged luciferin, NCL). Son application a été démontrée pour l'imagerie par bioluminescence de NTR *in vitro*, dans des bactéries et des cellules cancéreuses, ainsi que *in vivo* dans des modèles murins d'infection bactérienne et dans des xénogreffes de cellules tumorales exprimant les NTR. Nous estimons que cette sonde pourrait accélérer considérablement le développement d'approches thérapeutiques pour lutter contre le cancer basé sur la GDEPT ainsi que dans d'autres domaines où l'évaluation de l'expression des NTR est importante.

Dans le chapitre 3, nous décrivons le développement d'une sonde bioluminescente pour l'imagerie de sulfure d'hydrogène ( $H_2S$ ) en utilisant l'approche de "caged luciferin". L'objectif de cette recherche était de développer une sonde qui permet de détecter le  $H_2S$  endogène de façon non-invasive, en temps réel et sur des animaux vivants. Nous présentons une série de sondes "caged luciferin" qui ont été évalués sur la base de leur capacité à détecter  $H_2S$  rapidement et de manière sélective dans des expériences *in vitro*, dans des cellules et bactéries de culture. Les deux sondes sélec-

tionnées ont été utilisées pour l'imagerie du H<sub>2</sub>S exogène dans le tractus gastro-intestinal chez des souris vivantes. Nous nous attendons à de nouvelles applications de la sonde ayant été la plus performante, pour l'imagerie de la production de H<sub>2</sub>S par le microbiote intestinal chez la souris.

Dans le chapitre 4, nous présentons la conclusion générale suivie par les perspectives et les perspectives d'avenir.

## Mots-clés

Imagerie *in vivo*; bioluminescence; luciférine; luciférines masquées; sonde bioluminescente; nitroréductase; sulfure d'hydrogène.

# Contents

|   |              |
|---|--------------|
| <b>Acknowledgements .....</b>   | <b>v</b>     |
| <b>Abstract .....</b>   | <b>vii</b>   |
| <b>Keywords .....</b>   | <b>viii</b>  |
| <b>Résumé .....</b>   | <b>ix</b>    |
| <b>Mots-clés .....</b>  | <b>x</b>     |
| <b>Contents .....</b>   | <b>xi</b>    |
| <b>List of Figures .....</b>  | <b>xv</b>    |
| <b>List of Tables .....</b>   | <b>xix</b>   |
| <b>List of Schemes .....</b>  | <b>xxi</b>   |
| <b>Abbreviation .....</b>   | <b>xxiii</b> |
| <b>Chapter 1 Introduction .....</b>   | <b>25</b>    |
| 1.1 Bioluminescence imaging.....  | 25           |
| 1.1.1 Multi-modality imaging using BL .....   | 29           |
| 1.2 Caging of luciferin as a strategy for development of activatable BL probes .....          | 30           |
| 1.2.1 Enzyme- activatable BL probes .....   | 31           |
| 1.2.2 Small molecule- activatable BL probes .....   | 32           |
| 1.2.3 Staudinger ligation approach for the imaging of metabolic processes .....               | 34           |
| 1.2.4 BioLeT strategy for the development of activatable luciferin probes .....               | 34           |
| 1.3 Conclusion .....  | 36           |
| <b>Chapter 2 Development of a bioluminescent probe for nitroreductase (NTR) imaging .....</b> | <b>37</b>    |
| 2.1 Bacterial NTR and its application in cancer therapy (GDEPT) .....                         | 37           |
| 2.2 Strategies for probe development for imaging of NTR .....                                 | 38           |
| 2.3 Results .....   | 41           |
| 2.3.1 Probe design and synthesis.....   | 41           |

|                  |   |           |
|------------------|---|-----------|
| 2.3.2            | Validation of NCL in cell-free assays .....   | 42        |
| 2.3.3            | Stability profiling .....   | 43        |
| 2.3.4            | Imaging of NTR activity in <i>E. coli</i> .....   | 43        |
| 2.3.5            | Imaging of bacterial NTR <i>in vivo</i> in a mouse model of intramuscular infection .....       | 44        |
| 2.3.6            | Evaluation of NCL in NTR- and FLuc-expressing cancer cells .....                                | 45        |
| 2.3.7            | Imaging of NTR in cells not expressing luciferase .....   | 47        |
| 2.3.8            | The effect of hypoxia on the NCL probe in cells not expressing FLuc .....                       | 47        |
| 2.3.9            | Imaging of NTR activity in subcutaneous xenograft model of cancer .....                         | 48        |
| 2.4              | Conclusion .....  | 49        |
| 2.5              | Experimental section .....  | 50        |
| 2.5.1            | Chemical materials and methods .....  | 50        |
| 2.5.2            | General methods .....   | 52        |
| 2.6              | Supplementary figures .....   | 58        |
| <b>Chapter 3</b> | <b>Development of bioluminescent probes for hydrogen sulfide (H<sub>2</sub>S) imaging .....</b> | <b>65</b> |
| 3.1              | H <sub>2</sub> S as a third gasotransmitter .....   | 65        |
| 3.1.1            | Physico-chemical properties .....   | 65        |
| 3.1.2            | Host-derived H <sub>2</sub> S .....   | 66        |
| 3.1.3            | Bacterial-derived H <sub>2</sub> S .....  | 68        |
| 3.1.4            | Physiological effects of H <sub>2</sub> S in gastro-intestinal tract (GIT) .....                | 69        |
| 3.1.5            | Physiological concentrations of H <sub>2</sub> S in the body .....                              | 70        |
| 3.2              | H <sub>2</sub> S detection and measurement .....  | 71        |
| 3.3              | Strategies for probe development for the imaging of H <sub>2</sub> S <i>in vivo</i> .....       | 72        |
| 3.4              | Results .....   | 75        |
| 3.4.1            | Probe development .....   | 75        |
| 3.4.2            | Probe design and synthesis .....  | 76        |
| 3.4.3            | Kinetic analysis of the H <sub>2</sub> S-mediated reduction of Az-CL and Az-F-CL probes .....   | 79        |
| 3.4.4            | Validation of probes in luciferase assay <i>in vitro</i> .....                                  | 80        |
| 3.4.5            | Selectivity to H <sub>2</sub> S over biothiols .....  | 81        |
| 3.4.6            | Cell-based assays .....   | 82        |

|                  |  |            |
|------------------|--|------------|
| 3.4.7            | Detection limit of H <sub>2</sub> S and bioluminescence signal window..... | 85         |
| 3.4.8            | Detection of H <sub>2</sub> S in bacterial assays.....                     | 86         |
| 3.4.9            | Bioluminescence imaging of H <sub>2</sub> S in living mice.....            | 89         |
| 3.5              | Conclusion .....   | 95         |
| 3.6              | Future development .....   | 96         |
| 3.7              | Experimental section.....  | 97         |
| 3.7.1            | Chemical materials and methods .....                                       | 97         |
| 3.7.2            | General materials and methods .....  | 102        |
| 3.8              | Supplementary figures .....  | 105        |
| <b>Chapter 4</b> | <b>Conclusion and outlook .....</b>  | <b>115</b> |
| 4.1              | Conclusion .....   | 115        |
| 4.2              | Outlook.....   | 116        |
| <b>Chapter 5</b> | <b>References .....</b>  | <b>119</b> |
| <b>Chapter 6</b> | <b>Annexes .....</b>   | <b>131</b> |
| 6.1              | NMR spectra.....   | 131        |
| 6.2              | Curriculum Vitae .....   | 157        |





# List of Figures

|  |    |
|--|----|
| Figure 1.1 Luciferase-catalyzed conversion of D-luciferin (I) into oxyluciferin (V) .....  | 26 |
| Figure 1.2 Schematic representation of a caged luciferin approach .....  | 29 |
| Figure 2.1 Schematic representation of the GDEPT approach .....  | 38 |
| Figure 2.2 General strategy for imaging of NTR activity with Nitroreductase Caged Luciferin (NCL) probe .....  | 42 |
| Figure 2.3 Evaluation of NTR-specific uncaging of NCL probe .....  | 43 |
| Figure 2.4 Light production in <i>E. coli</i> by NTR-mediated uncaging of NCL.....   | 44 |
| Figure 2.5 <i>In vivo</i> activation of NCL probe by luciferase and nitroreductase expressing <i>E.coli</i> in a mouse model of thigh infection..... | 45 |
| Figure 2.6 Imaging of NTR activity in cells and in <i>in vivo</i> cancer model with NCL .....  | 46 |
| Figure 2.7 Imaging of NTR activity in HEK293T cells after cell lysis and addition of FLuc.....   | 47 |
| Figure 2.8 Imaging of intracellular reductase activity in A549 cells in hypoxic and normoxic conditions.....   | 48 |
| Figure S2.1 Analysis of NCL reduction by <i>E. coli</i> nitroreductase <i>in vitro</i> .....   | 58 |
| Figure S2.2 Kinetic measurements of NCL reduction by NTR <i>in vitro</i> .....   | 59 |
| Figure S2.3 Inhibition of NTR activity by dicoumarol <i>in vitro</i> .....   | 59 |
| Figure S2.4 Bioluminescent imaging of nitroreductase with NCL in enzyme assay.....   | 60 |
| Figure S2.5 Bioluminescence imaging of NTR by NCL in various <i>E. coli</i> strains .....  | 60 |
| Figure S2.6 Stability profiling .....  | 61 |
| Figure S2.7 <i>In vivo</i> comparison of NCL kinetics after IP and IV administration in a mouse model of thigh infection ..                          | 61 |
| Figure S2.8 Fluorescence imaging of NTR with CytoCy5S probe in MDA-MB-231-NTR-Fluc-EGFP and MDA-MB-231-luc cells.....                                | 61 |
| Figure S2.9 The CytoTox-Glo cytotoxicity assay .....   | 62 |

---

|   |    |
|---|----|
| Figure S2.10 Imaging of NTR with NCL in stably transfected cancer cells MDA-MB-231 <sup>GFP+Luc+NTR+</sup> compared to the control cells (MDA-MB-231 <sup>GFP+Luc+</sup> )..... | 62 |
| Figure S2.11 Imaging of NTR in a subcutaneous xenograft model of cancer .....   | 62 |
| Figure S2.12 Pimonidazole binding assay for immunohistochemical imaging of hypoxia .....  | 63 |
| Figure 3.1 Oxidation states of sulfur in inorganic and organic compounds .....  | 64 |
| Figure 3.2 Hydrogen sulfide states and their occurrence under physiological conditions in comparison to other biologically relevant thiols, cysteine and glutathione .....      | 65 |
| Figure 3.3 Selected biochemical pathways for the production and metabolism of hydrogen sulfide in living systems .....  | 66 |
| Figure 3.4 Enzymatic pathways of H <sub>2</sub> S production .....  | 66 |
| Figure 3.5 Concentration-dependent BL signal produced from Az-CL and Az-F-CL after 1 h of incubation with various NaHS concentrations in luciferase assay .....                 | 79 |
| Figure 3.6 Real-time BLI of H <sub>2</sub> S with Az-CL and Az-F-CL probes in luciferase assay.....   | 80 |
| Figure 3.7 Selectivity profiles of Az-CL and Az-F-CL towards biothiols in luciferase assay .....  | 81 |
| Figure 3.8 The signal produced in C2C12-FLuc cells from 10 µM Az-CL and Az-F-CL after 1 h of incubation with 10- 500 µM NaHS.....   | 82 |
| Figure 3.9 The signal produced in C2C12-FLuc cells from 25 µM Az-CL and Az-F-CL and 5- 250 µM NaHS .....  | 83 |
| Figure 3.10 Bioluminescence imaging of intracellular H <sub>2</sub> S in C2C12-FLuc cells.....  | 84 |
| Figure 3.11 The BL signal window between probes (grey) and luciferins (orange) in the luciferase assay and in FLuc-cells.....   | 85 |
| Figure 3.12 Structures of the probes used for the detection of H <sub>2</sub> S in the bacterial assay.....   | 86 |
| Figure 3.13 Imaging of H <sub>2</sub> S produced by bacteria after 8 h of culture with probes in EZ Rich Defined Medium (EZRDM) .....   | 87 |
| Figure 3.14 Kinetics of the bioluminescence signal produced from luciferins (A) or probes (B) in FVB-luc+ mice (n= 3) over 60 h.....  | 89 |
| Figure 3.15 Comparison of BL signal produced from probes in FVB-luc+ mice .....   | 90 |
| Figure 3.16 Localization of the BL signal produced from the Az-Bn-CL, Az-CL and NH <sub>2</sub> -L in the GIT of mice 1 and 24 h post OG ( <i>ex vivo</i> imaging) .....        | 91 |

---

|   |     |
|---|-----|
| Figure 3.17 BLI of H <sub>2</sub> S using Az-F-CL and Az-CL in living mice treated with NaHS in comparison to the control .....                                   | 92  |
| Figure 3.18 BLI of H <sub>2</sub> S using Az-CL in the GIT of living mice treated with NaHS .....   | 93  |
| Figure S3.1 HPLC-MS analysis of Az-CL and Az-Bn-CL reduction by H <sub>2</sub> S over 60 min <i>in vitro</i> .....  | 104 |
| Figure S3.2 Fluorescence from 10 µM Az-CL and Az-Bn-CL 60 min after the addition of NaHS <i>in vitro</i> .....  | 104 |
| Figure S3.3 HPLC-MS analysis of DNP-CL reduction by H <sub>2</sub> S <i>in vitro</i> .....  | 105 |
| Figure S3.4 Selectivity profiles of DNP-CL and Az-CL towards biologically relevant thiols <i>in vitro</i> .....   | 105 |
| Figure S3.5 Kinetic analysis of probes (Az-CL and Az-F-CL) reduction by H <sub>2</sub> S .....  | 106 |
| Figure S3.6 BLI of H <sub>2</sub> S after 1 h of pre-incubation with Az-CL and Az-F-CL in luciferase assay .....  | 107 |
| Figure S3.7 BLI of H <sub>2</sub> S with Az-CL and Az-F-CL in real-time in luciferase assay .....   | 107 |
| Figure S3.8 BLI of H <sub>2</sub> S after 1 h of pre-incubation with Az-CL and Az-F-CL in C2C12-FLuc cells .....  | 108 |
| Figure S3.9 BLI of exogenous H <sub>2</sub> S with Az-CL and Az-F-CL in real-time in C2C12-FLuc cells .....   | 109 |
| Figure S3.10 The cytotoxicity profile of Az-F-CL (red) and Az-CL (blue) in C2C12-FLuc cells measured with Alamar Blue assay .....                                 | 109 |
| Figure S3.11 Comparison of imaging of bacterial H <sub>2</sub> S from the probes in LB or EZ Rich Defined Medium (EZRD) ..  | 110 |
| Figure S3.12 Bacterial growth of <i>E. coli</i> <sup>H<sub>2</sub>S-LOW</sup> and <i>E. coli</i> <sup>H<sub>2</sub>S-HI</sup> in LB and EZRD .....                | 110 |
| Figure S3.13 Correlation between bioluminescence (A) and fluorescence (B) detection of H <sub>2</sub> S produced by bacteria using Az-CL and Az-F-CL probes ..... | 111 |
| Figure S3.14 A summary of the kinetics of the bioluminescence signal produced from luciferins (A) or probes (B) in FVB-luc+ mice (n= 3) over 60 h .....           | 112 |
| Figure S3.15 BLI of individual mice administered buffer + Az-CL (blue) and NaHS + Az-CL (red) .....   | 112 |



# List of Tables

|  |    |
|--|----|
| Table 1.1 BL pairs commonly used in <i>in vivo</i> imaging.....  | 24 |
| Table 1.2 Selected examples of caged luciferin probes used in <i>in vitro</i> and <i>in vivo</i> assays for imaging of enzyme activity, small molecules and metabolic processes..... | 32 |
| Table 2.1 Examples of activatable probes for NTR optical imaging.....  | 29 |
| Table 3.1 Selected examples of activatable probes for H <sub>2</sub> S optical imaging in living animals.....  | 73 |
| Table 3.2 Structures of caged luciferin (CL) probes for H <sub>2</sub> S imaging and corresponding free luciferins (L) formed after probe uncaging .....                             | 74 |
| Table 3.3 Limit of H <sub>2</sub> S detection (μM) for Az-CL and Az-F-CL .....   | 85 |



# List of Schemes

|  |    |
|--|----|
| Scheme 2.1 Original synthetic route of NCL .....   | 50 |
| Scheme 2.2 Improved synthetic route of NCL .....   | 50 |
| Scheme 3.1 Suggested mechanism for H <sub>2</sub> S-mediated reduction of the azide (1) to the amine (5) ..... | 75 |
| Scheme 3.2 Synthesis of NH <sub>2</sub> -L, Az-CL and Az-Bn-CL .....   | 76 |
| Scheme 3.3 Synthesis of Az-F <sub>4</sub> -Bn-CL.....  | 77 |
| Scheme 3.4 Synthesis of Az-F-CL and NH <sub>2</sub> -F-L .....   | 78 |





# Abbreviation

|                  |  |
|------------------|--|
| AMP              | Adenosine monophosphate                    |
| ATP              | Adenosine triphosphate                     |
| BL               | Bioluminescence                            |
| BLI              | Bioluminescence imaging                    |
| CT               | Computed tomography                        |
| Cys              | Cysteine                                   |
| DMF              | <i>N,N</i> -Dimethylformamide              |
| DMSO             | Dimethyl sulfoxide                         |
| EtOAc            | Ethyl acetate                              |
| FL               | Fluorescence                               |
| FLuc             | Firefly <i>Photinus pyralis</i> luciferase |
| FVB-Luc+         | FVB-Tg(CAG-luc,-GFP)L2G85Chco/J            |
| GSH              | Glutathione                                |
| H <sub>2</sub> S | Hydrogen sulfide                           |
| HCy              | Homocysteine                               |
| HPLC             | High-performance liquid chromatography     |
| IP               | Intraperitoneal                            |
| MeCN             | Acetonitrile                               |
| MeOH             | Methanol                                   |
| MR               | Magnetic resonance                         |
| NAD              | Nicotinamide adenine dinucleotide          |

|           |  |
|-----------|--|
| NADH      | Nicotinamide adenine dinucleotide reduced  |
| NaHS      | Sodium hydrogen sulfide                    |
| NIR       | Near-infrared                              |
| NTR       | Nitroreductase                             |
| OG        | Oral gavage                                |
| PBS       | Phosphate-buffered saline                  |
| PIPES     | Piperazine-N,N'-bis(2-ethanesulfonic acid) |
| PET       | Positron emission tomography               |
| RedFLuc   | <i>Luciola italica</i> luciferase          |
| S. c.     | Subcutaneous                               |
| SPECT     | Single-photon-emission computed tomography |
| $\lambda$ | Wavelength                                 |

# Chapter 1 Introduction

## 1.1 Bioluminescence imaging

Medical imaging technologies were developed at the beginning of the twentieth century as a way to complement morphological observations by creating visual representations of human anatomy and physiology. Present imaging techniques that provide anatomical and physiological information, such as computed tomography (CT), magnetic resonance imaging (MRI), and ultrasound, are well established in the clinic. However, they do not report on specific molecular events responsible for the disease. Hence, molecular imaging modalities evolved as a way to understand cellular and molecular functions within complex biological systems with a spatiotemporal resolution. Unlike histological studies, molecular imaging techniques do not require chemical fixation, isolation of tissues or organs which come with the need to sacrifice experimental animals, and can be performed noninvasively and repeatedly without perturbing living systems.

The most commonly used molecular imaging modalities include positron emission tomography (PET), single-photon-emission computed tomography (SPECT), magnetic resonance (MR) and optical modalities such as fluorescence and bioluminescence imaging (BLI) [1]. Optical imaging systems are simple, convenient and user-friendly. BLI offers the advantages of high sensitivity, relatively low cost and efficiency compared to other *in vivo* imaging techniques, and it is widely used in basic and applied research [2].

Luminescence is a general term that describes light emission as a form of non-thermal radiation. Light emitted as the result of a chemical reaction is termed chemiluminescence and the light produced from an enzymatic reaction is termed bioluminescence (BL).

Luciferases, enzymes catalyzing light emission from small molecule substrates, luciferins, are present in over 700 genera, about 80% of which are marine species. Even though luciferases are found in many different organisms, only a few of them have been applied in research. BL pairs commonly used in *in vivo* imaging can be classified into following categories (Table 1.1):

1. Luciferases from the sea pansy *Renilla reniformis* (RLuc) and the copepod *Gaussia princeps* (GLuc) oxidize coelenterazine with blue-green light emission [3, 4]. They require only oxygen and can function independently of cell environment, which lead to their extensive use as extracellular reporters. However, *in vivo* performance of this system is affected by poor solubility and high instability of the substrate.
2. In bacteria, reduced monoflavin phosphate (FMNH<sub>2</sub>) and long-chain aldehyde serve as substrates for bacterial luciferase LuxAB. The luxAB genes isolated from *Vibrio harveyi* and *Photobacterium luminescens* have been combined with genes required for the substrate biosynthesis and are transcribed from a single cassette called

luxCDABE [5]. The advantage of using this system is that the *lux* operon encodes all components necessary for light production resulting in ready-to-use imaging agents [6, 7].

- Luciferases isolated from click beetles, North American and Italian fireflies, emit red-shifted light (over 600 nm) and, therefore, are preferred reporters for *in vivo* imaging. The most studied BL system, *Photinus pyralis* firefly luciferase (FLuc)- D-luciferin pair, is exceptionally functional *in vitro* and *in vivo* and will be further discussed in detail.

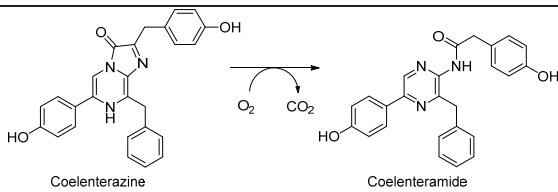
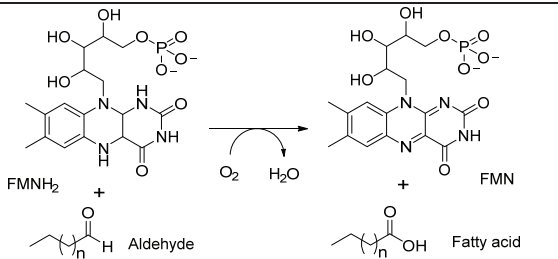
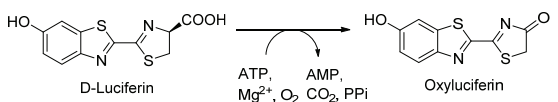
| Luciferase  | Luciferin                               | Enzymatic reaction   | $\lambda$ , nm | Reference  |
|---|---|--|----------------|------------|
| <i>Renilla reniformis</i> (RLuc)                        | Coelenterazine                          |    | 480            | [3]        |
| <i>Gaussia princeps</i> (GLuc)                          |   |  | 480            | [4], [8]   |
| Bacterial LuxAB ( <i>Vibrio harveyi</i> )               | FMNH <sub>2</sub> + long chain aldehyde |   | 490            | [9]        |
| North American firefly FLuc ( <i>Photinus pyralis</i> ) | D-luciferin                             |  | 612            | [10]       |
| Italian firefly ( <i>Luciola italica</i> )              |   |  | 610            | [11]       |
| Click beetle red ( <i>Pyrophorus plagiophthalmus</i> )  |   |  | 611            | [10], [12] |

Table 1.1 BL pairs commonly used in *in vivo* imaging (adapted from [13]).

**Firefly luciferase** is classified as *Photinus*-luciferin: oxygen 4-oxidoreductase (decarboxylating, ATP-hydrolysing) (EC 1.13.12.7). It is a monomeric protein (62 kDa) folded into two compact domains, a large N-terminal domain and a small C-terminal domain, joined by a flexible linker peptide, which creates a wide cleft between the two domains. The active site includes amino acid residues on the surface of both domains, which suggests that during the reaction the domains come close to cluster the substrate in the hydrophobic pocket, requiring a significant conformational change [14]. Interestingly, FLuc has the catalytic function of fatty acyl-CoA synthetase and can use CoA as a substrate [15, 16]. When CoA is added to the FLuc-luciferin reaction mixture, it helps to stabilize light emission by forming a product (L-CoA) which is a less-strong inhibitor of luciferase than L-AMP [17].

Fluc- luciferin bioluminescence has a quantum yield of  $0.41 \pm 0.07$  which is the highest of known bioluminescence systems [18]. The emission spectrum for FLuc is in the yellow-green region (550- 570 nm), with a peak at 562 nm at pH= 7.5- 7.8 at room temperature [19]. However, luciferase is a pH- and temperature- sensitive enzyme, and red shift in emission (620 nm) is observed at pH 5- 6 as well as at 37 °C [20]. The *in vitro* light emission follows a flash pattern, with a rapid rise in the intensity that decays to low level (about 5% of the initial burst) in a few seconds [21]. This flash profile is attributed to the formation of inhibitory products such as oxyluciferin ( $K_i = 0.50 \pm 0.03 \mu\text{M}$ ) and L-AMP ( $K_i = 3.8 \pm 0.7 \text{ nM}$ ) over the course of the reaction [22].

Several important features make Fluc- luciferin favorable over other reporters. The fast rate of enzyme turnover ( $t_{1/2} = 3 \text{ h}$ ) in the presence of D-luciferin allows real-time measurements as the enzyme does not accumulate intracellularly. BL is a quantitative method as the relationship between the enzyme concentration and the peak height of emitted light *in vitro* is linear up to 7- 8 orders of magnitude [1].

**Firefly luciferin** has the systematic name [(S)-2-(6'-hydroxy-2'-benzothiazolyl)-2-thiazoline-4-carboxylic acid] and is commonly named as D-luciferin. Interestingly, only the (S)-enantiomer (D-luciferin) can produce light with FLuc, while the (R)-enantiomer L-luciferin can be adenylated by luciferase, but is not a viable light emitter [23]. The synthesis of D-luciferin in fireflies still remains an open area of research; however, recent studies shed some light on its possible biosynthetic pathways [24-26].

D-luciferin has favorable biodistribution parameters for *in vivo* imaging such as high uptake in most organs and tissues and rapid clearance [27]. As D-luciferin is found exclusively in fireflies and evolved together with luciferase, it is not metabolized by mammalian enzymes and is stable *in vivo* over the time course of imaging.

Bioluminescence is a result of a series of reactions between luciferin, ATP,  $\text{Mg}^{2+}$  and oxygen catalyzed by Fluc (Figure 1.1). In the first step, Fluc catalyzes adenylation of D-luciferin (**I**) in the presence of ATP- $\text{Mg}^{2+}$  and produces enzyme-bound luciferyl-AMP (**II**) [28, 29]. Attachment of a good leaving group like AMP activates luciferin for subsequent oxidation and decarboxylation [30]. Removal of a proton from the C-4 carbon and addition of molecular oxygen produces activated dioxetanone (**III**) [31], which is unstable because of the high strain energy in the four-membered ring and weak peroxide bond [32]. The breakdown of this key intermediate generates oxyluciferin in the excited state (**IV**) and  $\text{CO}_2$  [30]. Further relaxation of the excited state to the ground state (**V**) is accompanied by the emission of a photon of light [33]. Besides the light-producing reaction, FLuc also catalyzes a dark reaction pathway in which luciferyl-AMP is oxidized to dehydroluciferyl-AMP [34].

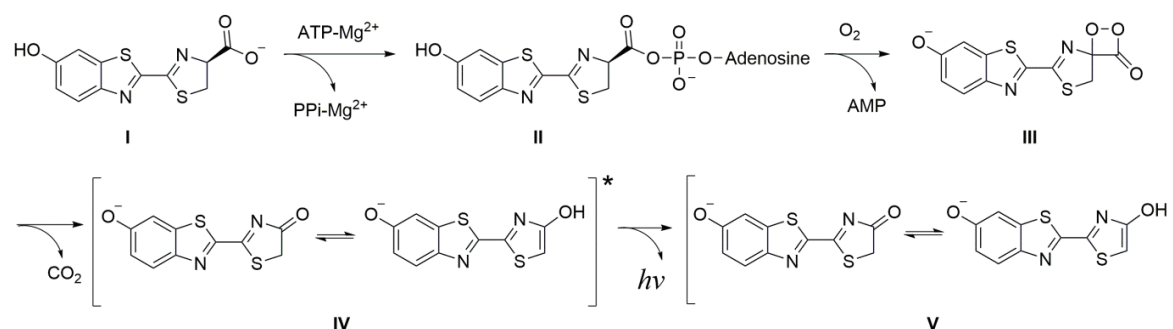


Figure 1.1 Luciferase-catalyzed conversion of D-luciferin (I) into oxyluciferin (V) (adapted from [35]).

BL *in vitro* assays are realized through the use of luciferase enzymes that have been isolated, sequenced, and expressed as DNA vectors [36]. Since the first report of the FLuc cDNA sequence in 1985 [37], luciferase was modified to optimize its expression in mammalian cells through optimized mammalian codon usage, removal of peroxisome targeting sites, and degradation signal addition [38]. Currently, mutagenesis studies on luciferase are aimed towards optimizing *in vivo* bioluminescence properties, such as red color emission [39, 40], higher emission intensity [41] and increased catalytic efficiency [42, 43].

Advances in synthetic biology and the need for expansion of bioluminescence technology for imaging of processes in living systems lead to the engineering of FLuc-expressing cells and animals. Luciferase-labeled cells are indispensable tools for monitoring physiological and pathological processes as they occur in living organisms. Many bioluminescent cancer cell lines labeled with a bright red-shifted luciferase from *Luciola italica* [11, 42] were recently developed and are commercially available.

For a typical bioluminescence *in vivo* imaging experiment, luciferase is genetically encoded and expressed in animals (in the form of cell injections, tumor xenografts or transgenic animals), while substrate molecules are injected into the animal immediately prior to imaging. Transgenic mouse models have been engineered to express luciferase in certain tissues or cell types using tissue-specific promoters [44-46] and ubiquitously in the whole animal under a constitutive promoter (e.g.  $\beta$ -actin promoter [47]). Transgenic mice ubiquitously expressing luciferase have found many applications in the field of biomedical research and have been used to evaluate the efficacy of siRNA delivery [48], measure ABCG2 efflux activity [49], trace homing of dendritic cells to lymph nodes [50], and track mesenchymal stem cells to tumors [51]. L2G85-FVB-luc<sup>+</sup> mice (full name FVB-Tg(CAG-luc,-GFP)L2G85Chco/J) developed in the laboratory of Prof. Contag [47] are invaluable tools for studies using bioluminescence-based probes and imaging of processes in real time *in vivo*. Selected examples include probes for imaging of caspase 3/7 [52], hydrogen peroxide [53], simultaneous detection of caspase 3/7 and hydrogen peroxide [54], fatty acid uptake [55], biodistribution of peptide conjugates [56] and novel luciferin derivatives [57, 58].

Optical imaging systems, such as IVIS Spectrum, allow non-invasive imaging of small animals. The IVIS Spectrum is equipped with an ultrasensitive, thermoelectrically-cooled charge-coupled device (CCD) camera (-90 °C) to detect bioluminescence from the animal [59]. The optical signal is digitalized by an analog-to-digital converter to create a

pseudo-color image based on the light intensity that is superimposed on a reference photograph of the animals. This relatively simple instrument allows imaging up to five animals simultaneously, providing means for a screening in cohort studies of large sample sizes like assessment of tumor size or infection [60]. It is also possible to measure the light emission for a specific range (e.g. 20 nm) by applying band pass filters and spectrally resolve BL signals with different emission maxima [40].

While the majority of studies with BL are performed in the 2D mode, 3D bioluminescence tomography techniques are being developed and used for quantitative 3D reconstruction of internal BL sources on the external surface of the mouse [61]. Multimodality modules used with IVIS systems allow the co- registration of bioluminescence with micro-CT which is an especially powerful strategy in bacterial imaging [7, 62-64].

The sensitivity of detection for BLI is determined by the photon flux from the source *in vivo*. The spatial resolution of BLI is depth-dependent being equal to the depth of the source (e.g. an object 3–5 mm deep has a ~3- to 5-mm spatial resolution) [65]. It was estimated from *in vitro* studies that the net reduction of BL signal is about ten-fold for every cm of tissue depth, varying with the tissue type [9]. Skin and muscle have the highest transmission and are relatively wavelength-dependent, whereas liver and spleen have the lowest transmission because of light absorption by oxyhemoglobin and deoxyhemoglobin [1]. Favorably, these limitations can be addressed by developing of luciferases or luciferins with red-shifted light emission [66].

Another limitation of BL is that the FLuc- luciferin system needs ATP, meaning that the light emission can only take place under physiological conditions within living cells expressing Fluc and that the read-out relies on the enzyme expression level. If BLI is to be applied to non-luciferase expressing animals or humans, a device has to be engineered to encapsulate FLuc-labeled cells analogous to the one reported by Aebischer and coworkers [67].

### 1.1.1 Multi-modality imaging using BL

Linking clinically relevant imaging modalities such as PET, SPECT and MRI with modalities used in small animal imaging (BLI, NIR fluorescence) is an emerging approach that helps to develop new strategies for human imaging.

Combination of imaging modalities offers a number of advantages. For example, high-sensitivity functional/molecular imaging (PET, optical imaging) combined with high- resolution anatomical imaging (CT, MRI) provides complementary diagnostic information [68]. This strategy can be used for the cross-validation of results obtained from various modalities and can aide in the evaluation of the effectiveness of each modality. Due to the availability of instrumentation, such as the IVIS Imaging System, a combination of BL and NIR fluorescence imaging is widely used in *in vivo* research. Although it seemed a daunting task over a decade ago [69], integration of BLI with MRI and PET has been recently demonstrated.

In oncology, a combination of BLI and MRI was used to monitor the effectiveness of anticancer treatment. In one study, this was realized by using Fluc-expressing cancer cells to monitor tumor blood supply and MRI contrast agent to label tumor cells [70]. After administration of a chemotherapeutic agent acting on tumor vasculature, a decrease in BL signal from the tumor correlated with MR signal confirmed the effectiveness of therapy. In another study, MRI and BLI

were used to monitor the effect of MRI-guided laser ablation on tumor viability [71]. Another interesting example is a study on tracking macrophages to experimental aortic aneurysms, where FLuc-macrophages were isolated from transgenic mice expressing luciferase and labeled with iron oxide nanoparticles for MRI [72].

BLI and PET combination was shown to be very useful for detecting reporter gene expression and cell viability. Otto-brini et al. implanted cells expressing BL reporter and PET reporter for the assessment of estrogen receptor activity in a breast cancer model *in vivo* [73]. Brader et al. applied this combination for imaging of bacteria targeted to tumors [74]. Using luciferase tagged probiotic *E. coli* Nissle 1917 and [ $^{18}\text{F}$ ]FEAU and [ $^{18}\text{F}$ ]FDG as bacterial PET tracers they demonstrated a correlation between the number of viable bacteria in tumors and PET and BL signal.

## 1.2 Caging of luciferin as a strategy for development of activatable BL probes

Currently, a hot topic in research is the design of specific and sensitive imaging probes. Advances in this area are realized through the development of novel approaches to probe design and chemistry [75].

A molecular imaging probe is an agent used to visualize, characterize and/or quantify biological processes in living systems [1, 76]. Imaging probes can be nonspecific, targeted and/ or activatable [77]. Nonspecific probes do not have a molecular target and are used to characterize physiological processes such as blood flow or tissue perfusion. Examples of nonspecific probes include fluorescein and indocyanine green dyes which are used for angiography studies [78].

Targeted and activatable probes are both directed specifically to the target, however activatable probes produce the signal only after interaction with their target and, therefore, are highly specific and yield a high signal-to-background ratio [79]. Activatable, or "smart", imaging probes can be genetically encoded or chemically synthesized. They are designed to undergo chemical or physicochemical changes in response to specific biomolecular recognition or interaction and produce amplification of optical signal. Therefore, performance of an activatable imaging probe depends on the probe design (dictated by the target of interest) and on the characteristics of a chosen imaging modality.

The term "caged" originally was used to describe fluorophores activated by light. The term "caged luciferin", along with the terms "pro-luciferin" or "bioluminogenic probe", is used to describe a probe that provides little to no bioluminescence in its native state but can be converted to a bright bioluminescent luciferin. However, unlike fluorescence probes, BL probes do not require exogenous illumination, which avoids cell phototoxicity or photobleaching of the probes. As caged luciferins are small molecules, they possess favorable pharmacokinetics for *in vivo* imaging and their properties can be tuned according to the imaging requirements.

Studies by McElroy and coworkers on the mechanism behind luciferin- luciferase reaction and screening of luciferin analogues [80, 81] allowed for the identification of structural modifications of the substrate that are tolerated by the enzyme and which gave the origins to the "caged luciferin" concept.

It was found that an electron-donating substituent at the 6'-position of luciferin is required for light emission (Table 1.2). Alkylated or acylated derivatives of 6'-hydroxy-luciferin did not produce light although they bind to FLuc [80]. The



first bright analogue of luciferin to be discovered was aminoluciferin, where an electron-donating amino group replaced the 6'-hydroxy group [81]. Aminoluciferin produces more red shifted light (605 nm) and is about 10% as bright compared to the classical substrate, 6'-hydroxy-luciferin, in the enzymatic assay with the FLuc [57]. Recent studies showed that N-alkylation of 6'-aminoluciferin generally leads to a decrease in light emission although some modifications (e.g. 3-hydroxypropyl) resulted in 1.2 times brighter substrate [82].

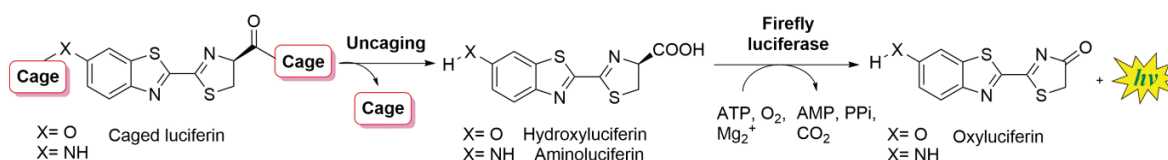


Figure 1.2 Schematic representation of a caged luciferin approach. Light emission is a result of a two-step process: conversion of caged luciferin to free luciferin and oxidation of luciferin by firefly luciferase.

"Cages" or functional groups that prevent light emission from luciferin can be introduced in the 6'-hydroxy-, 6'-amino- or carboxylic groups (Table 1:2). Conversion of the pro-luciferin to luciferin (uncaging) occurs as a result of a chemical reaction (e.g. reduction, hydrolysis) after interaction with the target and leads to release of free luciferin that is oxidized by luciferase (Figure 1.2). As the amount of produced light is related to the amount of available luciferin, this approach allows for the measurement of the activity of the target of interest. In the past ten years various caged luciferin probes have been designed for the detection of enzymatic activity and small molecules.

### 1.2.1 Enzyme- activatable BL probes

The high catalytic activity, diversity and abundance of enzymes enabled the development of activatable probes that could be used for the imaging of enzyme activities. In 1987, Geiger and Miska reported the development of first bioluminogenic substrates for carboxylic esterase, phosphatase, carboxypeptidases A and B, arylsulfatase and alkaline phosphatase [83]. The following work from the same group expanded the panel of caged luciferins to other targets, such as  $\alpha$ -chymotrypsin [84] and  $\beta$ -galactosidase [85]. Initially developed for *in vitro* assays, this technology proved to be highly sensitive (e.g. limit of detection (LOD) for  $\beta$ -galactosidase  $3.7 \times 10^{-17}$  mol [85]) than other analytical methods such as absorbance and fluorescence. Recent advances in molecular biology such as the development of Fluc-labeled cells and transgenic animals allowed the translation of caged luciferin technology from *in vitro* to *in vivo* studies (Table 1.2).

Probes for imaging protease activity are valuable tools for cancer research [79, 86] as overexpression of certain proteases is associated with cancer progression. In the caged luciferin approach, a peptide sequence which is recognized by proteases is usually attached to the 6'-amino- group of aminoluciferin via an amide bond. Riss and coworkers reported first peptide-aminoluciferin probes for measuring protease activity as a marker of cell death [87]. They later used these probes in a high-throughput screen to determine EC<sub>50</sub> values for specific proteasome inhibitors [88]. The DEVD-aminoluciferin probe was used in several studies to detect caspase-3/7 activity *in vitro* [89] and *in vivo* [90-92]. Similar caged luciferin probes were developed for the imaging of other proteases such as furin [93] and carboxypeptidase [94].

Our laboratory recently developed a split-luciferin approach for the BL imaging of proteases [52]. In this approach, the luciferin molecule is reconstituted from its synthetic precursors, OH-CBT and D-cysteine (D-Cys), the latter being released after cleavage by a protease from C- terminus of the substrate peptide such as DEVD-(D-Cys). This strategy allows for the imaging of caspase activity in living animals with about a two-fold increase in sensitivity compared to the full luciferin probe caged on 6'-amino- group (DEVD-aminoluciferin).

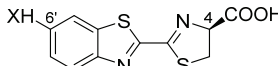
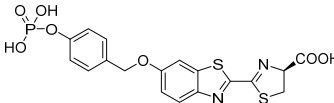
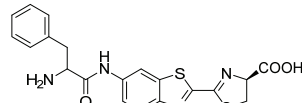
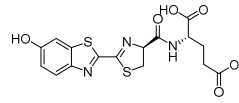
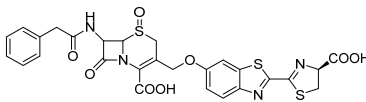
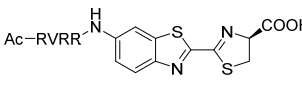
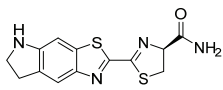
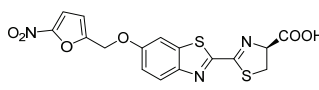
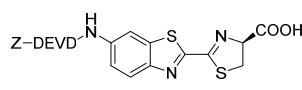
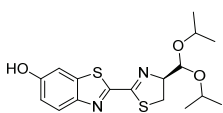
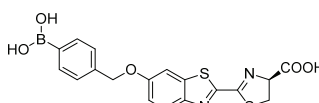
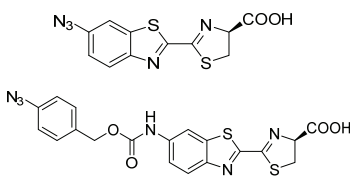
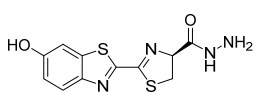
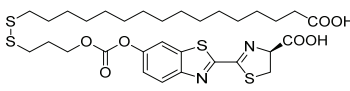
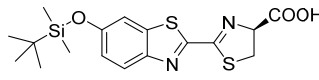
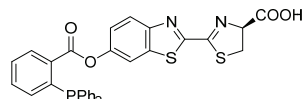
Highly specific probes can be developed by attaching a functional group which is a substrate for the enzyme to the 6'-hydroxyl of luciferin. Examples of such probe design include probes for imaging of  $\beta$ -galactosidase [85, 95]  $\beta$ -lactamase [96] and nitroreductase [97].

Acylation of the carboxylic group of luciferin was used as a strategy to develop probes for imaging of intracellular esterases [98, 99]. A luciferin acetal probe was applied to measure cytochrome P450 3A4 inhibition *in vitro* [100] and the effects of a drug on CYP3A4 in living mice [101].

### 1.2.2 Small molecule- activatable BL probes

Another application of the caged luciferin approach is the detection of various small molecules. As BL read-out relies on the speed of luciferin release from the probe (uncaging), the rate of the reaction of the probe with the target, selectivity and physiological concentrations of the target are key factors that define the success of this approach *in vitro* and *in vivo*.

Luciferin probes for measuring peptide uptake were the first reported example of luciferin uncaging by small molecules [109]. In this approach the linker containing a disulfide bond was placed between luciferin and an octa-arginine peptide. Arginine-rich peptides are readily taken up by cells and upon cell entry the disulfide bond is rapidly reduced by glutathione (GSH), the most abundant cell thiol (1- 10 mM), to release free luciferin. This method was developed to quantify the uptake of luciferin conjugates in real time, with luciferin emulating a drug in drug-conjugates, to estimate their uptake, intracellular release, and receptor interaction. This assay allowed for the measurement of the uptake and release of luciferin conjugates administered topically in real-time in living mice and to find linkers for optimal delivery of therapeutic agents [110].

| Applica-<br>tion  | Modification site of luciferin  |   |  |
|---|---|---|--|
|   | 6'-OH group   | 6'-NH <sub>2</sub> group  | C-4-COOH group   |
|   | <div><div>XH-6'</div><div></div><div>X = O, NH</div></div>                  |   |  |
| Imaging of enzyme activity  |   |   |  |
| <i>In vitro</i>   | <div>Alkaline phosphatase [83]</div> <div></div>                             | <div>α- Chymotrypsin [84]</div> <div></div>                           | <div>Carboxypeptidase G [94]</div> <div></div>                |
| <i>In vitro</i><br>and <i>in vivo</i>                                 | <div>β- Lactamase [96]</div> <div></div>                                     | <div>Furin [93]</div> <div></div>                                     | <div>Fatty Acid Amide Hydro-<br/>lase [102]</div> <div></div> |
| <i>In vitro</i><br>and <i>in vivo</i>                                 | <div>Nitroreductase [97]</div> <div></div>                                 | <div>Caspase 3/7 [89-92]</div> <div></div>                          | <div>Cytochrome P450 3A4<br/>[100, 101]</div> <div></div>   |
| Imaging of small molecules  |   |   |  |
| <i>In vitro</i><br>and <i>in vivo</i>                                 | <div>Hydrogen peroxide (H<sub>2</sub>O<sub>2</sub>) [53]</div> <div></div> | <div>Hydrogen sulfide (H<sub>2</sub>S) [103, 104]</div> <div></div> | <div>Copper (Cu<sup>2+</sup>) [105]</div> <div></div>       |
|   | <div>Fatty acid uptake via glutathione<br/>(GSH) [55]</div> <div></div>    |   |  |
|   | <div>Fluoride (F<sup>-</sup>) [106]</div> <div></div>                      |   |  |
| Staudinger ligation approach for imaging of metabolic processes [107] |   |   |  |
| <i>In vitro</i><br>and <i>in vivo</i>                                 | <div>Caged luciferin phosphine</div> <div></div>                           |   |  |

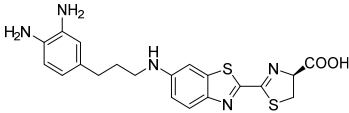
| BioLeT strategy for development of activatable luciferin probes [108] |  |   |  |
|---|--|---|--|
| <i>In vitro</i><br>and <i>in vivo</i>                                 |  | Nitric oxide (NO)<br> |  |

Table 1.2 Selected examples of caged luciferin probes used in *in vitro* and *in vivo* assays for imaging of enzyme activity, small molecules and metabolic processes.

Another useful demonstration of this release strategy by GSH was the development of a probe for measuring fatty acid uptake in cells and living mice [55]. A long chain fatty acid was conjugated to luciferin through a disulfide bond in a similar manner as described above to release luciferin as an indicator of cell uptake. The probe was validated in differentiated and non-differentiated cells. Uptake of the probe was inhibited in the presence of a natural fatty acid (oleic acid) and increased in cells expressing FATP5 transporter. Administration of the probe to FLuc- expressing mice allowed for the determination of the location of uptake in the gut and other organs, such as brown adipose tissue (BAT). Further experiments showed the dependence of the probe uptake by BAT on the metabolic state which was regulated by administration of a  $\beta$ -adrenergic agonist. Therefore, this probe can be used in animals as a valuable tool for imaging of intestinal fatty acid absorption and brown adipose tissue activation.

The high intrinsic reactivity of reactive oxygen species (ROS) enabled the development of many fluorescent probes for imaging the redox environment in cells [111]. However, the specificity of detection of a given oxidant in the presence of other reactive molecules remains a challenge [112]. Van de Bittner et al. developed a boronic acid- caged luciferin probe for the imaging of hydrogen peroxide fluxes in cells and living animals. The probe was shown to have good selectivity and reactivity in enzyme assays and detect  $\text{H}_2\text{O}_2$  in a concentration-dependent manner in living cells and in mice. Administration of an antioxidant lead to a decrease in the signal of the probe compared to untreated mice with basal levels of  $\text{H}_2\text{O}_2$ . The probe was applied to detect an increased  $\text{H}_2\text{O}_2$  production in prostate tumors upon treatment with testosterone *in vivo*.

### 1.2.3 Staudinger ligation approach for the imaging of metabolic processes

The Staudinger ligation is a biorthogonal reaction developed by Bertozzi and coworkers [113] that was applied to measure cell-surface glycosylation using a caged luciferin strategy [107]. The imaging probe consisted of two molecules: a caged-luciferin phosphine and an azido-sugar. Upon incorporation of sugar analogues via the cell biosynthetic machinery into the glycans on cell surface, the azide reacted with the phosphine to release luciferin. In theory, this approach could be used for bioluminescence imaging of any azide-containing biomolecule and studying biological processes in real-time *in vitro* and *in vivo*.

### 1.2.4 BioLeT strategy for the development of activatable luciferin probes

The group of Urano has recently developed a new design strategy for bioluminescence probes named BioLeT (BioLuminescent enzyme-induced electron Transfer) [108]. The idea behind this strategy is similar to the photoinduced elec-

tron transfer (PeT) principle used for the design of fluorescence probes: the electron-transfer process to or from the excited state of a fluorophore diminishes the fluorescence from the singlet excited state. It was shown that the bioluminescence of aminoluciferin analogues could be quenched through an electron-transfer process and that the "switch on/ off" occurred because of the difference in luminescence quantum efficiency from the singlet excited state.

It is interesting that the luminogenic substrate is processed by luciferase to yield an excited-state intermediate but does not emit strong bioluminescence. It means that when the probe is in "off state", it is converted by luciferase to the optically inactive form which decreases the sensitivity of this approach. When applied for imaging of nitric oxide (NO) in living rats expressing luciferase, the probe showed a four-fold increase in bioluminescence.

## 1.3 Conclusion

Bioluminescence imaging *in vivo* offers multiple advantages such as high sensitivity, low background signal due to the absence of tissue autoluminescence, low cost, relatively simple instrumentation and no requirements for radioactivity. As BLI is limited in use to genetically engineered cells and animals expressing luciferase, its clinical translation seems unlikely. However, preclinical studies using BLI are very attractive to researchers. The ability to noninvasively monitor the progress of the disease over time reduces the number of animals necessary to generate statistically meaningful data. Imaging of multiple animals simultaneously makes BLI suitable for screening and reduces the time scale of drug discovery. Studies in animal disease models using BLI allow for the rapid testing of lead drug candidates and the generation of data that provide valuable insights into how to improve existing therapy approaches and contribute to the understanding of disease.

Bioluminescence based on firefly luciferase- luciferin is a versatile platform for creating activatable probes for the molecular imaging of various targets. Previous studies showed that the structures of both luciferin and luciferase are amenable to modifications and, therefore, such modifications should be explored in more detail. It opens exciting possibilities for the expansion of the panel of BL substrate- enzyme pairs, novel probe designs, development of caged luciferin probes with improved characteristics and application of BLI to new areas of research.

## Chapter 2 Development of a bioluminescent probe for nitroreductase (NTR) imaging

This chapter is based on the publication by Vorobyeva AG, Stanton M, Godinat A, Lund KB, Karateev GG, et al. (2015) Development of a Bioluminescent Nitroreductase Probe for Preclinical Imaging. PLoS ONE 10(6): e0131037. doi: 10.1371/journal.pone.0131037.

I thank Grigory Karateev for developing the synthetic route for the NCL probe and supervising the synthesis (Scheme 2.1), Dr. Pavlo Khodakivskyi for optimizing the synthesis (Scheme 2.2), Michael Stanton for generating the data present in Figures 2.4, 2.5, S2.5, S2.7, Kjetil Lund for generating the data present in Figure S2.10, Dr. Elizabeth Allen, Ehud Drori and Aurélien Godinat for helping with the mouse tumor studies, Dr. K. Francis, Prof. E. McCormack and Dr. M. Tangney for valuable input, discussion and collaboration.

### 2.1 Bacterial NTR and its application in cancer therapy (GDEPT)

The nitroreductase (NTR) enzymes are widespread amongst bacteria and are known to metabolize nitrosubstituted compounds and quinones using NADH or NADPH as reducing agents [114-117]. They are important for the development of novel antibiotics being the main target for the treatment of infections caused by bacteria, e.g. *Mycobacterium tuberculosis* [118], *Helicobacter pylori* [119] and by parasites, e.g. *Trypanosoma* [120], *Giardia* and *Entamoeba* [121]. Their enzymatic activity in gut microbiota is linked to carcinogen production and etiology of colorectal cancer [122, 123]. In addition, they are used in biotechnology for degradation of environmental contaminants [114]. Due to their absence in mammalian cells they are also utilized as activating enzymes in gene-directed enzyme prodrug therapy (GDEPT) approaches for cancer chemotherapy [124] where the NTR gene is used to selectively transform cancer cells, providing unique targeted therapy of tumors over normal tissues [125, 126]. Nitroaromatic prodrug CB1954 in the complex with bacterial NTR is promising for GDEPT and has reached clinical trials for prostate cancer [127].

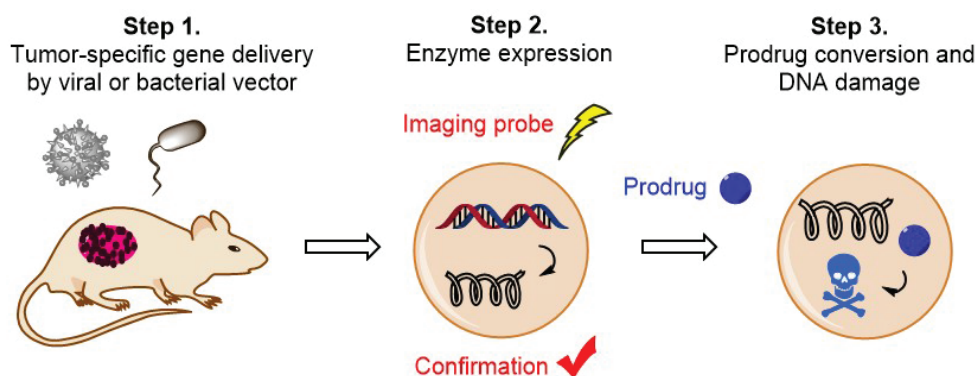


Figure 2.1 Schematic representation of the GDEPT approach (adapted from [126])

GDEPT (Figure 2.1) is based on: (1) introduction and expression of a foreign gene in tumor cells by means of a bacterial or viral vector; (2) administration of a non-toxic prodrug; (3) conversion of the prodrug into a cytotoxic agent by the product of gene expression in the tumor cells.

Following the recent first approval in Europe of a gene therapy medicine, the potential for clinical application of GDEPT is increasing [128]. However, both preclinical and clinical development of NTR-based GDEPT systems has been severely hampered by the lack of imaging tools that allow sensitive *in vivo* evaluation of transgene expression in living subjects. Quantification of the level of transgene expression is extremely important because it is directly linked to the effectiveness of the therapy and its assessment *in vivo* through noninvasive imaging may help develop efficient and safe gene therapy protocols [129, 130].

## 2.2 Strategies for probe development for imaging of NTR

Imaging of NTR activity is of a high interest to many researchers and several activatable probes were developed in nearly all optical modalities (**Table 2**). Many activatable fluorescent probes for NTR have their fluorescence maximum in the visible range of spectrum and they can only be applied for *in vitro* imaging [131-135]. One example of a red-shifted probe is Cy-NO<sub>2</sub> which consists of a nitroimidazole conjugated to tricarbochlorocyanine dye (Cy.7.Cl). The nitroimidazole quenches the fluorescence and upon reduction of nitro- to amino- group the probe exhibits a larger Stokes shift (55 nm), and shows maximum of fluorescence excitation and emission at 695 nm and 750 nm, respectively. This probe was applied to monitor the response of hypoxia in HepG2 cells via the detection of activity of endogenous reductases [136].

The only fluorescence probe reported for imaging of NTR *in vivo* is CytoCy5S [137-139] (GE Healthcare UK Ltd, currently discontinued). The probe is a membrane-permeable quenched substrate that is reduced by NTR to its fluorescent form and is retained within cells for a prolonged period of time making it suitable for live-cell imaging and for *in vivo* studies. It was applied for noninvasive monitoring of tumor progression and response to metronidazole treatment in orthotopic xenografts of disseminated leukemia, lung and metastatic breast cancer in mice [138]. Sekar et al. generated several cell lines expressing NTR for GDEPT studies and this probe was used to evaluate the efficiency of NTR transfection [139].



However, fluorescence imaging *in vivo* has several limitations, such as high tissue-derived background (autofluorescence), photobleaching and lack of quantification [140]. This prompted the development of NTR-activatable probes based on other optical modalities, such as bio- and chemiluminescence (Table 2.1).

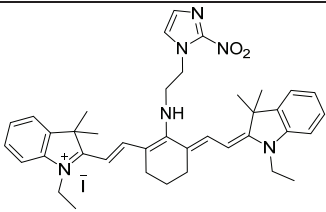
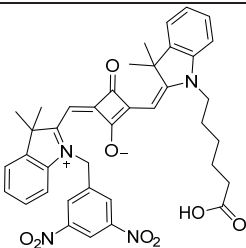
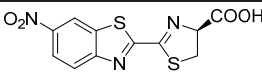
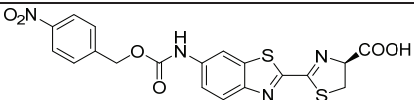
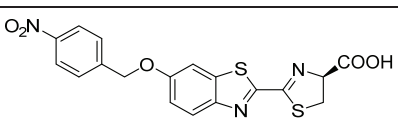
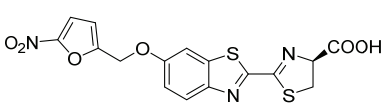
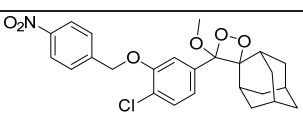
| Imaging probe  | Structure   | Demonstrated application  |
|--|---|---|
| <b>Activatable NIR fluorescence probes</b>                   |   |   |
| Cy-NO <sub>2</sub><br>( $\lambda_{\text{ex/em}}$ 695/750 nm) |    | <i>In vitro</i> (enzyme, imaging of endogenous reductases in hypoxia cell assays) [136]   |
| CytoCy5S<br>( $\lambda_{\text{ex/em}}$ 628/638 nm)           |   | <i>In vitro</i> (NTR enzyme, cell assays) [138, 139] and <i>in vivo</i> (NfsB-expressing tumors) [138]                                  |
| <b>Activatable BL probes (caged luciferins)</b>              |   |   |
| Luntr  |  | <i>In vitro</i> (enzyme and NfsB- cell assays), imaging of cell-cell interactions [143]   |
| Probe 1  |  | <i>In vitro</i> (enzyme, bacterial assays) [144] and <i>in vitro</i> (enzyme) [145]   |
| Probe 3  |  | <i>In vitro</i> (enzyme, cell assays) and <i>in vivo</i> (imaging of endogenous reductases in hypoxic tumors) [145]                     |
| NCL  |  | <i>In vitro</i> (enzyme, bacterial and NfsB- cell assays), <i>in vivo</i> (imaging of bacterial infection and NTR in NfsB- tumors) [97] |
| <b>Activatable chemiluminescence probes</b>                  |   |   |
| HyCL-2   |  | <i>In vitro</i> (enzyme assay) and <i>in vivo</i> (imaging of endogenous reductases in hypoxic tumors) [146]                            |

Table 2.1 Examples of activatable probes for NTR optical imaging.

Similar to BLI, chemiluminescence imaging *in vivo* offers the advantages of high sensitivity due to low background and high signal-to-noise ratios. Prior studies have elegantly demonstrated the application of chemiluminescence for imaging of myeloperoxidase [141] and beta-galactosidase activities [142] *in vivo*. Although chemiluminescence has an additional advantage of not requiring FLuc-transfected cells for the generation of light, expression of this enzyme allows

more elaborate disease models to be developed due to the researcher's ability to define its spatial localization. Moreover, most chemiluminescent agents suffer from low quantum yield, short maximal photon wavelength emission and high instability. For example, the quantum yield of aqueous luminol chemiluminescence is  $1.23 \pm 0.20\%$  [147] with a maximal emission of 424 nm [148], while the reported quantum yield of firefly BL is  $41.0 \pm 7.4\%$  [18], that is about 40 times higher, with D-hydroxyluciferin and D-aminoluciferin having wavelength at 560 nm and 603 nm respectively [149]. Recently, Zhang *et al.* [150] showed the advantage of using both near-infrared fluorescence and chemiluminescence imaging in combination, while addressing the wavelength issue associated with luminol chemiluminescence *in vivo* by shifting it into the near-infrared region utilizing quantum dots. A recently reported probe by Cao *et al.* demonstrated the possibility of using chemiluminescence for imaging of bacterial NTR *in vitro* and assessing the activity of endogenous reductases in tumor-bearing mice under various oxygenation conditions [146].

Several bioluminescence probes were recently developed for imaging of NTR. In a study by Porterfield *et al.* NTR was used as an alternative to a previously reported enzyme,  $\beta$ -galactosidase, as a tool to study cell-cell interaction [143]. The developed probe was applied to visualize two types of cells being in close contact with each other. When the probe was uncaged in NTR<sup>+</sup> cells, the released luciferin diffused and produced light in the neighbouring Fluc<sup>+</sup> cells. Although, the probe was a viable reporter of NTR activity, the caged probe produced a high background signal in enzyme assays (possible being a substrate for FLuc) and only four-fold S/N ratio when incubated with NTR which was attributed to the instability of the produced luciferin. These issues could be explained by the probe design and the fact that the product of probe uncaging is not a native substrate for FLuc, hydroxy-luciferin, but a hydroxylamino-luciferin.

The other reported BL probes were validated only in *in vitro* assays, with isolated enzyme or in live bacteria, and their applicability for imaging of bacterial NTR in living animals was not demonstrated [144, 145]. The work presented in this chapter describes the development of an NTR-specific probe that was extensively validated *in vitro* and *in vivo* with an emphasis on the GDEPT-related applications.

## 2.3 Results

### 2.3.1 Probe design and synthesis

The reduction of nitroaromatic compounds can occur through one- or two-electron mechanism [114]. Two types of bacterial NTRs have been described and they are classified according to the oxygen dependence. The NTRs used in our study (NfsA, NfsB) are type I oxygen-insensitive NTRs, they catalyze the reduction of the nitro group by addition of a pair of electrons, and their activity does not depend on the level of oxygen. However, the oxygen-sensitive NTRs (type II) catalyze the reduction of the nitro group by the addition of one electron, forming the nitro anion radical, which is oxidized back to the nitro group by oxygen. Bacteria contain both types of nitroreductases with type I being the most characterized among other NTRs. The independence of reduction from the level of oxygen in *E. coli* had been previously shown for an NTR-sensitive coumarin probe (7-nitrocoumarin-3-carboxylic acid) suggesting the prevalent involvement of type I NfsA and NfsB possibly along with other uncharacterized NTRs [151].

We have previously demonstrated the suitability of exploiting NTR activity as being sufficiently selective to distinguish bacterial cells from host background [152]. Several NTR-related enzymes have been identified in mammalian cells and they functionally relate to type I NTRs (NAD(P)H-quinone oxidoreductase (DT-diaphorase EC 1.6.99.2) and xanthine dehydrogenase EC 1.17.1.4). They can potentially contribute to reduction of nitroaromatics, although they are not phylogenetically related and do not exhibit the typical domain characteristic of NTR family. These properties were investigated in the study on FMISO imaging reagent, a derivative of nitroimidazole used as a hypoxia PET tracer [153]. It was reported that under hypoxic conditions xanthine dehydrogenase is converted to xanthine oxidase that reduces FMISO and other nitroimidazole-containing compounds. Similarly, eukaryotic NTRs that are functionally related to type II (aldehyde oxidase EC 1.2.3.1, cytochrome c oxidase EC 1.9.3.1, and NADPH cytochrome P450 reductase EC 1.6.2.4) can potentially reduce nitroaromatics anaerobically and are generally used as targets for hypoxia-activated prodrugs and imaging agents [154].

Therefore, several important factors need to be taken into account when designing the compounds activated selectively by bacterial or mammalian enzymes. For bacterial NTRs the activation is largely dependent on the redox potential of the nitroaromatics. For example, nitrofurans display relatively high redox potentials (reported from -250 to -270 mV) and are reductively activated by NAD(P)H nitroreductases of enteric bacteria. At the same time metronidazole (nitroimidazole) is only activated by anaerobic enzymes showing low redox potentials (-480 mV) in some bacteria and protozoa, making it well tolerated in humans when used as an antibiotic [155].

Substrate specificity of the designed compounds is also important, for example CB 1954 prodrug is efficiently reduced by bacterial NTRs and a human DT-diaphorase (NQO2) while being a poor substrate for a human paralogue NQO1 enzyme [156]. These and other important aspects of selectivity of bioreductive prodrugs are discussed in more details in a recent review by Wilson and Hay [157].

Our probe design is based on caging of D-luciferin with nitrofuryl moiety resulting in "Nitroreductase Caged Luciferin" (NCL) probe (Figure 2.2). 5-Nitrofuryl was selected as a cage as its derivatives (nitrofurazone, nitrofurantoin) were

shown to be efficiently activated by NTR in bacteria [155]. Upon the reduction of the nitro group by NTR the resulting electron-donating amino group promotes the cleavage of the C-O bond (uncaging), leading to the subsequent release of luciferin which is oxidized by luciferase and a photon of light is emitted. Therefore, release of free luciferin followed by light production is only possible in the presence of NTR.

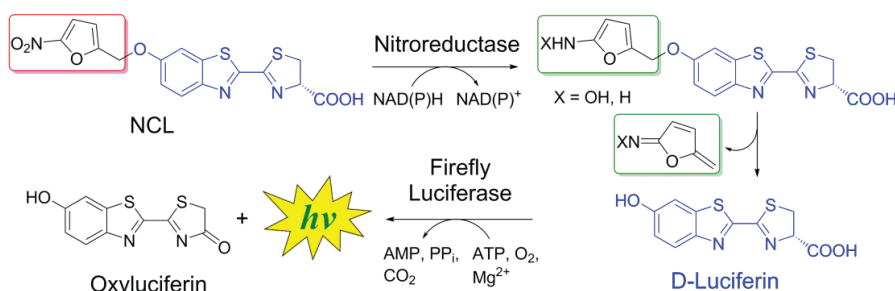


Figure 2.2 General strategy for imaging of NTR activity with Nitroreductase Caged Luciferin (NCL) probe

The caged luciferin probe NCL was originally synthesized in three steps with an overall yield of 17% (See 2.5 Experimental section, Scheme 2.1). The synthetic route was later optimized which allowed to obtain the probe in just two steps with an overall 63% yield (Scheme 2.2).

### 2.3.2 Validation of NCL in cell-free assays

We first investigated the specificity of probe uncaging by incubating NCL with a recombinant NTR enzyme from *E. coli* (NfsA) in the presence of NADH as a cofactor. The release of luciferin was followed by HPLC-MS analysis as a function of time (Figure S2.1). The resulting data demonstrated rapid conversion of NCL into free luciferin under these conditions, the calculated values of rate constant and NCL half-life, were  $5.8 \times 10^{-3} \text{ s}^{-1}$  and 119.5 s respectively (Figure S2.1).

Next, we determined the Michaelis-Menten kinetic parameters for the NTR-specific cleavage of NCL probe (Figure S2.2) using fluorescence to monitor release of luciferin ( $\lambda_{\text{ex/em}} = 330/530 \text{ nm}$ ) as the caged probe is not fluorescent. Both  $V_{\text{max}}$  and  $K_{\text{m}}$  values were found to be comparable to those previously reported for a NTR fluorescent substrate [133] and were determined to be  $0.057 \mu\text{M s}^{-1}$  and  $24.7 \mu\text{M}$  respectively. Catalytic efficiency of probe reduction by NTR ( $k_{\text{cat}}/K_{\text{m}}$ ) was determined to be  $2.25 \times 10^7 \text{ M}^{-1} \text{ s}^{-1}$ , which is two orders higher than that of luciferin-luciferase reaction ( $1.07 \times 10^5 \text{ M}^{-1} \text{ s}^{-1}$ ) [158]. To evaluate if the probe can be used as a reporter of NTR activity, we investigated the effect of the NTR inhibitor dicoumarol (competitive with NADH) on the efficiency of NCL uncaging. A gradual concentration-dependent decrease in signal was observed (Figure 2.3A) indicating that the uncaging of NCL depends on the activity of NTR. We also assayed quantitative capability of the probe against the amount of NTR by fluorescence and found the detection limit to be  $0.15 \mu\text{g/mL}$  (Figure S2.1).

To determine the utility of NCL as a bioluminescent reporter, we measured the light emission from increasing concentrations of NCL ( $0.25\text{--}5 \mu\text{M}$ ) in the presence or absence of NTR and firefly luciferase (Figure 2.3B) in real-time. The resulting signal was concentration-dependent and no significant light was produced in the absence of NTR, resulting in high signal to background noise ratios even at relatively low concentrations of the probe in comparison to that previ-

ously reported [53, 93]. In addition, NCL demonstrated an average 70% conversion into luciferin over 30 min, the highest uncaging efficiency among existing caged luciferin substrates reported to date [53, 93]. We also verified that NTR did not have any effect on the luciferin-luciferase reaction (Figure S2.4).

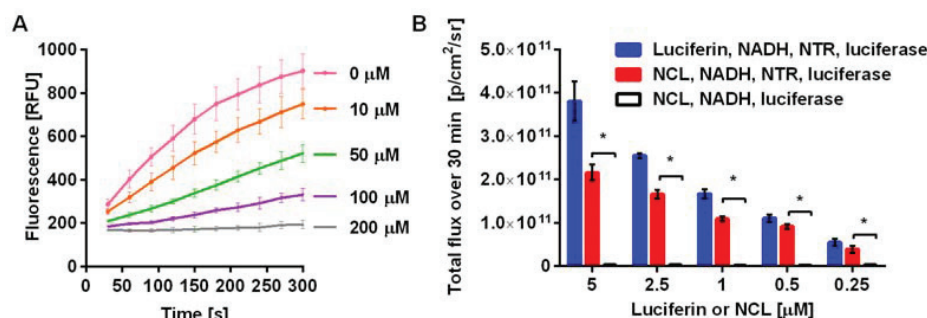


Figure 2.3 Evaluation of NTR-specific uncaging of NCL probe. (A) NCL (20  $\mu\text{M}$ ) uncaging by NTR (0.5  $\mu\text{g mL}^{-1}$ ) in the presence of NADH (100  $\mu\text{M}$ ) was inhibited by dicoumarol (0 to 200  $\mu\text{M}$ ). (B) Total luminescence over 30 min from luciferin or NCL (0.25–5  $\mu\text{M}$ ) with NADH, luciferase, and NTR, compared with the control (no NTR), \* $P < 0.001$ .

### 2.3.3 Stability profiling

Since an ideal imaging reagent should be non-toxic and stable in biological environments, we next investigated these parameters. The probe did not induce any toxicity in bacteria or mammalian cells (Figure S2.9). The half-life of NCL in mouse plasma *in vitro* was determined to be 53.7 h (Figure S2.6A), which readily permits robust BL imaging *in vivo*. In addition, NCL demonstrated excellent stability to liver microsomes *in vitro* (Figure S2.6B).

### 2.3.4 Imaging of NTR activity in *E. coli*

We approached the validation of NCL in a live biological system initially utilizing bacteria as a source of both NTR and luciferase. We investigated the potential of NCL probe for imaging NTR in *E. coli* naturally expressing NTR [115–117] and engineered to express luciferase. The resulting signal from NCL or luciferin control was compared between several *E. coli* strains: 1) *E. coli* wt, 2) *E. coli* engineered to stably express luciferase (*E. coli* *luc+*), 3) a strain of *E. coli* (*NTR KO luc+*) with three well-described NTR genes knocked out (*NfsA*, *NfsB* and *NemA*). First, as shown on Figure 2.4, significant signal above background was detected from *E. coli* *luc+* in comparison with *E. coli* wt, indicating the need of luciferase presence for light production. Both wt and *NTR KO luc+* strains showed similar levels of luciferase expression when treated with luciferin. However, with NCL the signal from parent strain was significantly higher than from the NTR mutant strain (*NTR KO luc+*), demonstrating probe selectivity for detection of NTR activity in bacteria. The presence of a signal in wells with *NTR KO luc+* strain indicates that reduction of the nitrofuryl cage is not exclusive or specific to any of the three major *E. coli* NTRs (*NfsA*, *NfsB* and *NemA*) and that cage reduction can be achieved at detectable levels in the presence of the remaining NTRs in *E. coli*. In *E. coli*, several nitroreductases (*NfsA* [115], *NfsB* [116], *YdjA* [117]) and reductases (*NemA* [159]) are characterized, while the exact functions of other reductase proteins remain unclear. Recent studies [117] indicate that *E. coli* reductases could also have additional nitroreductase activity.

We also investigated the signal dependence on different numbers of bacteria and significant signals were evident at concentrations of bacteria as low as  $10^4$  cells/mL ( $1.5 \times 10^3$  cells/ well) (Figure 2.4C). The average efficiency of probe uncaging in bacteria was calculated to be 35% (Figure 2.4D).

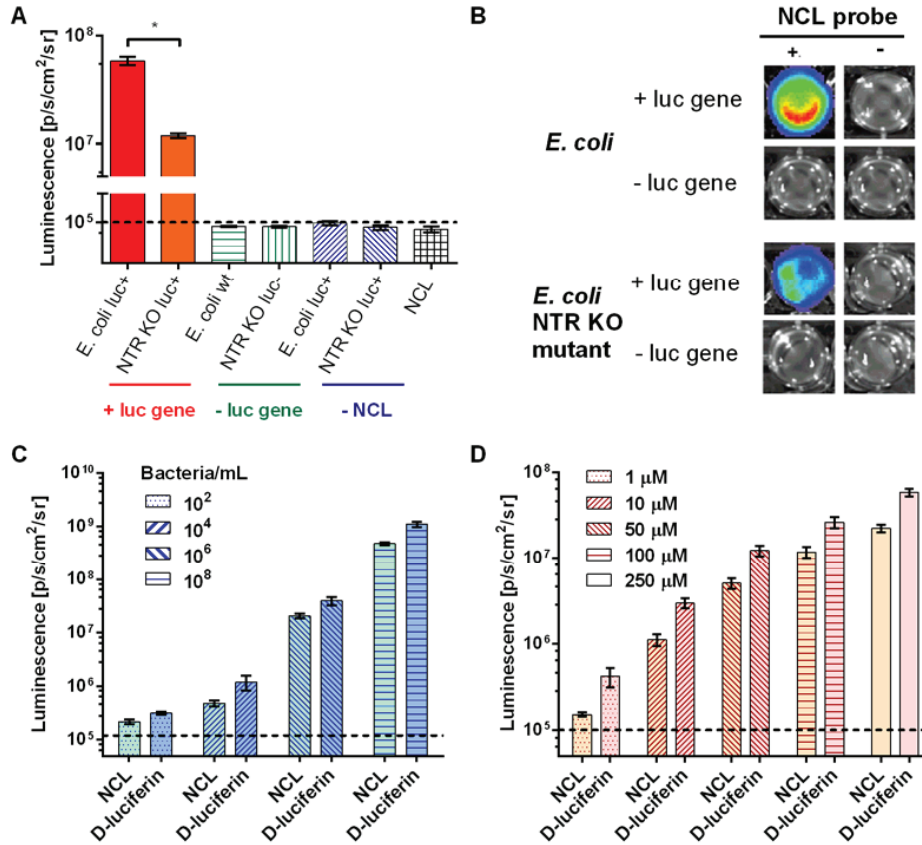


Figure 2.4 Light production in *E. coli* by NTR-mediated uncaging of NCL. (A). Light output from NCL (300 μM) after 2 h incubation in luciferase-expressing *E. coli* (+ luc gene) is significantly higher than in NTR mutant (NTR KO luc<sup>+</sup>) (\*P < 0.001) and in wild type (- luc gene). The dashed line indicates the background. (B). Overlay of a photographic image and bioluminescence from the assay described. (C). Bioluminescence from 100 μM NCL probe and luciferin incubated with various concentrations of luciferase expressing *E. coli* AB1157 ( $10^2$ – $10^8$  bacteria mL<sup>-1</sup>) for 10 min before imaging. (D). Bioluminescence from luciferase expressing *E. coli* luc<sup>+</sup> ( $10^8$  bacteria mL<sup>-1</sup>) incubated with various concentrations of NCL or luciferin (1–250 μM) for 10 min before imaging.

### 2.3.5 Imaging of bacterial NTR *in vivo* in a mouse model of intramuscular infection

The utility, and importantly, the specificity, of the probe *in vivo* was examined in a mouse model of thigh muscle infection, again utilizing bacteria as the source of both NTR and luciferase. Balb/c mice were injected in quadriceps with various numbers of *E. coli* luc<sup>+</sup> ( $5 \times 10^4$ – $5 \times 10^7$ ), followed by IP injection of NCL 30 min later (Figure 2.5A). Animals were imaged at various time points over 24 h (Figure 2.5B). Signal from the probe was detected 20 min post injection lasting for as long as 24 h and correlated with the amount of probe injected. The intensity increased over the first 4 h reaching plateau afterwards. The total photon flux produced during this time was approximately 1/3 of the total flux detected from the mice injected with luciferin, demonstrating high efficiency of uncaging by bacterial NTR *in vivo*

(Figure 2.5B). We also compared the probe kinetics after different administration routes in mouse model of *E. coli* intramuscular infection (Figure S2.7). Statistical analysis of the data showed no significant difference in signal from IP and IV administration of the probe in this model at 0.8 mg/mouse.

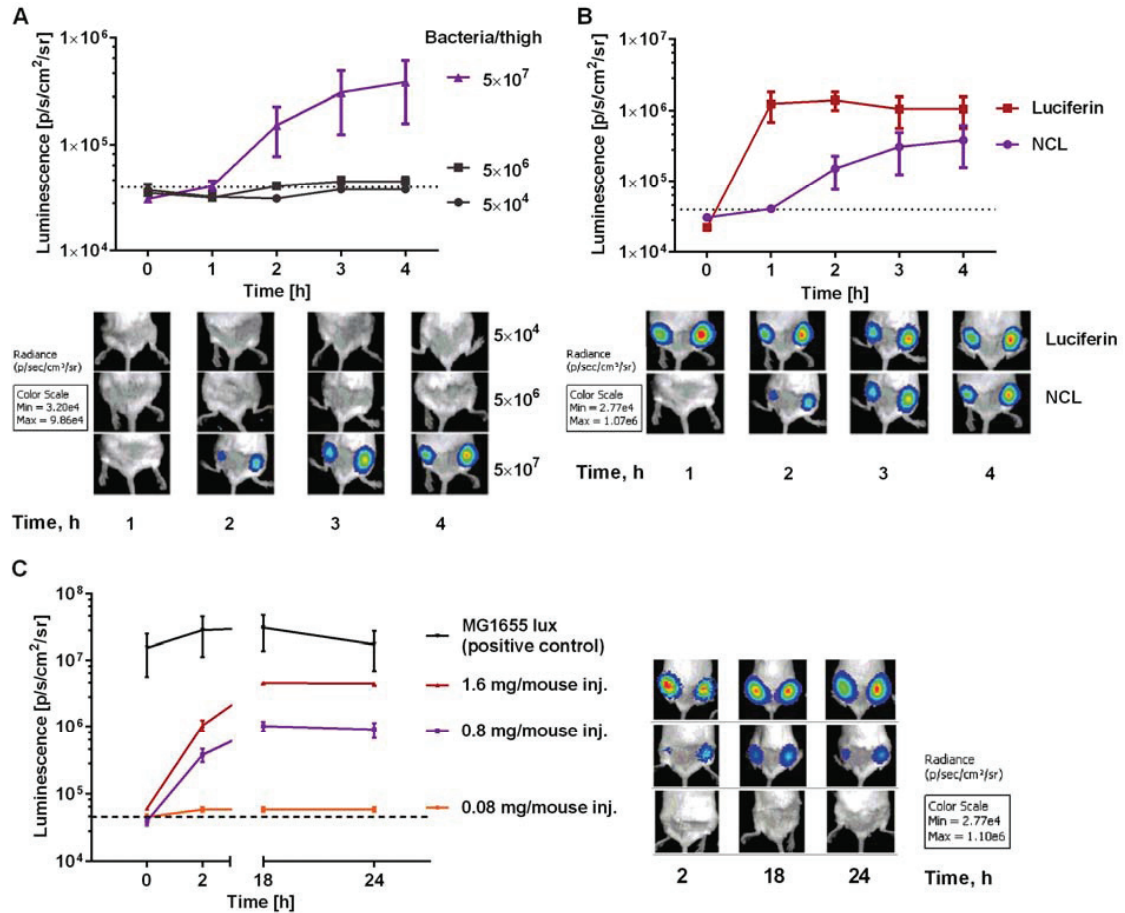


Figure 2.5 *In vivo* activation of NCL probe by luciferase and nitroreductase expressing *E. coli* in a mouse model of thigh infection. (A). Luminescence over 4 h from *E. coli* *luc+* infected quadriceps ( $5 \times 10^4$ – $5 \times 10^7$  bacteria) after IP injection of 0.8 mg NCL probe (200  $\mu$ L of 10 mM solution in PBS). (B). Luminescence over 4 h from *E. coli* *luc+* infected quadriceps ( $5 \times 10^7$  bacteria) following IP injection of 0.8 mg of probe or 0.63 mg of luciferin (200  $\mu$ L of 10 mM solution in PBS). (C). Luminescence imaging of mice over 24 h bearing  $5 \times 10^7$  bacteria, treated with various (0.08, 0.8 and 1.6 mg) NCL probe concentrations (200  $\mu$ L of 1, 10 and 20 mM solutions of NCL in PBS). As a positive control, mice were injected with equal amounts of *E. coli* MG1655 expressing lux luciferase that doesn't require exogenous substrate for light production [62]. The signal was collected over 24 h, n = 3 per group.

### 2.3.6 Evaluation of NCL in NTR- and FLuc-expressing cancer cells

As the next step we applied NCL for imaging of NTR activity in breast cancer cells, stably transfected with NTR and luciferase (MDA-MB-231-NTR+luc+) [139]. The expression of active NTR was confirmed by using the previously described NTR-specific fluorescent CytoCy5S probe (Figure S2.8). Addition of different concentrations of NCL to NTR+ cells resulted in rapid concentration-dependent signal increase, with up to 40 times signal-to-noise ratio at the highest concentration used (100  $\mu$ M) (Figure 2.6). Contrary to this, NTR- cells produced much lower signal of equal intensity at



all concentrations used (Figure 2.6B). The difference in brightness between the two cell lines due to different expression levels of luciferase was taken into account by normalizing the signal from NCL to the signal from equimolar quantities of luciferin control. The selectivity of NCL uncaging was also tested in another NTR-/NTR+ cancer cell line and similar results were observed (Figure S2.10).

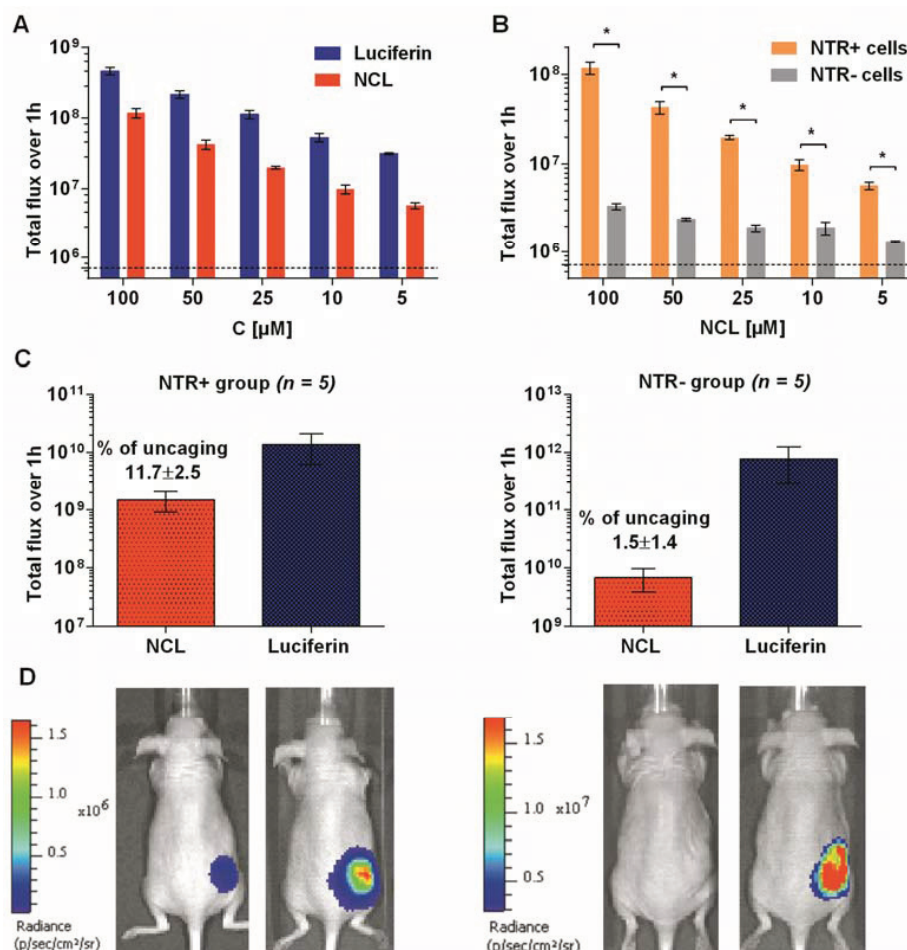


Figure 2.6 Imaging of NTR activity in cells and in *in vivo* cancer model with NCL. (A) Concentration-dependent uncaging of NCL in MDA-MB-231 NTR+luc+ cancer cells in comparison with luciferin. (B) Selectivity of NTR imaging by NCL in the same cells in comparison with NTR-luc+ cells. The dashed line indicates background (cells only), \* $P = 0.0001$ . (C) *In vivo* imaging of NTR activity in subcutaneous NTR+ and NTR- xenografts (n = 5). Total luminescence over 1 h from IP injection of luciferin (1.5 mg) and NCL (1.9 mg). (D) Representative images of mice 15 min post injection of luciferin or NCL.

The difference in kinetics of the signal from the probe in bacteria (Figure 2.4) and mammalian cells (Figure 2.6) can be explained by the fact that *E. coli* naturally expresses several types of nitroreductases, while the mammalian cell line used in our experiments was transfected with one type of nitroreductase (NfsB).



### 2.3.7 Imaging of NTR in cells not expressing luciferase

Several NTR-expressing cell lines have been generated for the GDEPT applications. However, they often do not have simultaneous co-expression of FLuc that is necessary for the BLI read-out. We therefore decided to demonstrate the applicability of our probe for imaging of NTR activity in cells not expressing FLuc.

After incubation of HEK293 NTR+ or wt cells with NCL or luciferin for one hour, the cells were lysed and FLuc was added to measure the amount of the probe uncaged by NTR. As shown in Figure 2.7A the probe produced a concentration-dependent signal with NTR+ cells which was significantly higher than the background signal in control cells. Luciferin was used as a positive control to check that the lysis procedure did not affect the BLI readout in both cell lines (Figure 2.7B).

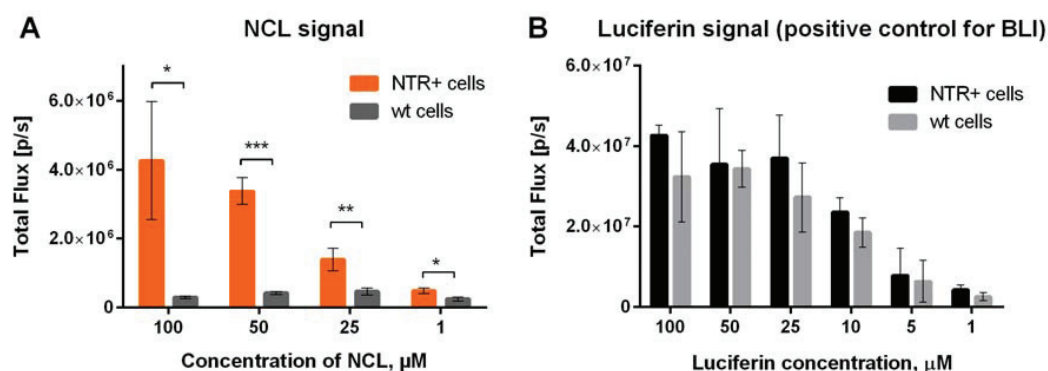


Figure 2.7 Imaging of NTR activity in HEK293T cells after cell lysis and addition of FLuc. (A) Concentration-dependent signal from NCL in HEK293T-NTR+ cells compared to the control HEK293 (wt). (B) Equal signal from luciferin in both cell lines confirmed that the lysis did not affect the BLI readout. Representative data at 40 min post-luciferase addition.

### 2.3.8 The effect of hypoxia on the NCL probe in cells not expressing FLuc

As mentioned earlier, eukaryotic cells have reductases that are functionally related to type II oxygen-sensitive NTRs (aldehyde oxidase EC 1.2.3.1, cytochrome c oxidase EC 1.9.3.1, and NADPH cytochrome P450 reductase EC 1.6.2.4) that can potentially reduce nitroaromatics anaerobically and are the targets for hypoxia-activated prodrugs and imaging agents [154, 157]. We decided to check whether our probe is a substrate for these enzymes and whether the reduction can occur in cells under hypoxic or normoxic conditions. We used cells that do not express FLuc and applied the detection method with cells lysis and exogenous addition of FLuc as described earlier.

First, a pimonidazole assay was used as a positive control for activity of intracellular reductases under hypoxia (Figure 2.8A). Pimonidazole-HCl is the gold standard immunochemical hypoxia marker widely used for imaging of regions of hypoxia in tumors *in vivo* and has been recently approved for clinical use in USA, Canada and Norway. Pimonidazole is a derivative of a nitro-imidazole where the nitro- group is reduced by one-electron oxygen-sensitive reductases under hypoxic conditions (at  $p\text{O}_2 \leq 10$  mm Hg). It is estimated that approximately 20% of reduced pimonidazole binds to cellular thiols and forms adducts that can be visualized by anti-pimonidazole antibody conjugated with a fluorescent

dye. This assay is based on the reduction of a nitro-aromatic system, therefore, it is an ideal control to check if our probe is a substrate for intracellular reductases in normoxic and hypoxic conditions, as the reduction of a nitro- group of NCL will lead to luciferin release and increase in probe signal. The mechanism of pimonidazole reduction and binding in hypoxic cells as well as additional controls for the experiment in Figure 2.8A is shown in Figure S2.12.

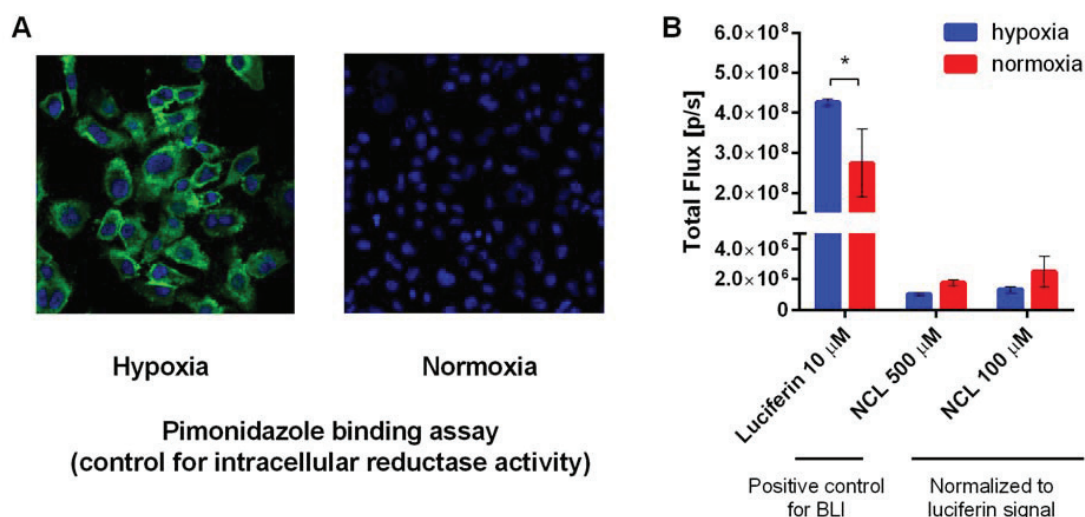


Figure 2.8 Imaging of intracellular reductase activity in A549 cells in hypoxic and normoxic conditions. (A) Pimonidazole trapping inside cells visualized by anti-pimonidazole FITC-mAb staining, green- FITC, blue- nucleus (Hoechst). (B) Bioluminescence signal from luciferin (positive control) or probe incubated with cells for 1 h in hypoxia or normoxia, after cell lysis and FLuc addition. The probe signal was normalized to the difference in luciferin signal in normoxic vs. hypoxic cells (2.1 times). Representative data at 10 min post-luciferase addition.

As can be seen in Figure 2.8A, a remarkably higher fluorescence signal was observed in cells incubated in hypoxic conditions for two hours than in the cells incubated in normoxic conditions (additional controls shown in Figure S2.12). This assay confirmed the activity of intracellular reductases in A549 cells under hypoxia and their ability to reduce the nitro-aromatic group of pimonidazole. However, when the NCL probe was incubated in A549 cells under hypoxia or normoxia, no difference in BL signal was observed between the two groups (Figure 2.8B). The overall signal intensity from high concentrations of the probe (100, 500  $\mu$ M) is about two orders of magnitude lower than for ten times lower concentration of luciferin (10  $\mu$ M), which corresponds to a very low background signal produced from the unspecific uncaging of the probe in cells (approximately 1% of the photon flux from luciferin). Moreover, there was no difference in the amount of light produced from 100 and 500  $\mu$ M of probe.

### 2.3.9 Imaging of NTR activity in subcutaneous xenograft model of cancer

In light of these positive results we decided to investigate the utility of NCL as a reporter of NTR activity in a cancer xenograft model in mice, using the same cell lines previously validated *in vitro* (Figure 2.5). Subcutaneous NTR+ or NTR- xenograft tumors were induced in two groups of mice (n = 5 per group) and were grown to an average volume of approximately 0.25 cm<sup>3</sup>. We chose to implant the NTR+ and NTR- cells in different mice to ensure that the signal produced from the probe is specific to the cell type and doesn't result from luciferin diffusion to the neighbouring tumor.

Another reason to implant the cells separately was the difference in light emission that could preclude accurate measurements for light sources of different intensity on a single mouse.

When caged luciferin probes are used to measure the activity of a biomolecule in various experimental settings, the light output needs to be calibrated to the amount of luciferase [52, 53, 160]. In our case this calibration takes into account variations between luciferase levels in tumors from one group to another. Therefore, in order to compare the performance of the probe in two different cancer cell lines with a various level of luciferase expression we normalized the signal from of the probe to the signal from equimolar amount of D-luciferin.

Both groups of mice were first injected IP with luciferin (1.5 mg) to determine the overall light emission from each tumor over 1 h. This signal was later used to calculate percentage of NCL uncaging in order to normalize tumor size and level of luciferase expression from NTR-/+ cell lines. 24 h later, all mice were injected IP with equimolar quantities of NCL (1.9 mg), followed by collection of light over 1 h (kinetics shown in Figure S2.11). Since the residual light from luciferin injection could contribute to the signal from the probe, the absence of residual signal was verified by imaging of mice before probe administration. The level of probe uncaging in NTR+ and NTR- groups was determined by quantifying light production from NCL in each mouse relative to luciferin. As shown in Figure 2.6C the efficiency of probe uncaging in the NTR+ group was approximately an order of magnitude higher than in the NTR- group ( $11.7 \pm 2.5\%$  and  $1.5 \pm 1.4\%$  respectively;  $p = 0.0001$ ), demonstrating the utility of this probe for imaging of NTR activity in tumors.

In a previously reported study of NTR imaging with CytoCy5S fluorescence of orthotopic xenograft tumors, probe activation by bacteria in the GIT resulted in background fluorescence in that cancer model requiring fluorescence lifetime gating to differentiate tumor signal from GIT signal [138]. Although we have not presented results of orthotopic tumors, it is anticipated that the bioluminescence based imaging tool in our study, permitting detection of the signal only with co-expression of both luciferase and NTR, would eliminate such issues.

## 2.4 Conclusion

In conclusion, we developed a new caged luciferin probe for bacterial nitroreductase imaging that can be readily synthesized in two steps in a high yield. The probe displayed minimal background signal, fast enzyme kinetics and high specificity to bacterial nitroreductases which resulted in high signal-to-background ratios in *in vitro* and *in vivo* experiments. The probe was extensively validated and its potential for *in vivo* imaging was demonstrated in several experimental models, which makes this reagent advantageous to other recently reported caged luciferin probes. Our results demonstrate that the NCL probe can be effectively used for non-invasive real-time imaging of NTR activity *in vitro*, in live bacteria and mammalian cells, as well as *in vivo*, in preclinical models of cancer and certain bacterial infections.

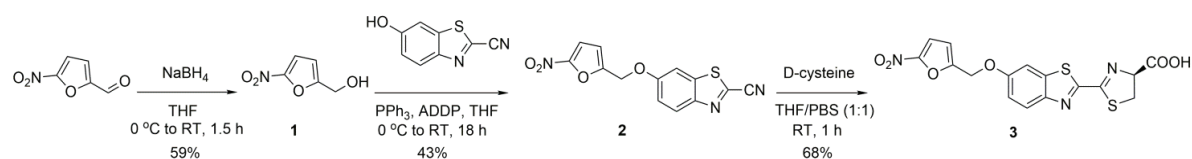
This novel reagent should significantly simplify screening of prodrugs *in vivo* and accelerate the preclinical development of enzyme-activatable therapeutics for translation into the clinic. In a recent review on NTR application in GDEPT Williams et al. highlighted that the development of tools for noninvasive imaging of NTR is one of the most exciting recent advances in this field and found our work to be of particular relevance to GDEPT [126].

## 2.5 Experimental section

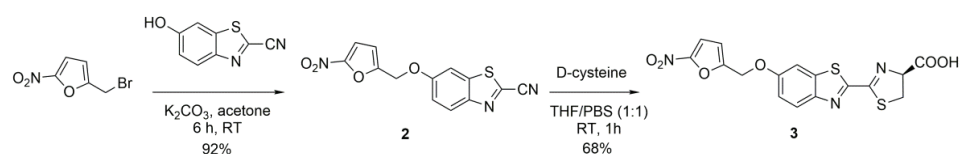
### 2.5.1 Chemical materials and methods

Chemicals were purchased from ABCR GmbH, Acros organics, AppliChem GmbH, Sigma-Aldrich, and were used as received. Firefly luciferase, *E. coli* nitroreductase NfsA, mouse male liver microsomes were purchased from Sigma-Aldrich. Mouse plasma was purchased from Harlan Laboratories. Analytical thin layer chromatography was performed using aluminum-backed SiO<sub>2</sub> TLC plates from Merck. HPLC analysis was performed on Agilent Infinity 1260 HPLC system (Agilent, Santa Clara, CA) with SunFire C18 column (2.6x20 mm, 3.5  $\mu$ m, Waters) using degassed HPLC gradient grade solvent from Fisher Chemicals (Loughborough, UK) and Millipore water. The products of the reaction were initially analyzed by Agilent 6120 Quadrupole LC/MS system (Agilent, Santa Clara, CA), directly connected to HPLC. Nuclear magnetic resonance (<sup>1</sup>H, <sup>13</sup>C NMR) data were acquired on a Bruker AV400 MHz spectrometer. NMR chemical shifts are reported in the standard  $\delta$  notation of parts per million using the peaks of residual proton and carbon signals of the solvent as internal references. Splitting patterns are designated as s (singlet), d (doublet), dd (doublet of doublets), t (triplet), m (multiplet). Coupling constants (*J*) are reported in hertz. HRESI-MS measurements were conducted at the EPFL ISIC Mass Spectrometry Service using Micro Mass QTOF Ultima (Waters Corp., Milford, MA).

#### Chemical synthesis



Scheme 2.1 Original synthetic route of NCL (3 steps, overall yield 17%).



Scheme 2.2 Improved synthetic route of NCL (2 steps, overall yield 63%).

#### (5-Nitrofuran-2-yl)methanol (1)

Compound **2** was synthesized using a method described in the literature [161]. 5-Nitro-2-furaldehyde (2.0 g, 14.2 mmol) was dissolved in THF (25 mL). Sodium borohydride (0.45 g, 14.2 mmol) in water (2 mL) was added slowly dropwise to the THF solution at 0 °C. After the addition, the ice bath was removed and the reaction mixture was left to stir at room temperature for 1 h 30 min. THF was evaporated, 20 mL of water was added to the reaction mixture and extracted with ethyl acetate (3 x 30 mL). The combined organic extracts were washed with saturated NaCl solution, dried (Na<sub>2</sub>SO<sub>4</sub>) and evaporated. After evaporation the desired product was obtained as a dark-yellow liquid (1.19 g, 59%). <sup>1</sup>H NMR (400 MHz, CDCl<sub>3</sub>)  $\delta$  = 7.29 (d, 1H), 6.56 (d, 1H), 4.72 (s, 2H), 2.40 (1H, br). Data is consistent with the literature [161].

**6-((5-Nitrofuran-2-yl)methoxy)benzo[d]thiazole-2-carbonitrile (2)**

**Scheme 2.1.** To a solution of compound **1** (0.25 g, 1.75 mmol), 2-cyano-6-hydroxybenzothiazole (0.277 g, 1.57 mmol), and triphenylphosphine (0.642 g, 2.45 mmol) in anhydrous THF (7 mL) under N<sub>2</sub>, was added a solution of 1,1'-(azodicarbonyl)dipiperidine (ADDP) (0.617 g, 2.45 mmol) in anhydrous THF (4 mL) dropwise at 0°C. After 1.5 h, the reaction mixture was placed at room temperature and stirred for 18 h. The solvent was evaporated and crude mixture was purified using Biotage (SNAP C18 12g column, H<sub>2</sub>O:THF, 3-100% THF over 30 min). Purification yielded 0.226 g (43%) of compound **2**. <sup>1</sup>H NMR (400 MHz, (CD<sub>3</sub>)<sub>2</sub>CO) δ = 8.16 (d, *J* = 9.1 Hz, 1H), 7.98 (d, *J* = 2.6 Hz, 1H), 7.54 (d, *J* = 3.7 Hz, 1H), 7.45 (dd, *J* = 9.1, 2.6 Hz, 1H), 7.03 (d, *J* = 3.7 Hz, 1H), 5.43 (s, 2H). <sup>13</sup>C NMR (101 MHz, (CD<sub>3</sub>)<sub>2</sub>CO) δ = 159.5, 154.0, 153.3, 148.3, 138.4, 135.3, 126.6, 119.7, 114.6, 114.0, 113.3, 106.3, 63.3. HRMS: calculated for C<sub>13</sub>H<sub>7</sub>N<sub>3</sub>O<sub>4</sub>S [MH]<sup>+</sup> 302.0229, found 302.0236.

**Scheme 2.2.** To a solution of bromide (**0.116 g**, 0.56 mmol) in anhydrous acetone (8 mL) was added 2-cyano-6-hydroxybenzothiazole (0.09 g, 0.51 mmol) and K<sub>2</sub>CO<sub>3</sub> (0.141 g, 1.02 mmol) under N<sub>2</sub> at room temperature. The reaction was monitored by HPLC-MS and after 6 h the disappearance of starting compound **3** was observed, the reaction mixture was filtered, the filtrate was evaporated to give the product **2** (95% purity by <sup>1</sup>H NMR) in excellent yield (0.141 g, 92%).

**2-((5-nitrofuran-2-yl)methoxy)benzo[d]thiazol-2-yl)-4,5-dihydrothiazole-4-carboxylic acid (3)**

To a solution of compound **2** (0.048 g, 0.16 mmol) in THF (1.5 mL) was added a solution of D-cysteine (0.029 g, 0.24 mmol) in degassed PBS (1.2 mL) under N<sub>2</sub>. After 1 h, solvent was evaporated and crude material was purified by preparative HPLC (C8 column, H<sub>2</sub>O+5mM HCOONH<sub>4</sub>:ACN, 5-95% ACN over 30 min), affording pure product **3** (0.044 g, 68%). <sup>1</sup>H NMR (400 MHz, CD<sub>3</sub>CN) δ = 7.97 (d, *J*=9.0 Hz, 1H), 7.63 (d, *J*=2.6 Hz, 1H), 7.41 (d, *J*=3.7 Hz, 1H), 7.22 (dd, *J*=9.1, 2.6 Hz, 1H), 6.83 (d, *J*=3.7 Hz, 1H), 5.27 (t, *J*=9.2 Hz, 1H), 5.20 (s, 2H), 3.71 (d, *J*=6.2 Hz, 1H), 3.68 (d, *J*=5.5 Hz, 1H). <sup>13</sup>C NMR (101 MHz, (CD<sub>3</sub>)<sub>2</sub>CO) δ = 171.3, 166.1, 159.7, 158.4, 154.4, 153.2, 149.2, 138.5, 126.0, 118.2, 114.4, 113.4, 106.6, 79.3, 63.2, 35.5. HRMS: calculated for C<sub>16</sub>H<sub>11</sub>N<sub>3</sub>O<sub>6</sub>S<sub>2</sub> [MH]<sup>+</sup> 406.0168, found 406.0171.

## 2.5.2 General methods

**HPLC analysis.** HPLC analysis was performed on Agilent Infinity 1260 HPLC system (Agilent, Santa Clara, CA) with Sun-Fire C18 column (2.6 × 20 mm, 3.5 μm, Waters) using degassed HPLC gradient grade solvent from Fisher Chemicals (Loughborough, UK) and Millipore water. The products of the reaction were initially analyzed by Agilent 6120 Quadrupole LC/MS system (Agilent, Santa Clara, CA), directly connected to HPLC. NCL and luciferin were detected at 320 nm, testosterone was detected at 240 nm. Conditions of the method were the following: mobile phase 5 mM HCOONH<sub>4</sub>:ACN, 5:95% ACN over 2 min, the injection volume 3 μL and the flow rate 1 mL/min. Standard curve for NCL was constructed by plotting the peak areas vs. diluted concentrations (in a range of 1- 50 μM) of stock solutions of the compound.

**Nitroreductase assay (Figure S2.1).** The reduction of NCL probe by *E. coli* nitroreductase (NTR) was monitored by HPLC analysis. The reaction solution containing 700 μL of PBS (pH 7.4), 100 μL of 10 mM NADH, 100 μL of 10 μg/mL NTR and 100 μL of 10 mM NCL solution in PBS (pH 7.4) was performed at 37 °C. Aliquots of 100 μL were taken from reaction mixture at 0, 0.5, 1, 3, 5, 7, 9 and 30 min, and were quenched with 100 μL of acetonitrile. The samples were analyzed by HPLC. Kinetics of the reaction was calculated assuming pseudo-first-order kinetics and a plot of ln of probe concentration versus time was established. The half-life of reduction was calculated on the basis of the disappearance of the substrate assuming pseudo-first-order kinetics.

**In vitro stability in mouse plasma (Figure S2.6).** The *in vitro* stability of NCL was studied in mouse plasma (Harlan Laboratories) according to the procedure described in the literature [162]. The reactions were initiated by the addition of 100 μL of 1mM solution of NCL in PBS (pH 7.4) to 400 μL of preheated plasma solution to yield a final concentration of 200 μM. The assays were performed in a shaking water bath at 37 °C. Samples (50 μL) were taken at 0, 15, 30, 45, 60 min, 2, 6 and 24 h and added to 150 μL of ice-cold methanol. The samples were subjected to brief vortex mixing and centrifugation for 10 min at 14000 rpm. The clear supernatants were analyzed by HPLC. The *in vitro* plasma half-life ( $t_{1/2}$ ) was calculated using the expression  $t_{1/2} = \ln 2/b$ , where b is the slope found in the linear fit of the natural logarithm of the fraction remaining of the NCL vs. incubation time.

**In vitro mouse liver microsome stability assay (Figure S2.6).** The assay was performed according to the procedure described in the literature [163]. The reaction mixture contained 390 μL of PBS (pH 7.4), 10 μL of microsomes (20 mg/mL) with or without 50 μL of 10 mM NADPH. The reaction was initiated by the addition of 50 μL of 1 mM solution of NCL in PBS (pH 7.4) to the reaction mixture. At 20, 40 and 60 min 100 μL aliquots were taken and quenched with 150 μL of ice-cold methanol. The samples were subjected to brief vortex mixing and centrifugation for 10 min at 14000 rpm. The clear supernatants were analyzed by HPLC. The microsomal activity was monitored using testosterone as a positive control.

**Kinetics of NCL reaction with NTR by fluorescence (Figure S2.2).** Fluorescence was measured using a Tecan Infinite M1000 (Tecan Austria GmbH) plate reader. Kinetic measurements of NCL (5–50 μM) uncaging by NTR (0.25 μg mL<sup>-1</sup>) were performed in the presence of NADH (500 μM) at 37°C in PBS buffer (pH 7.4). The kinetics rate of luciferin release from NCL was measured by fluorescence at 330 nm excitation and 530 nm emission wavelengths. The fluorescence

calibration curve for luciferin was used to calculate the rate (Figure S2.2). Kinetic parameters  $K_m$  and  $V_{max}$  were determined from Michaelis-Menten model and Lineweaver-Burk plot was used to display the data. The  $k_{cat}$  value was calculated by dividing the  $V_{max}$  value, obtained from the data acquired for the determination of the corresponding  $K_m$  values for the probe, by the concentration of the nitroreductase in the assay.

**Inhibition assay of NTR by dicoumarol in enzyme assay (Figure 2.3A).** NCL (20  $\mu$ M) uncaging by NTR (0.5  $\mu$ g mL<sup>-1</sup>) in the presence of NADH (100  $\mu$ M) was inhibited by various concentrations of dicoumarol (0 to 200  $\mu$ M). Luciferin release from NCL was measured by fluorescence at 330 nm excitation and 530 nm emission wavelengths over time. Inhibitory activity of dicoumarol is expressed as a percentage compared to uninhibited control (Figure S2.3).

**Bioluminescent imaging of NTR with NCL in enzyme assay (Figure 2.3B).** *In vitro* imaging studies were performed in clear bottom black 96 well plates from Becton Dickinson and Company. An IVIS Spectrum (PerkinElmer) was used to measure the amount of bioluminescent imaging (BLI) signal production. The data are presented as pseudocolor images indicating light intensity (red being the most intense and blue the least intense), which are superimposed over the grayscale reference photographs. Bioluminescence was quantified using region of interest (ROI) analysis of individual wells and the average signal expressed as the total number of photons emitted per second per cm<sup>2</sup> per steradian (p/sec/cm<sup>2</sup>/sr) from each of the three wells was calculated by using the Living Image software. Total luminescence was calculated by integrating the area under corresponding kinetic curves. Luciferase buffer was prepared as following: 2 mM ATP, 5 mM MgSO<sub>4</sub> in PBS (pH 7.4). Stock solutions of luciferase in luciferase buffer, NADH, NCL, luciferin and NTR in PBS (pH 7.4), were freshly prepared and aliquoted in a 96-well plate to give the following final concentrations in the total volume of 100  $\mu$ L/well: luciferase (60  $\mu$ g mL<sup>-1</sup>), NADH (100  $\mu$ M), NTR (10  $\mu$ g mL<sup>-1</sup>), luciferin or NCL (0.25–5  $\mu$ M); luciferin and NCL were added at the last step with a multichannel pipette from the additional 96-well plate. Bioluminescence signal from the plate was acquired immediately every 1 min with 0.5 s integration time for 30 min.

**Bacterial strains, plasmids and culture conditions.** *E. coli* K-12 MG1655 (- luc gene) and *E. coli* K-12 AB1157, containing the luciferase expressing pUC57 Click beetle red (CBR) plasmid (+ luc gene) was a kind gift from Daniel Ansaldi (Perkin Elmer). The NTR triple mutant, *E. coli* K-12 AB502Nema, was a kind gift from Dr. Antonio Valle (University of Cádiz, Cádiz, Spain) and was transformed with the pUC57 CBR plasmid for production of luciferase. *E. coli* MG1655 lux, expressing lux luciferase, was generated as previously described [62]. All strains were grown aerobically at 37°C in Luria Bertani (LB) medium supplemented with 100  $\mu$ g mL<sup>-1</sup> ampicillin (Amp).

**Bioluminescent imaging of NTR activity by NCL in *E. coli* (Figure 2.4C, D).** An IVIS-100 (PerkinElmer) was used to measure the amount of BLI signal production. Stock solutions of luciferin and NCL in PBS (pH 7.4) were freshly prepared and aliquoted in a 96-well plate to give the final concentrations (1–250  $\mu$ M) in the total volume of 200  $\mu$ L/well. The volume of bacterial suspension was 150  $\mu$ L/well. Bioluminescence signal from the plate was acquired immediately every 2 min with 10 s integration time for 1 h.

**Bacterial viability assay.** *E. coli* K-12 AB1157 CBR and *E. coli* K-12 AB502Nema CBR were cultured aerobically overnight. Bacteria were then subcultured and divided into two groups (untreated and probe treated) in triplicate in fresh media and grown until cultures reached OD<sub>600</sub> of 0.2. At this point, NCL probe treated group was treated with 100  $\mu$ M



probe. At hourly time points, aliquots from all cultures were subjected to serial dilution before plating on Amp selective agar to determine cfu/mL values. Cultures were also tested for changes in luminescence over time to identify if any differences existed between bacteria grown alone and bacteria grown in the presence of the probe.

#### Cell lines and cell culture.

Cell lines MDA-MB-231-NTR-Fluc-EGFP (NTR+luc+) (Figure 2.6) and HEK293T-NTR+ (Figure 2.7) were kindly provided by Dr. R. Paulmurugan (Stanford University School of Medicine, Stanford, USA) [139]. The cells were generated as described below with a reference to Sekar et al. [139]. The cloning vectors, expressing bacterial nitroreductase gene (NTR2) and Fluc-EGFP fusion constructs, were from the plasmid bank (Cellular Pathway Imaging Laboratory, Stanford). To make MDA-MB-231 stable cell line, modified pcDNA3.1 (PURO) vector expressing NTR was transfected using Lipofectamine 2000 Transfection Reagent (Invitrogen). 24 hours later medium was changed and the cells were treated with 100 ng mL<sup>-1</sup> of puromycin. The process was continued until no further cell death was observed. The cells were plated in low dilution (1 cell/100  $\mu$ L) in a 96 well plate. Single colonies of cells expressing NTR were expanded for further transduction with lentivirus expressing Fluc-EGFP fusion protein. To control the level of Fluc-EGFP at near equal expression, cells were sorted by FACS in a similar window after transduction. MDA-MB-231 stable cells were maintained in puromycin stress throughout the study. Single colonies of stable cells were evaluated for the functionality of NTR enzyme by incubating with a CytoCy5S (red-shifted NTR substrate; GE Healthcare) for the detection of fluorescent signal ( $\lambda_{exc/em}$  = 628 nm/ 638 nm).

Cell line MDA-MB-231-luc-D3H2LN Bioware (NTR-luc+), used as NTR negative control for *in vitro* and *in vivo* experiments (Figure 2.6), was purchased from PerkinElmer, cell lines HEK293, A549 (Figures 2:7, 2:8) were kindly provided by Dr. E. Allen (EPFL, Lausanne, Switzerland) and were maintained in Dulbecco's Modified Eagle's Medium supplemented with 10% (v/v) heat-inactivated FBS, 1% (v/v) penicillin/streptomycin (all reagents purchased from Life Technologies).

Cell lines used for *in vitro* experiments (Figure S2.10) were generated as described in the work of McCormack et al. [138] The triple negative mammary carcinoma MDA-MB-231<sup>wt</sup> and MDA-MB-231<sup>GFP+Luc+</sup> were kindly provided by Prof. J. Lorens (University of Bergen, Norway). The MDA-MB-231<sup>GFP+Luc+</sup> cells were transfected with the retroviral expression vector L149 pTra Puro2AGFP2ALuciferase2NTR (Entrez: EU753858) containing genes expressing *E. coli* enzyme Nitroreductase (NTR) and green fluorescence protein (GFP), and was named MDA-MB-231<sup>GFP+Luc+NTR+</sup>.<sup>4</sup> The MDA-MB-231 cell lines were maintained in Dulbecco's Modified Eagle's Medium. The media were supplemented with 10% heat-inactivated FBS (HyClone, Thermo Scientific), 1% penicillin/streptomycin (PS; Sigma-Aldrich) and 1% L-glutamin (Sigma-Aldrich). The cells were incubated in a humidified atmosphere at 37°C in 5% CO<sub>2</sub>. Authentication of all cell lines was done by DNA fingerprinting using the AmpFISTR Profiler Plus PCR Amplification kit (Applied Biosystems) in April 2013.

**BLI of NTR by NCL in stable cell lines** (Figure 2.6) MDA-MB-231-NTR-Fluc-EGFP cells and control MDA-MB-231-luc cells were plated at a density  $3 \times 10^4$  cells/well in two black 96-well plates with clear bottom, after 48 h the growth medium was removed, and 100  $\mu$ L of NCL probe or luciferin solutions (1–100  $\mu$ M) in cell culture medium was added to the



wells. The plates were immediately placed in IVIS Spectrum and were imaged every 1 min for 1 h. Observed BLI signal was quantified using ROI analysis with Living Image software.

**BLI of NTR by NCL in stable cell lines (Figure S2.10).** MDA-MB-231<sup>wt</sup> and MDA-MB-231<sup>GFP+Luc+</sup> cells were seeded in a 96 well plate in triplicates with descending concentrations of compounds in 100  $\mu$ L of media (NCL probe, luciferin, cells only and media only). The cells were set in the incubator for two hours after seeding before imaging. Descending concentrations of NCL probe or luciferin (10  $\mu$ L) were added to each well with a multichannel Finnpiptette F2 (Thermo Labsystems, Milford, MA, USA). Bioluminescence images were acquired using KODAK In Vivo Multispectral Imaging System FX (Carestream Healt, NY, US) every two minutes for 1 h without filters. The images were acquired over 90 s with 30 s of rest between each acquisition. Images were analyzed using Carestream Molecular Imaging Software (version 5.0.6.20).

**BLI of NTR by NCL in cells not expressing FLuc (Figure 2.7).** HEK293T-NTR+ and HEK293T (wild type) cells were plated at the concentration  $6 \times 10^4$  cells/well in two corresponding 96 well plates. After 24 h the media from cells was removed, 100  $\mu$ L of NCL or luciferin solutions in media was added to cells, after 1 h of incubation at 37 °C the cells were lysed by three freeze-thaw cycles (each cycle included 10 min incubation of the well plate on dry ice followed by 10 min at 37 °C). Then 10  $\mu$ L of Fluc solution (100  $\mu$ g/ml, 10 mM ATP, 25 mM MgSO<sub>4</sub> in PBS) was added to each well with 100  $\mu$ L of lysate and the BL was acquired using IVIS Spectrum for 1 h.

**Pimonidazole binding assay (Figure 2.8A).** *In vitro* imaging of hypoxia with Hypoxyprobe™ Green Kit from Hypoxyprobe Inc., USA (Pimonidazole and anti-pimonidazole IgG1 mouse monoclonal antibody conjugated to FITC) was performed as described in [164]. A549 cells were seeded in 8 well chamber slide (Lab-Tek Chamber Glass) at a density of  $1 \times 10^4$  cells/well in 200  $\mu$ L of medium/well and left for 24 h in normoxia (standard incubator) or hypoxia (incubator with 1% O<sub>2</sub>). After 24 h medium was removed, 200  $\mu$ M of Pimonidazole solution in medium was added, cells were put for 1 h in normoxia or hypoxia. Then the cells were washed 2 times with PBS and fixed with 70% ethanol 10 min, permeabilized with PBS containing 0.1% Triton-X and 4% FBS for 10 min, washed 3 times with PBS. FITC-mAb was added to the cells (1/200 dilution) and incubated for 4 h at RT, washed 3 times with PBS. Then cells were incubated with Hoechst dye (1:5000 dilution) for 10 min, washed 2 times with PBS. Cells were left in PBS overnight at 4 °C. The slides were coverslip with Prolong® Gold Antifade Reagent. Fluorescence imaging was performed using Zeiss LSM700 confocal microscope, fluorescence intensity was quantified using ImageJ software.

**BLI of NCL in cells not expressing FLuc under hypoxia or normoxia (Figure 2.8B).** A549 cells were plated at the concentration  $1 \times 10^4$  cells/well in a 96 well plate. After 1 week of culture in normoxia (standard incubator) or hypoxia (incubator with 1% O<sub>2</sub>) the media from cells was removed, 100  $\mu$ L of NCL or luciferin solutions in media was added to cells, after 1 h of incubation at 37 °C the cells were lysed by three freeze-thaw cycles (each cycle included 10 min incubation of the well plate on dry ice followed by 10 min at 37 °C). Then 10  $\mu$ L of Fluc solution (100  $\mu$ g/ml, 10 mM ATP, 25 mM MgSO<sub>4</sub> in PBS) was added to each well with 100  $\mu$ L of lysate and the BL was acquired using IVIS Spectrum for 30 min.

**Cell viability assay (Figure S2.9).** MDA-MB-231 (NTR-luc+) cells were plated at a density  $1 \times 10^4$  cells/well in a 96 well plate, the next day cells were treated with different concentrations of NCL probe (5–150  $\mu$ M solutions in cell culture medium) for 1 h, control group was incubated with medium only. CytoTox-Glo™ reagent was prepared as indicated and 80  $\mu$ L of solution was added to each well. After 20 min luminescence was measured using a plate reader Tecan Infinite M1000 (Tecan Austria GmbH) with integration time 0.5 s.

**Ethics statement.** All animal procedures on imaging of bacterial NTR in a mouse model of thigh infection were performed in accordance with the national ethical guidelines prescribed by the Health Products Regulatory Authority (HPRA). Protocols were approved by the animal ethics committee of University College Cork (AERR #2010/003 and #2012/015). Experiments on imaging of NTR in a mouse model of subcutaneous cancer were carried out in strict accordance to the Swiss regulation on animal experimentation and the protocol (VD 2363) was approved by the authority of the Canton Vaud, Switzerland (EXPANIM (Expérience sur animaux)–SCAV, Département de la sécurité et de l'environnement, Service de la consommation et des affaires vétérinaires). All efforts were made to minimize suffering.

**Bacterial administration and imaging of bacterial nitroreductase in mice (Figure 2.5).** Bacteria were grown at 37°C in a shaking incubator until reaching OD<sub>600</sub> of 0.6 in LB medium, containing 100  $\mu$ g mL<sup>-1</sup> Amp. Cultures were harvested by centrifugation (4000  $\times$  g for 10 min) and washed three times in PBS. After washing, bacteria were resuspended in one tenth volume of PBS. Mice were kept at a constant room temperature (22°C) with a natural day/night light cycle in a conventional animal colony. Standard laboratory food and water were provided ad libitum. Mice were afforded an adaptation period of at least 7 days before the beginning of experiments. Female BALB/c mice (Harlan, Oxfordshire, UK) in good condition, without infections, weighing 18–22 g and 6–8 weeks old, were kept as previously described [45] and were included in experiments. BALB/c mice were anaesthetized and the fur on the rear legs was removed. Mice were injected directly into the right quadriceps muscle at a depth of approximately 5 mm with 50  $\mu$ L of bacteria suspended in PBS. The concentration of bacterial suspensions used for injection ranged from  $10^6$  to  $10^9$  bacteria/mL. Mice also received an intramuscular injection of 50  $\mu$ L sterile PBS in the left rear quadriceps (control) and lux MG1655 *E. coli* (positive control). 1 h post bacterial injection, mice received an IP injection of 200  $\mu$ L of 10 mM NCL probe (0.8 mg) or 200  $\mu$ L of 10 mM D-luciferin potassium salt (0.63 mg) in PBS. For *in vivo* experiments involving varying concentrations of the probe, the concentration of NCL probe injected was 200  $\mu$ L of 1, 10 or 20 mM solutions in PBS (0.08, 0.8 or 1.6 mg of NCL probe). Mice were imaged for bioluminescence at regular intervals beginning immediately after probe injection using IVIS 100. Mice that were infected with bacteria for experimental purposes were monitored for signs of illness for the duration of the experiment. No adverse symptoms were reported. Following bioluminescence imaging, or at experiment end, animals were euthanized by cervical dislocation.

**Mice and tumor induction (Figure 2.6).** Swiss nu/nu mice were obtained from Charles River Labs. Mice were maintained at the EPFL UDP animal facility under pathogen free conditions and group housed in individually ventilated cages at 22°C with 12/12 light cycle. Before experiments the mice were afforded an adaptation period of at least 7 days. Female mice in good condition, weighing 18–25 g and 6 weeks of age were randomly divided in two experimental groups (n = 5 per group). For tumor induction,  $1 \times 10^6$  cells in 100  $\mu$ L of FBS-free medium/Matrigel (BD Biosci-

ences) (50:50) was injected subcutaneously into the flank of the mice. One group was injected with MDA-MB-231-NTR-Fluc-EGFP cells and the other group- with MDA-MB-231-luc cell (control). The viability of cells used for inoculation was more than 95% as determined by Trypan Blue Dye Exclusion (Gibco). Following tumor establishment, the health parameters that may lead to the endpoints were carefully monitored in xenograft mice three times a week: cachexia (acute weight loss), lack of activity and loss of appetite. Weight was measured and general behavior as well as body conditions was assessed. Tumor size was carefully monitored to ensure that it doesn't exceed maximal allowed size of 1 cm<sup>3</sup>. Tumor volume was measured by caliper and calculated according to the formula  $1/2(\text{length} \times \text{width}^2)$ . When tumors reached approximately 0.1 cm<sup>3</sup> in volume, the mice were imaged with luciferin (1.5 mg/mouse in 50 µL of PBS IP) for 1 h once a week to estimate the light emission and the optimal imaging window. Bioluminescence was acquired using IVIS Spectrum, every 1 min for 1 h with the auto-exposure mode. Following bioluminescence imaging at experiment end animals were euthanized by CO<sub>2</sub> inhalation or cervical dislocation.

**Imaging of nitroreductase in a mouse model of subcutaneous cancer (Figure 2.6).** Potassium salt of D-luciferin (Intrace Medical) was dissolved in PBS (pH 7.2), solution was filter sterilized through 0.22 µm filter, aliquoted and kept at -20°C. NCL probe was dissolved in PEG400 (Sigma-Aldrich) and diluted with sterile PBS (pH 7.2) 1:5 (20% (v/v) of PEG400 in the total volume of 200 µL), fresh solution was prepared before every imaging. The dose of NCL probe (1.9 mg/mouse) was equivalent (4.7 µmol) to the dose of luciferin (1.5 mg/mouse). Mice were anesthetized prior to injection and during imaging via inhalation of isoflurane (Piramal Critical Care, Inc). When the total photon flux over 1 h from the mice imaged with luciferin reached  $1 \times 10^8$ , the mice entered the experiment. On day 1 of the experiment all mice were injected IP with luciferin (1.5 mg/mouse in 50 µL of PBS) and bioluminescence was acquired immediately every 1 min for 1 h with the auto-exposure mode. On day 2 of the experiment (24 h after the luciferin imaging) all mice were injected IP with NCL probe (1.9 mg/mouse in 200 µL of PBS containing 20% (v/v) PEG400) and bioluminescence was acquired immediately every 1 min for 1 h with the auto-exposure mode.

**Data analysis from a cancer model experiment.** Bioluminescence was quantified using ROI analysis of the tumor area individually for each mouse. Total luminescence was calculated by integrating the area under corresponding kinetic curves. Percent of the NCL probe uncaging was calculated individually for each mouse using the formula: % of uncaging = (Total photon flux over 1 h from NCL/ Total photon flux over 1 h from luciferin) × 100%. Two-tailed Student's t-test was used to determine statistical significance (GraphPad Prism 6.03, GraphPad Software).

## 2.6 Supplementary figures

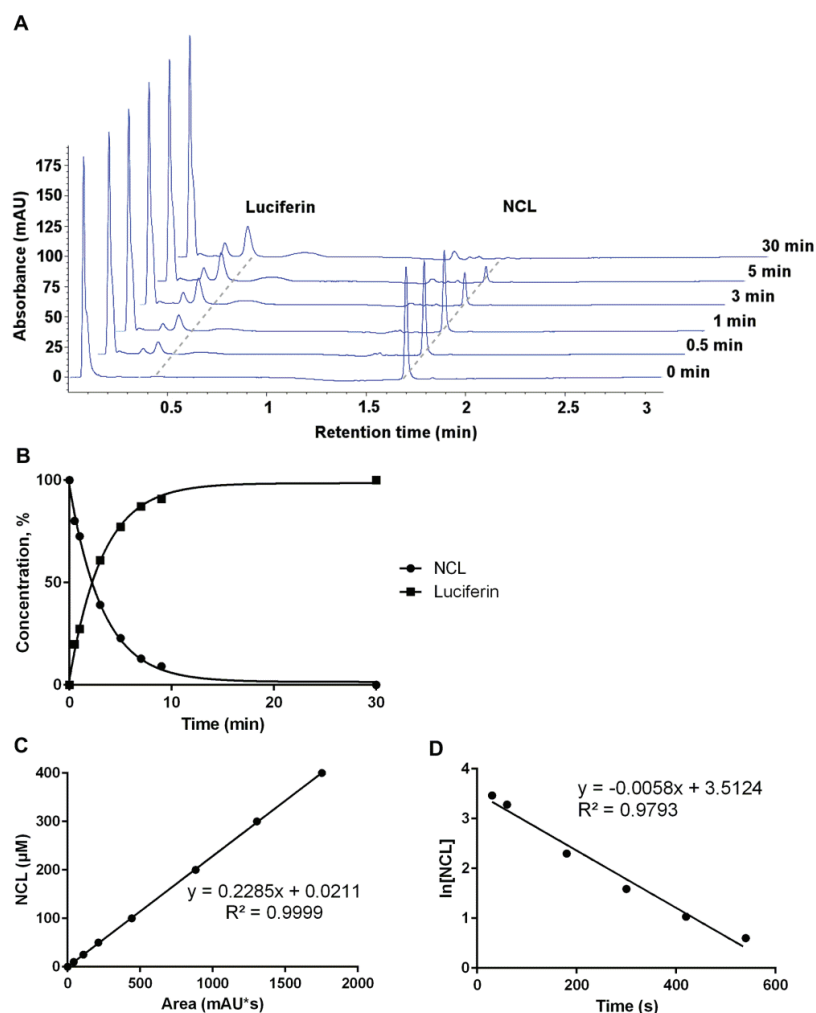


Figure S2.1 Analysis of NCL reduction by *E. coli* nitroreductase *in vitro*. (A). UV HPLC profiles (detected at 320 nm) of NCL reduction by NTR over 30 min, peak at 0.4 min corresponds to luciferin ( $m/z$  281), peak at 1.7 min corresponds to NCL ( $m/z$  406). (B). Time course of the conversion of NCL to luciferin, the distribution of reaction products was quantified by HPLC analysis on the basis of absorbance at 320 nm. (C). Absorbance calibration curve for NCL. (D). Pseudo-first-order kinetics of NCL reduction, rate constant  $5.8 \cdot 10^{-3} \text{ s}^{-1}$ ,  $t_{1/2}$ : 119.5 s.

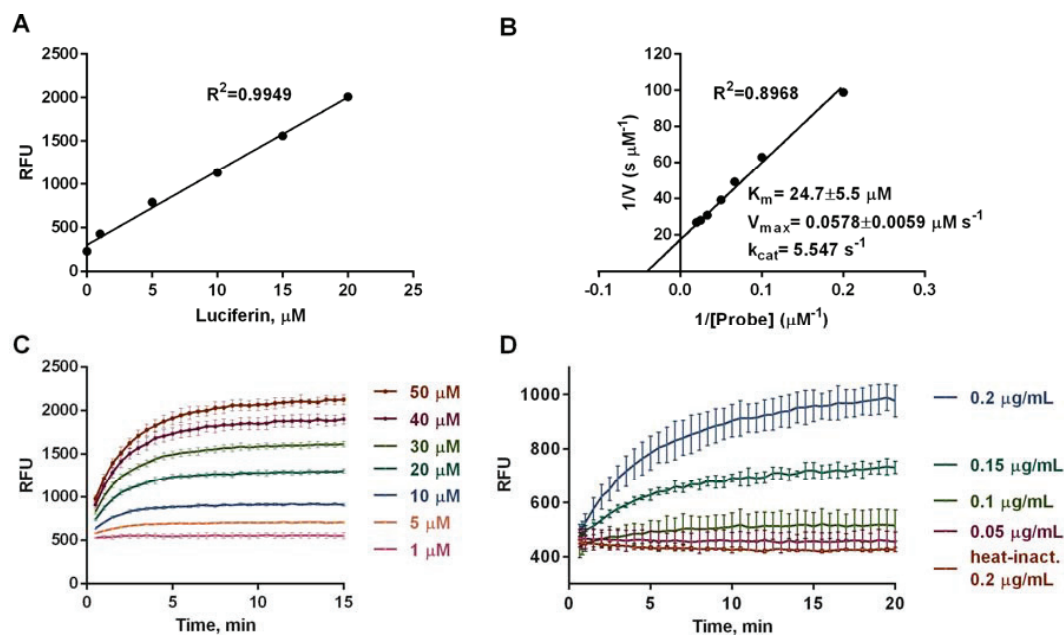


Figure S2.2 Kinetic measurements of NCL reduction by NTR *in vitro*. (A). Calibration curve for luciferin fluorescence at  $\lambda_{\text{exc/em}} = 330/530 \text{ nm}$ . (B). Lineweaver-Burk plot of NCL probe reduction (5–50  $\mu\text{M}$ ) by NTR from *E. coli* NfsA (0.25  $\mu\text{g/mL}$ ) in the presence of NADH (500  $\mu\text{M}$ ) at 37°C in PBS buffer (pH 7.4). Kinetic parameters  $K_m$  and  $V_{\max}$  were determined from Michaelis-Menten model. (C). A plot of fluorescence intensity at  $\lambda_{\text{exc/em}} = 330/530 \text{ nm}$  of different amounts of NCL (1–50  $\mu\text{M}$ ) over an incubation time of 15 min with 1  $\mu\text{g/mL}$  of NTR from *E. coli* NfsA and 500  $\mu\text{M}$  of NADH at 37°C in PBS buffer (pH 7.4). (D). A plot of fluorescence intensity at  $\lambda_{\text{exc/em}} = 330/530 \text{ nm}$  of 20  $\mu\text{M}$  of NCL, 500  $\mu\text{M}$  of NADH and different amounts of NTR from *E. coli* NfsA (0.05–0.2  $\mu\text{g/mL}$ ) over an incubation time of 20 min at 37°C in PBS buffer (pH 7.4).

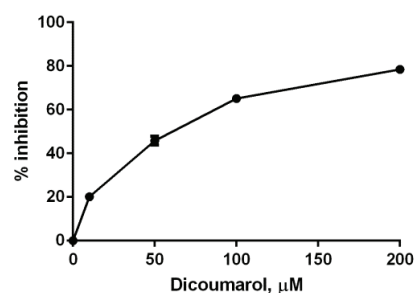


Figure S2.3 Inhibition of NTR activity by dicoumarol *in vitro*. NCL (20  $\mu\text{M}$ ) reduction by NTR (0.5  $\mu\text{g/mL}$ ) in the presence of NADH (100  $\mu\text{M}$ ) was inhibited by dicoumarol (0 to 200  $\mu\text{M}$ ) (Figure 2.2A). Inhibitory activity of dicoumarol is expressed as a percentage compared to uninhibited control.

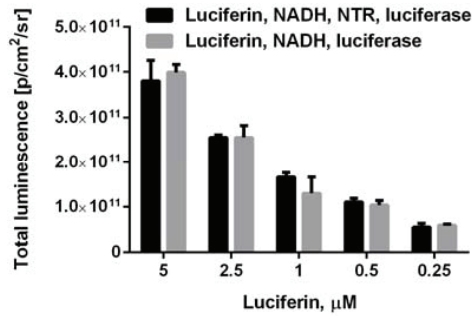


Figure S2.4 Bioluminescent imaging of nitroreductase with NCL in enzyme assay. Light emission from luciferin in the presence and absence of NTR, NTR did not have any effect on the luciferin-luciferase reaction. Total luminescent signal integrated over 30 min from luciferin (0.25–5 μM) with NADH (100 μM), luciferase (60 μg/mL) and NTR (10 μg/mL) compared to the control (without NTR).

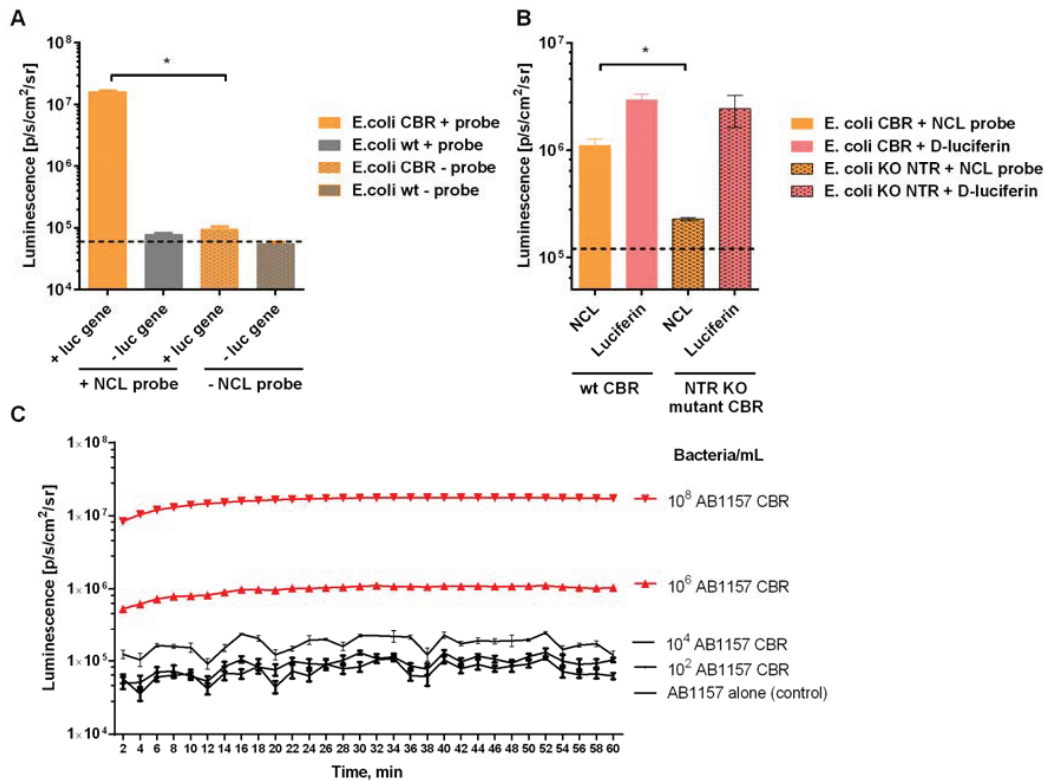


Figure S2.5 Bioluminescence imaging of NTR by NCL in various *E. coli* strains. (A). Bioluminescence from 100 μM NCL probe incubated with the wild type AB1157 and luciferase expressing AB1157 CBR *E. coli* strains (10⁷ bacteria/mL) for 2 h at 37 °C before imaging. The dotted line indicates background, calculated as the average signal from wells containing bacteria only. (B). Bioluminescence from NCL probe and luciferin (10 μM) incubated with luciferase expressing *E. coli* AB1157 CBR (parent strain) and AB502Nema CBR NTR KO (mutant strain) (10⁸ bacteria/mL) for 10 min before imaging. A significant difference in signal from the probe is observed between parent and NTR mutant strains ( $p = 0.0062$ ) while the luciferin signal is the same. (C). Signal kinetics over 1 h from 100 μM NCL and indicated concentrations of bacteria/mL AB1157 CBR.

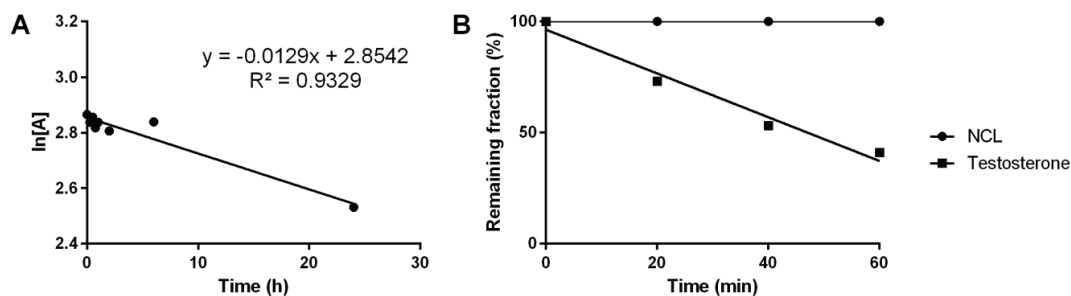


Figure S2.6 Stability profiling. (A) NCL *in vitro* stability in mouse plasma,  $t_{1/2} = 53.7$  h. (B) NCL stability in mouse liver microsomes *in vitro*. Testosterone was used as a positive control.

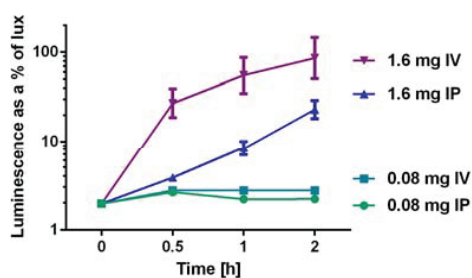


Figure S2.7 *In vivo* comparison of NCL kinetics after IP and IV administration in a mouse model of thigh infection (Luciferase and nitroreductase expressing *E. coli*). Luminescence over 2 h from infected mice that received NCL as a percentage of luminescence from mice that were injected with *E. coli* lux (positive control for bacterial number)<sup>5</sup>. Mice were infected with  $5 \times 10^7$  *E. coli*, NCL was administered by IV or IP injection,  $n = 2-4$  per group. Statistical analysis was performed using a two way ANOVA with Bonferroni post-test showing no significant difference between IV and IP administration of NCL at 0.8 mg. The error bars were calculated using the following equation: (Luminescence SEM/Average lux)  $\times 100$ .

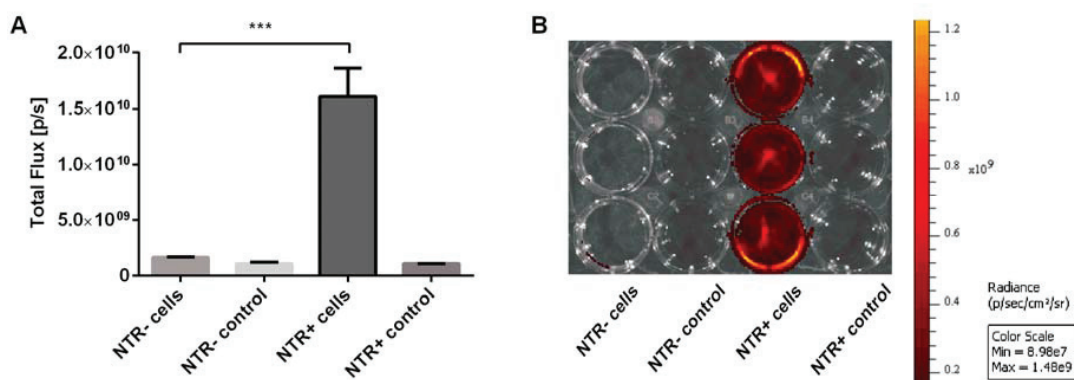


Figure S2.8 Fluorescence imaging of NTR with CytoCy5S probe in MDA-MB-231-NTR-Fluc-EGFP and MDA-MB-231-luc cells. (A). The cells were incubated with 400 ng/mL of CytoCy5S in HBSS or HBSS only (control) for 1.5 h, washed with HBSS once and imaged for fluorescence (excitation 640 nm, emission 700 nm) in IVIS Spectrum. Error bars are  $\pm$ SD of



three wells, \*\*\*P = 0.0006. (B). Image overlay of a photographic image and epi-fluorescence from the well plate used in the assay.

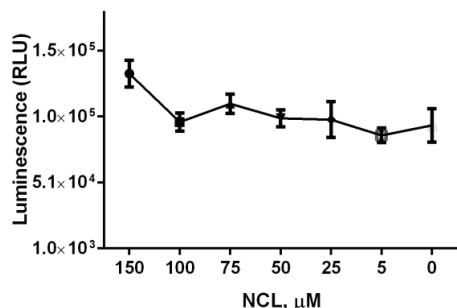


Figure S2.9 The CytoTox-Glo Cytotoxicity Assay (Promega). MDA-MB-231-luc cells were treated with various concentrations of NCL for 1 h and the level of ATP was measured using CytoTox-Glo reagent.

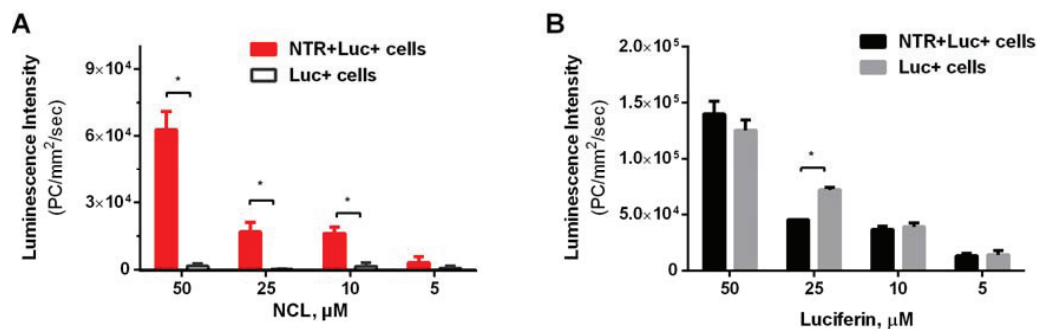


Figure S2.10 Imaging of NTR with NCL in stably transfected cancer cells MDA-MB-231<sup>GFP+Luc+NTR+</sup> compared to the control cells (MDA-MB-231<sup>GFP+Luc+</sup>). (A). Bioluminescence from NCL (50–5  $\mu\text{M}$ ) 15 min after addition to the cells. (B). Luciferin signal (50–5  $\mu\text{M}$ ) 15 min after addition to the cells confirmed equal levels of luciferase in both cell lines. Imaging was performed for 1 h, a single image presented here is at 15 min time point.

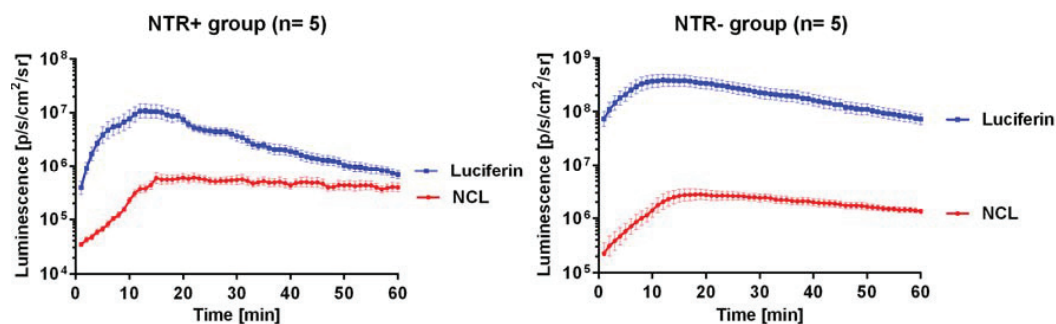


Figure S2.11 Imaging of NTR in a subcutaneous xenograft model of cancer. Signal kinetics over 1 hour from luciferin and NCL in NTR+ and NTR- groups (n = 5).



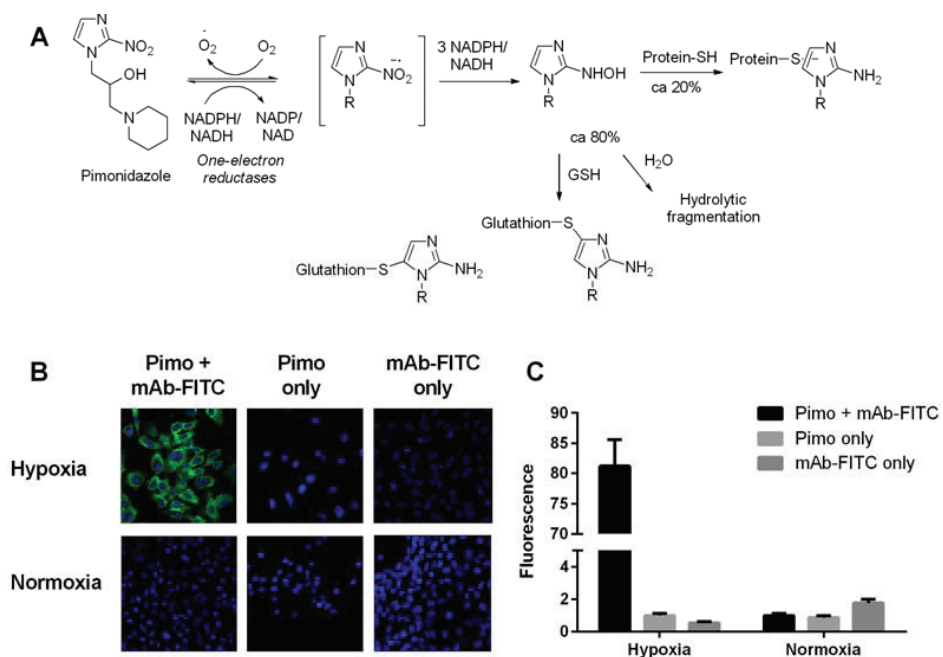


Figure S2.12 Pimonidazole binding assay for immunohistochemical imaging of hypoxia. (A) Proposed mechanism for the activation and binding of pimonidazole to hypoxic cells (adapted from [165]). (B) Immunohistochemical staining of pimonidazole binding in A549 cells in hypoxic and normoxic conditions, green- FITC, blue- nucleus (Hoechst). Fluorescence intensity was quantified using ImageJ software.



# Chapter 3 Development of bioluminescent probes for hydrogen sulfide (H<sub>2</sub>S) imaging

## 3.1 H<sub>2</sub>S as a third gasotransmitter

### 3.1.1 Physico-chemical properties

H<sub>2</sub>S, a colorless gas with the odor of rotten eggs, is an important component of the biogeochemical sulfur cycle. Sulfur exists in several oxidation states ranging from -2 in H<sub>2</sub>S to +6 in sulfates (Figure 3.1) and H<sub>2</sub>S/HS<sup>-</sup> can be readily oxidized to other biologically relevant reactive sulfur species. H<sub>2</sub>S is a weak acid with a first pK<sub>a1</sub> of 7.0, and a second pK<sub>a2</sub> of 19 [166] (Figure 3.2). Under physiological conditions hydrogen sulfide mainly exists as HS<sup>-</sup> (about 80%), as neutral H<sub>2</sub>S- about 20%, and less than 0.1% as S<sup>2-</sup> [167]; therefore, the term "H<sub>2</sub>S" will be used to refer to the sum of these species.

| Sulfur Oxidation States |                  |            |  |   |  |   |
|-------------------------|------------------|------------|--|---|--|---|
|                         | -2               | -1         | 0  | +2  | +4   | +6  |
| <b>Inorganic</b>        | H <sub>2</sub> S |            | S (S <sup>0</sup> /S <sub>8</sub> )<br>elemental                                   | SO  | SO <sub>2</sub> , SO <sub>3</sub> <sup>2-</sup>  | SO <sub>3</sub> , SO <sub>4</sub> <sup>2-</sup>   |
| <b>Organic</b>          | R-S-H            | R-S-S-R    | $\begin{array}{c} \text{O} \\ \parallel \\ \text{R}-\text{S}-\text{R} \end{array}$ | $\begin{array}{c} \text{O} \\ \parallel \\ \text{R}-\text{S}-\text{R} \\ \parallel \\ \text{O} \end{array}$ | $\begin{array}{c} \text{O} \\ \parallel \\ \text{R}-\text{S}-\text{OH} \\ \parallel \\ \text{O} \end{array}$ | $\begin{array}{c} \text{O} \\ \parallel \\ \text{R}-\text{O}-\text{S}-\text{O}-\text{R} \\ \parallel \\ \text{O} \end{array}$ |
|                         | thiols           | disulfides | sulfoxide  | sulfones  | sulfonic acids   | sulfate ester   |
|                         | R-S-R            |            | R-S-OH   | $\begin{array}{c} \text{O} \\ \parallel \\ \text{R}-\text{S}-\text{OH} \end{array}$                         | $\begin{array}{c} \text{O} \\ \parallel \\ \text{R}-\text{O}-\text{S}-\text{O}-\text{R} \end{array}$         |   |
|                         | sulfides         |            | sulfenic acids   | sulfinic acids  | sulfite ester  |   |

Figure 3.1 Oxidation states of sulfur in inorganic and organic compounds.

H<sub>2</sub>S has been recently recognized as a gasotransmitter in addition to the well-known nitric oxide (NO) and carbon monoxide (CO) [168]. A gasotransmitter is a gaseous signaling molecule that is endogenously produced and degraded in a regulated manner and that induces physiological changes in a cell. The H<sub>2</sub>S molecule can penetrate the lipid bi-layer of cell membranes, however, it is less cell permeable than NO and CO (dipole moments of H<sub>2</sub>S being 0.97, NO 0.16, and CO 0.13) [167]. HS<sup>-</sup> is a good nucleophile that can react with different electrophilic cellular targets via sulphydration, e.g. with cysteines on proteins to form S-sulphydrates. It has recently been shown about 10- 25% of liver proteins are sulphydrated under physiological conditions and that S-sulphydration appears to be a posttranslational modification for proteins [169]. H<sub>2</sub>S has a high affinity for metalloproteins, demonstrated by its potent inhibition of heme-

containing cytochrome *c* oxidase ( $K_i = 0.2 \mu\text{M}$ ) [170]. At low concentrations, H<sub>2</sub>S stimulates oxygen consumption by the mitochondrial respiratory chain, but at concentration higher than 20  $\mu\text{M}$  the respiratory chain is inhibited [171]. Additionally, H<sub>2</sub>S/HS<sup>-</sup> can act as a reductant and be oxidized to other reactive sulfur species forming sulfane sulfur clusters (pools) which provides a way of sulfide storage and transport in cells and tissues (Figure 3.3).

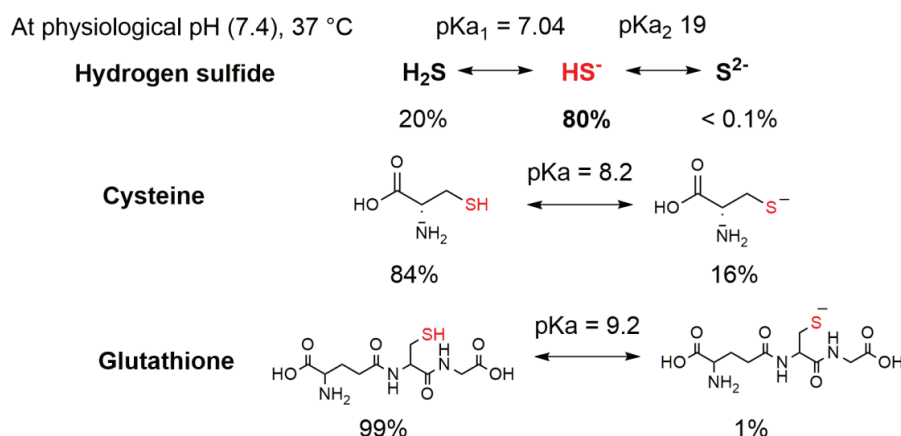


Figure 3.2 Hydrogen sulfide states and their occurrence under physiological conditions in comparison to other biologically relevant thiols, cysteine and glutathione.

### 3.1.2 Host-derived H<sub>2</sub>S

Signaling molecules such as neurotransmitters and hormones are usually stored in vesicles and the concentrations are controlled such that only a small amount is released at a time. However, gasotransmitters cannot be stored in this manner and are synthesized on demand [172]. As H<sub>2</sub>S can be toxic at certain concentrations, its free level in the tissues is tightly regulated [173]. It was shown that most tissues maintain high turnover rates of sulfur through H<sub>2</sub>S to rapidly regulate its concentration [174, 175]. The half-life for H<sub>2</sub>S under aerobic conditions in liver, kidney, and brain homogenate was found to be 2.0, 2.8, and 10.0 min, respectively [174].

Generation of H<sub>2</sub>S in mammalian cells during enzymatic activity is mediated by three enzymes: cystathionine  $\gamma$ -lyase (CSE, EC 4.4.1.1), cystathionine- $\beta$ -synthase (CBS, EC 4.2.1.22), and 3-mercaptopyruvate sulfur transferase (3-MST, EC 2.8.1.2)/cysteine aminotransferase (CAT, EC 2.6.1.3) (Figure 3.4). The elimination of cysteine catalyzed by CSE is the major source of H<sub>2</sub>S, accounting for 70% of its production, whereas the elimination of homocysteine (HCy) accounts for approximately 29% of H<sub>2</sub>S generated by CSE [176]. The  $K_m$  of human CSE for H<sub>2</sub>S generation from Cys is 1.7 mM [176]. CSE is the dominant enzyme for the formation of H<sub>2</sub>S in liver, brain, colon, lungs, kidneys [177], and CSE-deficient mice show a marked depletion of H<sub>2</sub>S level in those tissues [178].

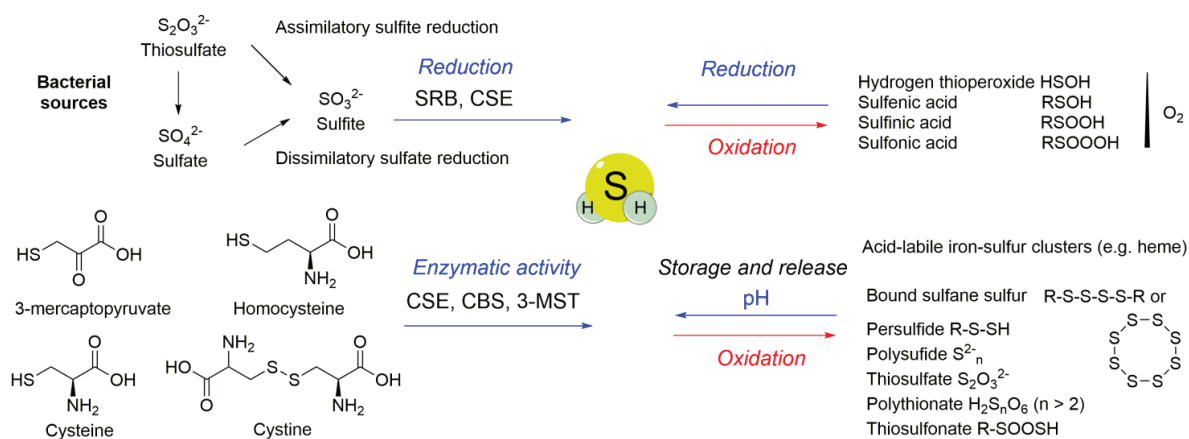


Figure 3.3 Selected biochemical pathways for the production (blue) and metabolism (red) of hydrogen sulfide in living systems (adapted from [179] and [180]).

CBS is expressed predominantly in the brain and uses Hcy and serine to generate cystathionine, which is converted by CSE to cysteine. As the  $K_m$  values of mammalian CBS for serine and Cys ( $\sim 1.9$  mM and  $\sim 6.5$  mM, respectively) are higher than intracellular concentrations, the extent to which serine will be used vs. Cys as a substrate for cystathionine synthesis will depend on the tissue concentrations of these substrates [177]. Cysteine serves as a substrate for both CSE and CBS and the catalyzed reactions yield H<sub>2</sub>S. A third H<sub>2</sub>S-generating pathway is mediated by MST. The sulfur of 3-mercaptopyruvate reacts with a Cys residue in the active site of MST (MST-SH) to produce a persulfide (MST-SSH), which then releases H<sub>2</sub>S in the presence of a reductant (R-SH) [172]. In addition to H<sub>2</sub>S production CBS plays a role in maintaining Hcy levels in vivo. Patients with homocysteinaemia have impaired CBS activity, increased levels of Hcy and cardiovascular disability [181]. Mice lacking CBS also show homocysteinaemia as well as severe growth retardation and developmental defects, which lead to death by 4 weeks of age [182].

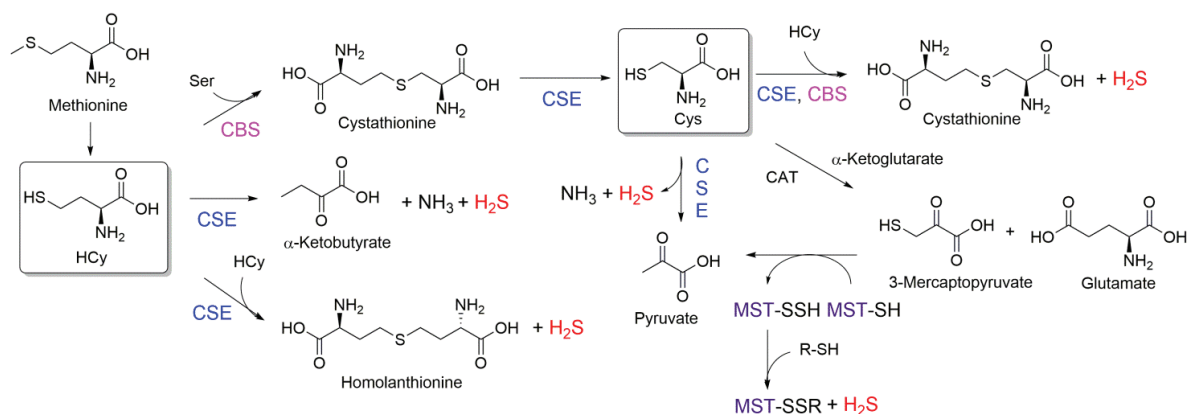


Figure 3.4 Enzymatic pathways of H<sub>2</sub>S production. H<sub>2</sub>S (red); CSE (blue): cystathionine  $\gamma$ -lyase; CBS (pink): cystathionine  $\beta$ -synthase; 3-MST (violet): 3-mercaptopyruvate sulfurtransferase; CAT: cysteine aminotransferase; Hcy: homocysteine. Adapted from [172].

Catabolism of H<sub>2</sub>S occurs primarily by oxidation in many tissues including colonic mucosa, liver, lungs, kidney, and brain. It was shown that the rate of thiosulfate production from H<sub>2</sub>S in rat colonic mucosa was eight times higher than

for non-colonic tissues [183]. This suggests that colon epithelium might have a protective function and prevent the entry of high level of locally produced H<sub>2</sub>S by intestinal bacteria into the systemic circulation [183]. At the cellular level mitochondrial detoxification of H<sub>2</sub>S is catalyzed by sulfur quinone reductase (EC 1.8.5.4), rhodanese (EC 2.8.1.2) and sulfur dioxygenase (EC 1.13.11.18), the latter converts H<sub>2</sub>S into sulfite and thiosulfate [184]. Sulfite oxidase (EC 1.8.3.1) produces sulfate as a final product, which is responsible for 77- 92% of the total urinary sulfur output [185]. The other methods for H<sub>2</sub>S excretion include expiration and methylation, although they are not as efficient as oxidation (methylation was shown to be ~10000 times slower than the oxidation of H<sub>2</sub>S in colonic mucosa [186]).

### 3.1.3 Bacterial-derived H<sub>2</sub>S

Bacterial production of H<sub>2</sub>S by the typhoid bacillus was recognized as early as in 1895 and was used as a test to differentiate paratyphoid and enteritidis groups [187]. Modern reports of production of H<sub>2</sub>S by bacteria exist for about 60 bacterial species with main substrates identified as cystine, cysteine, thiosulfate, sulfite and sulfate. Tests for H<sub>2</sub>S production are used to detect *Salmonella*, *Citrobacter*, *Proteus*, *Edwardsiella* and *Klebsiella* associated with fecal contamination in drinking and environmental water [188, 189].

The colonic bacteria of humans and animals produce a variety of flatus gases. It was found that H<sub>2</sub>, CO<sub>2</sub>, and CH<sub>4</sub> comprise more than a half of flatus while sulfur-containing gases, e.g. hydrogen sulfide, methanethiol, and dimethyl sulfide are generally present at low concentration (up to 15% of total amount) [190]. About 70% of H<sub>2</sub>S production in the colon is attributed to sulfate-reducing bacteria (SRB) of the genus *Desulfovibrio* in the class  $\delta$ -Proteobacteria [191]. SRB are the most efficient consumers of H<sub>2</sub> which is formed during fermentation and they use sulfate as an electron acceptor to maintain redox balance while maximizing their energy production [192]. It was shown that SRB isolated from patients with colitis produced higher level of H<sub>2</sub>S than SRB from healthy volunteers [193, 194]. The association of SRB (particularly, *Desulfovibrio piger*) with inflammation was reported [195, 196], however H<sub>2</sub>S was shown to exert both pro- and anti-inflammatory effects in the gut [197, 198].

H<sub>2</sub>S can also be produced from cysteine and methionine by bacteria expressing desulfhydrases which belong to the groups *Enterococci*, *Enterobacteria*, and *Clostridia*, including *E. coli* [199]. Reduction of sulfite by sulfite reductases (EC 1.8.99.1) in certain  $\gamma$ -Proteobacteria, such as *Salmonella*, *Enterobacteria*, *Klebsiella*, and in Firmicutes, including *Bacillus* and *Staphylococcus*, is another source of bacterial H<sub>2</sub>S produced in the colon.

The contribution of the microbiota to host H<sub>2</sub>S metabolism remains poorly understood. Wallace and colleagues estimated that approximately a half of the H<sub>2</sub>S detected in feces is derived from eukaryotic cells [200]. They did not find any differences in the H<sub>2</sub>S production *in vitro* from feces isolated from germ-free mice and mice colonized with altered Schaedler flora, which contain *Bacteroides* and *Fusobacterium* and could contribute to H<sub>2</sub>S production [200]. However, in a study by Shen et al. significant differences in total tissue H<sub>2</sub>S level (free, acid-labile, bound sulfane sulfur) and CSE activity were measured between germ-free and conventionally housed mice [201]. These results indicate that gut microbiota regulates H<sub>2</sub>S homeostasis not only locally, in the gut, but also systemically. The variations in results between two studies might be attributed to the method of detection; the methylene blue assay used by Wallace and colleagues is prone to experimental artefacts [202, 203] while the monobromobimane (MBB) HPLC-based assay used

by Shen et al. is very sensitive (sulfide limit of detection 2 nM [204]) and allows for the measurement of the concentrations of the various sulfide forms.

Interestingly, bacteria have been recently found to have similar enzymatic systems for H<sub>2</sub>S synthesis to those in mammals, including orthologues of the genes encoding CSE, CBS and MST [205]. Shatalin et al. showed that H<sub>2</sub>S in bacteria acts as a cytoprotectant from redox stress caused by antibiotics. Bacteria in which CSE, CBS and MST have been deleted showed increased sensitivity to the antibiotics. Therefore, inhibitors of bacterial H<sub>2</sub>S production may be used to potentiate the effectiveness of the antibiotic therapies [205].

### 3.1.4 Physiological effects of H<sub>2</sub>S in gastro-intestinal tract (GIT)

Hydrogen sulfide is involved in a variety of physiological processes, including vasodilation [206], neurotransmission [207] and nociception [208]. It is produced throughout the gastro-intestinal tract and it has been shown to regulate intestinal smooth muscle contraction [209, 210], epithelial secretion [211] and mucosal defense [212]. Due to its protective properties on gut mucosa it can prevent the formation of nonsteroidal anti-inflammatory drug (NSAID)-induced ulcers and promote healing [213, 214]. Naproxen, diclofenac and celecoxib coupled to an H<sub>2</sub>S-releasing moiety have been reported to cause less gastrointestinal and cardiovascular injury than parent NSAIDs in preclinical models [215, 216].

In addition to H<sub>2</sub>S synthesized in the gut tissues, the intestinal mucosa is constantly exposed to H<sub>2</sub>S generated by bacteria. Given the toxicity and the reported effects of this signaling molecule in the GIT, it has been recognized that H<sub>2</sub>S may affect many aspects of gut function. Luminal H<sub>2</sub>S was proposed as a causative factor in intestinal cancers and chronic intestinal inflammation, however multiple studies showed that the role of H<sub>2</sub>S in intestinal inflammation is very complex and at times contradictory [217].

Ulcerative colitis (UC) is a mucosal inflammation of the colon characterized by epithelial cell damage with an accumulation of neutrophils and eosinophils that form crypt abscesses. Some studies report an increased level of H<sub>2</sub>S in patients with UC and the reduction in its level after anti-inflammatory treatment [218]. However, despite its well-known cytotoxic properties H<sub>2</sub>S was shown to have an anti-inflammatory effect in animal models of UC [198, 219, 220]. Moreover, scavenging of H<sub>2</sub>S by administration of bismuth salts did not prevent the colitis in rats [221] while inhibition of endogenous H<sub>2</sub>S synthesis significantly worsened the disease state [198].

Nowadays, it has been generally recognized that the microbial community inhabiting the gut markedly affects physiology and health [222-225]. The gut bacteria are highly metabolically active and may have not only local but also systemic effects. As the production of gaseous metabolites by the microbiome can be studied by manipulating the dietary composition, this strategy was applied to observe the H<sub>2</sub>S level produced in the gut as a function of various diets.

It was shown that fasting dramatically reduced H<sub>2</sub>S levels in rat colon. Supplementation of the diet with carrageenan, a poorly absorbed organic sulfate from seaweed, resulted in a massive increase in cecal H<sub>2</sub>S that could be quenched by the addition of zinc acetate to the diet [226]. When another sulfate source, chondroitin sulfate, was added to a high fat/high sugar diet in mice, it was shown to increase the level of SRB *D. piger* and H<sub>2</sub>S. However, no adverse effects on

intestinal mucosa, uptake of nutrients or body weight of mice were noted [227]. High fat diet alone was reported to increase the expression of CSE and CBS and H<sub>2</sub>S in the liver as a response to the hepatic oxidative stress in mice [228]. An *in vitro* study showed that lactate can stimulate sulfide production in *D. piger* with possible consequences for colitis [229].

In humans, fecal sulfide was shown to correlate with meat uptake [230]. The H<sub>2</sub>S level was increased about 4 times (from 160 to 750 nmol/g of feces) in subjects on diets containing 60 versus 420 g meat, while the level of free sulfide in blood did not change significantly [231]. The study on dietary restriction of sulfur amino acids (cysteine and methionine) is also of particular interest to the field as it was shown that H<sub>2</sub>S serves as a mediator of positive dietary effects on stress resistance and longevity in mammals and lower organisms [232].

Despite a large number of reports that study the effects of H<sub>2</sub>S in various experimental settings, the molecular mechanisms of its cellular actions are poorly understood. Some of the effects might be related to the mitochondrial functions and cytochrome c oxidase [171, 233], while its effects on gene expression might be mediated via the NFκB and ERK pathways [234, 235]. The molecular details, however, are still unknown [236].

### 3.1.5 Physiological concentrations of H<sub>2</sub>S in the body

There are significant discrepancies in the current literature on what constitutes biologically relevant levels of H<sub>2</sub>S. The majority of early studies report on micromolar concentrations of H<sub>2</sub>S in healthy tissues e.g., brain: 47 μM to 166 μM [237-240]; liver: 26 μM [241], 144 μM [238]; kidney: 40 μM [241], 200 μM [238]; heart: 130 μM [241]; and lung: 30 μM [233]. Plasma values of H<sub>2</sub>S were reported to be 34 μM [242], 38 μM [243], 46 μM [206] and 274 μM [244]. The concentration of H<sub>2</sub>S in the rat colon was found to be 40 μM (~1000 ppm) [226] and about 0.1- 0.7 μmol/g in wet human feces [231, 245]. It has been measured that the rat colon absorbs 340 μmol of sulfide per day and that only 1% of sulfide in feces exists in its free form; the rest is bound into complexes or quickly metabolized by colonic mucosa [245].

On the contrary, several studies reported values that are orders of magnitude lower. Using a gas chromatography-based chemiluminescent method Furne et al. estimated free H<sub>2</sub>S in blood to be 100 pM and 15 nM in tissues, as opposed to the μM values mentioned previously [246]. Whitfield et al. found the blood H<sub>2</sub>S level to be about 100 nM using a polarographic sensor [247].

The reported differences in values are attributed to the different methods used for analysis [248]. High micromolar values were found when samples were processed in acidic conditions (e.g. Zn-trapping assay or methylene blue assay), which liberates sulfur from its bound form in sulfide pools, iron-sulfur clusters or sulfhydrated proteins, which lead to the overestimation of the free sulfide level. Although commonly used, these methods report on total sulfide level rather than on free H<sub>2</sub>S/HS<sup>-</sup>.

To summarize, there is a considerable number of studies that suggest an important role of H<sub>2</sub>S in the gastrointestinal physiology and in pathological conditions. Importantly, the results of several studies were found to depend on the method of H<sub>2</sub>S detection. Therefore, an accurate and reliable method for measuring H<sub>2</sub>S *in vivo* is needed. Such meth-



od would help to better understand the contribution of this molecule to the pathogenesis and to develop new therapeutic approaches for the treatment of various gut disorders.

### 3.2 H<sub>2</sub>S detection and measurement

Sensitive and selective detection of H<sub>2</sub>S represents one of the major challenges in studying this molecule in living systems. Commonly used methods for sulfide quantification, such as spectrophotometry, chromatography, and ion-selective electrode, were initially developed for analysis of H<sub>2</sub>S in environmental samples and, therefore, can only be used for *ex vivo* analysis of biological samples [167, 172]. Another drawback is that they require destructive sample preparation which is not representative of the real-time situation in biological systems. The following is a summary of the various sulfide detection methods, along with their specific drawbacks.

- **Spectrophotometry**

The classical method involves H<sub>2</sub>S trapping with zinc or lead, followed by acidification and the reaction of sulfide with *N,N*-dimethyl-*p*-phenylenediamine. This forms methylene blue that absorbs at 670 nm and can be quantified [249]. The method requires acidic conditions and, as mentioned earlier, it reports total H<sub>2</sub>S values and does not distinguish between free or bound form [250]. Other disadvantages of this method are the lack of sensitivity (LOD 2 μM [202]) and that the absorbance of methylene blue is linear only at low μM concentrations due to the interference from dimers and trimers of methylene blue [166].

- **Gas chromatography**

By contrast, gas chromatography can detect H<sub>2</sub>S in the nanomolar range and can distinguish free sulfide from acid-labile sulfide [251]. However, the primary analytical drawback of the GC/MS methods for H<sub>2</sub>S measurement is the absence of a specific H<sub>2</sub>S internal standard required to perform quantification [252].

- **RP-HPLC with fluorescence detection**

Recently a novel sensitive method (LOD 5 nM) was developed by Kevil and colleagues [202-204]. It is based on the reaction of monobromobimane (mBB) with HS<sup>-</sup> under basic conditions at room temperature to produce fluorescent sulfide-dibimane. RP-HPLC allows for the separation of the free, reductant-labile/sulfane-sulfur, and acid-labile sulfide pools, enabling more detailed investigations of complex sulfide content in the same sample. Additionally, the mBB method was used to detect and quantify reactive sulfur-containing compounds, such as L-cysteine hydropersulfide [253].

- **Electrochemical methods**

A polarographic (amperometric) electrode allows for the direct measurement of H<sub>2</sub>S production in real-time in cell culture and in plasma of unanesthetized animals and has a detection limit of 10 to 20 nM H<sub>2</sub>S gas or 100- 200 nM total sulfide [247, 254]. However, the detector electrodes have a limited performance in small sample volumes and are pressure and temperature sensitive, and, therefore, need to be frequently calibrated [255]. A comparison of the am-

perometric H<sub>2</sub>S sensor to the mBB method showed that both methods produced identical responses to H<sub>2</sub>S in buffer or blood plasma [256].

- **Optical imaging**

Reaction-based probes for H<sub>2</sub>S detection offer higher spatiotemporal resolution and better compatibility with living systems compared to other methods. Fluorescent probes can detect local H<sub>2</sub>S production in specific cellular organelles [257-260] or in the cytoplasm [261, 262] of live cells. Because of their design strategy they report the accumulated fluorescence signal from the probe activation over time rather than the real-time H<sub>2</sub>S dynamics, and have a detection limit in the micromolar range [263]. Different strategies for the development of optical probes for H<sub>2</sub>S imaging will be covered in detail in the following section.

### 3.3 Strategies for probe development for the imaging of H<sub>2</sub>S *in vivo*

After the recognition of H<sub>2</sub>S as an important biomolecule and the acknowledgment of a limited number of tools available to study its role and effects in living systems, the field of fluorescence imaging witnessed a rapid progress in the area of probe development. Even though a large number of optical imaging probes are being reported, only a few of them were applied for H<sub>2</sub>S detection in intact living systems.

The two major strategies used for the development of activatable probes for H<sub>2</sub>S imaging are based on the reductive and nucleophilic properties of HS<sup>-</sup>, which is the most abundant form of H<sub>2</sub>S in physiological conditions [180, 264].

The most commonly used functional group in the design of H<sub>2</sub>S-sensitive probes is the azide. Azides are relatively stable and compatible with living cells [265] and animals [266, 267] which explains their extensive use as a biorthogonal functional group in chemical biology [268]. The reduction of an azide to an amine was recognized early-on as a versatile strategy to manipulate the emission state of the fluorophore. A combination of the two above mentioned factors resulted in the dramatic increase in the use of this approach with over 65 papers published on azide-based probes for H<sub>2</sub>S imaging since the original rhodamine-based probes reported by Chang and colleagues [269].

The SF5-AM is second-generation probe based on the rhodamine scaffold by Chang [262] (Table 3:1). Two azido-groups were used for quenching the fluorescence and lowering the background signal and the acetoxymethyl (AM) ester group was added to increase cellular retention. The probe could detect H<sub>2</sub>S *in vitro* with a limit of detection of 0.25 μM and was used in cell assays. However, leakage of the dye from live cells was noted after 60 min. The same probe was later applied for imaging H<sub>2</sub>S production in a mouse model of acute inflammation [270]. The probe reported on the synthesis of H<sub>2</sub>S in primary mouse microphage cultures with comparable efficiency to the methylene blue assay. The probe was injected IP in mice with a zymosan-induced air pouch model to report on the H<sub>2</sub>S synthesis by tissue and infiltrating leukocytes over 48 h. The fluorescence response observed *in vivo* was broadly consistent with the data obtained by methylene blue assay from exudates; however, it was noted that SF5 fluorescence is not a quantifiable method of measuring H<sub>2</sub>S synthesis and that methylene blue formation was more efficient in test-tube assays than SF5.

Another azido-based fluorescent probe was recently reported by Pluth and colleagues and was applied for the imaging of H<sub>2</sub>S production in the gut of live zebrafish [271]. The probe is based on *O*-methylrhodol scaffold with an azide group locking the fluorophore in a spirocyclic lactone form (Table 3:1). The reduction of the azide by H<sub>2</sub>S to the amine leads to opening of the cycle and fluorescence. The probe can detect H<sub>2</sub>S in a test-tube assay with a limit of 0.09  $\mu$ M and shows 32-fold selectivity over 5 mM GSH. The ability of the probe to respond to endogenous H<sub>2</sub>S produced *in vivo* was tested after oral gavage of the probe and a slow-releasing H<sub>2</sub>S donor mixed with GSH in zebrafish. Imaging of the intestinal bulb using light sheet fluorescence microscopy revealed about 2.5-fold increase in fluorescence from zebrafish treated with H<sub>2</sub>S donor compared to the ones treated with the probe alone.

| Imaging probe   | Structure | Demonstrated application   |
|---|-----------|--|
| <b>Activatable NIR fluorescence probes</b>                    |           |  |
| Probe 1<br>( $\lambda_{\text{ex/em}}$ 385/453 nm)             |           | <i>In vitro</i> (test-tube, cell assays) and <i>in vivo</i> (imaging of H <sub>2</sub> S in endogenous lysosomal injury model in <i>C. elegans</i> ) [272]                   |
| MeRho-Az<br>( $\lambda_{\text{ex/em}}$ 476/516 nm)            |           | <i>In vitro</i> (test-tube, cell assays) and <i>in vivo</i> (imaging of H <sub>2</sub> S production in GIT from H <sub>2</sub> S-donor using probe (OG) in zebrafish) [271]  |
| SF5-AM<br>( $\lambda_{\text{ex/em}}$ 480/520 nm)              |           | <i>In vitro</i> (test-tube, cell assays)[262] and <i>in vivo</i> (whole-body imaging of H <sub>2</sub> S production in a mouse model of inflammation using probe (IP)) [270] |
| NIR-HS<br>( $\lambda_{\text{ex/em}}$ 695/750 nm)              |           | <i>In vitro</i> (test-tube, cell assays) and <i>in vivo</i> (whole-body imaging of exogenous NaHS (IP) using probe (IP) in mice) [273]                                       |
| XC-H <sub>2</sub> S<br>( $\lambda_{\text{ex/em}}$ 670/725 nm) |           | <i>In vitro</i> (test-tube, cell assays) and <i>in vivo</i> (whole-body imaging of exogenous NaHS (IP) using probe (IP) in mice) [274]                                       |
| <b>Activatable BL probes (caged luciferins)</b>               |           |  |
| Probe 1   |           | <i>In vitro</i> (enzyme, cell assays), <i>in vivo</i> (whole-body imaging of exogenous NaHS (IV) using probe (IP))   |

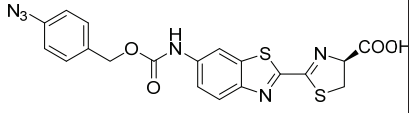
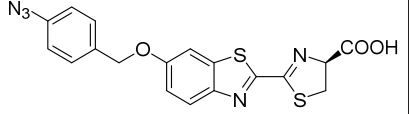
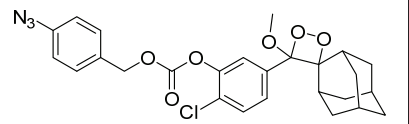
|   |   |   |
|---|---|---|
|   |   | in mice [103]) and (imaging of exogenous NaHS in FLuc-tumors as a BL reporter [104])  |
| Probe 2                                     |  | <i>In vitro</i> (test-tube assays) [103]  |
| Probe 3                                     |  | <i>In vitro</i> (test-tube assays) [103]  |
| <b>Activatable chemiluminescence probes</b> |   |   |
| CHS-3                                       |  | <i>In vitro</i> (test-tube, cells) and <i>in vivo</i> (whole-body imaging of exogenous Na <sub>2</sub> S (IP) using probe (IP) in mice) [275] |

Table 3.1 Selected examples of activatable probes for H<sub>2</sub>S optical imaging in living animals. All reported BL probes for *in vitro* and *in vivo* imaging are shown.

Despite being valuable tools in *in vitro* assays, these probes are limited by high autofluorescence background from blood and tissues which precludes their wide application in *in vivo* studies. As a way to improve the performance of the probes for *in vivo* imaging several groups utilized near-infrared fluorophores to develop H<sub>2</sub>S-responsive probes.

Two examples of the NIR probes that were validated in living mice are based on another sensing strategy, the nucleophilic attack of HS<sup>-</sup> on the 2,4-dinitrophenyl (DNP) ether moiety. The attack leads to the cleavage of the ether bond (thiolysis) and release of the free fluorophore. The probe NIR-HS (Table 3:1) showed a low detection limit for H<sub>2</sub>S *in vitro* (0.04 μM), and sulfide-induced increase of the fluorescence intensity in living cells and in living mice after IP administration of Na<sub>2</sub>S [273]. Another probe, XC-H<sub>2</sub>S, is based on a xanthene-cyanine platform with a reported limit of H<sub>2</sub>S detection of 0.16 μM and only 6-fold selectivity over 1 mM GSH in a test-tube assay. It was shown to be cell permeable and upon IP administration to live mice it produced NaHS-dependent fluorescence. However, when the background signal from the probe alone was compared with the full fluorophore, it became apparent that the dynamic range was quite low (only 5-fold difference in signal) which might be explained by the side-reaction of the probe with endogenous GSH.

A chemiluminescent probe, CHS-3 (Table 3:1), carrying the azido-benzyl moiety showed about 4-fold increase in the luminescence response in the Na<sub>2</sub>S treated mice versus the vehicle controls [275].

Interestingly, the same functionality was employed as an H<sub>2</sub>S-sensitive group in a series of bioluminescent probes for H<sub>2</sub>S imaging recently reported by Ke et al. [103]; however, it was found less reactive than the Probe 1 (Table 3:1) when the azide was installed directly in the 6'-position of luciferin. Probe 1 was independently reported by two research groups as a tool for BL imaging of H<sub>2</sub>S in living mice; Tian et al. showed the validation of this probe in a FLuc-tumor model in mice and Ke et al. used it for the whole-body imaging of H<sub>2</sub>S in FVB-luc<sup>+</sup> mice. Injection of NaSH IV 5 min

prior to the IP injection of the probe 1 (equimolar) resulted in a 2-fold increase in BL in the H<sub>2</sub>S-treated group compared to the control group.

In summary, several fluorescent probes for imaging H<sub>2</sub>S in living animals were reported, however, some of them operate in the visible range and are not suitable for *in vivo* imaging and the ones with the NIR properties suffer from high background and low specificity. Recently, one bioluminescent probe for H<sub>2</sub>S imaging in living animals was described, which demonstrates a high potential of this approach and opportunities for further probe development in this area.

### 3.4 Results

#### 3.4.1 Probe development

We designed and synthesized a series of caged luciferin probes carrying azides or dinitroaryl groups, analogous to the caging approach of the fluorescent imaging probes discussed earlier. Reducing the azides in probes 1 and 2 (Table 3:2) would lead to the direct formation of amino-luciferin (NH<sub>2</sub>-L, NH<sub>2</sub>-F-L) or lead to the uncaging and formation of hydroxy-luciferin (OH-L) (probes 3 and 4, Table 3 :2). In the probe 5 the nucleophilic attack of HS<sup>-</sup> would lead to the cleavage of the ether bond (thiolysis) and release of OH-L.

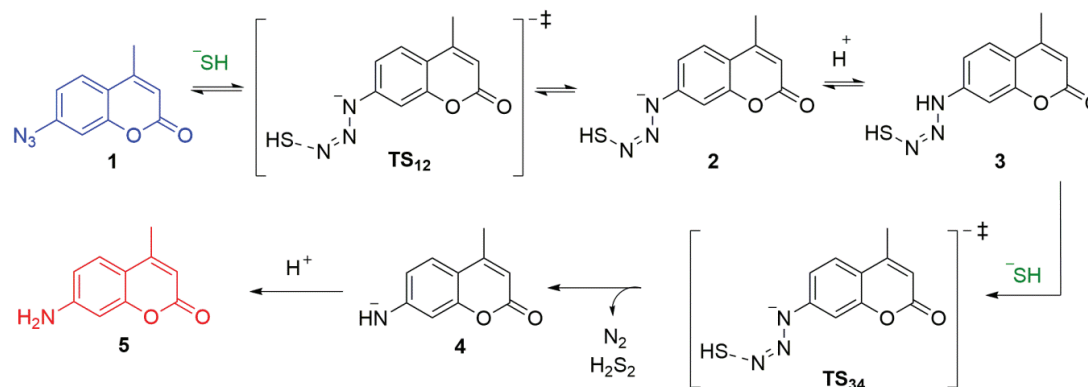
| N | Caged Luciferin (CL) | Abbreviation             | Free Luciferin (L) | Abbreviation         |
|---|----------------------|--------------------------|--------------------|----------------------|
| 1 |                      | Az-CL                    |                    | NH <sub>2</sub> -L   |
| 2 |                      | Az-F-CL                  |                    | NH <sub>2</sub> -F-L |
| 3 |                      | Az-Bn-CL                 |                    | OH-L                 |
| 4 |                      | Az-F <sub>4</sub> -Bn-CL |                    | OH-L                 |
| 5 |                      | DNP-CL                   |                    | OH-L                 |

Table 3.2 Structures of caged luciferin (CL) probes for H<sub>2</sub>S imaging and corresponding free luciferins (L) formed after probe uncaging.

We have chosen aromatic azides as caging groups, as it was previously shown that aryl azides are more reactive towards thiols than alkyl azides [276, 277]. The suggested mechanism of the azide reduction by H<sub>2</sub>S is shown in Scheme 3:1 (adapted from [278]).

### 3.4.1.1 Suggested mechanism of azide reduction by H<sub>2</sub>S

In a recent study Henthorn et al. investigated the mechanism of the reaction between H<sub>2</sub>S and an aromatic azide (4-methyl-7-azidocoumarin) [278]. First, they showed that HS<sup>-</sup>, rather than H<sub>2</sub>S, is the active species responsible for the reduction, and that two equivalents of HS<sup>-</sup> is required for complete reduction of azide. Second, the reaction is first-order with respect to azide and NaSH (second order overall), which is consistent with HS<sup>-</sup> acting as a one electron reductant.



Scheme 3.1 Suggested mechanism for H<sub>2</sub>S-mediated reduction of the azide (1) to the amine (5) (adapted from [278]).

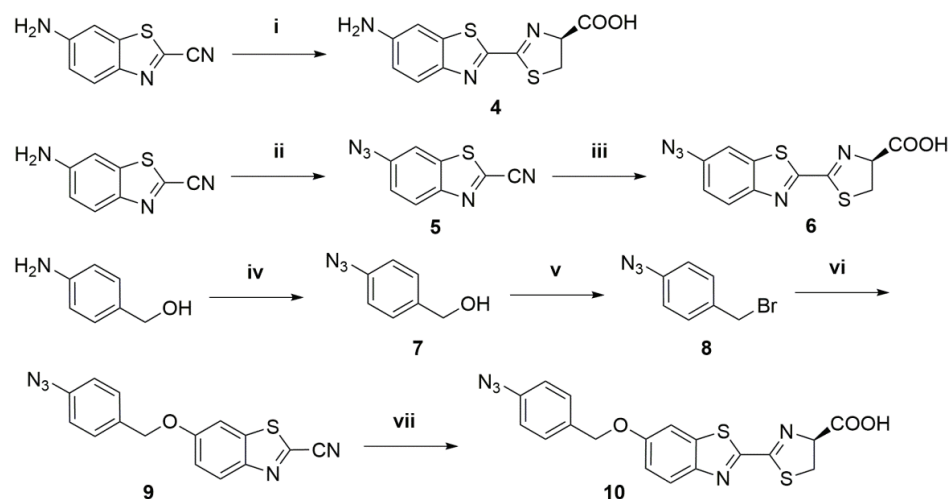
In a first reversible step HS<sup>-</sup> acts as a nucleophile and attacks the terminal azide nitrogen of Az-CL (**1**), which is the most electrophilic nitrogen of the azide [279]. In analogous reactions of azides with other nucleophilic reductants, such as phosphines in the Staudinger reaction [280, 281], nucleophilic attack takes place on the terminal nitrogen as well. This generates anionic azidothiol (**2**), which is later protonated to generate neutral intermediate (**3**), which is then attacked by a second equivalent of HS<sup>-</sup> to release N<sub>2</sub>, H<sub>2</sub>S<sub>2</sub>, and the deprotonated amine (**4**), which undergoes proton transfer mediated by the solvent to generate the final product NH<sub>2</sub>-L (**5**).

From the mechanism suggested above it is possible to conclude the advantages and limitations of using azide group for H<sub>2</sub>S sensing. As under physiological conditions hydrogen sulfide exists mainly in HS<sup>-</sup> form, the azide reduction reports on the most prevalent state of H<sub>2</sub>S. However, because the initial addition of HS<sup>-</sup> to the azide is reversible, generation of the intermediate (**2**) may be difficult if sulfide concentrations are very low. It is also possible that other sulfhydryl-containing biomolecules, such as glutathione and cysteine, may participate in the reaction decreasing the selectivity of the system.

### 3.4.2 Probe design and synthesis

As different aromatic azides might have a different reactivity to H<sub>2</sub>S we decided to synthesize two azido-caged luciferin in probes, Az-CL, where the azide was installed directly in the 6'-position of luciferin, and Az-Bn-CL, where the *p*-azido-benzyl group was attached to the 6'-hydroxy-luciferin. Upon the reaction with H<sub>2</sub>S Az-CL is converted to the amino-luciferin (NH<sub>2</sub>-L), while the Az-Bn-CL is converted to hydroxy-luciferin (OH-L), both luciferins are classical substrates for FLuc.

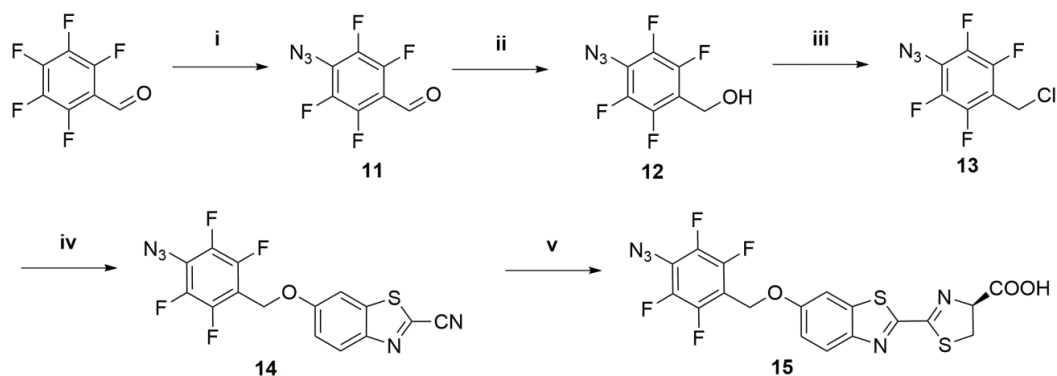
The NH<sub>2</sub>-L was synthesized in 1 step in 72% yield, the Az-CL probe was synthesized in 2 steps with an overall yield 63%, the Az-Bn-probe was synthesized in 4 steps with an overall yield 24% (Scheme 3.2).



Scheme 3.2 Synthesis of NH<sub>2</sub>-L (4), Az-CL (6) and Az-Bn-CL (10). Reagents and conditions: (i) D-cysteine, THF/H<sub>2</sub>O (1:1), RT, 1 h; (ii) 1. NaNO<sub>2</sub>, HCl; 2. NaN<sub>3</sub>; 0 °C to RT, 1 h; (iii) D-cysteine, ACN/H<sub>2</sub>O (1:1), RT, 0.5 h; (iv) 1. NaNO<sub>2</sub>, HCl; 2. NaN<sub>3</sub>; 0 °C to RT, 1 h; (v) PBr<sub>3</sub>, RT, 1 h; (vi) 2-Cyano-6-hydroxybenzothiazole, K<sub>2</sub>CO<sub>3</sub>, DMF, 0 °C to RT, 4 h; (vii) D-cysteine, THF/H<sub>2</sub>O (1:1), RT, 2 h.

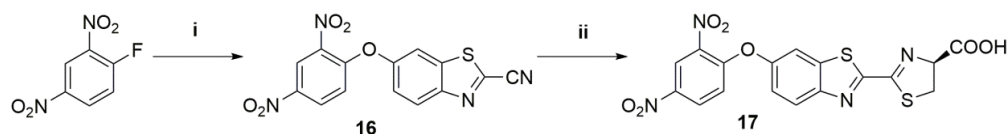
With the two probes in hand, we first measured their reactivity to H<sub>2</sub>S by HPLC-MS analysis. NaHS was used as a source of H<sub>2</sub>S in all experiments. Upon the addition of NaHS solution to the caged luciferins, both probes released free luciferin (Figure S3.1), however, the release of OH-L from the Az-Bn-CL probe was slower than the release of NH<sub>2</sub>-L from the Az-CL probe. After 60 min Az-CL was fully converted to NH<sub>2</sub>-L, while, only about the half of the Az-Bn-CL probe was converted to OH-L. The difference in the luciferin release between the two probes was also observed using a fluorescence assay (Figure S3.2).

As the speed of luciferin release is crucial for the probe performance in the BL assay, we aimed to increase the reactivity of Az-Bn-CL probe by designing a new probe, Az-F<sub>4</sub>-Bn-CL. It was previously reported that functionalization of the aromatic ring with fluorine atoms accelerated the reduction of aryl azides by H<sub>2</sub>S [282-284]. The Az-F<sub>4</sub>-Bn-CL probe was synthesized in 5 steps with an overall yield 7% (Scheme 3.3). When the probe was added to the NaHS solution and the reaction was analyzed by HPLC-MS, surprisingly, no free luciferin was detected. The HPLC-MS analysis suggested that the azide was reduced by H<sub>2</sub>S to the amine, however, no uncaging occurred. This might be explained by the fact that the electron-withdrawing fluorine atoms introduced on the aromatic ring decrease the aromaticity [285] which might prevent the distribution of electrons from an electron-donating amino group to the C-O bond and preclude the cleavage of this bond and release of luciferin.



Scheme 3.3 Synthesis of Az-F<sub>4</sub>-Bn-CL (15). Reagents and conditions: (i) NaN<sub>3</sub>, acetone/H<sub>2</sub>O reflux, 8 h; (ii) (CH<sub>3</sub>)<sub>2</sub>NH·BH<sub>3</sub>, 55 °C, 1 h; (iii) SOCl<sub>2</sub>, DCM, 0 °C to RT, 6 h; (iv) 2-Cyano-6-hydroxybenzothiazole, K<sub>2</sub>CO<sub>3</sub>, acetone, 0 °C to RT, 5 h; (v) D-cysteine, THF/H<sub>2</sub>O (1:1), RT, 1 h.

In addition to the azido-caged luciferins we designed and synthesized 2,4-dinitrophenyl (DNP) caged luciferin, DNP-CL (Table 3:2). We were encouraged by the reports of several caged NIR fluorescent probes for imaging of H<sub>2</sub>S in living animals [273, 274] and we wanted to compare two commonly used functional groups, azide and DNP, in the caged luciferin approach for the detection of H<sub>2</sub>S. The DNP-CL probe was synthesized in 2 steps with an overall yield 47% (Scheme 3.4).



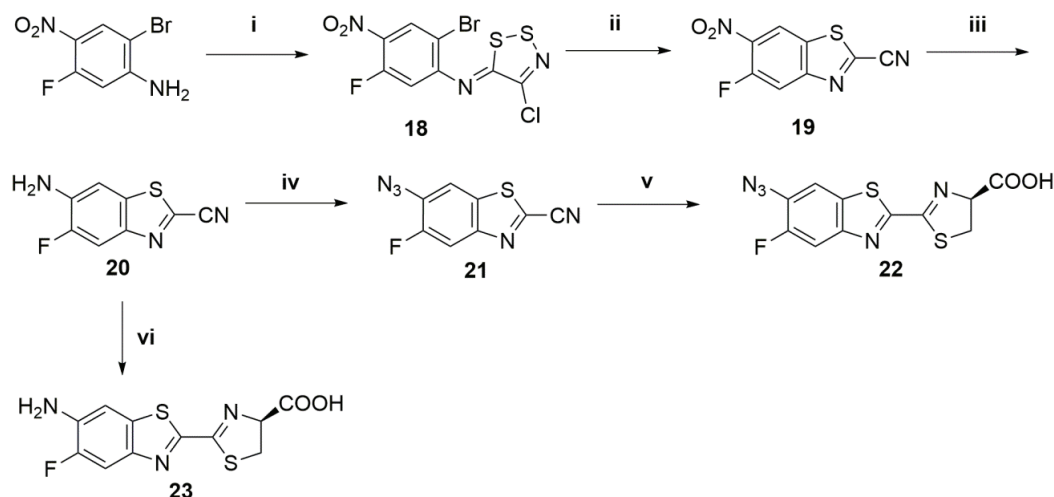
Scheme 3.4 Synthesis of DNP-CL (17). Reagents and conditions: (i) 2-Cyano-6-hydroxybenzothiazole, K<sub>2</sub>CO<sub>3</sub>, acetone, RT, 0.5 h; (ii) D-cysteine, ACN/H<sub>2</sub>O (1:1), RT, 1.5 h.

HPLC-MS analysis of the reaction mixture of DNP-CL with NaHS showed that the reaction was slow and only about 10% of luciferin was released in 30 min (Figure S3.3), while the Az-CL probe was fully converted to luciferin in 30 min. Moreover, when the two probes were tested in the selectivity assay with biothiols, the DNP-CL probe reacted 10-fold more selectively with Cys and 12-fold with GSH over H<sub>2</sub>S, while the Az-CL probe showed 6-fold selectivity to H<sub>2</sub>S vs. Cys and GSH over 1 h (Figure S3.4). On the basis of these results we have chosen Az-CL for further studies.

After the recent literature reports of Az-CL and its application for H<sub>2</sub>S imaging in living animals [103, 104] we decided to further optimize the performance of this probe by improving its reactivity to H<sub>2</sub>S. We chose to introduce a fluorine atom in the *o*-position to the azide on the basis of a similar strategy reported for fluorescent probes for H<sub>2</sub>S [282, 284]. As it could be introduced in two possible positions of luciferin, 5'- or 7'-, we chose the 5'-position as it was shown that 5'-F-OH-L produces twice more light than 7'-F-substituted analogue [286] and FLuc tolerates modifications of luciferin structure in the 5'-position [287]. We hypothesized that electron-withdrawing fluorine would increase the electrophilicity of the azide and the rate of its reduction by nucleophilic sulfide.



The probe Az-F-CL was synthesized in 5 steps with an overall yield 20%, the corresponding NH<sub>2</sub>-F-L luciferin was synthesized in 5 steps with an overall yield 27% (Scheme 3.5).



Scheme 3.5 Synthesis of Az-F-CL (22) and NH<sub>2</sub>-F-L (23). Reagents and conditions: (i) Appel's salt, pyridine (2 eq.), DCM, RT, 2 h; (ii) CuI, pyridine, MW, 90 W, 110 °C, 15 min; (iii) SnCl<sub>2</sub>·2H<sub>2</sub>O (14 eq.), EtOAc, 70 °C, 2 h; (iv) 1. NaNO<sub>2</sub>, HCl; 2. NaN<sub>3</sub>; 0 °C to RT, 1.5 h; (v) D-cysteine, THF/H<sub>2</sub>O (2:1), RT, 1 h; (vi) D-cysteine, THF/H<sub>2</sub>O (2:1), RT, 1 h.

### 3.4.3 Kinetic analysis of the H<sub>2</sub>S-mediated reduction of Az-CL and Az-F-CL probes

We next decided to measure the kinetics of the reduction of Az-CL and Az-F-CL to compare their reactivity to H<sub>2</sub>S.

The kinetics of the reaction between probes and NaHS was monitored by HPLC-MS analysis. Treatment of aqueous buffered solutions of probes with excess of NaSH solution (pseudo-first-order conditions) resulted in decrease of the peaks of the probes (Az-CL, Az-F-CL) and formation of corresponding luciferins (NH<sub>2</sub>-L, NH<sub>2</sub>-F-L). Under our experimental conditions observed reaction rates were  $k_{\text{obs}} = (6.4\text{--}11.2) \times 10^{-4} \text{ M}^{-1} \text{ s}^{-1}$  for Az-CL and  $k_{\text{obs}} = (8.6\text{--}21) \times 10^{-4} \text{ M}^{-1} \text{ s}^{-1}$  for Az-F-CL (Figure S3.5A, B). The plot of  $k_{\text{obs}}$  vs. [NaHS] gave a straight line passing through the origin (Figure S3.5C, D). This indicates that the reaction is first order to sulfide, which is consistent with previously reported data for azide reduction by H<sub>2</sub>S [278]. The slope of the best-fit line provided second order rate constants  $k_2 = 0.1 \text{ M}^{-1} \text{ s}^{-1}$  for Az-L and  $k_2 = 0.2 \text{ M}^{-1} \text{ s}^{-1}$  for Az-F-L (Figure S3.5C, D). This data shows that the addition of fluorine in the *o*-position to the azide improved the reaction rate by about two-fold which is in agreement with previous studies on activatable fluorescent probes for imaging of H<sub>2</sub>S [282, 284].

It should be noted that the rate constants of the reaction between CL probes and H<sub>2</sub>S are lower than the reported values for the azide-containing fluorescent probes, such as azido-coumarin 4-Az-7-MC ( $k_2 = 4.6 \text{ M}^{-1} \text{ s}^{-1}$ ) [282], or for other caged luciferin probes for imaging of small molecules, such as hydrogen peroxide probe, PCL-1 ( $k_2 = 3.8 \pm 0.34 \text{ M}^{-1} \text{ s}^{-1}$ ) [53].

We have also estimated by HPLC-MS analysis that the solutions of probes prepared from DMSO stocks in PBS at pH 7.4 are stable for at least 3 hours at room temperature which is sufficient for the duration of the imaging experiment *in vitro* and *in vivo*.

We, therefore, have chosen these two probes, Az-CL and Az-F-CL, for further validation and side-by-side comparison.

### 3.4.4 Validation of probes in luciferase assay *in vitro*

We next examined the response of Az-CL and Az-F-CL probes to different concentration of H<sub>2</sub>S in the bioluminescence assays where firefly luciferase was added to detect the luciferin formed during the reaction. We performed two types of assays: (1) pre-incubation of probes with H<sub>2</sub>S for 1 h followed by the BL read-out and (2) detection of H<sub>2</sub>S in real-time.

#### 3.4.4.1 BL detection of H<sub>2</sub>S after pre-incubation with probes

The probes were incubated with various concentrations of NaHS for 1 h and the released luciferin was measured after addition of luciferase for 1 h. The plot of the total photon flux vs. the concentration of NaHS provided a linear fit for both probes, which shows that the probes can quantify H<sub>2</sub>S over a 2-order-of-magnitude range, from 10-1000  $\mu$ M (Figure S3.6B). Az-F-CL produced 7-times lower background signal and, as expected from its higher reaction rate, 2 to 3 times higher BL response to NaHS compared to the Az-CL (Figure 3.5).

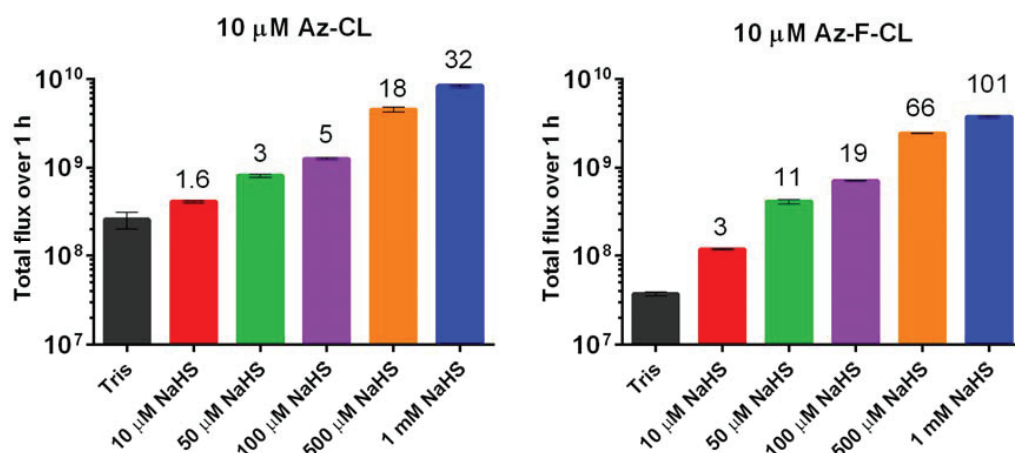


Figure 3.5 Concentration-dependent BL signal produced from Az-CL and Az-F-CL after 1 h of incubation with various NaHS concentrations in luciferase assay. Numbers indicate the ratio over the background (probe in Tris), the differences are statistically significant (t-test),  $n = 3$ .

The limit of H<sub>2</sub>S detection was calculated as the concentration at which the BL equals that of [blank + 3  $\times$  SD<sub>blank</sub>] according to a linear regression fit of the data (Figure S3.6B) and determined to be  $13.6 \pm 4.1$   $\mu$ M for Az-CL and  $0.09 \pm 0.02$   $\mu$ M for Az-F-CL. This data shows that H<sub>2</sub>S detection limit of Az-F-CL is about 150-times lower than of Az-CL and is on par with the most sensitive fluorescence probes for H<sub>2</sub>S reported [271]. We also checked that NaHS had no effect on the bioluminescence read-out (Figure S3.6C).

### 3.4.4.2 BL detection of H<sub>2</sub>S in real-time

In order to determine the utility of the probes for H<sub>2</sub>S detection under biologically relevant conditions, e.g. in cells where luciferase will oxidize luciferin as soon as it is released from the probes, we performed BL imaging of H<sub>2</sub>S in real-time. After addition of the probes, NaHS and luciferase, BL was detected for 90 min. The plot of the total photon flux vs. the concentration of NaHS provided a linear fit for both probes (Figure S3.7B), however the Az-F-CL probe shows a higher dynamic range (higher signal-to-background ratio) (Figure 3.6). The detection limit of H<sub>2</sub>S was determined to be  $4.2 \pm 1.4 \mu\text{M}$  for Az-CL and  $3.4 \pm 0.3 \mu\text{M}$  for Az-F-CL. Therefore, Az-F-CL can more reliably differentiate between low levels of H<sub>2</sub>S than Az-CL. When the data was compared with the signal produced from corresponding luciferins, it was estimated that after 90 min of reaction with 50 eq. of NaHS (500  $\mu\text{M}$ ) about 20% of Az-F-CL was uncaged, while for Az-CL it was only 8%.

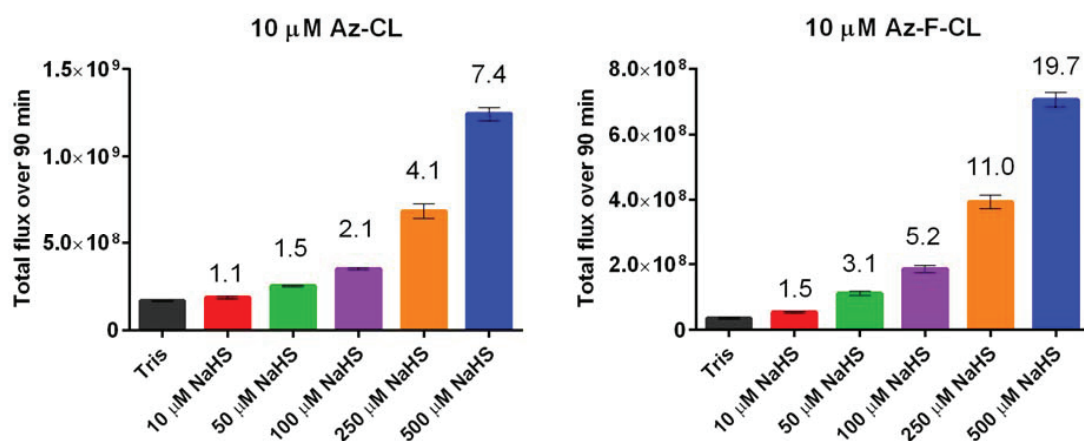


Figure 3.6 Real-time BLI of H<sub>2</sub>S with Az-CL and Az-F-CL probes in luciferase assay. Numbers indicate the ratio over the background (probe in Tris), the differences are statistically significant (t-test),  $n = 3$ .

### 3.4.5 Selectivity to H<sub>2</sub>S over biothiols

As it was mentioned earlier the SH-containing biomolecules, such as glutathione and cysteine, may participate in the reduction of the azide decreasing the selectivity. The selectivity of the probe for H<sub>2</sub>S over Cys and GSH is achieved due to the differences in  $pK_a$  values (Figure 3.1). The  $pK_a$  of the thiol group in cysteine has been determined to be 8.2 [288], which means that at pH 7.4 about 16% of the total amount of cysteine exists in the thiolate form; for 100  $\mu\text{M}$  intracellular concentration this number translates to 16  $\mu\text{M}$  concentration. In glutathione, the most abundant thiol in the cytosol, cysteine residue has a  $pK_a$  of 9.2 [288, 289], at pH 7.4 about 1.6% exists in the thiolate form (for 5 mM intracellular concentration about 80  $\mu\text{M}$  exists in the thiolate form). As concentration of H<sub>2</sub>S was estimated to be in the nanomolar to low micromolar range in the cells and high micromolar to millimolar in the lumen of the gut, it was important to examine the selectivity of the probes.

The selectivity of the probes for H<sub>2</sub>S detection was determined by incubating the probes with Cys or GSH for 20, 40 or 60 min and adding luciferase for the bioluminescence read-out (Figure 3.7). Az-CL probe (5  $\mu\text{M}$ ) showed 8-fold reactiv-

ity with H<sub>2</sub>S and produced 1.3-fold signal with 2000 eq. of GSH (10 mM) and 20 eq. of Cys (100  $\mu$ M) over the background after 1 h of incubation. Az-F-CL probe showed 14-fold higher signal with H<sub>2</sub>S, 2-fold signal with GSH and 1.3-fold signal with Cys over the background. However, despite the twice higher reaction rate of Az-F-CL towards H<sub>2</sub>S, the selectivity has dropped about 1.5-times. From these results it can be calculated that both Az-CL and Az-F-CL have about 6-times preferential reactivity to H<sub>2</sub>S over other biothiols which results in a similar selectivity profile.

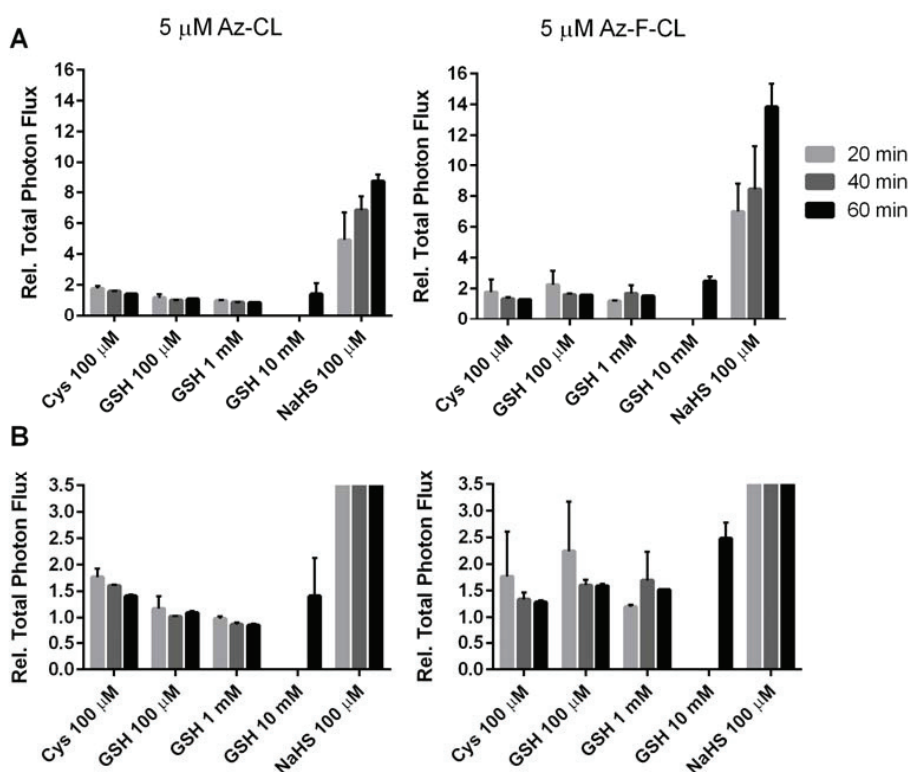


Figure 3.7 Selectivity profiles of Az-CL and Az-F-CL towards biothiols in luciferase assay. (A) Relative BL over 1 h from 5  $\mu$ M of the probe incubated with 100  $\mu$ M Cys, 1 and 10 mM GSH or 100  $\mu$ M NaHS for 20, 40 or 60 min and measured after the addition of luciferase (50  $\mu$ g/mL) in Tris pH 7.8 (relative to the signal from the probes alone). (B) Zoom-in of the graph (A); n= 3

### 3.4.6 Cell-based assays

Having determined that both probes are selective to H<sub>2</sub>S over other thiols in a test-tube assay, we next wanted to examine whether the performance of the probes would translate to cell culture as live cells contain thiols that might interfere with the H<sub>2</sub>S detection. For initial validation with cells being a source of luciferase, we chose C2C12-FLuc cell line that does not express H<sub>2</sub>S-producing enzymes in order to have an estimation of a background signal produced from probes in cells.

#### 3.4.6.1 BLI of exogenous H<sub>2</sub>S using cells as a read-out

First, the probes were incubated with various concentrations of NaHS for 1 h, then the solutions were added to C2C12-FLuc cells (mouse myoblast cells) and the BL signal was acquired for 1 h. As can be seen in Figure 3.8A both

probes produced a concentration-dependent BL signal when the reaction mixture was added to cells, however, a signal from as low as 50  $\mu$ M H<sub>2</sub>S could be detected with the Az-F-CL probe, while the Az-CL probe produced a signal above background only from 250  $\mu$ M H<sub>2</sub>S.

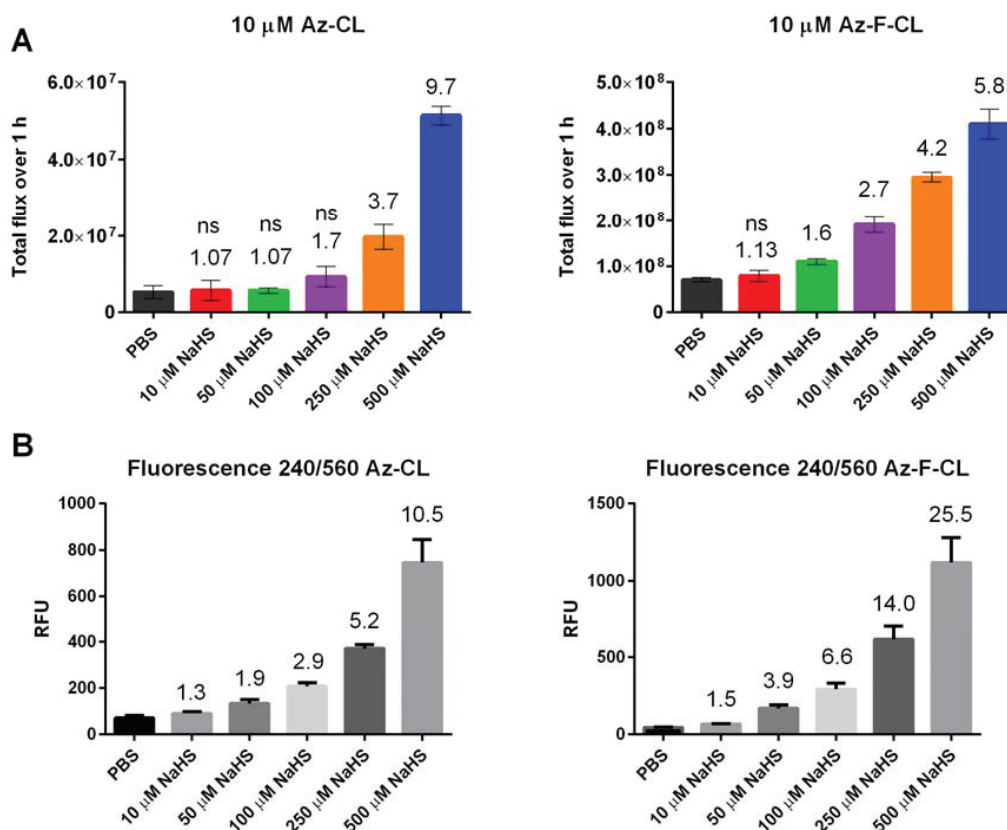


Figure 3.8 The signal produced in C2C12-FLuc cells from 10  $\mu$ M Az-CL and Az-F-CL after 1 h of incubation with 10- 500  $\mu$ M NaHS. (A) Bioluminescence signal over 1 h. (B) Fluorescence at  $\lambda_{\text{ex/em}}$  240/560 nm from the same plate after the BL acquisition (2 h after starting the reactions). Numbers indicate the ratio over the background (probe in PBS); the differences are statistically significant (t-test), "ns"- non-significant; n= 3.

As caged luciferin probes are not fluorescent and free luciferins are, fluorescence can be used as an additional control. Interestingly, we found that fluorescence provided a more robust read-out in this experiment than BL, probably, because fluorescence reports on the amount of luciferin directly and BL reports via luciferase (Figure 3.8B). It should be noted that high concentrations of H<sub>2</sub>S (> 20  $\mu$ M) inhibit the mitochondrial respiration which might affect the cell metabolism and explain the decrease of BL signal at 250 and 500  $\mu$ M NaHS (Figure S3.8A). The plot of the fluorescence vs. NaHS concentration provides a better fit and a lower detection limit than that of BL (Figure S3.8B, C; Table 3.3).

#### 3.4.6.2 Real-time BLI of exogenous H<sub>2</sub>S in cells

After we determined that the probes can be used for imaging of H<sub>2</sub>S in living cells we decided to see if the probes can report on exogenous H<sub>2</sub>S in real-time in cells. The solutions of both probes and NaHS were added to

C2C12-Fluc cells simultaneously and the BL was acquired for the duration of the signal peak (30 min). Luciferins were used as a control to check the effect of H<sub>2</sub>S on BL signal (Figure S3.9A).

As can be seen in Figures 3.8 and 3.9, the signal-to-noise ratio in the pre-incubation assay and in the real-time imaging assay in cells is very similar. This indicates that cells do not interfere with the reaction between probes and H<sub>2</sub>S and that exogenous H<sub>2</sub>S can be monitored in real-time in living cells using these probes.

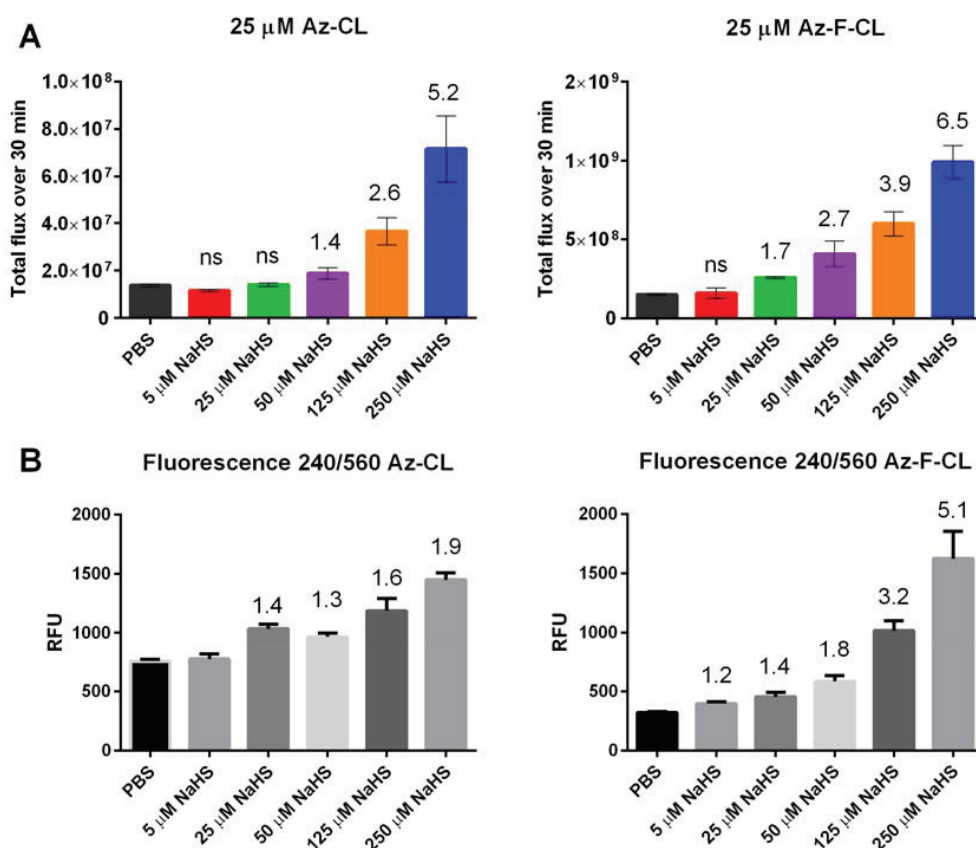


Figure 3.9 The signal produced in C2C12-FLuc cells from 25  $\mu$ M Az-CL and Az-F-CL and 5- 250  $\mu$ M NaHS. (A) Total photon flux produced over 30 min. (B) Fluorescence at  $\lambda_{ex/em}$  240/ 560 nm from the same plate after the BL acquisition. Numbers indicate the ratio over the background (probe in PBS); the differences are statistically significant (t-test), "ns"- non-significant; n= 3.

We next examined if the probes can detect intracellular H<sub>2</sub>S after incubation of cells with NaHS solutions and washing. C2C12-Fluc cells were incubated with 10- 500  $\mu$ M NaHS solutions for 10 min, then washed, then 10  $\mu$ M of the probes were added and bioluminescence was acquired for 1 h. As can be seen in Figure 3.10 the Az-F-CL probe provided more sensitive detection of H<sub>2</sub>S than the Az-CL probe, detecting as low as 10  $\mu$ M H<sub>2</sub>S inside cells. We also used a commercially available fluorescent probe for H<sub>2</sub>S imaging, 7-azido-4-methylcoumarine, as a control to verify the H<sub>2</sub>S activity in cells (Figure 3.10C).



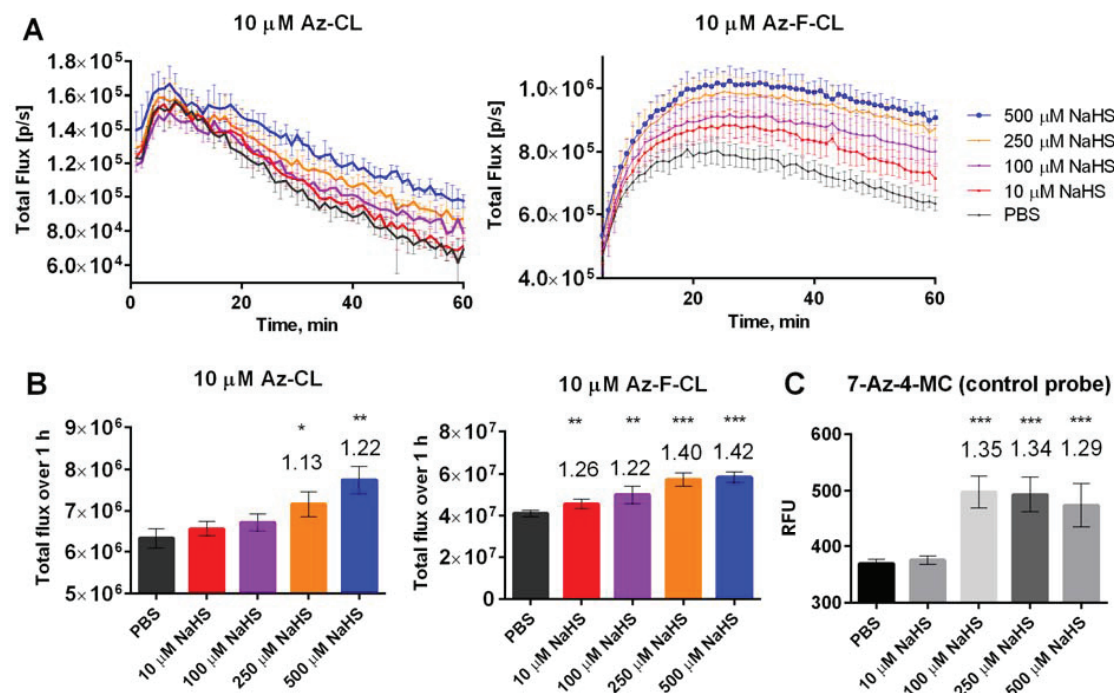


Figure 3.10 Bioluminescence imaging of intracellular H<sub>2</sub>S in C2C12-FLuc cells. Cells were incubated with 10- 500 μM NaHS for 10 min, washed and loaded with 10 μM probes. (A) Kinetics of BL signal over 1 h. (B) Total photon flux produced over 1 h. (C) Fluorescence from the control probe 7-Az-4-MC (λ<sub>ex/em</sub> 365/450 nm). Numbers indicate the ratio over the background (probe in PBS); \* p < 0.05, \*\* p < 0.01, \*\*\* p < 0.001 (t-test); n = 3.

### 3.4.6.3 Cytotoxicity assay

The cytotoxic effect of the two probes was determined after 1 h of incubation with C2C12-FLuc cells using Alamar Blue assay. The Az-F-CL probe showed higher cytotoxicity in cells (IC<sub>50</sub> = 1198 ± 18 μM) than Az-CL (IC<sub>50</sub> = 1604 ± 43 μM) (Figure S3.10), however, these value are far below the working concentrations used in the BLI assays.

### 3.4.7 Detection limit of H<sub>2</sub>S and bioluminescence signal window

The data on the limit of H<sub>2</sub>S detection for Az-CL and Az-F-CL probes for each assay is summarized in the Table 3.3. Az-F-CL provides higher sensitivity in almost every assay and equal sensitivity to Az-CL in the real-time assay with luciferase. It can be estimated that the sensitivity drops about 10 times for Az-CL and about 4 times for Az-F-CL when comparing the real-time imaging in enzyme and cell assays. Also, as mentioned before, fluorescence imaging was used as an additional control in these assays and it generally provided a better fit than BLI in cell assays.

| Assay                           | Az-CL       | Az-F-CL     |
|---------------------------------|-------------|-------------|
| Pre-incubation + luciferase- BL | 13.6 ± 4.1  | 0.09 ± 0.02 |
| Real-time + luciferase- BL      | 4.2 ± 1.4   | 3.4 ± 0.3   |
| Pre-incubation + cells- BL      | 84.4 ± 15.0 | 12.5 ± 3.2  |
| Pre-incubation + cells- FL      | 20.7 ± 1.5  | 1.9 ± 1.5   |

|                       |            |            |
|-----------------------|------------|------------|
| Real-time + cells- BL | 43.2 ± 2.8 | 13.5 ± 5.7 |
| Real-time + cells- FL | 14.1 ± 4.9 | 2.1 ± 0.2  |

Table 3.3 Limit of H<sub>2</sub>S detection (μM) for Az-CL and Az-F-CL calculated using the following formula  $LOD = [blank + 3 \times SD_{blank}]$ . BL-bioluminescence, FL- fluorescence.

An important parameter to estimate the performance of imaging probes is the signal window between the background (signal from the probe alone) and the maximum achievable signal (equimolar concentration of luciferin). As can be seen in Figure 3.10 both probes showed a very high signal window in luciferase assay, 101 times difference between the BL produced from Az-F-CL and NH<sub>2</sub>-F-CL and 92 times difference between the Az-CL and NH<sub>2</sub>-CL. This allows to detect H<sub>2</sub>S with a two log dynamic range (from 10<sup>-10</sup> to 1000 μM). However, in cell assays Az-F-CL showed a high background signal, which decreases the signal window to only 5 times which is 10 times lower than for Az-CL. This data shows that Az-CL is potentially a better performing probe for *in vivo* imaging applications in living animals.

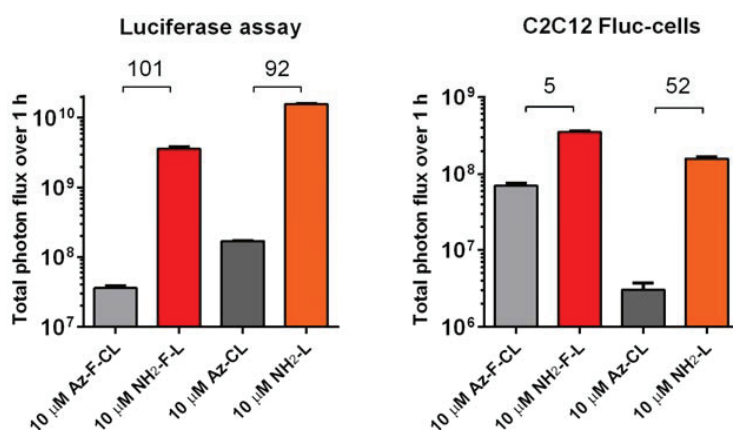


Figure 3.11 The BL signal window between probes (grey) and luciferins (orange) in the luciferase assay and in Fluc-cells. Numbers indicate the ratio of the mean values; n= 3.

### 3.4.8 Detection of H<sub>2</sub>S in bacterial assays

After characterizing the performance of both probes for detection of H<sub>2</sub>S in enzyme and cell assays we decided to apply them for imaging of H<sub>2</sub>S production by bacteria, as the microbiota is a major source of H<sub>2</sub>S production in mammals.

As a negative control we used wild type (wt) *Escherichia coli* (*E. coli*) K12 strain BW25113 that does not naturally produce high levels of H<sub>2</sub>S. To create a strain producing high levels of H<sub>2</sub>S we transformed BW25113 with either pTrc99a (an Isopropyl β-D-1-thiogalactopyranoside {IPTG} inducible vector with no gene inserted upstream of the promoter), or pSB74 (pTrc99a carrying the thiosulfate reductase operon *phsABC* from *Salmonella enterica* serovar Typhimurium strain LT2). Overexpression of the *phsABC* operon in *E. coli* has previously been shown to produce high levels of H<sub>2</sub>S from inorganic thiosulfate, or sulfite [126].

The bacterial strains, BW25113 + pTrc99a (*E. coli*<sup>H<sub>2</sub>S-LOW</sup>), BW25113 + pSB74 (*E. coli*<sup>H<sub>2</sub>S-HI</sup>), were grown with the probes or luciferins (as a control) for 8 h anaerobically (BD GasPak EZ system) as a planktonic broth in either Luria Bertani



medium (LB) or EZ Rich Defined Medium (EZRD), the cultures were centrifuged and the supernatant was analyzed using BL and fluorescence imaging. To compare the performance of our probes with commercially available probes we used WSP-5 and 7-Az-4-MC and the corresponding fluorophores (fluorescein and 4-methylcoumarin) as controls (Figure 3.11). NaHS was used as a positive control, probe in buffer served as a negative control.

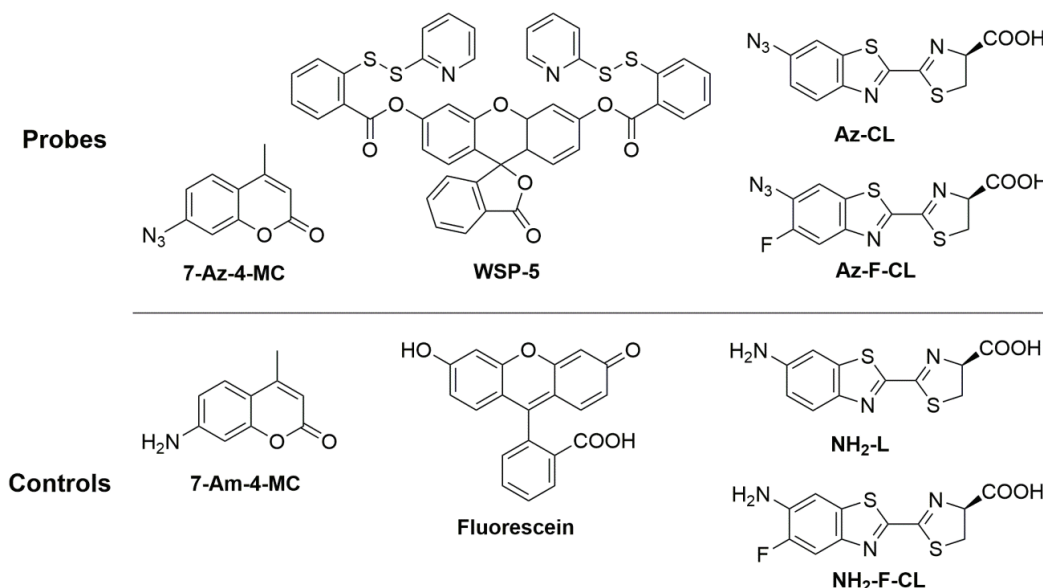


Figure 3.12 Structures of the probes used for the detection of H<sub>2</sub>S in the bacterial assay.

First, it was noted that all probes responded to H<sub>2</sub>S with a higher signal-to-background ratio in EZ Rich Defined Medium (EZRD) than in LB (Figure S3.11), especially from the positive control (NaHS). EZRD has a well-defined biochemical composition, which facilitates rapid growth of *E. coli*, with growth rates comparable to LB, which are not observed in standard M9 minimal medium. Importantly, this medium has less components that might react with H<sub>2</sub>S, e.g. thiol-containing peptides, that could interfere with H<sub>2</sub>S detection. We also quantified bacterial growth in LB and EZRD and no significant differences ( $p > 0.05$ ) between the growth rate in two media were observed (Figure S3.12).

As can be seen in Figure 3.12A both BL probes were capable of detecting H<sub>2</sub>S produced by bacteria with a similar sensitivity, despite the two fold higher background signal from Az-F-CL compared to Az-CL. Importantly, we detected between a 5-7 fold increase in BL signal from *E. coli*<sup>H<sub>2</sub>S-HI</sup> compared to *E. coli*<sup>H<sub>2</sub>S-LOW</sup>, which is in agreement with the original report describing the generation of H<sub>2</sub>S-overproducing *E. coli* DH5α [126]. Importantly, *E. coli*<sup>H<sub>2</sub>S-LOW</sup> showed a 3 fold increase in BL signal above the background signal which can be explained either by production of low levels of H<sub>2</sub>S by the 3-mercaptopyruvate sulfurtransferase (3-MST) [205] and by L-cysteine desulfhydrase [292] present in *E. coli* or by the reaction of probes with endogenous GSH and cysteine.

Although we did not quantify the absolute amount of H<sub>2</sub>S production in our bacterial growth assays, it can be estimated that the amount of H<sub>2</sub>S produced by *E. coli*<sup>H<sub>2</sub>S-HI</sup> over 8 h is below 500 μM, when compared to the positive control (500 μM NaHS), which is in relative agreement with the literature. *E. coli* DH5α + pSB74 has been reported to produce

377  $\mu\text{M}$  H<sub>2</sub>S in 5 h, and 389  $\mu\text{M}$  H<sub>2</sub>S in 24 h using a sulfide electrode [126]). We anticipate that the level of H<sub>2</sub>S can be quantified by constructing a standard curve (BL signal vs. NaHS concentration) and interpolating the measured values to obtain the concentration of H<sub>2</sub>S in the growth medium.

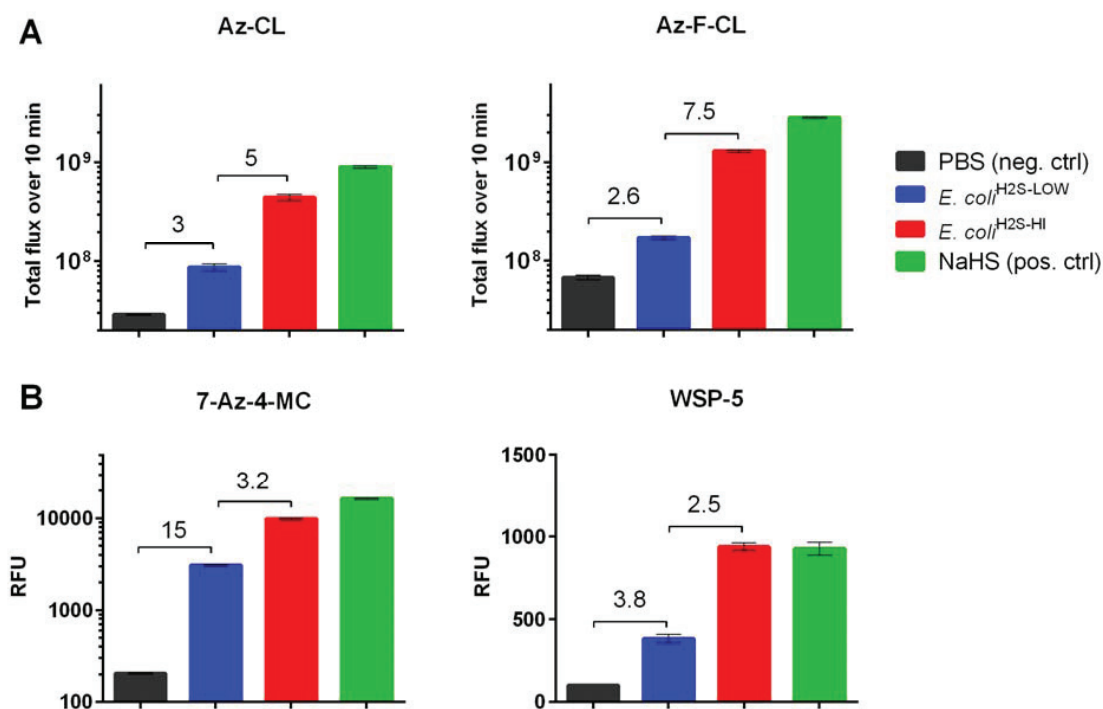


Figure 3.13 Imaging of H<sub>2</sub>S produced by bacteria after 8 h of culture with probes in EZ Rich Defined Medium (EZRD). (A) Total photon flux from 50  $\mu\text{M}$  CL probes in the culture supernatant measured after the addition of luciferase (62.5  $\mu\text{g}/\text{mL}$ ). (B) Fluorescence from control probes WSP-5 and 7-Az-4-MC (50  $\mu\text{M}$ ) in the culture supernatant. Numbers indicate the ratio of the mean values. The experiment was repeated three times, representative data is shown;  $n=3$ .

The control fluorescent probe 7-Az-4-MC has an azide and employs the same reaction for the detection of H<sub>2</sub>S as Az-CL probes. WSP-5 probe contains a disulfide group and detects H<sub>2</sub>S through sulfide-mediated nucleophilic addition followed by an intramolecular cyclization and release of the fluorophore. 7-Az-4-MC showed a lower background but a similar trend in signal as the caged luciferins (Figure 3.12B). By contrast, WSP-5 probe did not differentiate between the level of H<sub>2</sub>S produced by SL1344, *E. coli*<sup>H<sub>2</sub>S-HI</sup> and NaHS (positive control). The low level of sensitivity might be explained by the solubility issues previously described for this class of probes [128].

The data from the BL imaging correlated with the fluorescence of the caged luciferin probes (Figure S3.13), which means that both of these imaging modalities can be used for the detection of H<sub>2</sub>S production by bacteria.

### 3.4.9 Bioluminescence imaging of H<sub>2</sub>S in living mice

On the basis of results from the validation of caged luciferin probes in enzyme, cell and bacterial assays we sought to establish their efficacy for detecting H<sub>2</sub>S produced in the gastrointestinal tract (GIT) in living mice.

As discussed earlier, the Az-CL probe was recently reported for BLI of H<sub>2</sub>S in living mice in two studies, in one study the FLuc-tumors were used for the BL read-out and in another study a whole-body H<sub>2</sub>S imaging was performed after sequential injections of NaHS (IV) and the probe (IP) in mice ubiquitously expressing luciferase (FVB-luc+ mice).

It is important to consider that in our approach the detection of bioluminescence from the GIT might be potentially challenged by the depth of the gut tissues. We were encouraged by the study of fatty acid uptake in FVB-luc+ mice using the caged luciferin probe [55]. After administration of the probe by oral gavage (OG), it was absorbed in the gut and the released luciferin was distributed through the circulation and produced the signal from the whole body, which could be detected and quantified.

#### 3.4.9.1 Characterization of caged luciferin probes in living mice

All experiments were performed using FVB-Luc+ mice [47]. Because little is known about the signal kinetics of luciferin administered by OG in mice, we first focused on the characterization of signal produced from luciferin and probes in living mice over time.

Four groups of mice with three mice per group were used. The first two groups were orally gavaged with classical substrates OH-L and NH<sub>2</sub>-L (0.73  $\mu$ mol in 100  $\mu$ L of PEG400, at the dose equivalent to 0.2 mg/mouse of OH-L) and bioluminescence was measured until the disappearance of the signal (before the OG, at 0.5, 1, 6, 18, 24, 48 and 60 h time points post OG; Figure 3.13). When the initial time point (0.5 h) is taken as 100% intensity it can be estimated that after 6 h the amount of signal for OH-L decreased to  $42 \pm 8\%$ , while for NH<sub>2</sub>-L to  $20 \pm 6\%$ . After 18 h the signal for OH-L decreased to  $11 \pm 3\%$ , while for NH<sub>2</sub>-L to  $1.1 \pm 0.3\%$ , and at 48 h about 0.2% of the initial signal could be detected for both luciferins. It should be noted that the signal for OH-L decreased to the background level after 60 h.

The next two groups of mice were administered a slow-reacting probe Az-Bn-CL and a fast-reacting probe Az-CL. Notably, the signal from Az-Bn-CL was slowly increasing over the first 6 h, reached the maximum around 18 h and decreased with the same efficiency as for the OH-L. Az-CL probe showed similar signal kinetics as NH<sub>2</sub>-L, reaching the equal signal intensity at 18 h.

We have also performed the same kinetic studies for the Az-F-CL and NH<sub>2</sub>-F-L and a similar trend to Az-CL and NH<sub>2</sub>-L was observed (Figure S3.14).

In summary, this data shows that the clearance time for the free luciferins and probes after administration by OG is 2 to 3 days.

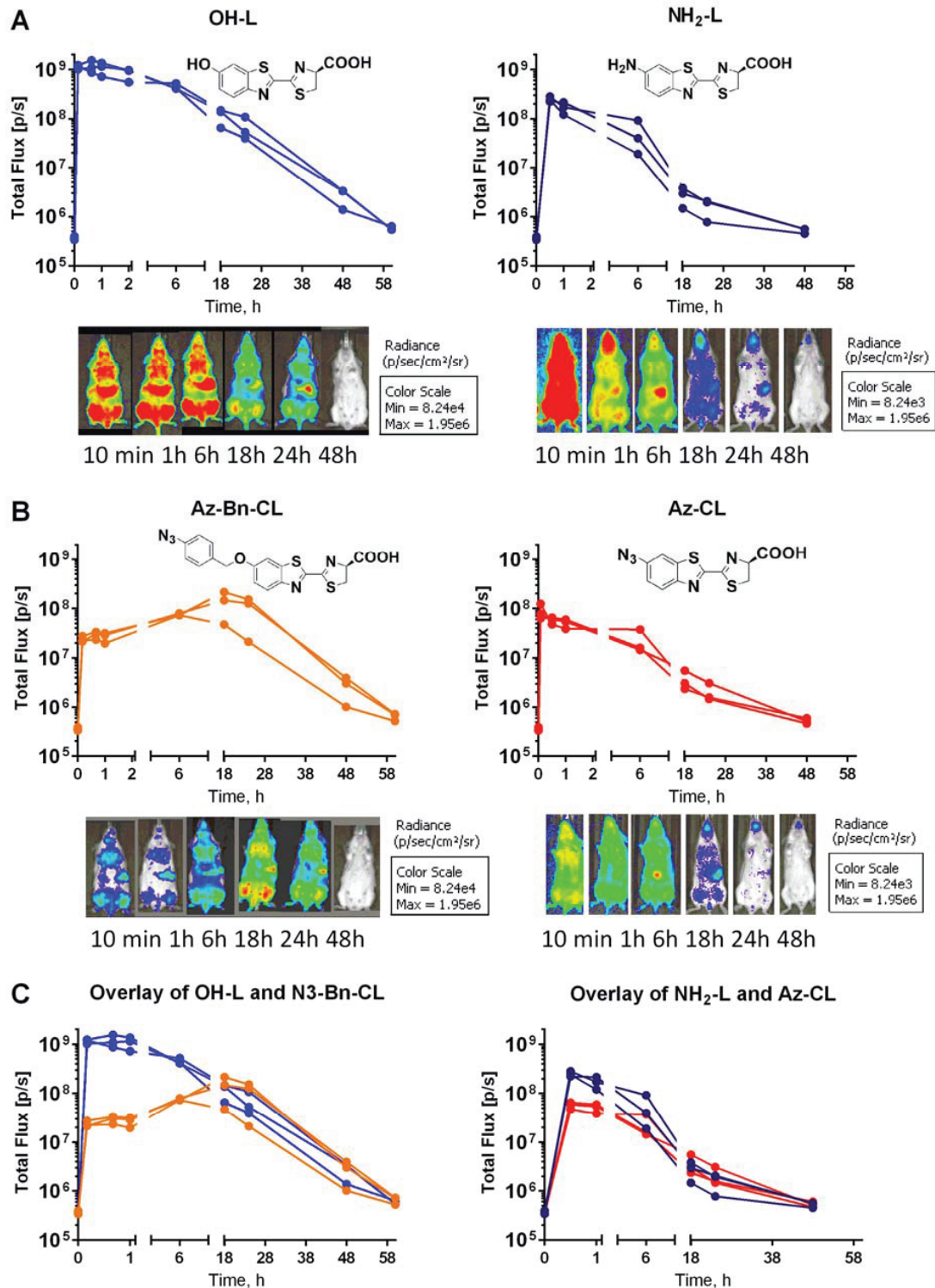


Figure 3.14 Kinetics of the bioluminescence signal produced from luciferins (A) or probes (B) in FVB-luc<sup>+</sup> mice (n = 3) over 60 h. (C) Overlay of the kinetic curves from (A) and (B). Luciferins or probes were administered by OG (0.73  $\mu$ mol in 100  $\mu$ L of PEG400) at the dose equivalent to 0.2 mg of OH-L. The color scales for ventral luminescent/photographic images were adjusted separately for OH-L/Az-Bn-CL group and for NH<sub>2</sub>-L/Az-CL group; n = 3.

As can be seen in the luminescence images of mice in Figure 3.13, both luciferins and probes produced a detectable signal from the whole body with a localized signal in the stomach area. As the compounds are administered by OG and stomach is the largest organ in the gut located closer to the surface than the other organs, it is likely to appear brighter in 2D bioluminescence imaging.

To compare the signal intensity produced from the probes and corresponding luciferins mice were orally gavaged with the compounds (0.73  $\mu$ mol in 100  $\mu$ L of PEG400, at the dose equivalent to 0.2 mg of OH-L) and the bioluminescence was acquired every min for 45 min. Az-Bn-CL and Az-CL produced the signal of a similar intensity, however, Az-F-CL produced a 40-fold higher signal (Figure 3.14). When the total photon flux over 45 min from the probes was compared to corresponding luciferins, it was calculated that Az-Bn-CL/OH-L pair had the largest signal window (82 times difference), followed by Az-CL/NH<sub>2</sub>-L (12 times) and Az-F-CL/NH<sub>2</sub>-F-L (7 times). As previously observed in cell assays (Figure 3.10), the low signal window for the Az-F-CL probe could be explained by its reactivity towards endogenous GSH.

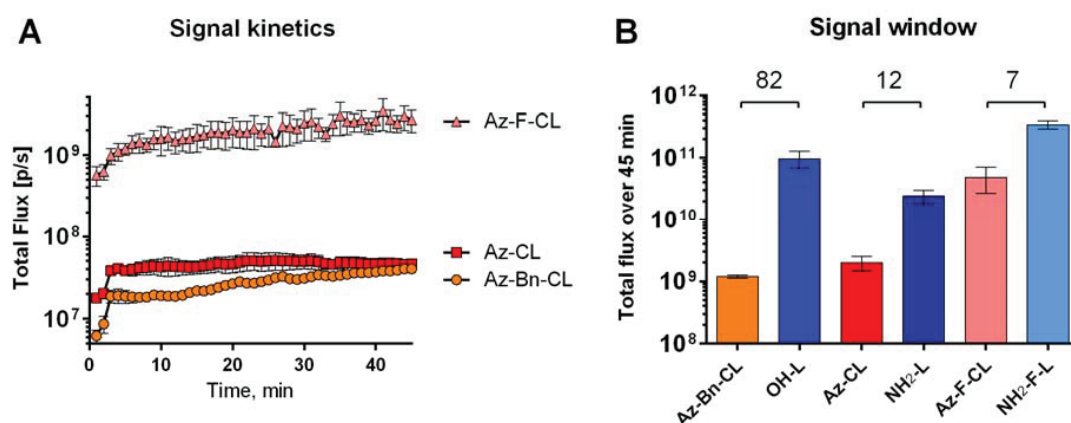


Figure 3.15 Comparison of BL signal produced from probes in FVB-luc<sup>+</sup> mice. (A) Signal kinetics from the CL probes over 45 min. (B) The BL signal window between probes and luciferins. Luciferins or probes were administered by OG (0.73  $\mu$ mol in 100  $\mu$ L of PEG400) at the dose equivalent to 0.2 mg of OH-L. Numbers indicate the ratio of the mean values,  $n = 2$ , mean  $\pm$  SEM.

To study the localization of the signal produced from the Az-Bn-CL and Az-CL probes in the gut, mice were sacrificed at 1 and 24 h post OG and the GI tract was excised from the stomach to the colon. Importantly, 1 h after the gavage of both probes the strongest signal localized to the cecum and colon was observed (Figure 3.15). This observation is in excellent agreement with the known location of sulfate-reducing bacteria populations in the mouse intestine [294]. It was also reported that average H<sub>2</sub>S concentrations in mouse gut varied from 0.1 mM (stomach) to 1 mM (cecum) [294] which might explain the residual signal from the stomach. Furthermore, the signal in the cecum could be detected even 24 h after the OG of the probes. Contrary to this, amino-luciferin (NH<sub>2</sub>-L) showed the signal of equal intensity through the whole GIT 1 h after OG and almost no signal 24 h after OG which points out to the specificity of the signal produced by the probes.

On the basis of the *in vitro* and *in vivo* data, the reactivity, selectivity and a bioluminescence signal window, we have selected Az-CL as the best performing probe for further experiments.



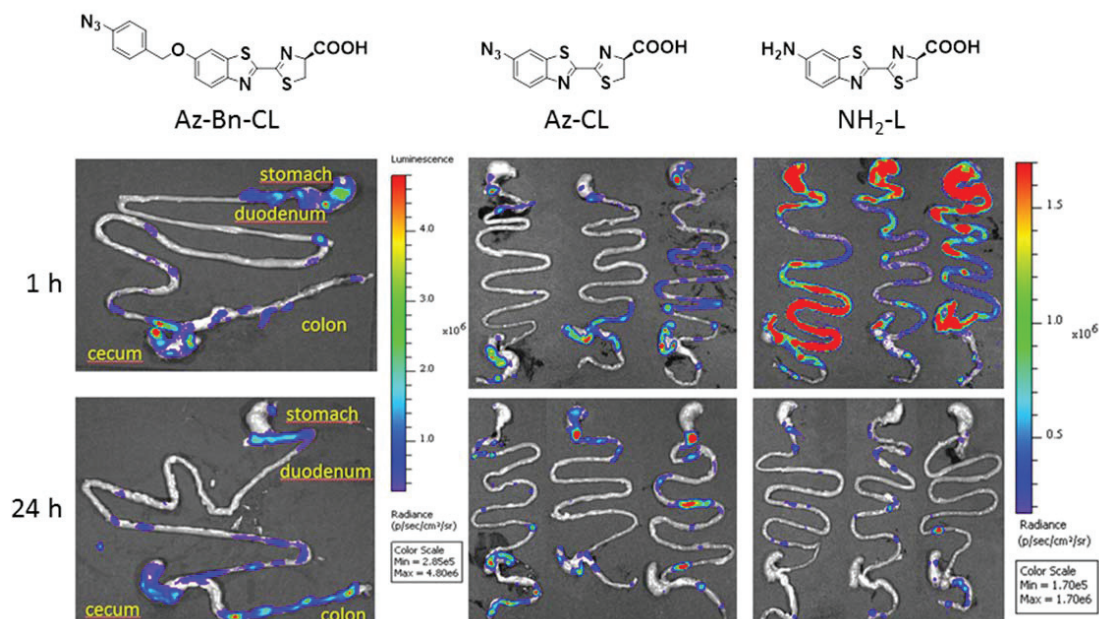


Figure 3.16 Localization of the BL signal produced from the Az-Bn-CL, Az-CL and NH<sub>2</sub>-L in the GIT of mice 1 and 24 h post OG (*ex vivo* imaging).

#### 3.4.9.2 Modulation of H<sub>2</sub>S level in the GIT of mice treated with H<sub>2</sub>S donor

To establish Az-CL as an *in vivo* H<sub>2</sub>S reporter, we next examined its ability to report on the H<sub>2</sub>S level in the GIT.

In the pilot study the efficiency of H<sub>2</sub>S detection was compared between Az-CL and Az-F-CL. Four groups of mice with two mice per group were used. Mice were fasted 16 to 18 h before the experiment as it was reported that fasting reduces the H<sub>2</sub>S level in the gut [226]. The dose of the probes was decreased 24 fold compared to the previous study (from 0.73  $\mu$ mol to 0.03  $\mu$ mol, 0.01 mg/ mouse). First, two mice in each group were administered the H<sub>2</sub>S donor solution (NaHS in HEPES pH 7.4, 40 equiv., 1.308  $\mu$ mol) and two mice received the buffer alone, 5 min after the probes were administered by OG to all mice and the bioluminescence was acquired for 2 h for the Az-F-CL probe (to follow the signal growth) and for 1.5 h for Az-CL (Figure 3.16). Despite showing the low signal window, the Az-F-CL probe gave a response to H<sub>2</sub>S, however, it was slow, reaching only 2-fold over 90 min. Notably, the Az-CL probe demonstrated a 3-fold lower background, a fast response which was detectable 15 min after probe gavage and reached 3.8-fold over 90 min. This data demonstrates that Az-CL is a better reporter than Az-F-CL for imaging of H<sub>2</sub>S in living mice.

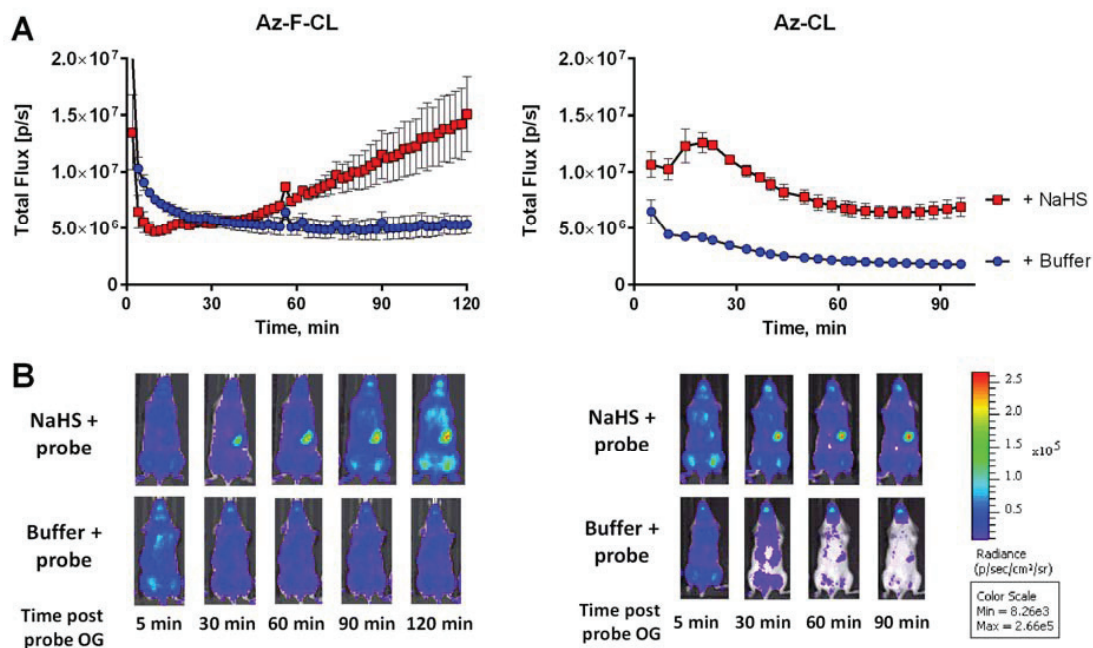


Figure 3.17 BLI of H<sub>2</sub>S using Az-F-CL and Az-CL in living mice treated with NaHS in comparison to the control. (A) Kinetics of the BL signal. (B) Overlay of ventral luminescent/ photographic images of mice. N= 2, data presented as mean  $\pm$  SEM. NaHS was administered by OG (40 equiv., 1.308  $\mu$ mol, 100  $\mu$ L of HEPES (pH 7.4)), 5 min later probes were administered by OG (0.03  $\mu$ mol, 0.01 mg, 100  $\mu$ L of HEPES with 2% DMSO).

Finally, we decided to apply Az-CL for H<sub>2</sub>S imaging in a setup when each mouse would serve as its own control. The experimental outline was similar to the previous experiment. One group of mice (n= 3) was first administered the buffer, followed by the probe, and imaged for 2 h. Three days after the same mice were administered NaHS solution, followed by the probe, and imaged again (Figure 3.17). When the mice were administered NaHS a steady increase in signal was detected, reaching 4-fold after 2 h. The total amount of signal produced from the NaHS treatment over 2 h was 3-fold higher than the background. Next, the imaging with amino-luciferin (NH<sub>2</sub>-L) was performed with the same mice, followed by NaHS + NH<sub>2</sub>-L imaging three days later, to check if NaHS treatment affects the BL signal. No difference in the total flux over 2 h was detected.

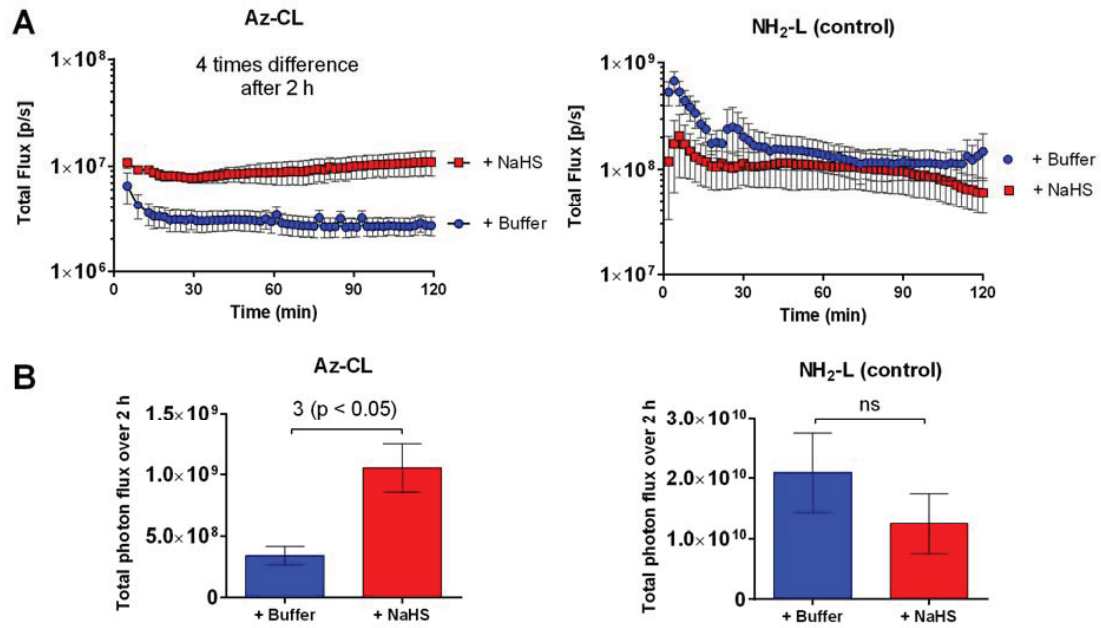


Figure 3.18 BLI of H<sub>2</sub>S using Az-CL in the GIT of living mice treated with NaHS. NH<sub>2</sub>-L was used to check the BL signal before and after the treatment. Each mouse served as its own control. (A) Kinetics of the BL signal. (B) Total photon flux measured over 2 h. N= 3, data presented as mean  $\pm$  SEM.



### 3.5 Conclusion

We rationally designed and synthesized a series of H<sub>2</sub>S-responsive caged luciferin probes, two of which were recently reported by other groups. We first evaluated the probes on the basis of two key parameters, the rate of the bioluminescence response to H<sub>2</sub>S and the selectivity of H<sub>2</sub>S detection over endogenous thiols *in vitro*.

The kinetic studies of the reaction between the two probes and H<sub>2</sub>S showed that the introduction of a single fluorine atom in *o*-position to the azide increased the reactivity of the probe with H<sub>2</sub>S by two-fold. This strategy allowed for the development of a fast responsive probe, Az-F-CL, with the limit of H<sub>2</sub>S detection of approximately 100 nM, that can be used for a quantitative analysis of H<sub>2</sub>S in a pre-incubation assay *in vitro*.

After initial validation the two best performing probes, Az-CL and Az-F-CL, were selected and further applied for the detection of H<sub>2</sub>S in live bacterial and mammalian cell-based assays, as well as in living animals. Both probes effectively detected H<sub>2</sub>S produced by bacteria in culture, while Az-F-CL provided a more sensitive read-out than Az-CL in mammalian cells.

We next characterized the signal produced from three probes (Az-Bn-CL, Az-CL, Az-F-CL) and three luciferins (OH-L, NH<sub>2</sub>-L, NH<sub>2</sub>-F-L) in living mice. The specificity of the signal produced from the Az-Bn-CL and Az-CL probes in the GIT was confirmed by *ex vivo* imaging.

Finally, we compared the efficiency of Az-CL and Az-F-CL for the detection of exogenous H<sub>2</sub>S in real-time in living mice and observed that Az-CL provided a better bioluminescence response to H<sub>2</sub>S than Az-F-CL. On the basis of these results we anticipate a further application of Az-CL probe for the detection of H<sub>2</sub>S in the GIT in living animals.

We believe that the results presented here will contribute to a better understanding of the caged luciferin probe design principles. When designing imaging probes it is important to consider the interplay between the reactivity and the selectivity, and, as demonstrated here, an increase in probe's reactivity might lead to a decrease in selectivity and narrow down the bioluminescence signal window in living systems.

**Note.** Parallel to this work two research groups have independently reported the development of bioluminescent probes for imaging of hydrogen sulfide (probes Az-Bn-CL and Az-CL) [103, 104].

### 3.6 Future development

The described caged luciferin probes can be applied in various areas of research. For example, the Az-F-CL probe could be used for the *in vitro* analysis of H<sub>2</sub>S levels or bacterial H<sub>2</sub>S production in environmental samples.

Another potential application of these probes could be screening of H<sub>2</sub>S-releasing drugs (e.g. novel anti-inflammatory drugs) in *in vitro* and *in vivo* assays to develop novel therapies for inflammatory bowel disease, hypertension and atherosclerosis.

Our future directions include application of the Az-CL probe for the detection of H<sub>2</sub>S production by gut microbiota in mice. It is of particular interest to investigate if the changes in the dietary composition could cause a change in the H<sub>2</sub>S production by bacteria and if these changes could be detected using Az-CL. For example, if the diet enriched with the sources of H<sub>2</sub>S, such as cysteine and sulfate, could cause an increase of H<sub>2</sub>S production in the GIT of mice. These assays could ultimately help to better understand the contribution of this signaling molecule to the pathogenesis of various gastrointestinal diseases, like ulcerative colitis and inflammatory bowel disease, and to develop new therapeutic approaches.

## 3.7 Experimental section

### 3.7.1 Chemical materials and methods

Chemicals were purchased from ABCR GmbH, Acros organics, Fluorochem, Sigma-Aldrich, and were used as received. Firefly luciferase was purchased from Sigma-Aldrich. Analytical thin layer chromatography was performed using glass-backed SiO<sub>2</sub> TLC plates from Merck. HPLC-MS analysis was performed either on Agilent Infinity 1260 HPLC system (Agilent, Santa Clara, CA) with SunFire® C18 column (2.6 × 20 mm, 3.5 μm, Waters) directly connected to Agilent 6120 Quadrupole LC/MS system (Agilent, Santa Clara, CA) or on Waters Acquity UPLC system with Acquity UPLC® BEH C18 column (2.1 × 50 mm, 1.7 μm) directly connected to Waters Acquity LC/MS system using HPLC gradient grade solvents from Fisher Chemicals (Loughborough, UK) and Millipore water. Purification of compounds was performed either on Agilent Infinity 1260 preparative HPLC system using Zorbax SB-C8 column (21.2 × 250 mm, 7 μm, Agilent) or on Waters preparative HPLC system using SunFire® PrepC18 OBD™ column (30 × 50 mm, 5 μm, Waters). Nuclear magnetic resonance (<sup>1</sup>H, <sup>13</sup>C, <sup>19</sup>F NMR) data were acquired on a Bruker AV400 MHz spectrometer. NMR chemical shifts are reported in the standard δ notation of parts per million using the peaks of residual proton and carbon signals of the solvent as internal references. Splitting patterns are designated as s (singlet), d (doublet), dd (doublet of doublets), t (triplet), m (multiplet). Coupling constants (*J*) are reported in hertz. HRESI-MS measurements were conducted at the EPFL ISIC Mass Spectrometry Service using Micro Mass QTOF Ultima (Waters Corp., Milford, MA).

**Known compounds:** the following compounds have previously been reported in the literature: 4, 5, 6, 7, 8, 9, 10, 11, 12, 13.

**(S)-2-(6-aminobenzo[104]thiazol-2-yl)-4,5-dihydrothiazole-4-carboxylic acid (4).** The compound was synthesized by a modified method described in [295]. To a solution of 2-cyano-6-aminobenzothiazole (0.020 g, 0.114 mmol) in THF (0.5 mL) was added a solution of D-cysteine (0.021 g, 0.171 mmol) in degassed H<sub>2</sub>O (1.0 mL) under N<sub>2</sub>. After 30 min the reaction was analyzed by HPLC-MS, full conversion to product was observed, crude reaction mixture was purified by preparative HPLC (C18 column, H<sub>2</sub>O+0.1% HCOOH:ACN, 5-95% ACN over 10 min), affording pure product **4** (0.023 g, 72%). <sup>1</sup>H NMR (400 MHz, (CD<sub>3</sub>)<sub>2</sub>SO) δ 7.77 (d, *J* = 8.9 Hz, 1H), 7.07 (d, *J* = 2.2 Hz, 1H), 6.85 (dd, *J* = 8.9, 2.2 Hz, 1H), 5.83 (s, 2H), 5.36 (dd, *J* = 9.7, 8.2 Hz, 1H), 3.72 (dd, *J* = 11.2, 9.7 Hz, 1H), 3.63 (dd, *J* = 11.2, 8.2 Hz, 1H). <sup>13</sup>C NMR (101 MHz, (CD<sub>3</sub>)<sub>2</sub>SO) δ 171.4, 164.3, 153.2, 149.3, 144.2, 137.8, 124.6, 115.9, 103.0, 78.0, 39.5, 34.6. HRMS: calculated for C<sub>11</sub>H<sub>11</sub>N<sub>3</sub>O<sub>2</sub>S<sub>2</sub> [MH]<sup>+</sup> 280.0215, found 280.0215; calculated for C<sub>11</sub>H<sub>9</sub>N<sub>3</sub>O<sub>2</sub>S<sub>2</sub>Na [MH]<sup>+</sup> 302.0034, found 302.0034. Data is consistent with the literature [104].

Compounds **5** and **6** were synthesized as previously described [103].

**6-azidobenzo[d]thiazole-2-carbonitrile (5).** To a suspension of 2-cyano-6-aminobenzothiazole (0.05 g, 0.285 mmol) in 6N HCl (0.5 mL) at 0 °C was added a solution of NaNO<sub>2</sub> (0.03 g, 0.428 mmol) in water (1 mL) dropwise and stirred for 30 min, then a solution of NaN<sub>3</sub> (0.037 g, 0.570 mmol) in water (1 mL) was added and the reaction was stirred at 0 °C. The reaction was followed by TLC, after completion (1 h) the solution was extracted with ethyl acetate (3 × 10 mL), the organic phase was washed with a NaHCO<sub>3</sub> saturated aqueous solution, then with brine and dried over MgSO<sub>4</sub>. The

evaporation of the solvent *in vacuo* gave azide **5** (0.055 g, 96%) which was used in the next step without purification. <sup>1</sup>H NMR (400 MHz, CDCl<sub>3</sub>) δ 8.18 (d, *J* = 8.9 Hz, 1H), 7.60 (d, *J* = 2.2 Hz, 1H), 7.31 (dd, *J* = 8.9, 2.2 Hz, 1H). Data is consistent with the literature [103].

**(S)-2-(6-azidobenzo[d]thiazol-2-yl)-4,5-dihydrothiazole-4-carboxylic acid (6).** To a solution of compound **5** (0.035 g, 0.174 mmol) in ACN (0.5 mL) was added a solution of D-cysteine (0.042 g, 0.348 mmol) in degassed PBS (0.5 mL) under N<sub>2</sub>. After 30 min, reaction mixture was diluted with water to the total volume of 2 mL and was purified by preparative HPLC (C8 column, H<sub>2</sub>O+0.1% HCOOH:ACN, 5-95% ACN over 33 min), affording pure product (0.035 g, 66%). <sup>1</sup>H NMR (400 MHz, (CD<sub>3</sub>)<sub>2</sub>SO) δ 13.25 (br s, 1H), 8.16 (d, *J* = 8.8 Hz, 1H), 8.05 (d, *J* = 1.7 Hz, 1H), 7.32 (dd, *J* = 8.8, 1.7 Hz, 1H), 5.44 (dd, *J* = 9.8, 8.3 Hz, 1H), 3.79 (dd, *J* = 11.3, 9.8 Hz, 1H), 3.71 (dd, *J* = 11.3, 8.3 Hz, 1H). <sup>13</sup>C NMR (101 MHz, (CD<sub>3</sub>)<sub>2</sub>SO) δ 171.0, 164.3, 160.3, 150.1, 139.0, 137.0, 125.2, 119.4, 112.7, 78.2, 34.8. HRMS: calculated for C<sub>11</sub>H<sub>7</sub>N<sub>5</sub>O<sub>2</sub>S<sub>2</sub> [MH]<sup>+</sup> 306.0119, found 306.0119. Data is consistent with the literature [104].

**(4-azidophenyl)methanol (7)** was prepared following the literature procedure [296]. To a solution of 4-aminobenzylalcohol (0.3 g, 2.436 mmol) in HCl 6N (3 mL) was added NaNO<sub>2</sub> (0.252 g, 3.654 mmol) in water (3 mL) dropwise at 0°C. The reaction was stirred at 0°C for 30 min, then NaN<sub>3</sub> (0.316 g, 4.872 mmol) in water (3 mL) was added dropwise. The reaction was followed by TLC and after 30 min the reaction mixture was extracted with EtOAc (3 × 10 mL), the organic phase was washed with a NaHCO<sub>3</sub> saturated aqueous solution, then with brine and dried over MgSO<sub>4</sub>. The evaporation of the solvent *in vacuo* gave the azide **7** in 79% yield (0.289 g) which was used without further purification. <sup>1</sup>H NMR (400 MHz, CDCl<sub>3</sub>) δ 7.31 (d, *J* = 8.2 Hz, 2H), 6.99 (d, *J* = 8.3 Hz, 2H), 4.60 (s, 2H), 2.40 (br, 1H). <sup>13</sup>C NMR (101 MHz, CDCl<sub>3</sub>) δ 139.4, 137.6, 128.6, 119.2, 64.6. Data is consistent with the literature [296].

**1-azido-4-(bromomethyl)benzene (8)** was prepared following the literature procedure [296]. (4-azidophenyl)methanol (0.289 g, 1.938 mmol) was dissolved in dry DCM (10 mL) under N<sub>2</sub> before PBr<sub>3</sub> (0.22 mL, 2.325 mmol) was added dropwise at rt. The reaction was followed by TLC, after completion (1 h) the reaction was quenched with a NaHCO<sub>3</sub> saturated aqueous solution. The organic phase was washed with water and then dried over MgSO<sub>4</sub> before evaporation of the solvent *in vacuo*. The crude material (0.22 g, 53%) was used in the next step without further purification. <sup>1</sup>H NMR (400 MHz, MeOD) δ 8.76 (d, *J* = 8.5 Hz, 2H), 8.36 (d, *J* = 8.5 Hz, 2H), 5.90 (s, 2H). <sup>13</sup>C NMR (101 MHz, MeOD) δ 141.1, 136.1, 131.7, 120.2, 33.8. Data is consistent with the literature [296].

**6-((4-Azidobenzyl)oxy)benzo[d]thiazole-2-carbonitrile (9).** To a stirred solution of 2-cyano-6-hydroxybenzothiazole (0.021 g, 0.118 mmol) in DMF (0.5 mL) at 0 °C was added K<sub>2</sub>CO<sub>3</sub> (0.036 g, 0.260 mmol), 5 min after the bromide **8** in DMF (0.5 mL) was added dropwise. After 30 min the reaction was put at rt and stirred at rt for 3.5 h. After the completion of the reaction (analyzed by HPLC-MS) the reaction mixture was poured in 0.5M HCl (20 mL), white precipitate was filtered through a glass filter, yielding pure product **9** (0.027 g, 75%). <sup>1</sup>H NMR (400 MHz, CDCl<sub>3</sub>) δ 8.10 (d, *J* = 9.1 Hz, 1H), 7.44 (d, *J* = 8.5 Hz, 2H), 7.41 (d, *J* = 2.5 Hz, 1H), 7.30 (dd, *J* = 9.1, 2.5 Hz, 1H), 7.07 (d, *J* = 8.5 Hz, 2H), 5.14 (s, 2H). <sup>13</sup>C NMR (101 MHz, CDCl<sub>3</sub>) δ 159.4, 147.2, 140.4, 137.5, 133.8, 132.5, 129.3, 126.1, 119.5, 119.1, 113.3, 104.4, 70.3. HRMS: calculated for C<sub>15</sub>H<sub>9</sub>N<sub>5</sub>OS [MH]<sup>+</sup> 308.0606, found 308.0602.

**(R)-2-(6-((4-Azidobenzyl)oxy)benzo[d]thiazol-2-yl)-4,5-dihydrothiazole-4-carboxylic acid (10).** To a solution of compound **9** (0.027 g, 0.087 mmol) in THF (0.5 mL) was added a solution of D-cysteine (0.021 g, 0.175 mmol) in degassed PBS (0.5 mL) under N<sub>2</sub>. After 2 h, reaction mixture was dissolved in ACN:H<sub>2</sub>O (7:3) and purified by preparative HPLC (C8 column, H<sub>2</sub>O+0.1% HCOOH:ACN, 5-95% ACN over 33 min), affording pure product **10** (0.027 g, 75%). <sup>1</sup>H NMR (400 MHz, (CD<sub>3</sub>)<sub>2</sub>SO) δ 8.05 (d, *J* = 9.0 Hz, 1H), 7.85 (d, *J* = 2.5 Hz, 1H), 7.53 (d, *J* = 8.5 Hz, 2H), 7.26 (dd, *J* = 9.0, 2.5 Hz, 1H), 7.16 (d, *J* = 8.5 Hz, 2H), 5.41 (dd, *J* = 9.8, 8.3 Hz, 1H), 5.19 (s, 2H), 3.77 (dd, *J* = 11.2, 9.8 Hz, 1H), 3.68 (dd, *J* = 11.2, 8.3 Hz, 1H). <sup>13</sup>C NMR (101 MHz, (CD<sub>3</sub>)<sub>2</sub>SO) δ 171.2, 164.3, 158.0, 157.9, 147.2, 139.2, 137.1, 133.4, 129.8, 124.8, 119.2, 117.5, 105.9, 78.2, 69.4, 34.8. HRMS: calculated for C<sub>18</sub>H<sub>13</sub>N<sub>5</sub>O<sub>3</sub>S<sub>2</sub> [M+H]<sup>+</sup> 412.0538, found 412.0537.

**4-azido-2,3,5,6-tetrafluorobenzaldehyde (11)** was prepared following the literature procedure [297]. A mixture of NaN<sub>3</sub> (0.30 g, 4.6 mmol) and pentafluorobenzaldehyde (0.88 g, 4.3 mmol) in acetone (8 mL) and water (3 mL) was refluxed for 8 h. The mixture was cooled, diluted with water (10 mL) and extracted with ether (3 × 10 mL). The organic phase was dried (MgSO<sub>4</sub>), the solvent was evaporated *in vacuo*. The crude was purified by flash chromatography (silica gel, 1:3 EtOAc: hexane) to give the product **11** (0.7 g, 67% yield) with 10% impurity (estimated by <sup>1</sup>H NMR).

**(4-azido-2,3,5,6-tetrafluorophenyl)methanol (12)** was prepared following the literature procedure [297]. A stirred solution of **11** (0.7 g, containing 0.63 g of **11**, 2.88 mmol) and (CH<sub>3</sub>)<sub>2</sub>NH·BH<sub>3</sub> (0.23 g, 3.45 mmol) in acetic acid (15 mL) was heated at 55 °C for 1 h. The solvent was removed by aspirator at 45 °C. The residue was dissolved in DCM (20 mL), washed with 5% Na<sub>2</sub>CO<sub>3</sub> (2 × 15 mL) and water (15 mL), dried (MgSO<sub>4</sub>), and evaporated to leave yellow oil which was purified by chromatography (silica gel, 1:3 EtOAc: hexane) to afford 0.623 g (63% yield) of the mixture, containing product **12** and impurity (2:1 estimated by <sup>1</sup>H NMR and <sup>19</sup>F NMR), which was used in the next step. <sup>1</sup>H NMR (400 MHz, CDCl<sub>3</sub>) δ 4.78 (s, 2H). <sup>19</sup>F NMR (376 MHz, CDCl<sub>3</sub>) δ -144.68 (m, 2F), -151.80 (m, 2F).

**1-azido-4-(chloromethyl)-2,3,5,6-tetrafluorobenzene (13)** was prepared following the literature procedure [297]. To a stirred solution of **12** (0.623 g, 2.82 mmol) in DCM at 0 °C was added SOCl<sub>2</sub> (0.67 g, 5.64 mmol) dropwise. The mixture was stirred at 0 °C for 1 h, then put at rt and stirred at rt for another 4 h. Then the reaction mixture was evaporated to dryness and the crude material was purified by chromatography (silica gel, 1:4 EtOAc: hexane) to give 0.24 g (34% yield) of the product **13** containing 15% of impurity (estimated by <sup>1</sup>H NMR). The product (0.08 g) was purified in 2 runs by preparative TLC (hexane) to give 0.07 g of **13** as a yellow liquid, which solidified at rt. <sup>1</sup>H NMR (400 MHz, CDCl<sub>3</sub>) δ 4.64 (t, 2H). <sup>13</sup>C NMR (101 MHz, CDCl<sub>3</sub>) δ 145.1 (m), 140.7 (m), 120.9 (m, *J* = 12.1 Hz), 111.8 (t, *J* = 17.4, 17.4 Hz), 31.7 (m, *J* = 4.1, 4.1, 2.2, 2.2 Hz).

**6-((4-azido-2,3,5,6-tetrafluorobenzyl)oxy)benzo[d]thiazole-2-carbonitrile (14).** A mixture of compound **13** (0.069 g, 0.29 mmol), 2-cyano-6-hydroxybenzothiazole (0.046 g, 0.264 mmol), and K<sub>2</sub>CO<sub>3</sub> (0.073 g, 0.523 mmol) in anhydrous acetone (1 mL) under N<sub>2</sub> was stirred at rt for 3 h, then 0.01 g of **13** was added and the reaction mixture was stirred at rt overnight. The reaction mixture was filtered, evaporated to dryness, the solid material was washed and sonicated with hexane (3 × 3 mL) and dried *in vacuo* to afford the product **14** (0.084 g, 84% yield). <sup>1</sup>H NMR (400 MHz, CDCl<sub>3</sub>) δ 8.12 (d, *J* = 9.1 Hz, 1H), 7.48 (d, *J* = 2.5 Hz, 1H), 7.27 (dd, *J* = 9.1 Hz, 2.5 Hz, 1H), 5.22 (s, 2H). <sup>13</sup>C NMR (101 MHz, CDCl<sub>3</sub>) δ 158.6, 147.5, 145.6 (d, *J*<sub>CF</sub> = 250.5 Hz), 140.5 (dd, *J*<sub>CF</sub> = 250.5 Hz, <sup>2</sup>*J*<sub>CF</sub> = 17.2 Hz), 137.3, 134.2, 126.2, 121.4, 118.6,

113.0, 109.4 (t,  $^2J_{CF}$  = 17.2 Hz), 104.6, 58.3. **<sup>19</sup>F NMR** (376 MHz, CDCl<sub>3</sub>) δ -145.81 (m, 2F), -154.38 (m, 2F), C<sub>6</sub>F<sub>6</sub> (-164.90) was used as internal standard. **HRMS**: calculated for C<sub>15</sub>H<sub>5</sub>F<sub>4</sub>N<sub>5</sub>OS for [M+H]<sup>+</sup> 380.0229, found 380.0235.

**(S)-2-(6-((4-azido-2,3,5,6-tetrafluorobenzyl)oxy)benzo[d]thiazol-2-yl)-4,5-dihydrothiazole-4-carboxylic acid (15)**. To a solution of compound **14** (0.038 g, 0.10 mmol) in THF (2.2 mL) was added a solution of D-cysteine (0.029 g, 0.24 mmol) in degassed water (0.6 mL) under N<sub>2</sub>. After 1 h the solvent was evaporated, the crude material was sonicated in water and filtered. The crude was purified by preparative HPLC (C18 column, H<sub>2</sub>O+0.1% HCOOH:ACN, 5-95% ACN over 10 min), affording pure product **15** (0.029 g, 61% yield). **<sup>1</sup>H NMR** (400 MHz, (CD<sub>3</sub>)<sub>2</sub>SO) δ 13.23 (s, 1H), 8.09 (d,  $J$  = 9.0 Hz, 1H), 7.94 (d,  $J$  = 2.6 Hz, 1H), 7.27 (dd,  $J$  = 9.0, 2.6 Hz, 1H), 5.42 (dd,  $J$  = 9.8, 8.3 Hz, 1H), 5.30 (s, 2H), 3.78 (dd,  $J$  = 11.3, 9.8 Hz, 1H), 3.69 (dd,  $J$  = 11.3, 8.3 Hz, 1H). **<sup>13</sup>C NMR** (101 MHz, (CD<sub>3</sub>)<sub>2</sub>SO) δ 171.6, 164.8, 159.0, 157.7, 148.2, 145.4 (m,  $J_{CF}$  = 248.5 Hz), 140.6 (m,  $J_{CF}$  = 250.5 Hz), 137.5, 125.4, 121.4 (m), 117.7, 110.1 (t,  $^2J_{CF}$  = 18.0 Hz), 106.8, 78.7, 58.6, 35.3. **<sup>19</sup>F NMR** (376 MHz, (CD<sub>3</sub>)<sub>2</sub>SO) δ -146.19 (dd,  $J$  = 22.5, 9.7 Hz), -154.30 (dd,  $J$  = 22.5, 9.7 Hz), C<sub>6</sub>F<sub>6</sub> (-164.90) was used as internal standard. **HRMS**: calculated for C<sub>18</sub>H<sub>9</sub>F<sub>4</sub>N<sub>5</sub>O<sub>3</sub>S<sub>2</sub> [M+Na]<sup>+</sup> 505.9981, found 505.9986.

**6-(2,4-dinitrophenoxy)benzo[d]thiazole-2-carbonitrile (16)**. To a solution of 2-cyano-6-hydroxybenzothiazole (0.03 g, 0.170 mmol) and K<sub>2</sub>CO<sub>3</sub> (0.026 g, 0.187 mmol) in anhydrous acetone (1 mL) under N<sub>2</sub> was added 1-fluoro-2,4-dinitrobenzene (23.5 μL, 0.187 mmol) stirred at rt for 0.5 h, then the reaction mixture was filtered through 0.22 μm filter, the filtrate was evaporated *in vacuo*, the crude material was purified by silica gel column chromatography (starting with 1:8 EtOAc: hexane, the product eluted at 1:4) to give the product **16** (0.049 g, 84%). **<sup>1</sup>H NMR** (400 MHz, CDCl<sub>3</sub>) δ 8.90 (s, 1H), 8.41 (d,  $J$  = 9.1 Hz, 1H), 8.32 (d,  $J$  = 9.0 Hz, 1H), 7.73 (s, 1H), 7.45 (d,  $J$  = 9.0 Hz, 1H), 7.16 (d,  $J$  = 9.1 Hz, 1H). **<sup>13</sup>C NMR** (101 MHz, CDCl<sub>3</sub>) δ 154.8, 154.5, 150.2, 142.8, 140.5, 137.4, 137.3, 129.2, 127.4, 122.4, 121.1, 120.1, 112.6, 77.5, 77.2, 76.8, 29.9.

**(S)-2-(6-(2,4-dinitrophenoxy)benzo[d]thiazol-2-yl)-4,5-dihydrothiazole-4-carboxylic acid (17)**. To a solution of compound **16** (0.026 g, 0.076 mmol) in THF (0.5 mL) was added a solution of D-cysteine (0.010 g, 0.076 mmol) in degassed water (0.3 mL) under N<sub>2</sub>. After 1.5 h the HPLC-MS analysis showed disappearance of starting material, the crude mixture was diluted with water and purified by preparative HPLC (C8 column, H<sub>2</sub>O+5 mM NH<sub>4</sub>COOH:ACN, 5-95% ACN over 33 min), affording pure product **17** (0.019 g, 54% yield). **<sup>1</sup>H NMR** (400 MHz, (CD<sub>3</sub>)<sub>2</sub>SO) δ 8.93 (d,  $J$  = 2.7 Hz, 1H), 8.47 (dd,  $J$  = 9.3, 2.8 Hz, 1H), 8.29 (d,  $J$  = 8.9 Hz, 1H), 8.15 (d,  $J$  = 2.4 Hz, 1H), 7.54 (dd,  $J$  = 8.8, 2.5 Hz, 1H), 7.37 (d,  $J$  = 9.3 Hz, 1H), 5.44 (t,  $J$  = 9.1, 9.1 Hz, 1H), 3.80 (t,  $J$  = 10.6, 10.6 Hz, 1H), 3.72 (t,  $J$  = 11.2, 8.4 Hz, 1H). **<sup>13</sup>C NMR** (101 MHz, (CD<sub>3</sub>)<sub>2</sub>SO) δ 171.1, 164.1, 161.4, 154.4, 153.0, 150.4, 142.0, 139.8, 137.0, 129.8, 125.9, 122.0, 120.5, 120.2, 113.9, 78.5, 35.0.

**(Z)-N-(2-bromo-5-fluoro-4-nitrophenyl)-4-chloro-5H-1,2,3-dithiazol-5-imine (18)** was prepared following a modified method described in [295]. 4,5-Dichloro-1,2,3-dithiazole (0.781 g, 3.74 mmol) and 2-bromo-5-fluoro-4-nitroaniline (0.800 g, 3.40 mmol) were added to a 100 mL round-bottom flask and placed under N<sub>2</sub>. Dry DCM (6 mL) was then added and the resulting solution was stirred for 10 min at rt, then dry pyridine (0.55 mL, 6.80 mmol) was added drop-wise to the flask. The mixture was stirred for 2 h (when TLC with 3:7 EtOAc: hexane indicated no starting aniline), the solvent was evaporated *in vacuo*. The crude material was purified by silica gel column chromatography (eluting with 1:9 to 1:1 DCM: hexane, the product eluted at 1:1) to provide **18** as a bright dark-yellow solid (1.160 g, 92%). **<sup>1</sup>H NMR**

(400 MHz, CDCl<sub>3</sub>)  $\delta$  8.42 (d,  $J$  = 7.5 Hz, 1H), 7.04 (d,  $J$  = 11.2 Hz, 1H). **<sup>13</sup>C NMR** (101 MHz, CDCl<sub>3</sub>)  $\delta$  163.2, 156.0 (d,  $J_{CF}$  = 269.1 Hz), 156.0 (d,  $J_{CF}$  = 9.25 Hz), 147.3, 134.2 (d,  $J_{CF}$  = 7.9 Hz), 131.4 (d,  $J_{CF}$  = 2.2 Hz), 109.8 (d,  $J_{CF}$  = 3.8 Hz), 108.4 (d,  $J_{CF}$  = 23.8 Hz). **<sup>19</sup>F NMR** (376 MHz, CDCl<sub>3</sub>)  $\delta$  -117.32 (s), C<sub>6</sub>F<sub>6</sub> (-164.90) was used as internal standard **HRMS**: calculated for C<sub>8</sub>H<sub>2</sub>BrClFN<sub>3</sub>O<sub>2</sub>S<sub>2</sub> [M+H]<sup>+</sup> 371.8499, found 371.8506.

**5-fluoro-6-nitrobenzo[d]thiazole-2-carbonitrile (19)** was prepared following the method for the synthesis of 2-cyanobenzothiazoles described in [298]. To a 10 mL microwave vessel with a stir-bar was added CuI (0.086 g, 0.45 mmol) and compound **18** (0.152 g, 0.41 mmol) in dry pyridine. The microwave irradiation synthesis was carried out in a CEM–Discover monomode microwave synthesizer. The reaction vessel was sealed with a Teflon septum and placed in the microwave cavity. The reaction mixture was irradiated at 90 W, 110 °C for 15 min, then the reaction was cooled to rt with gas jet cooling. The solvent was evaporated *in vacuo*, the crude mixture was washed with EtOAc (5 × 20 mL), the organic phase was filtered through a celite cake (1 cm), the filtrate was evaporated and the crude material was purified by silica gel column chromatography (starting with 1:9 to 1:3 EtOAc: hexane, the product eluted at 1:3) to provide **19** as a light-yellow solid (0.05 g, 55%). In some cases the crude material (analyzed by <sup>1</sup>H NMR) was used in the next step without further purification. Aqueous workup was avoided as it led to the hydrolysis of the product and formation of the amide (analyzed by HPLC-MS). **<sup>1</sup>H NMR** (400 MHz, CDCl<sub>3</sub>)  $\delta$  8.77 (d,  $J$  = 6.7 Hz, 1H), 8.14 (d,  $J$  = 10.4 Hz, 1H). **<sup>13</sup>C NMR** (101 MHz, CDCl<sub>3</sub>)  $\delta$  155.1 (d,  $J_{CF}$  = 11.7 Hz), 155.0 (d,  $J_{CF}$  = 264.5 Hz), 143.5, 138.1 (d,  $J_{CF}$  = 10.9 Hz), 130.5 (d,  $J_{CF}$  = 2.5 Hz), 120.4 (d,  $J_{CF}$  = 1.6 Hz), 113.9 (d,  $J_{CF}$  = 23.4 Hz), 111.7. **<sup>19</sup>F NMR** (376 MHz, CDCl<sub>3</sub>)  $\delta$  -120.48 (dd,  $J_{HF}$  = 10.3, 6.7 Hz), C<sub>6</sub>F<sub>6</sub> (-164.90) was used as internal standard in <sup>19</sup>F-NMR studies.

**6-amino-5-fluorobenzo[d]thiazole-2-carbonitrile (20)** was prepared following the procedure described in [299]. A mixture of **19** (0.038 g, 0.17 mmol) and SnCl<sub>2</sub>·2H<sub>2</sub>O (0.545 g, 2.41 mmol) in EtOAc (3 mL) was heated at 70 °C under N<sub>2</sub>, the reaction was analyzed by TLC and HPLC-MS, after 2 h when the starting material disappeared, the reaction was stopped, the reaction mixture was cooled down, saturated aqueous solution of NaHCO<sub>3</sub> was added dropwise on ice till pH 6-7 (white precipitate was formed), the reaction mixture was extracted with EtOAc (3 × 10 mL), the organic phase was separated, washed with brine, dried over Na<sub>2</sub>SO<sub>4</sub>, the solvent was evaporated *in vacuo*, the crude material was purified by silica gel column chromatography (starting with 1:9 EtOAc: hexane, the product eluted at 3:7) to provide **20** as a bright yellow-orange solid (0.027 g, 82%). **<sup>1</sup>H NMR** (400 MHz, (CD<sub>3</sub>)<sub>2</sub>CO)  $\delta$  7.82 (d,  $J$  = 11.5 Hz, 1H), 7.49 (d,  $J$  = 8.3 Hz, 1H), 5.70 (s, 2H). **<sup>13</sup>C NMR** (101 MHz, (CD<sub>3</sub>)<sub>2</sub>CO)  $\delta$  153.5 (d,  $J_{CF}$  = 242.4 Hz), 144.5 (d,  $J_{CF}$  = 12.2 Hz), 140.6 (d,  $J_{CF}$  = 15.4 Hz), 134.6, 132.3 (d,  $J_{CF}$  = 1.0 Hz), 114.4, 110.5 (d,  $J_{CF}$  = 21.6 Hz), 105.20 (d,  $J_{CF}$  = 5.0 Hz). **<sup>19</sup>F NMR** (376 MHz, (CD<sub>3</sub>)<sub>2</sub>CO)  $\delta$  -133.53, C<sub>6</sub>F<sub>6</sub> (-164.90) was used as internal standard. **HRMS**: calculated for C<sub>8</sub>H<sub>4</sub>FN<sub>3</sub>S [M+H]<sup>+</sup> 194.0188, found 194.0186.

**6-azido-5-fluorobenzo[d]thiazole-2-carbonitrile (21)**. To a suspension of benzothiazole **20** (0.064 g, 0.331 mmol) in 6N HCl (2 mL) at 0 °C was added a solution of NaNO<sub>2</sub> (0.034 g, 0.497 mmol) in water (1 mL) dropwise and stirred for 30 min, then a solution of NaN<sub>3</sub> (0.043 g, 0.663 mmol) in water (1 mL) was added, the reaction was stirred at 0 °C. The reaction was followed by TLC, after completion (1 h) the solution was extracted with ethyl acetate (3 × 10 mL), the organic phase was washed with brine and dried over Na<sub>2</sub>SO<sub>4</sub>, evaporation of the solvent *in vacuo* gave crude material which was purified by silica gel column chromatography (starting with 1:9 EtOAc: hexane, the product eluted first, **20**



eluted at 2:8) to provide the azide **21** (0.053 g, 74%). <sup>1</sup>H NMR (400 MHz, CDCl<sub>3</sub>) δ 7.92 (d, *J* = 10.7 Hz, 1H), 7.63 (d, *J* = 7.5 Hz, 1H). <sup>13</sup>C NMR (101 MHz, CDCl<sub>3</sub>) δ 155.3 (d, *J*<sub>CF</sub> = 252.0 Hz), 149.5 (d, <sup>3</sup>*J*<sub>CF</sub> = 11.7 Hz), 137.5, 132.0 (d, <sup>4</sup>*J*<sub>CF</sub> = 1.9 Hz), 131.2 (d, <sup>2</sup>*J*<sub>CF</sub> = 13.8 Hz), 112.5, 112.4 (d, <sup>3</sup>*J*<sub>CF</sub> = 2.2 Hz), 112.0 (d, <sup>2</sup>*J*<sub>CF</sub> = 21.9 Hz). <sup>19</sup>F NMR (376 MHz, CDCl<sub>3</sub>) δ -126.64 (s), C<sub>6</sub>F<sub>6</sub> was used as internal standard (-164.90).

**(S)-2-(6-azido-5-fluorobenzo[d]thiazol-2-yl)-4,5-dihydrothiazole-4-carboxylic acid (22).** To a solution of compound **21** (0.041 g, 0.187 mmol) in THF (1.5 mL) was added a solution of D-cysteine (0.023 g, 0.187 mmol) in degassed water (0.5 mL) under N<sub>2</sub>. After 1 h the HPLC-MS analysis showed the disappearance of starting material **19**, the crude mixture was diluted with water and purified by preparative HPLC (C18 column, H<sub>2</sub>O+0.1% HCOOH:ACN, 5-95% ACN over 10 min), affording pure product **22** (0.039 g, 65% yield). <sup>1</sup>H NMR (400 MHz, (CD<sub>3</sub>)<sub>2</sub>SO) δ 8.26 (d, *J* = 8.1 Hz, 1H), 8.19 (d, *J* = 11.5 Hz, 1H), 5.45 (dd, *J* = 9.8, 8.3 Hz, 1H), 3.80 (dd, *J* = 11.3, 9.8 Hz, 1H), 3.71 (dd, *J* = 11.3, 8.3 Hz, 1H). <sup>13</sup>C NMR (101 MHz, (CD<sub>3</sub>)<sub>2</sub>SO) δ 171.0, 164.2, 162.3, 153.4 (d, *J*<sub>CF</sub> = 247.0 Hz), 149.8 (d, <sup>3</sup>*J*<sub>CF</sub> = 11.7 Hz), 132.1, 128.4 (d, <sup>2</sup>*J*<sub>CF</sub> = 13.2 Hz), 114.5, 111.0 (d, <sup>2</sup>*J*<sub>CF</sub> = 21.3 Hz), 78.2, 34.9. <sup>19</sup>F NMR (376 MHz, (CD<sub>3</sub>)<sub>2</sub>SO) δ -128.88 (dd, *J*<sub>HF</sub> = 11.5, 8.1 Hz), C<sub>6</sub>F<sub>6</sub> was used as internal standard (-164.90). HRMS: calculated for C<sub>11</sub>H<sub>6</sub>FN<sub>5</sub>O<sub>2</sub>S<sub>2</sub> [M+H]<sup>+</sup> 324.0025, found 324.0027.

**(S)-2-(6-amino-5-fluorobenzo[d]thiazol-2-yl)-4,5-dihydrothiazole-4-carboxylic acid (23).** To a solution of compound **20** (0.082 g, 0.424 mmol) in THF (3 mL) was added a solution of D-cysteine (0.051 g, 0.424 mmol) in degassed water (1.5 mL) under N<sub>2</sub>. After 1 h the HPLC-MS analysis showed disappearance of starting material, the crude mixture was diluted with water and purified by preparative HPLC (C18 column, H<sub>2</sub>O+0.1% HCOOH:ACN, 5-95% ACN over 10 min), affording pure product **23** (0.080 g, 64% yield). <sup>1</sup>H NMR (400 MHz, (CD<sub>3</sub>)<sub>2</sub>SO) δ 13.19 (broad, 1H), 7.83 (d, *J* = 11.8 Hz, 1H), 7.30 (d, *J* = 8.5 Hz, 1H), 5.91 (s, 2H), 5.37 (dd, *J* = 9.7, 8.2 Hz, 1H), 3.68 (m, 2H). <sup>13</sup>C NMR (101 MHz, (CD<sub>3</sub>)<sub>2</sub>SO) δ 171.3, 164.1, 155.8, 151.3 (d, *J*<sub>CF</sub> = 240.4 Hz), 143.3 (d, <sup>3</sup>*J*<sub>CF</sub> = 12.1 Hz), 138.3 (d, <sup>2</sup>*J*<sub>CF</sub> = 15.4 Hz), 133.1, 109.3 (d, <sup>2</sup>*J*<sub>CF</sub> = 20.9 Hz), 104.7 (d, <sup>3</sup>*J*<sub>CF</sub> = 5.2 Hz), 78.1, 34.6. <sup>19</sup>F NMR (376 MHz, (CD<sub>3</sub>)<sub>2</sub>SO) δ -134.93 (dd, *J*<sub>HF</sub> = 11.8, 8.5 Hz). C<sub>6</sub>F<sub>6</sub> was used as internal standard (-164.90). HRMS: calculated for C<sub>11</sub>H<sub>8</sub>FN<sub>3</sub>O<sub>2</sub>S<sub>2</sub> [M+H]<sup>+</sup> 298.0120, found 298.0124.

### 3.7.2 General materials and methods

Buffers used for the preparation of solutions of H<sub>2</sub>S were degassed by vigorous sparging with N<sub>2</sub> (for at least 30 min). Anhydrous sodium hydrogen sulfide (NaSH) was purchased from Strem Chemicals and was used to prepare H<sub>2</sub>S solutions. Because of volatility and potential oxidation of sulfide, all solutions were prepared in degassed buffer immediately prior to use. WSP-5 probe was purchased from Cayman Chemical, 7-Az-4-MC probe was purchased from Sigma-Aldrich. Stock solutions of the probes and luciferins were prepared in DMSO (10 mM) and stored at -20 °C until immediately prior to use. Recombinant firefly luciferase was purchased from Sigma-Aldrich, the aliquots were prepared at the concentration of 2 mg/mL in Tris pH 7.8 and stored at -20 °C. Luciferase was desalted using Zeba™ Spin Desalting Columns, 7K MWCO (Thermo Fisher Scientific) to remove DTT which contributes to azide reduction the assays. The luciferase buffer containing 2 mM ATP, 5 mM MgSO<sub>4</sub> (final concentrations) in 100 mM Tris pH 7.8 was prepared immediately prior to use.

**Kinetic analysis of the reaction between probes and H<sub>2</sub>S.** The reactions between probes (50 μM final concentration) and NaHS (5, 7.5, 10 mM final concentration) were monitored by HPLC-MS analysis. HPLC-MS analysis was performed



using Waters Acquity UPLC system with Acquity UPLC® BEH C18 column (2.1 × 50 mm, 1.7 μm) directly connected to Waters Acquity LC/MS system. Conditions of the method were the following: mobile phase H<sub>2</sub>O+0.1% FA:ACN, 5:95% ACN over 2 min, injection volume 3 μL and flow rate 1 mL/min. Standard curves for luciferins were constructed by plotting the peak areas (absorbance) vs. diluted concentrations (in a range of 1- 50 μM) prepared from 10 mM stock solutions in DMSO. Stock solutions of NaHS were prepared in a degassed buffer (bubbling N<sub>2</sub> for 30 min). The reactions were carried out in PIPES buffer (50 mM PIPES, 100 mM KCl, pH 7.4) at room temperature with caffeine (50 μM) added as a reference. The reaction was initiated by adding sulfide solution (200 μL) to the probe solution (200 μL) in a sealed glass vial, total reaction volume 400 μL. The reaction was analyzed at 120, 360, 600 and 840 s post-sulfide addition, time between HPLC runs was 240±5 s. The pseudo-first-order rate constants ( $k_{\text{obs}}$ ) were determined as slopes of the plot of ln of concentrations of the substrate vs. reaction time. The second rate constants ( $k_2$ ) were determined as slopes of the plot of  $k_{\text{obs}}$  vs. [NaHS].

**BL detection of H<sub>2</sub>S after pre-incubation with probes in luciferase assay.** Solutions of the probes (25 μL, 10 μM final) or corresponding luciferins (25 μL, 10 μM final) were added to 25 μL of NaHS solutions of the indicated final concentrations (0.01 to 1 mM) in the Tris pH 7.8 in a 96 well-plate, the plate was sealed with an aluminum tape (Corning). After incubation for 60 min at RT 50 μL of the Tris buffer containing 50 μg/ mL luciferase, 2 mM ATP, 5 mM MgSO<sub>4</sub> was added to the 50 μL solutions in the plate and the acquisition of BL started immediately for 60 min using IVIS 100.

**BL detection of H<sub>2</sub>S in real-time in luciferase assay.** Solutions of the probes (25 μL, 10 μM final) or corresponding luciferins (25 μL, 10 μM final) (as a control) were added to 25 μL of NaHS solutions of the indicated final concentrations (0.01 to 0.5 mM) in the Tris pH 7.8 using two multichannel pipettes in a 96 well-plate. Then 50 μL of the Tris buffer containing 50 μg/ mL luciferase, 2 mM ATP, 5 mM MgSO<sub>4</sub> was added to the 50 μL solutions in the plate and the acquisition of bioluminescence started immediately for 90 min using IVIS 100.

**Selectivity to biothiols.** In the 96 well-plate 25 μL of the probes (5 μM final) or corresponding luciferins (0.5 μM final) (as a control) were added to 25 μL of biothiols of the indicated final concentrations (0.1, 1 or 10 mM) in the Tris pH 7.8. After incubation for 20, 40, or 60 min 50 μL of the Tris buffer containing 100 μg/ mL luciferase, 2 mM ATP, 5 mM MgSO<sub>4</sub> was added to 50 μL of the mixture containing probes or luciferins and the bioluminescence was acquired for 60 min using IVIS 100.

**Cell lines and cell culture.** C2C12-FLuc cells were kindly provided by Prof. Aebischer (EPFL, Lausanne, Switzerland). Cells were cultured in DMEM with 10% heat-inactivated FBS and 1% P/S and subcultured at 60-70% confluency.

**BLI of H<sub>2</sub>S pre-incubated with probes using cells as a read-out.** C2C12-Fluc cells were seeded in a 96 well-plate at concentration  $3 \times 10^4$  cells/well 24 h before the assay. Solutions of the probes (50 μL, 10 μM final) or corresponding luciferins (50 μL, 10 μM final) (as a control) were added to 50 μL of NaHS solutions of the indicated final concentrations (10- 500 μM final) in PBS 7.2 to 0.5 mL PCR tubes and incubated for 1 h. After that the solutions were transferred to a 96 well plate and added to the cells cleared from media with two multichannel pipettes, the bioluminescence was acquired for 60 min using IVIS 100. After the BLI fluorescence at  $\lambda_{\text{ex/em}}$  240/ 560 nm was measured on the same plate as a control.

**BLI of exogenous H<sub>2</sub>S using cells in real-time.** C2C12-Fluc cells were seeded in a 96 well-plate at concentration  $3 \times 10^4$  cells/well 24 h before the assay. Cells were cleared from media, washed with PBS and loaded first with 100  $\mu$ L of probes (25  $\mu$ M final) or corresponding luciferins (2.5  $\mu$ M final) as a control and after that with 100  $\mu$ L of NaHS solutions in PBS 7.2 (10- 500  $\mu$ M final). The bioluminescence was acquired for 60 min using IVIS 100. After the BLI fluorescence at  $\lambda_{\text{ex/em}}$  240/ 560 nm was measured on the same plate as a control.

**BLI of intracellular H<sub>2</sub>S in C2C12-Fluc cells.** C2C12-Fluc cells were seeded in a 96 well-plate at concentration  $3 \times 10^4$  cells/well 24 h before the assay. Cells were cleared from media, washed with PBS and loaded with 100  $\mu$ L of NaHS solutions in PBS 7.2 (10- 500  $\mu$ M). After 10 min of incubation at 37 °C the cells were washed with PBS and loaded with 100  $\mu$ L of BL and 4-Az-7-MC probes (10  $\mu$ M) or corresponding luciferins (1  $\mu$ M) as a control. The bioluminescence was acquired for 60 min using IVIS 100. After the BLI fluorescence at  $\lambda_{\text{ex/em}}$  240/ 560 nm was measured on the same plate as a control.

**Cytotoxicity assay.** C2C12-Fluc cells were seeded in a 96 well-plate at concentration  $3 \times 10^4$  cells/well 24 h before the assay. Solutions of probes were prepared from 10 mM stock in DMSO in PBS at 1, 10, 100, 250, 500, 750 and 1000  $\mu$ M final concentrations. Cells were cleared from media, washed with PBS and loaded with 50  $\mu$ L of probes or control (corresponding amount of DMSO in PBS). After 1 h of incubation at 37 °C 25  $\mu$ L of alamarBlue® (Thermo Fisher Scientific) was added to each well, the plate was covered with aluminum foil and incubated for 1 h at 37 °C. Fluorescence was measured with Tecan Infinite 1000M plate reader (exc 570 nm; em 585 nm).

**Bacterial strains, plasmids and culture conditions.** *E. coli* K12 BW25113 was obtained from American Type Culture Collection (Rockville, Md). Plasmids pTrc99A (empty vector) and pSB74 (pTrc99A containing the thiosulfate reductase operon *phsABC* from *S. enterica* serovar Typhimurium LT2) were a kind gift of Prof. Keasling (University of California, Berkeley). For the bacterial growth curves the cultures were started in 100  $\mu$ L of LB or EZRDM at an OD<sub>600</sub> of 0.1 in a 96 well-plate, the plate was covered with a lid, placed in the plate reader and kept at 37 °C with a 5 min shaking cycle (1.5 mm, 216 rpm) and OD<sub>600</sub> measurement every 30 min for 8 h.

**Analysis of H<sub>2</sub>S production in bacteria.** The solutions containing growth media (LB or EZRDM), 3 mM IPTG, 10 mM Na<sub>2</sub>S<sub>2</sub>O<sub>3</sub> and 50  $\mu$ M of the probes were sterilized by filtration (0.22  $\mu$ m), aliquoted (1 mL/tube) and kept at – 20 °C. For the assay bacteria were grown aerobically overnight in 15 mL of LB, next day diluted to the OD<sub>600</sub> of 1.0 in LB, pelleted by centrifugation (10 000 rpm  $\times$  5 min), washed three times in PBS, and the cultures were started in 1 mL of previously prepared and aliquoted LB or EZRDM with 100  $\mu$ g/mL ampicillin. The cultures were wrapped in aluminum foil, placed in an anaerobic jar (BD GasPak EZ system, BD diagnostics) containing a CO<sub>2</sub>-generating envelop (Oxoid AnaeroGen Sachet, Thermo Fisher Scientific) and were grown statically for 8 h at 37 °C. After 8 h bacteria were pelleted by centrifugation (10 000 rpm  $\times$  5 min), the supernatant was aliquoted in a 96-well plate and analyzed using bioluminescence or fluorescence. For BL analysis 50  $\mu$ L of luciferase (62.5  $\mu$ g/mL in Tris 7.8 containing 6 mM ATP, 15 mM MgSO<sub>4</sub>) was added to 100  $\mu$ L of the supernatant in a well and the BL was acquired immediately for 10 min using an IVIS 100. After the BLI fluorescence at  $\lambda_{\text{ex/em}}$  240/560 nm was measured on the same plate as a control. For WSP-5 and fluorescein the fluorescence was measured at  $\lambda_{\text{ex/em}}$  502/525 nm and for 7-Az-4-MC and 7-Amino-4-MC at  $\lambda_{\text{ex/em}}$  365/450 nm.

## 3.8 Supplementary figures

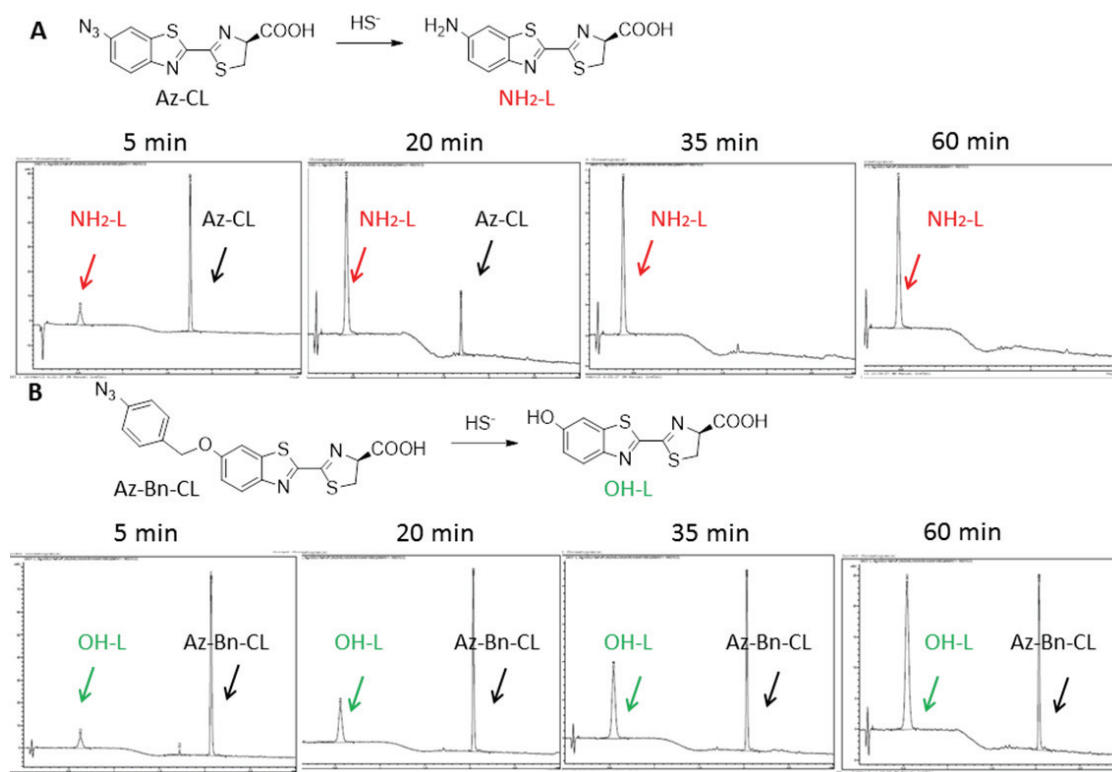


Figure S3.1 HPLC-MS analysis of Az-CL and Az-Bn-CL reduction by H<sub>2</sub>S over 60 min *in vitro*. 100  $\mu$ M of the probe was added to 10 mM NaHS solution in degassed PBS 7.2 and the reaction mixture was analyzed at 5, 20, 35 and 60 min post-addition. (A). UV HPLC profiles (at 320 nm) of Az-CL reduction, peak at 0.4 min corresponds to amino-luciferin (M+H 280), peak at 1.5 min corresponds to Az-CL (M+H 306). (B). UV HPLC profiles (at 320 nm) of Az-Bn-CL reduction, peak at 0.4 min corresponds to hydroxy-luciferin (M+H 281), peak at 1.9 min corresponds to Az-Bn-CL (M+H 412).

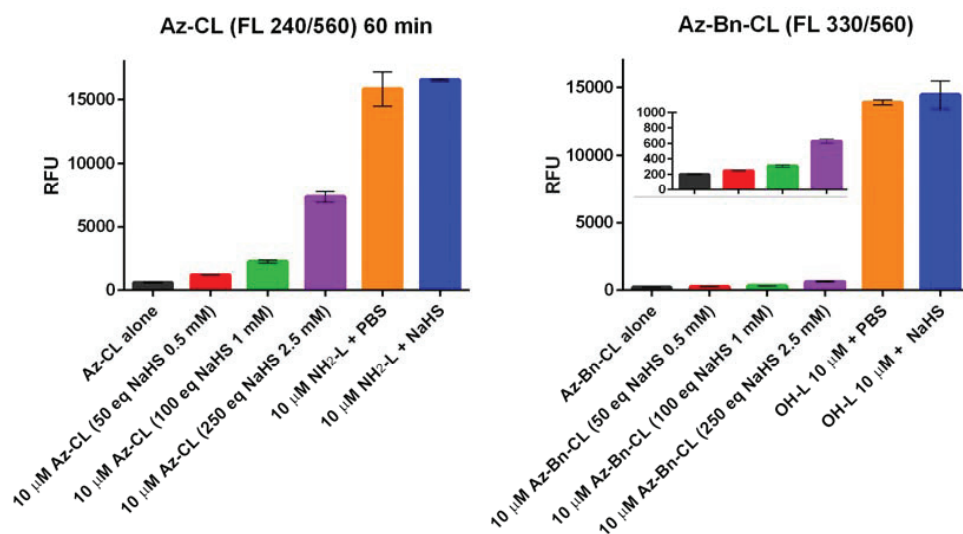


Figure S3.2 Fluorescence from 10  $\mu$ M Az-CL and Az-Bn-CL 60 min after the addition of NaHS (0.5, 1 and 2.5 mM) *in vitro*. Fluorescence was measured at  $\lambda_{ex/em}$  240/560 nm.

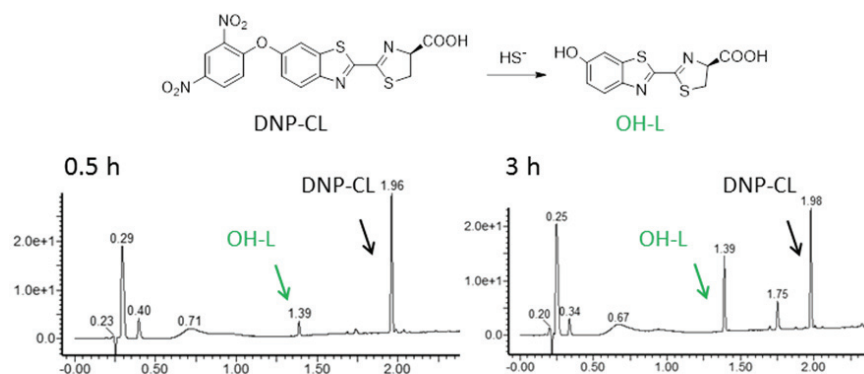


Figure S3.3 HPLC-MS analysis of DNP-CL reduction by H<sub>2</sub>S *in vitro*. 100  $\mu$ M of the probe was added to 10 mM NaHS solution in degassed PBS 7.2 and the reaction mixture was analyzed at 0.5 h and 3 h post-addition. Peak at 1.4 min corresponds to hydroxy-luciferin ( $m/z$  280), peak at 1.9 min corresponds to DNP-CL ( $m/z$  446).

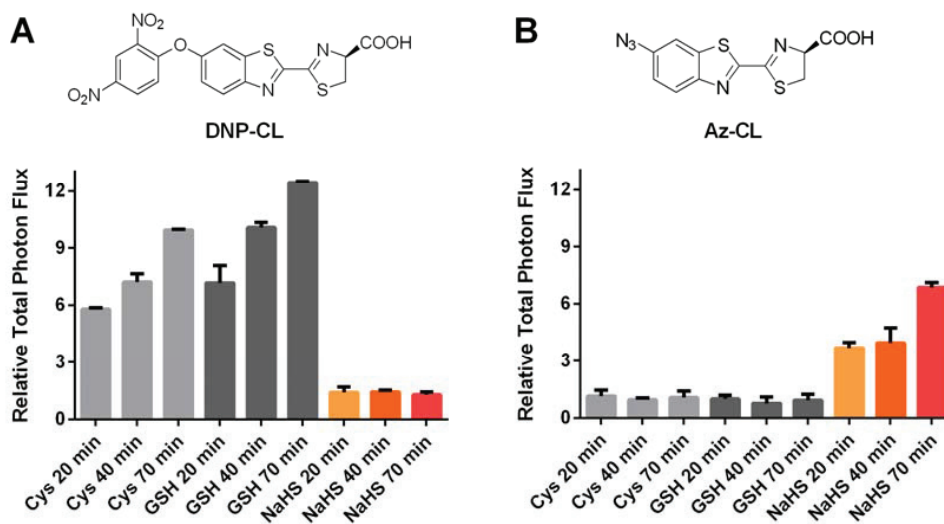


Figure S3.4 Selectivity profiles of DNP-CL and Az-CL towards biologically relevant thiols *in vitro*. Relative BL over 1 h from 5  $\mu$ M DNP-CL (A) or Az-CL (B) incubated with 100  $\mu$ M Cys, GSH or NaHS for 20, 40 or 70 min before addition of luciferase (relative to the signal from the probes alone).

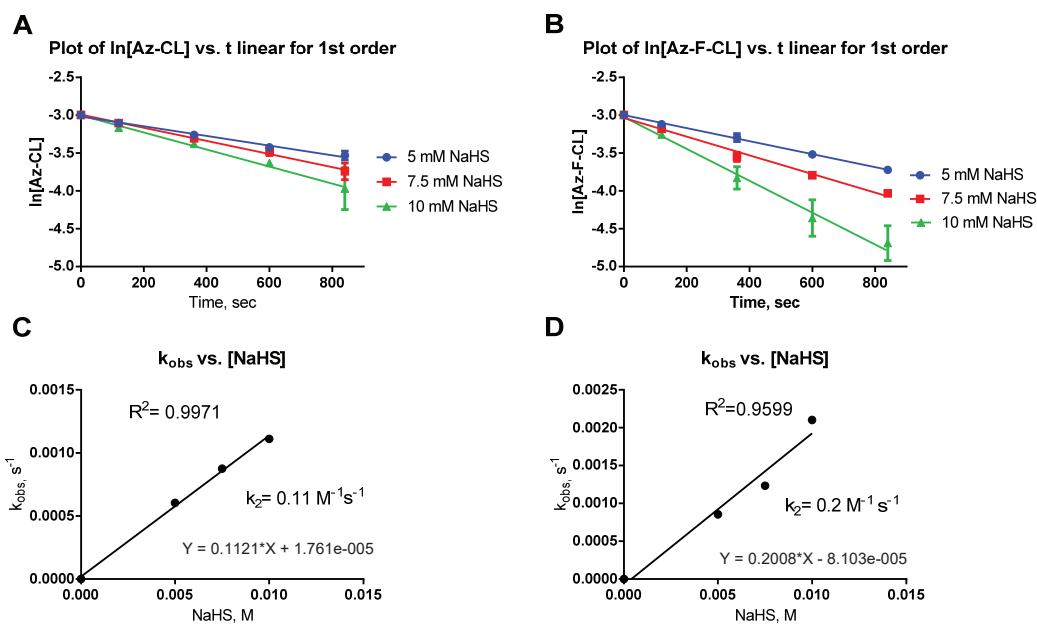


Figure S3.5 Kinetic analysis of probes (Az-CL and Az-F-CL) reduction by H<sub>2</sub>S. (A) The plot of the logarithm of [Az-CL] vs. time is a straight line with  $k = -\text{slope of the line}$ , which indicates a first order reaction. (B) The plot of the logarithm of [Az-F-CL] vs. time is a straight line with  $k = -\text{slope of the line}$ , which indicates a first order reaction. (C) The plot of  $k_{\text{obs}}$  vs [NaHS] for the reactions of 0.005- 0.01 M NaHS with 50  $\mu\text{M}$  Az-CL. (D) Plot of  $k_{\text{obs}}$  vs [NaHS] for the reactions of 0.005- 0.01 M NaHS with 50  $\mu\text{M}$  Az-F-CL. Standard conditions: 50 mM PIPES, 100 mM KCl, pH 7.4, 25 °C. Each measurement was performed in triplicate.

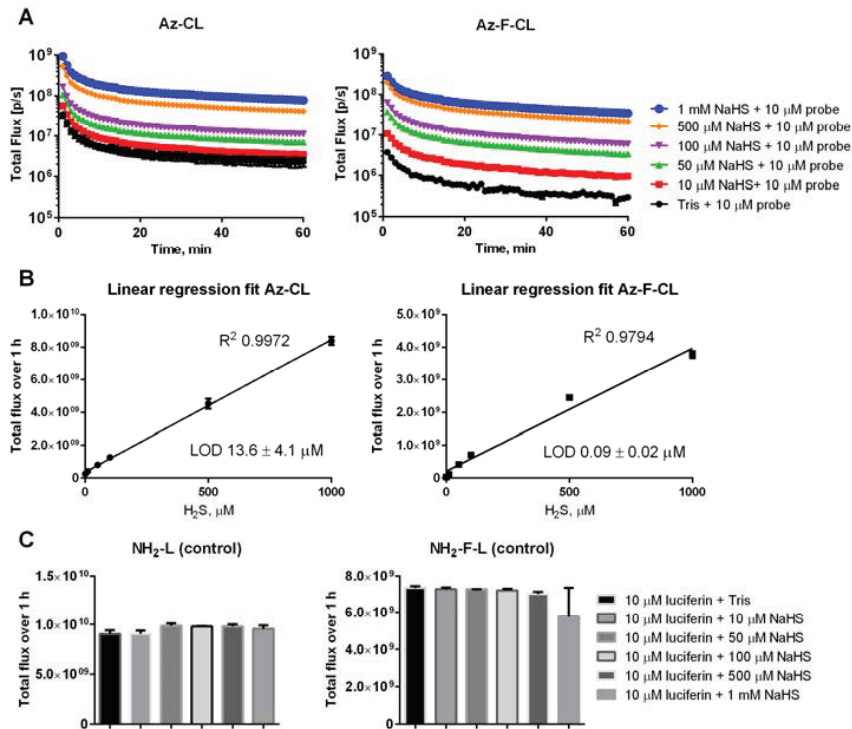


Figure S3.6 BLI of H<sub>2</sub>S after 1 h of pre-incubation with Az-CL and Az-F-CL in luciferase assay. (A) Kinetic curves of BL signal over 1 h. (B) Linear regression fit of total photon flux produced from probes over 1 h. (C) Total photon flux from luciferin over 1 h as a control for BL.

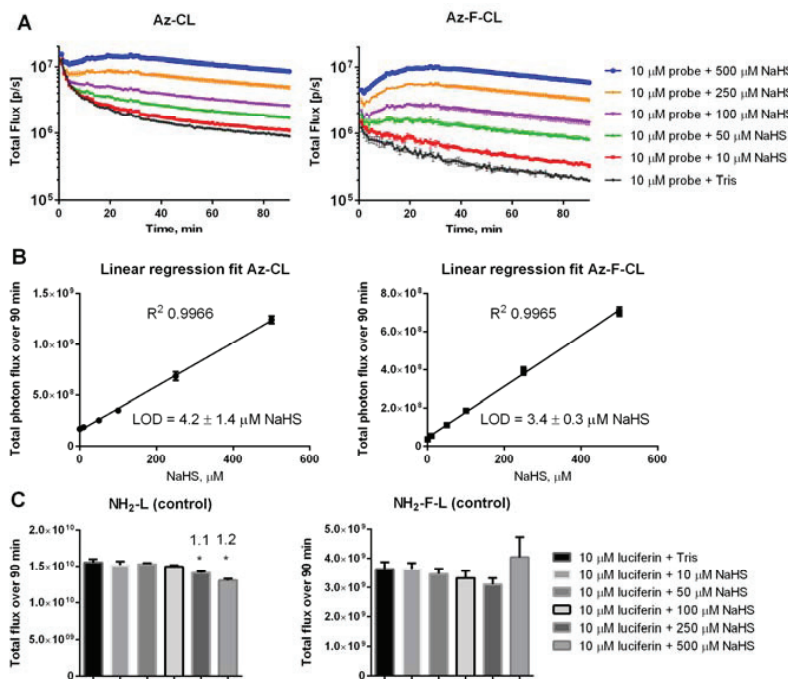


Figure S3.7 BLI of H<sub>2</sub>S with Az-CL and Az-F-CL in real-time in luciferase assay. (A) Kinetic curves of BL signal over 1 h. (B) Linear regression fit of total photon flux produced from probes over 1 h. (C) Total photon flux from luciferin over 1 h as a control for BL.

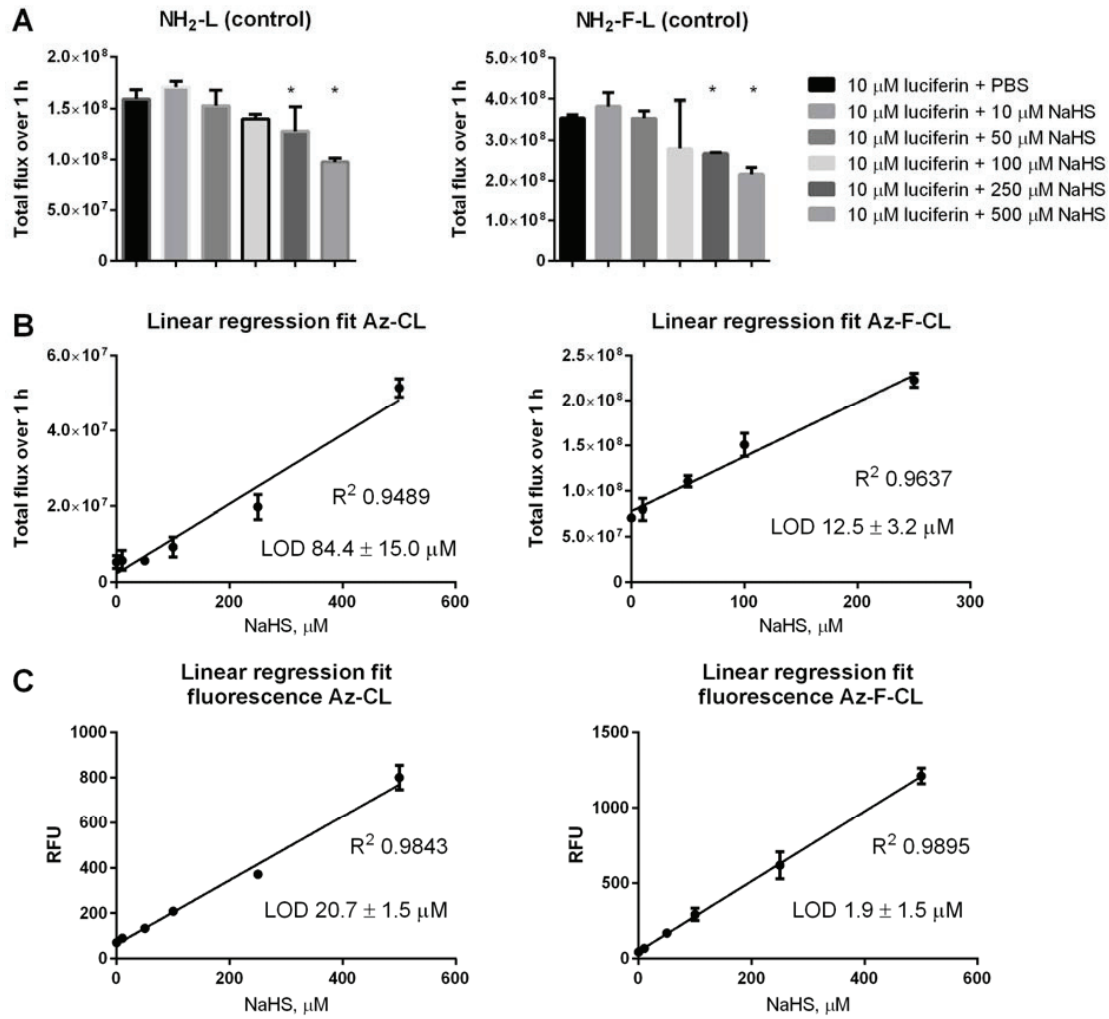


Figure S3.8 BLI of H<sub>2</sub>S after 1 h of pre-incubation with Az-CL and Az-F-CL in C2C12-FLuc cells. (A) Total photon flux from luciferin over 1 h as a control for BL. (B) Linear regression fit of total photon flux produced from probes over 1 h. (C) Linear regression fit of fluorescence measured from probes ( $\lambda_{ex/em}$  240/560 nm).



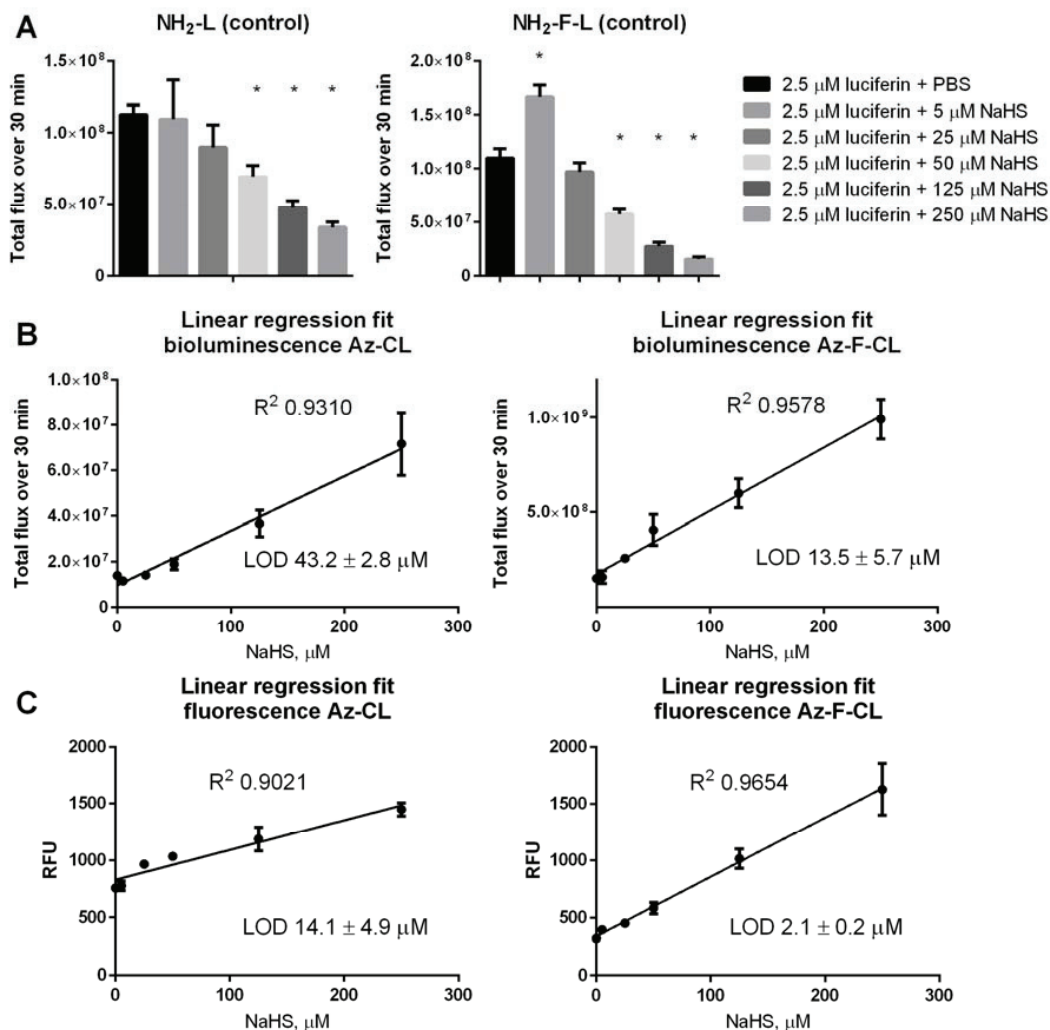


Figure S3.9 BLI of exogenous H<sub>2</sub>S with Az-CL and Az-F-CL in real-time in C2C12-FLuc cells. (A) Total photon flux from luciferin over 1 h as a control for BL. (B) Linear regression fit of total photon flux produced from probes over 1 h. (C) Linear regression fit of fluorescence measured from probes ( $\lambda_{ex/em}$  240/560 nm).

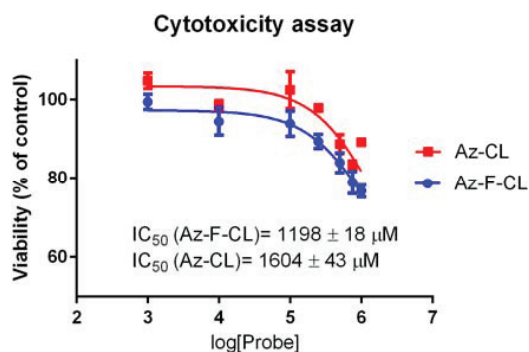


Figure S3.10 The cytotoxicity profile of Az-F-CL (red) and Az-CL (blue) in C2C12-FLuc cells measured with Alamar Blue assay



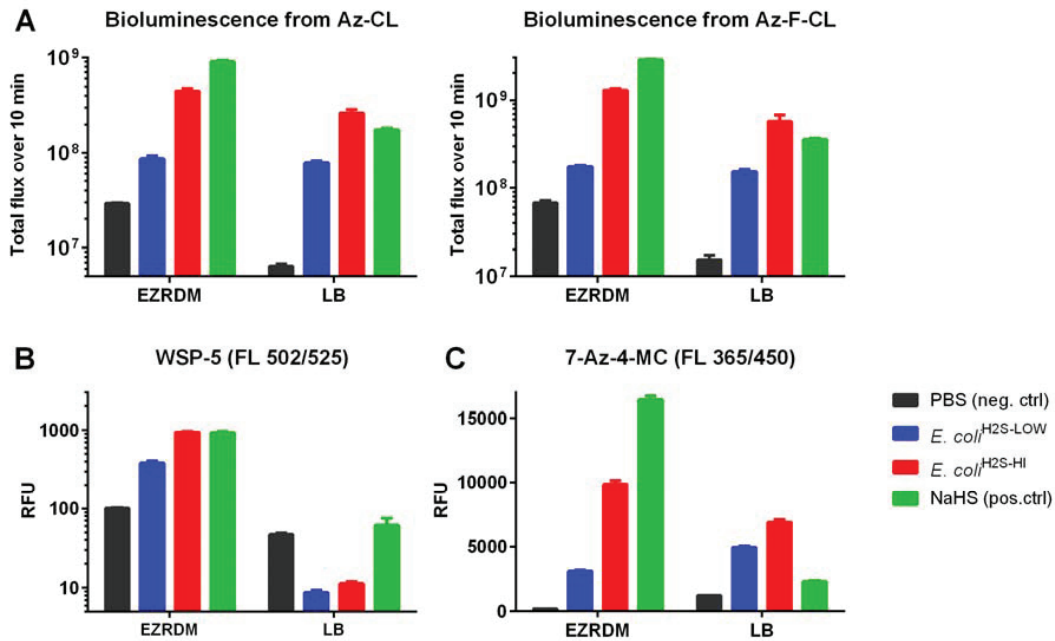


Figure S3.11 Comparison of imaging of bacterial H<sub>2</sub>S from the probes in LB or EZ Rich Defined Medium (EZRDM). (A) Bioluminescence over 10 min produced from the bacterial supernatant with Az-CL or Az-F-CL probes after the addition of luciferase (62.5 µg/ mL). (B) Fluorescence from WSP-5 probe (λ<sub>ex</sub>/em 502/525 nm). (C) Fluorescence from 7-Az-4-MC probe (λ<sub>ex</sub>/em 365/450 nm). The signal from the NaHS (positive control) is lower in the LB than in the EZRDM.

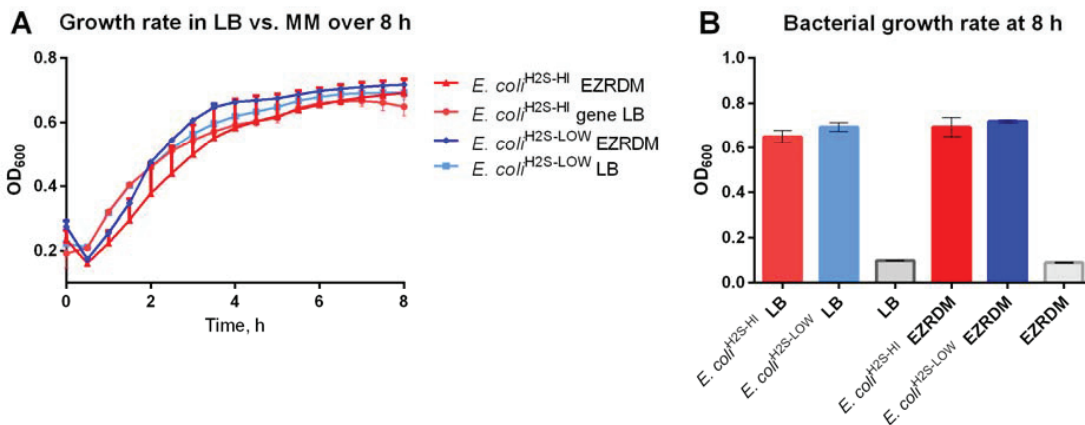


Figure S3.12 Bacterial growth of *E. coli*<sup>H<sub>2</sub>S-LOW</sup> and *E. coli*<sup>H<sub>2</sub>S-HI</sup> in LB and EZRDM. (A) Growth curves over 8 h anaerobic growth as a planktonic broth. (B) The differences between the growth of the bacterial strains following 8 h anaerobic growth as a planktonic broth.

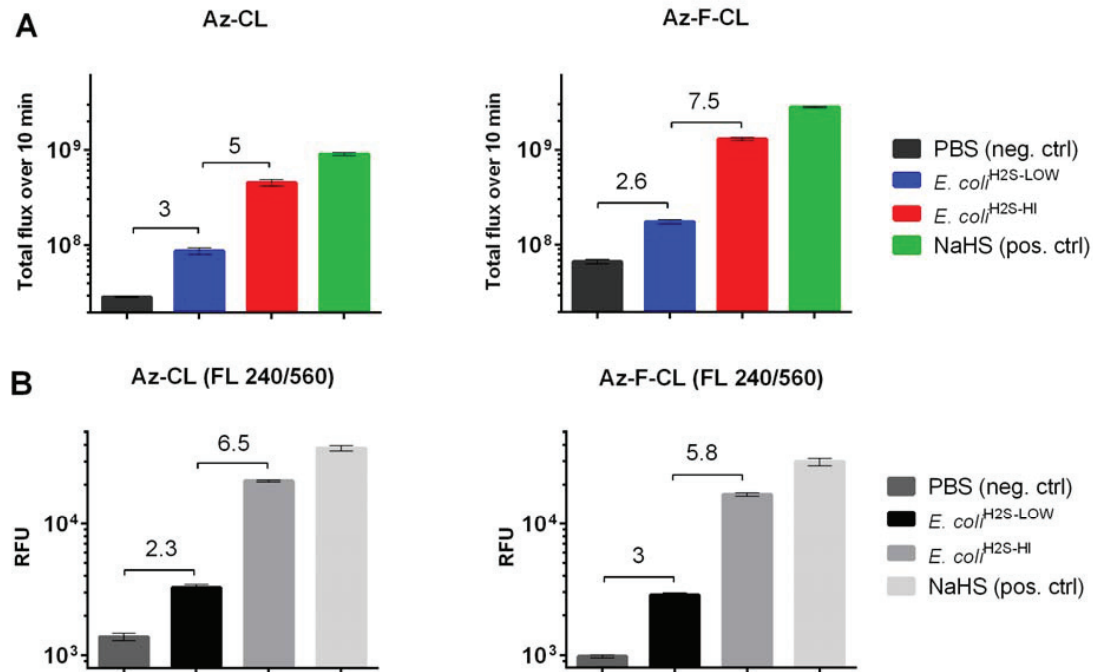


Figure S3.13 Correlation between bioluminescence (A) and fluorescence (B) detection of H<sub>2</sub>S produced by bacteria using Az-CL and Az-F-CL probes. Fluorescence was measured at  $\lambda_{\text{ex/em}}$  240/560 nm.

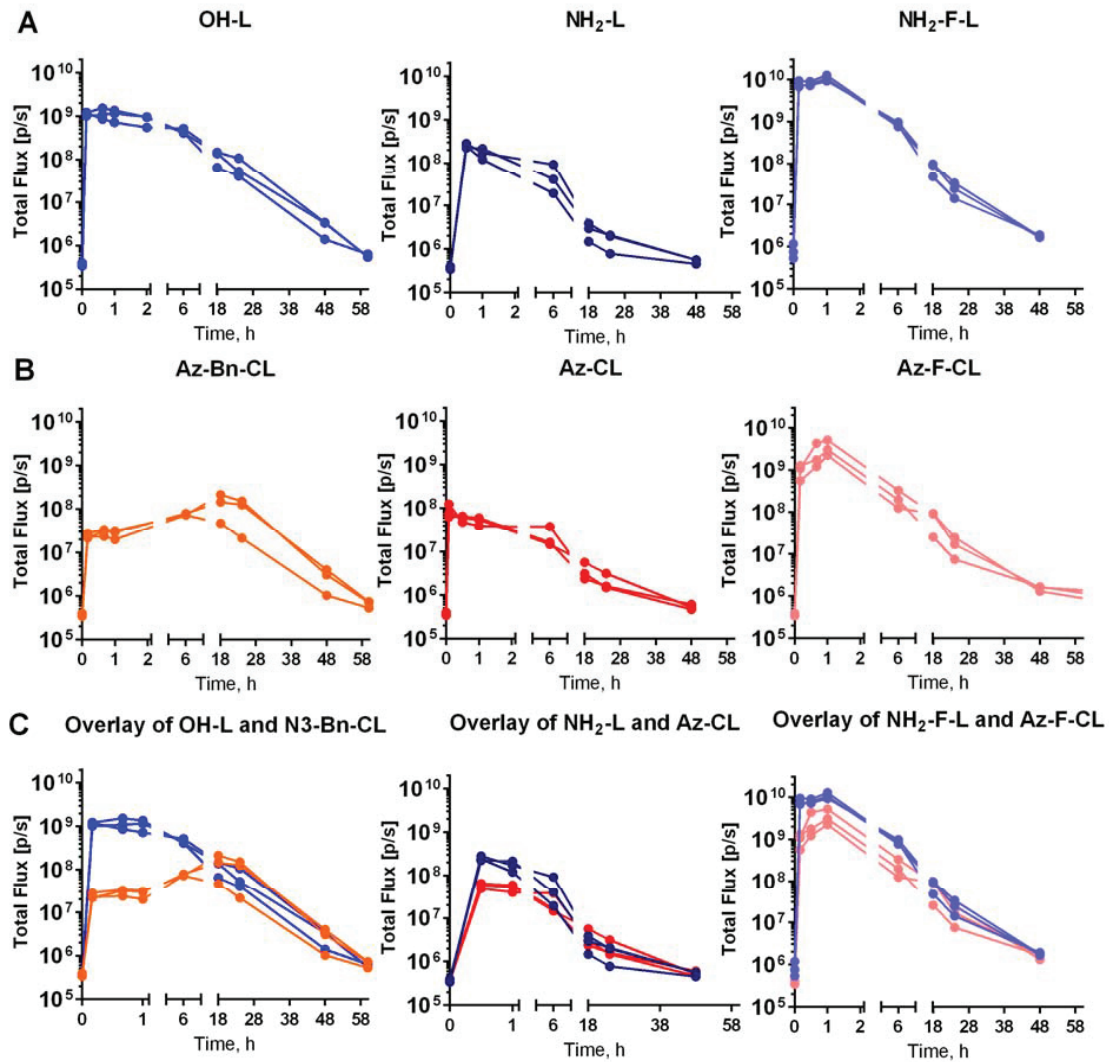


Figure S3.14 A summary of the kinetics of the bioluminescence signal produced from luciferins (A) or probes (B) in FVB-luc<sup>+</sup> mice (n = 3) over 60 h.

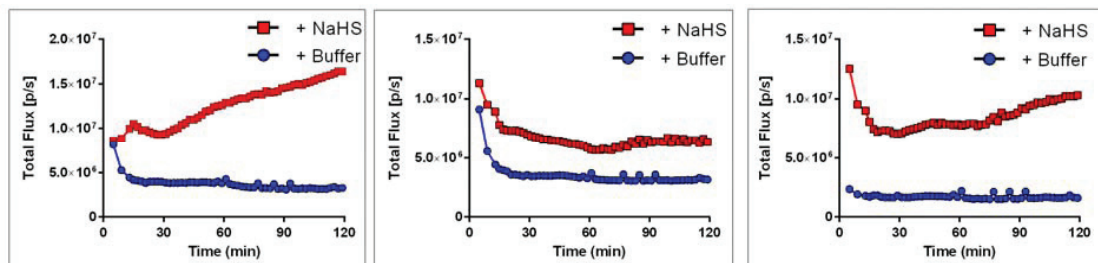


Figure S3.15 BLI of individual mice administered buffer + Az-CL (blue) and NaHS + Az-CL (red).



## Chapter 4 Conclusion and outlook

### 4.1 Conclusion

The field of molecular imaging has witnessed rapid expansion over the past ten years. A large number of molecular probes for optical imaging of various biological molecules *in vitro* are actively being developed, however, only a small fraction of them can be applied to living systems mainly due to the instability of the probes and low selectivity of detection in a complex biological environment. Advances in organic chemistry prompt the discovery of novel biocompatible reactions that can be employed to design activatable probes responsive to the biomolecules of interest for *in vivo* imaging.

A key advantage of bioluminescence imaging in comparison to other optical imaging modalities is its high sensitivity. Due to the linear relationship between the concentration of luciferin/ luciferase, and the emitted light, bioluminescence is widely used for quantitative analysis of biological processes *in vitro* and *in vivo*. Importantly, the structure of luciferin is amenable to modifications which open exciting possibilities for the design of molecular imaging probes using the caged luciferin approach. As the resulting light emission depends on the amount of free luciferin that is released proportional to the activity of the biomolecules of interest, this system can report the dynamic processes of probe activation and luciferin release as they occur in real-time within the living systems.

In this thesis we described the development of novel activatable probes for the bioluminescence imaging of two biological molecules, nitroreductase and hydrogen sulfide. The probes were designed using the caged luciferin approach and successfully synthesized. We demonstrated the examples of probe design was based on the classical luciferase substrates, hydroxy-luciferin (OH-L) and amino-luciferin (NH<sub>2</sub>-L), exploring the 6'-modifications of the luciferin core. The probes were extensively validated in several *in vitro* and *in vivo* models for non-invasive real-time imaging applications.

The process of validation of the probes generally included a number of *in vitro* assays followed by the *in vivo* assays. First, the probes were evaluated on the basis of their reactivity towards the biomolecule of interest and the ability to produce a dose-dependent light emission in the presence of the biomolecule and luciferase *in vitro*. Next, the selectivity of the probes for the detection of the biomolecule was evaluated in the corresponding *in vitro* assays. The applicability of the probes for the bioluminescence imaging in cell-based assays was demonstrated using bacterial and mammalian cells *in vitro*. In order to evaluate the selectivity of the probes in living systems and to demonstrate their potential for noninvasive real-time bioluminescence imaging *in vivo*; the probes were evaluated in a suitable mouse model.

In Chapter 2 we described the development of the Nitroreductase Caged Luciferin (NCL) probe. The probe demonstrated the highest uncaging efficiency by NTR among existing caged luciferin substrates reported to date. Due to the specificity of the cage reduction to bacterial NTR, the probe efficiently reported NTR activity in mammalian systems. We showed the application of this probe for imaging of NTR in *E. coli* bacterial infection model and preclinical model of cancer which is particularly relevant to GDEPT approach for targeted cancer chemotherapy.

In Chapter 3 we described the development of a series of caged luciferin probes for imaging of hydrogen sulfide. In order to show the relationship between the structure of the probes and their reactivity towards  $H_2S$ , five caged luciferin probes were designed and successfully synthesized. The two probes with the highest reactivity towards  $H_2S$  and selectivity of  $H_2S$  detection over endogenous biothiols were evaluated side-by-side in a number of *in vitro* assays. The probes effectively detected  $H_2S$  produced by bacteria in culture and were applied for the real-time imaging of exogenous  $H_2S$  in the gastro-intestinal tract of living mice expressing luciferase. The best performing probe detected exogenous  $H_2S$  with high signal-to-background ratio and is a promising tool for non-invasive real-time bioluminescence imaging of  $H_2S$  production in the gastro-intestinal tract.

The results described in this thesis provide valuable insights in the probe design for the development of novel caged luciferin probes for imaging of enzymatic activity and small biomolecules. The developed caged luciferin probes have expanded the toolbox of reagents that allow non-invasive real-time imaging in living animals and broaden the scope of BLI applications for preclinical research.

## 4.2 Outlook

The developed NCL probe can be applied in various areas of research where evaluation of NTR activity is important. As NTRs are widespread among bacteria, the NCL probe could be applied for the discovery of bacterial strains with enhanced bioremediation rates that degrade nitro-aromatics, known environmental pollutants formed from the combustion of fossil fuels and during many industrial processes.

NTRs are involved in the activation of 5-nitro heterocyclic antibiotics by bacteria and parasites and are responsible for the efficiency of antimicrobial therapy. Mutations in the NTR genes lead to a diminished enzyme capacity to activate antibiotic prodrugs and often occur in the drug-resistance bacteria strains. The NCL probe could find application in drug discovery assays such as *in vitro* screening of NTRs that catalyze the conversion of 5-nitrofurane antibiotics and aid in the development of new antibacterial drugs.

For GDEPT applications the above mentioned screen could be performed for the identification of NTR variants with high catalytic efficiency for cancer prodrug activation. The NCL probe could be particularly useful to evaluate novel gene delivery systems (such as extracellular vesicles) and the efficiency of NTR transgene expression in cell culture *in vitro* and in cancer models *in vivo*.

Previous studies showed that NTR activity in the gut microbiota varied depending on the diet composition, for example consumption of high meat diet was shown to increase NTR activity. As NTRs could participate in carcinogen pro-

duction (amines, nitrosamines) in the gut, it is promising to investigate the effect of diet on intestinal microflora and human health.

The developed caged luciferin probes allow for the non-invasive imaging of NTR activity and H<sub>2</sub>S production in the gut of living animals which is more representative of bacterial metabolism in a host and relevant to *in vivo* systems than the commonly used *ex vivo* detection methods.

Hydrogen sulfide is a gasotransmitter involved in multiple physiological and pathological processes in the gut. The developed probes for imaging of H<sub>2</sub>S could advance our understanding of its contribution to the pathogenesis and ultimately help to develop new therapeutic approaches for the treatment of gut disorders.

Understanding the relationship between gut microbiota and the host H<sub>2</sub>S metabolism is becoming more important as it was recently discovered that H<sub>2</sub>S possesses not only local but also systemic effects, and was shown to participate in stress resistance and longevity.

Imaging of H<sub>2</sub>S level in the gut in real-time in living animals could address many questions related to the contribution of bacterial and mammalian (host) production to the total level of H<sub>2</sub>S. As the level of H<sub>2</sub>S in the gut was shown to vary with diet, it could be of interest to study if the consumption of certain dietary elements could lead to an increased or decreased H<sub>2</sub>S production in the gut. Given the important role of H<sub>2</sub>S in inflammation, these studies could help to investigate the role of H<sub>2</sub>S in the development and progression of gut inflammatory diseases, such as inflammatory bowel disease (IBD) and ulcerative colitis (UC).

In addition to the real-time imaging applications in living animals the developed caged luciferin probes can be applied for the detection of NTR activity or H<sub>2</sub>S production in fecal samples *ex vivo*. Such screening assays could be developed for a number of other bacterial enzymes and analytes of interest and could be used for the profiling and diagnostics of healthy versus diseased patients.





## Chapter 5      References

1. Massoud, T.F. and S.S. Gambhir, *Molecular imaging in living subjects: seeing fundamental biological processes in a new light*. Genes Dev, 2003. **17**(5): p. 545-80.
2. Rudin, M. and R. Weissleder, *Molecular imaging in drug discovery and development*. Nat Rev Drug Discov, 2003. **2**(2): p. 123-31.
3. Bhaumik, S. and S.S. Gambhir, *Optical imaging of Renilla luciferase reporter gene expression in living mice*. Proc Natl Acad Sci U S A, 2002. **99**(1): p. 377-82.
4. Tannous, B.A., et al., *Codon-optimized Gaussia luciferase cDNA for mammalian gene expression in culture and in vivo*. Mol Ther, 2005. **11**(3): p. 435-43.
5. Riedel, C.U., et al., *Improved luciferase tagging system for Listeria monocytogenes allows real-time monitoring in vivo and in vitro*. Appl Environ Microbiol, 2007. **73**(9): p. 3091-4.
6. Cronin, M., et al., *Development of a luciferase-based reporter system to monitor Bifidobacterium breve UCC2003 persistence in mice*. BMC Microbiol, 2008. **8**: p. 161.
7. Baban, C.K., et al., *Bioluminescent bacterial imaging in vivo*. J Vis Exp, 2012(69): p. e4318.
8. Santos, E.B., et al., *Sensitive in vivo imaging of T cells using a membrane-bound Gaussia princeps luciferase*. Nature Medicine, 2009. **15**(3): p. 338-344.
9. Contag, C.H., et al., *Photonic detection of bacterial pathogens in living hosts*. Mol Microbiol, 1995. **18**(4): p. 593-603.
10. Zhao, H., et al., *Emission spectra of bioluminescent reporters and interaction with mammalian tissue determine the sensitivity of detection in vivo*. J Biomed Opt, 2005. **10**(4): p. 41210.
11. Maguire, C.A., et al., *Codon-optimized Luciola italica luciferase variants for mammalian gene expression in culture and in vivo*. Mol Imaging, 2012. **11**(1): p. 13-21.
12. Miloud, T., C. Henrich, and G.J. Hammerling, *Quantitative comparison of click beetle and firefly luciferases for in vivo bioluminescence imaging*. J Biomed Opt, 2007. **12**(5): p. 054018.
13. Prescher, J.A. and C.H. Contag, *Guided by the light: visualizing biomolecular processes in living animals with bioluminescence*. Curr Opin Chem Biol, 2010. **14**(1): p. 80-9.
14. Conti, E., N.P. Franks, and P. Brick, *Crystal structure of firefly luciferase throws light on a superfamily of adenylate-forming enzymes*. Structure, 1996. **4**(3): p. 287-98.
15. Oba, Y., M. Ojika, and S. Inouye, *Firefly luciferase is a bifunctional enzyme: ATP-dependent monooxygenase and a long chain fatty acyl-CoA synthetase*. FEBS Lett, 2003. **540**(1-3): p. 251-4.
16. Oba, Y., et al., *Enzymatic and genetic characterization of firefly luciferase and Drosophila CG6178 as a fatty acyl-CoA synthetase*. Biosci Biotechnol Biochem, 2005. **69**(4): p. 819-28.
17. Fraga, H., et al., *Coenzyme A affects firefly luciferase luminescence because it acts as a substrate and not as an allosteric effector*. FEBS J, 2005. **272**(20): p. 5206-16.
18. Ando, Y., et al., *Firefly bioluminescence quantum yield and colour change by pH-sensitive green emission*. Nat Photon, 2008. **2**(1): p. 44-47.
19. Seliger, H.H., et al., *The Spectral Distribution of Firefly Light*. J Gen Physiol, 1964. **48**: p. 95-104.
20. Seliger, H.H. and W.D. McElroy, *The Colors of Firefly Bioluminescence: Enzyme Configuration and Species Specificity*. Proc Natl Acad Sci U S A, 1964. **52**(1): p. 75-81.
21. Mc, E.W., *Properties of the reaction utilizing adenosinetriphosphate for bioluminescence*. J Biol Chem, 1951. **191**(2): p. 547-57.
22. Ribeiro, C. and J.C. Esteves da Silva, *Kinetics of inhibition of firefly luciferase by oxyluciferin and dehydroluciferyl-adenylate*. Photochem Photobiol Sci, 2008. **7**(9): p. 1085-90.
23. Seliger, H.H., et al., *Stereo-specificity and firefly bioluminescence, a comparison of natural and synthetic luciferins*. Proc Natl Acad Sci U S A, 1961. **47**: p. 1129-34.
24. Niwa, K., M. Nakamura, and Y. Ohmiya, *Stereoisomeric bio-inversion key to biosynthesis of firefly D-luciferin*. FEBS Lett, 2006. **580**(22): p. 5283-7.

25. Oba, Y., et al., *Biosynthesis of Firefly Luciferin in Adult Lantern: Decarboxylation of L-Cysteine is a Key Step for Benzothiazole Ring Formation in Firefly Luciferin Synthesis*. PLoS ONE, 2014. **8**(12): p. e84023.
26. Kanie, S., et al., *One-pot non-enzymatic formation of firefly luciferin in a neutral buffer from p-benzoquinone and cysteine*. Sci Rep, 2016. **6**: p. 24794.
27. Berger, F., et al., *Uptake kinetics and biodistribution of 14C-D-luciferin--a radiolabeled substrate for the firefly luciferase catalyzed bioluminescence reaction: impact on bioluminescence based reporter gene imaging*. Eur J Nucl Med Mol Imaging, 2008. **35**(12): p. 2275-85.
28. Green, A. and W.D. McElroy, *Function of adenosine triphosphate in the activation of luciferin*. Arch Biochem Biophys, 1956. **64**(2): p. 257-71.
29. Rhodes, W.C. and E.W. Mc, *Enzymatic synthesis of adenylyl-oxyluciferin*. Science, 1958. **128**(3318): p. 253-4.
30. Hopkins, T.A., et al., *The chemiluminescence of firefly luciferin. A model for the bioluminescent reaction and identification of the product excited state*. J Am Chem Soc, 1967. **89**(26): p. 7148-50.
31. DeLuca, M. and W.D. McElroy, *Kinetics of the firefly luciferase catalyzed reactions*. Biochemistry, 1974. **13**(5): p. 921-5.
32. White, E.H., et al., *Chemi- and bioluminescence of firefly luciferin*. J Am Chem Soc, 1969. **91**(8): p. 2178-80.
33. Suzuki, N., et al., *Studies on firefly bioluminescence—I*. Tetrahedron, 1972. **28**(15): p. 4065-4074.
34. Rhodes, W.C. and E.W. Mc, *The synthesis and function of luciferyl-adenylate and oxyluciferyl-adenylate*. J Biol Chem, 1958. **233**(6): p. 1528-37.
35. Marques, S.M. and J.C. Esteves da Silva, *Firefly bioluminescence: a mechanistic approach of luciferase catalyzed reactions*. IUBMB Life, 2009. **61**(1): p. 6-17.
36. Greer, L.F., 3rd and A.A. Szalay, *Imaging of light emission from the expression of luciferases in living cells and organisms: a review*. Luminescence, 2002. **17**(1): p. 43-74.
37. de Wet, J.R., et al., *Cloning of firefly luciferase cDNA and the expression of active luciferase in Escherichia coli*. Proc Natl Acad Sci U S A, 1985. **82**(23): p. 7870-3.
38. Sherf B.A., W.K.V., *Firefly luciferase engineered for improved genetic reporting*, in *Promega Notes*. 1994. p. 14- 21.
39. Branchini, B.R., et al., *Red-emitting luciferases for bioluminescence reporter and imaging applications*. Anal Biochem, 2010. **396**(2): p. 290-7.
40. Mezzanotte, L., et al., *Sensitive dual color in vivo bioluminescence imaging using a new red codon optimized firefly luciferase and a green click beetle luciferase*. PLoS One, 2011. **6**(4): p. e19277.
41. Fujii, H., et al., *Increase in bioluminescence intensity of firefly luciferase using genetic modification*. Anal Biochem, 2007. **366**(2): p. 131-6.
42. Branchini, B.R., et al., *Luciferase from the Italian firefly Luciola italica: molecular cloning and expression*. Comparative biochemistry and physiology. Part B, Biochemistry & molecular biology, 2006. **145**(2): p. 159-167.
43. Hirokawa, K., N. Kajiyama, and S. Murakami, *Improved practical usefulness of firefly luciferase by gene chimerization and random mutagenesis*. Biochim Biophys Acta, 2002. **1597**(2): p. 271-9.
44. Huang, C., et al., *Blocking activator protein-1 activity, but not activating retinoic acid response element, is required for the antitumor promotion effect of retinoic acid*. Proc Natl Acad Sci U S A, 1997. **94**(11): p. 5826-30.
45. Carlsen, H., et al., *In vivo imaging of NF-kappa B activity*. J Immunol, 2002. **168**(3): p. 1441-6.
46. Wilsbacher, L.D., et al., *Photic and circadian expression of luciferase in mPeriod1-luc transgenic mice invivo*. Proc Natl Acad Sci U S A, 2002. **99**(1): p. 489-94.
47. Cao, Y.A., et al., *Shifting foci of hematopoiesis during reconstitution from single stem cells*. Proc Natl Acad Sci U S A, 2004. **101**(1): p. 221-6.
48. Svensson, R.U., et al., *Assessing siRNA pharmacodynamics in a luciferase-expressing mouse*. Mol Ther, 2008. **16**(12): p. 1995-2001.
49. Kumar, J.S., et al., *Bioluminescent imaging of ABCG2 efflux activity at the blood-placenta barrier*. Sci Rep, 2016. **6**: p. 20418.
50. Creusot, R.J., et al., *Lymphoid-tissue-specific homing of bone-marrow-derived dendritic cells*. Blood, 2009. **113**(26): p. 6638-47.
51. Wang, H., et al., *Trafficking mesenchymal stem cell engraftment and differentiation in tumor-bearing mice by bioluminescence imaging*. Stem Cells, 2009. **27**(7): p. 1548-58.
52. Godinat, A., et al., *A biocompatible in vivo ligation reaction and its application for noninvasive bioluminescent imaging of protease activity in living mice*. ACS Chem Biol, 2013. **8**(5): p. 987-99.

53. Van de Bittner, G.C., et al., *In vivo imaging of hydrogen peroxide production in a murine tumor model with a chemoselective bioluminescent reporter*. Proc Natl Acad Sci U S A, 2010. **107**(50): p. 21316-21.
54. Van de Bittner, G.C., C.R. Bertozzi, and C.J. Chang, *Strategy for dual-analyte luciferin imaging: in vivo bioluminescence detection of hydrogen peroxide and caspase activity in a murine model of acute inflammation*. J Am Chem Soc, 2013. **135**(5): p. 1783-95.
55. Henkin, A.H., et al., *Real-time noninvasive imaging of fatty acid uptake in vivo*. ACS Chem Biol, 2012. **7**(11): p. 1884-91.
56. Dubikovskaya, E.A., et al., *Overcoming multidrug resistance of small-molecule therapeutics through conjugation with releasable octaarginine transporters*. Proc Natl Acad Sci U S A, 2008. **105**(34): p. 12128-33.
57. Shinde, R., J. Perkins, and C.H. Contag, *Luciferin derivatives for enhanced in vitro and in vivo bioluminescence assays*. Biochemistry, 2006. **45**(37): p. 11103-12.
58. Evans, M.S., et al., *A synthetic luciferin improves bioluminescence imaging in live mice*. Nat Methods, 2014. **11**(4): p. 393-5.
59. Rice, B.W., M.D. Cable, and M.B. Nelson, *In vivo imaging of light-emitting probes*. J Biomed Opt, 2001. **6**(4): p. 432-40.
60. Luker, G.D. and K.E. Luker, *Optical imaging: current applications and future directions*. J Nucl Med, 2008. **49**(1): p. 1-4.
61. Wang, G., et al., *Overview of bioluminescence tomography--a new molecular imaging modality*. Front Biosci, 2008. **13**: p. 1281-93.
62. Cronin, M., et al., *High resolution in vivo bioluminescent imaging for the study of bacterial tumour targeting*. PLoS One, 2012. **7**(1): p. e30940.
63. Bernthal, N.M., et al., *Combined in vivo optical and microCT imaging to monitor infection, inflammation, and bone anatomy in an orthopaedic implant infection in mice*. J Vis Exp, 2014(92): p. e51612.
64. Collins, J.W., et al., *4D multimodality imaging of Citrobacter rodentium infections in mice*. J Vis Exp, 2013(78).
65. Massoud, T.F., A. Singh, and S.S. Gambhir, *Noninvasive Molecular Neuroimaging Using Reporter Genes: Part I, Principles Revisited*. American Journal of Neuroradiology, 2008. **29**(2): p. 229-234.
66. Kuchimaru, T., et al., *A luciferin analogue generating near-infrared bioluminescence achieves highly sensitive deep-tissue imaging*. Nat Commun, 2016. **7**: p. 11856.
67. Lathuiliere, A., et al., *A high-capacity cell macroencapsulation system supporting the long-term survival of genetically engineered allogeneic cells*. Biomaterials, 2014. **35**(2): p. 779-91.
68. Zaidi, H., *Molecular Imaging of Small Animals: Instrumentation and Applications*. 2014: Springer New York.
69. Contag, C.H. and M.H. Bachmann, *Advances in in vivo bioluminescence imaging of gene expression*. Annu Rev Biomed Eng, 2002. **4**: p. 235-60.
70. Zhao, D., et al., *Antivascular effects of combretastatin A4 phosphate in breast cancer xenograft assessed using dynamic bioluminescence imaging and confirmed by MRI*. FASEB J, 2008. **22**(7): p. 2445-51.
71. Thompson, S.M., et al., *Molecular bioluminescence imaging as a noninvasive tool for monitoring tumor growth and therapeutic response to MRI-guided laser ablation in a rat model of hepatocellular carcinoma*. Invest Radiol, 2013. **48**(6): p. 413-21.
72. Miyama, N., et al., *Bioluminescence and magnetic resonance imaging of macrophage homing to experimental abdominal aortic aneurysms*. Mol Imaging, 2012. **11**(2): p. 126-34.
73. Ottobri, L., et al., *Development of a bicistronic vector for multimodality imaging of estrogen receptor activity in a breast cancer model: preliminary application*. Eur J Nucl Med Mol Imaging, 2008. **35**(2): p. 365-78.
74. Brader, P., et al., *Escherichia coli Nissle 1917 facilitates tumor detection by positron emission tomography and optical imaging*. Clin Cancer Res, 2008. **14**(8): p. 2295-302.
75. Rao, J. and C.H. Contag, *More Chemistry Is Needed for Molecular Imaging*. Bioconjug Chem, 2016. **27**(2): p. 265-6.
76. Weissleder, R. and U. Mahmood, *Molecular imaging*. Radiology, 2001. **219**(2): p. 316-33.
77. Rudin, M., *Molecular Imaging: Basic Principles and Applications in Biomedical Research*. 2013: World Scientific Publishing Company.
78. Brancato, R. and G. Trabucchi, *Fluorescein and indocyanine green angiography in vascular chorioretinal diseases*. Semin Ophthalmol, 1998. **13**(4): p. 189-98.
79. Lee, S., J. Xie, and X. Chen, *Activatable molecular probes for cancer imaging*. Curr Top Med Chem, 2010. **10**(11): p. 1135-44.
80. Denburg, J.L., R.T. Lee, and W.D. McElroy, *Substrate-binding properties of firefly luciferase. I. Luciferin-binding site*. Arch Biochem Biophys, 1969. **134**(2): p. 381-94.

81. White, E.H., et al., *Amino Analogs of Firefly Luciferin and Biological Activity Thereof*. Journal of the American Chemical Society, 1966. **88**(9): p. 2015-2019.
82. Woodroffe, C.C., et al., *N-Alkylated 6'-aminoluciferins are bioluminescent substrates for Ultra-Glo and QuantiLum luciferase: new potential scaffolds for bioluminescent assays*. Biochemistry, 2008. **47**(39): p. 10383-93.
83. Miska, W. and R. Geiger, *Synthesis and characterization of luciferin derivatives for use in bioluminescence enhanced enzyme immunoassays. New ultrasensitive detection systems for enzyme immunoassays, I*. J Clin Chem Clin Biochem, 1987. **25**(1): p. 23-30.
84. Monsees, T., W. Miska, and R. Geiger, *Synthesis and characterization of a bioluminogenic substrate for alpha-chymotrypsin*. Anal Biochem, 1994. **221**(2): p. 329-34.
85. Geiger, R., et al., *A new ultrasensitive bioluminogenic enzyme substrate for beta-galactosidase*. Biol Chem Hoppe Seyler, 1992. **373**(12): p. 1187-91.
86. Drake, C.R., D.C. Miller, and E.F. Jones, *Activatable Optical Probes for the Detection of Enzymes*. Curr Org Synth, 2011. **8**(4): p. 498-520.
87. Niles, A.L., et al., *A homogeneous assay to measure live and dead cells in the same sample by detecting different protease markers*. Anal Biochem, 2007. **366**(2): p. 197-206.
88. Moravec, R.A., et al., *Cell-based bioluminescent assays for all three proteasome activities in a homogeneous format*. Analytical Biochemistry, 2009. **387**(2): p. 294-302.
89. Liu, J.J., et al., *Bioluminescent imaging of TRAIL-induced apoptosis through detection of caspase activation following cleavage of DEVD-aminoluciferin*. Cancer Biology & Therapy, 2005. **4**(8): p. 885-892.
90. Shah, K., et al., *In vivo imaging of S-TRAIL-mediated tumor regression and apoptosis*. Mol Ther, 2005. **11**(6): p. 926-31.
91. Hickson, J., et al., *Noninvasive molecular imaging of apoptosis in vivo using a modified firefly luciferase substrate, Z-DEVD-aminoluciferin*. Cell Death Differ, 2010. **17**(6): p. 1003-10.
92. Scabini, M., et al., *In vivo imaging of early stage apoptosis by measuring real-time caspase-3/7 activation*. Apoptosis, 2011. **16**(2): p. 198-207.
93. Dragulescu-Andrasi, A., G. Liang, and J. Rao, *In vivo bioluminescence imaging of furin activity in breast cancer cells using bioluminogenic substrates*. Bioconjug Chem, 2009. **20**(8): p. 1660-6.
94. Chang, Y.C., P.W. Chao, and C.H. Tung, *Sensitive luciferin derived probes for selective carboxypeptidase activity*. Bioorg Med Chem Lett, 2011. **21**(13): p. 3931-4.
95. Wehrman, T.S., et al., *Luminescent imaging of beta-galactosidase activity in living subjects using sequential reporter-enzyme luminescence*. Nat Methods, 2006. **3**(4): p. 295-301.
96. Yao, H., M.K. So, and J. Rao, *A bioluminogenic substrate for in vivo imaging of beta-lactamase activity*. Angew Chem Int Ed Engl, 2007. **46**(37): p. 7031-4.
97. Vorobyeva, A.G., et al., *Development of a Bioluminescent Nitroreductase Probe for Preclinical Imaging*. PLoS ONE, 2015. **10**(6): p. e0131037.
98. Craig, F.F., et al., *Membrane-permeable luciferin esters for assay of firefly luciferase in live intact cells*. Biochem J, 1991. **276** ( Pt 3): p. 637-41.
99. Yang, J. and D.B. Thomason, *An easily synthesized, photolyzable luciferase substrate for in vivo luciferase activity measurement*. Biotechniques, 1993. **15**(5): p. 848-50.
100. Meisenheimer, P.L., et al., *Proluciferin acetals as bioluminogenic substrates for cytochrome P450 activity and probes for CYP3A inhibition*. Drug Metab Dispos, 2011. **39**(12): p. 2403-10.
101. Roncoroni, C., et al., *Molecular imaging of cytochrome P450 activity in mice*. Pharmacol Res, 2012. **65**(5): p. 531-6.
102. Mofford, D.M., et al., *Luciferin Amides Enable in Vivo Bioluminescence Detection of Endogenous Fatty Acid Amide Hydrolase Activity*. Journal of the American Chemical Society, 2015. **137**(27): p. 8684-8687.
103. Ke, B., et al., *Bioluminescence Probe for Detecting Hydrogen Sulfide in Vivo*. Anal Chem, 2016. **88**(1): p. 592-5.
104. Tian, X., et al., *Visualization of in Vivo Hydrogen Sulfide Production by a Bioluminescence Probe in Cancer Cells and Nude Mice*. Anal Chem, 2015. **87**(22): p. 11325-31.
105. Zheng, Z., et al., *Hydrazide d-luciferin for in vitro selective detection and intratumoral imaging of Cu(2.)*. Biosens Bioelectron, 2016. **83**: p. 200-4.
106. Ke, B., et al., *Cell and in vivo imaging of fluoride ion with highly selective bioluminescent probes*. Anal Chem, 2015. **87**(18): p. 9110-3.
107. Cohen, A.S., et al., *Real-time bioluminescence imaging of glycans on live cells*. J Am Chem Soc, 2010. **132**(25): p. 8563-5.



108. Takakura, H., et al., *New class of bioluminogenic probe based on bioluminescent enzyme-induced electron transfer: BioLeT*. J Am Chem Soc, 2015. **137**(12): p. 4010-3.
109. Jones, L.R., et al., *Releasable luciferin-transporter conjugates: tools for the real-time analysis of cellular uptake and release*. J Am Chem Soc, 2006. **128**(20): p. 6526-7.
110. Wender, P.A., et al., *Real-time analysis of uptake and bioactivatable cleavage of luciferin-transporter conjugates in transgenic reporter mice*. Proc Natl Acad Sci U S A, 2007. **104**(25): p. 10340-5.
111. Gomes, A., E. Fernandes, and J.L. Lima, *Fluorescence probes used for detection of reactive oxygen species*. J Biochem Biophys Methods, 2005. **65**(2-3): p. 45-80.
112. Winterbourn, C.C., *The challenges of using fluorescent probes to detect and quantify specific reactive oxygen species in living cells*. Biochim Biophys Acta, 2014. **1840**(2): p. 730-8.
113. Saxon, E. and C.R. Bertozzi, *Cell surface engineering by a modified Staudinger reaction*. Science, 2000. **287**(5460): p. 2007-10.
114. Oliveira, I.M., Bonatto, D. , Henriques, J. A., *Nitroreductases: Enzymes with Environmental, Biotechnological and Clinical Importance*. Current Research, Technology and Education Topics in Applied Microbiology and Microbial Biotechnology, ed. A. Méndez-Vilas. Vol. 2. 2010, Spain: Formatex Badajoz.
115. Zenno, S., et al., *Biochemical characterization of NfsA, the Escherichia coli major nitroreductase exhibiting a high amino acid sequence homology to Frp, a Vibrio harveyi flavin oxidoreductase*. J Bacteriol, 1996. **178**(15): p. 4508-14.
116. Zenno, S., et al., *Gene cloning, purification, and characterization of NfsB, a minor oxygen-insensitive nitroreductase from Escherichia coli, similar in biochemical properties to FRase I, the major flavin reductase in Vibrio fischeri*. J Biochem, 1996. **120**(4): p. 736-44.
117. Prosser, G.A., et al., *Discovery and evaluation of Escherichia coli nitroreductases that activate the anti-cancer prodrug CB1954*. Biochem Pharmacol, 2010. **79**(5): p. 678-87.
118. Cellitti, S.E., et al., *Structure of Ddn, the deazaflavin-dependent nitroreductase from Mycobacterium tuberculosis involved in bioreductive activation of PA-824*. Structure, 2012. **20**(1): p. 101-12.
119. Jenks, P.J. and D.I. Edwards, *Metronidazole resistance in Helicobacter pylori*. Int J Antimicrob Agents, 2002. **19**(1): p. 1-7.
120. Patterson, S. and S. Wyllie, *Nitro drugs for the treatment of trypanosomatid diseases: past, present, and future prospects*. Trends in Parasitology, 2014. **30**(6): p. 289-298.
121. Pal, D., et al., *Giardia, Entamoeba, and Trichomonas enzymes activate metronidazole (nitroreductases) and inactivate metronidazole (nitroimidazole reductases)*. Antimicrob Agents Chemother, 2009. **53**(2): p. 458-64.
122. McBain, A.J. and G.T. Macfarlane, *Ecological and physiological studies on large intestinal bacteria in relation to production of hydrolytic and reductive enzymes involved in formation of genotoxic metabolites*. J Med Microbiol, 1998. **47**(5): p. 407-16.
123. Louis, P., G.L. Hold, and H.J. Flint, *The gut microbiota, bacterial metabolites and colorectal cancer*. Nat Rev Micro, 2014. **12**(10): p. 661-672.
124. Xu, G. and H.L. McLeod, *Strategies for enzyme/prodrug cancer therapy*. Clin Cancer Res, 2001. **7**(11): p. 3314-24.
125. Cronin, M., et al., *Bacterial vectors for imaging and cancer gene therapy: a review*. Cancer Gene Ther, 2012. **19**(11): p. 731-40.
126. Williams, E.M., et al., *Nitroreductase gene-directed enzyme prodrug therapy: insights and advances toward clinical utility*. Biochem J, 2015. **471**(2): p. 131-53.
127. Patel, P., et al., *A phase I/II clinical trial in localized prostate cancer of an adenovirus expressing nitroreductase with CB1954 [correction of CB1984]*. Mol Ther, 2009. **17**(7): p. 1292-9.
128. Bryant, L.M., et al., *Lessons learned from the clinical development and market authorization of Glybera*. Hum Gene Ther Clin Dev, 2013. **24**(2): p. 55-64.
129. Waerzeggers, Y., et al., *Methods to monitor gene therapy with molecular imaging*. Methods, 2009. **48**(2): p. 146-160.
130. Fass, L., *Imaging and cancer: a review*. Mol Oncol, 2008. **2**(2): p. 115-52.
131. Cui, L., et al., *A new prodrug-derived ratiometric fluorescent probe for hypoxia: high selectivity of nitroreductase and imaging in tumor cell*. Org Lett, 2011. **13**(5): p. 928-31.
132. Shi, Y., S. Zhang, and X. Zhang, *A novel near-infrared fluorescent probe for selectively sensing nitroreductase (NTR) in an aqueous medium*. Analyst, 2013. **138**(7): p. 1952-5.
133. Li, Z., et al., *Nitroreductase detection and hypoxic tumor cell imaging by a designed sensitive and selective fluorescent probe, 7-[(5-nitrofuran-2-yl)methoxy]-3H-phenoxazin-3-one*. Anal Chem, 2013. **85**(8): p. 3926-32.

134. James, A.L., et al., *Fluorogenic substrates for the detection of microbial nitroreductases*. Lett Appl Microbiol, 2001. **33**(6): p. 403-8.
135. Li, Z., et al., *7-((5-Nitrothiophen-2-yl)methoxy)-3H-phenoxazin-3-one as a spectroscopic off-on probe for highly sensitive and selective detection of nitroreductase*. Chem Commun (Camb), 2013. **49**(52): p. 5859-61.
136. Xu, K., et al., *High selectivity imaging of nitroreductase using a near-infrared fluorescence probe in hypoxic tumor*. Chem Commun (Camb), 2013. **49**(25): p. 2554-6.
137. Bhaumik, S., et al., *Noninvasive optical imaging of nitroreductase gene-directed enzyme prodrug therapy system in living animals*. Gene Ther, 2012. **19**(3): p. 295-302.
138. McCormack, E., et al., *Nitroreductase, a near-infrared reporter platform for in vivo time-domain optical imaging of metastatic cancer*. Cancer Res, 2013. **73**(4): p. 1276-86.
139. Sekar, T.V., et al., *Noninvasive Theranostic Imaging of HSV1-sr39TK-NTR/GCV-CB1954 Dual-Prodrug Therapy in Metastatic Lung Lesions of MDA-MB-231 Triple Negative Breast Cancer in Mice*. Theranostics, 2014. **4**(5): p. 460-74.
140. Leblond, F., et al., *Pre-clinical whole-body fluorescence imaging: Review of instruments, methods and applications*. J Photochem Photobiol B, 2010. **98**(1): p. 77-94.
141. Gross, S., et al., *Bioluminescence imaging of myeloperoxidase activity in vivo*. Nat Med, 2009. **15**(4): p. 455-61.
142. Liu, L. and R.P. Mason, *Imaging beta-galactosidase activity in human tumor xenografts and transgenic mice using a chemiluminescent substrate*. PLoS One, 2010. **5**(8): p. e12024.
143. Porterfield, W.B., et al., *A "Caged" Luciferin for Imaging Cell-Cell Contacts*. Journal of the American Chemical Society, 2015. **137**(27): p. 8656-8659.
144. Wong, R.H.F., et al., *Real time detection of live microbes using a highly sensitive bioluminescent nitroreductase probe*. Chemical Communications, 2015. **51**(21): p. 4440-4442.
145. Feng, P., et al., *Real-Time Bioluminescence Imaging of Nitroreductase in Mouse Model*. Anal Chem, 2016. **88**(11): p. 5610-4.
146. Cao, J., et al., *In Vivo Chemiluminescent Imaging Agents for Nitroreductase and Tissue Oxygenation*. Anal Chem, 2016. **88**(9): p. 4995-5002.
147. Ando, Y., et al., *Development of a quantitative bio/chemiluminescence spectrometer determining quantum yields: re-examination of the aqueous luminol chemiluminescence standard*. Photochem Photobiol, 2007. **83**(5): p. 1205-10.
148. White, E.H. and D.F. Roswell, *Chemiluminescence of Organic Hydrazides*. Accounts of Chemical Research, 1970. **3**(2): p. 54-8.
149. Viviani, V.R., et al., *Bioluminescence of beetle luciferases with 6'-amino-D-luciferin analogues reveals excited keto-oxyluciferin as the emitter and phenolate/luciferin binding site interactions modulate bioluminescence colors*. Biochemistry, 2014. **53**(32): p. 5208-20.
150. Zhang, N., et al., *Enhanced detection of myeloperoxidase activity in deep tissues through luminescent excitation of near-infrared nanoparticles*. Nat Med, 2013. **19**(4): p. 500-5.
151. Mercier, C., et al., *Characteristics of major Escherichia coli reductases involved in aerobic nitro and azo reduction*. J Appl Microbiol, 2013. **115**(4): p. 1012-22.
152. Stanton, M., et al., *In Vivo Bacterial Imaging without Engineering; A Novel Probe-Based Strategy Facilitated by Endogenous Nitroreductase Enzymes*. Curr Gene Ther, 2015. **15**(3): p. 277-88.
153. Prekeges, J.L., et al., *Reduction of fluoromisonidazole, a new imaging agent for hypoxia*. Biochem Pharmacol, 1991. **42**(12): p. 2387-95.
154. Krohn, K.A., J.M. Link, and R.P. Mason, *Molecular imaging of hypoxia*. J Nucl Med, 2008. **49 Suppl 2**: p. 129S-48S.
155. Sisson, G., et al., *Enzymes associated with reductive activation and action of nitazoxanide, nitrofurans, and metronidazole in Helicobacter pylori*. Antimicrob Agents Chemother, 2002. **46**(7): p. 2116-23.
156. Celli, C.M., et al., *NRH:quinone oxidoreductase 2 (NQO2) catalyzes metabolic activation of quinones and anti-tumor drugs*. Biochem Pharmacol, 2006. **72**(3): p. 366-76.
157. Wilson, W.R. and M.P. Hay, *Targeting hypoxia in cancer therapy*. Nat Rev Cancer, 2011. **11**(6): p. 393-410.
158. Branchini, B.R., et al., *Site-directed mutagenesis of firefly luciferase active site amino acids: a proposed model for bioluminescence color*. Biochemistry, 1999. **38**(40): p. 13223-30.
159. Miura, K., et al., *Molecular cloning of the nemA gene encoding N-ethylmaleimide reductase from Escherichia coli*. Biol Pharm Bull, 1997. **20**(1): p. 110-2.
160. Sellmyer, M.A., et al., *Visualizing cellular interactions with a generalized proximity reporter*. Proc Natl Acad Sci U S A, 2013. **110**(21): p. 8567-72.

161. Borch, R.F., et al., *Synthesis and evaluation of nitroheterocyclic phosphoramidates as hypoxia-selective alkylating agents*. J Med Chem, 2000. **43**(11): p. 2258-65.
162. Konsoula, R. and M. Jung, *In vitro plasma stability, permeability and solubility of mercaptoacetamide histone deacetylase inhibitors*. Int J Pharm, 2008. **361**(1-2): p. 19-25.
163. Hill, J.R., *In vitro drug metabolism using liver microsomes*. Curr Protoc Pharmacol, 2004. **Chapter 7**: p. Unit7 8.
164. Bao, B., et al., *In vivo imaging and quantification of carbonic anhydrase IX expression as an endogenous biomarker of tumor hypoxia*. PLoS One, 2012. **7**(11): p. e50860.
165. Raleigh, J.A. [cited 2016 June 17th]; Available from: <http://www.hypoxyprobe.com/faq.html#mechanism>.
166. Hughes, M.N., M.N. Centelles, and K.P. Moore, *Making and working with hydrogen sulfide: The chemistry and generation of hydrogen sulfide in vitro and its measurement in vivo: a review*. Free Radic Biol Med, 2009. **47**(10): p. 1346-53.
167. Wang, R., *Physiological implications of hydrogen sulfide: a whiff exploration that blossomed*. Physiol Rev, 2012. **92**(2): p. 791-896.
168. Wang, R., *Two's company, three's a crowd: can H<sub>2</sub>S be the third endogenous gaseous transmitter?* FASEB J, 2002. **16**(13): p. 1792-8.
169. Mustafa, A.K., et al., *H<sub>2</sub>S signals through protein S-sulfhydration*. Sci Signal, 2009. **2**(96): p. ra72.
170. Petersen, L.C., *The effect of inhibitors on the oxygen kinetics of cytochrome c oxidase*. Biochim Biophys Acta, 1977. **460**(2): p. 299-307.
171. Cooper, C.E. and G.C. Brown, *The inhibition of mitochondrial cytochrome oxidase by the gases carbon monoxide, nitric oxide, hydrogen cyanide and hydrogen sulfide: chemical mechanism and physiological significance*. J Bioenerg Biomembr, 2008. **40**(5): p. 533-9.
172. Paul, B.D. and S.H. Snyder, *H<sub>2</sub>S signalling through protein sulfhydration and beyond*. Nat Rev Mol Cell Biol, 2012. **13**(8): p. 499-507.
173. Stein, A. and S.M. Bailey, *Redox Biology of Hydrogen Sulfide: Implications for Physiology, Pathophysiology, and Pharmacology*. Redox Biol, 2013. **1**(1): p. 32-39.
174. Vitvitsky, V., O. Kabil, and R. Banerjee, *High turnover rates for hydrogen sulfide allow for rapid regulation of its tissue concentrations*. Antioxid Redox Signal, 2012. **17**(1): p. 22-31.
175. Bartholomew, T.C., et al., *Oxidation of sodium sulphide by rat liver, lungs and kidney*. Biochem Pharmacol, 1980. **29**(18): p. 2431-7.
176. Chiku, T., et al., *H<sub>2</sub>S biogenesis by human cystathionine gamma-lyase leads to the novel sulfur metabolites lanthionine and homolanthionine and is responsive to the grade of hyperhomocysteinemia*. J Biol Chem, 2009. **284**(17): p. 11601-12.
177. Linden, D.R., et al., *Production of the gaseous signal molecule hydrogen sulfide in mouse tissues*. J Neurochem, 2008. **106**(4): p. 1577-85.
178. Yang, G., et al., *H<sub>2</sub>S as a physiologic vasorelaxant: hypertension in mice with deletion of cystathionine gamma-lyase*. Science, 2008. **322**(5901): p. 587-90.
179. Kolluru, G.K., et al., *Hydrogen sulfide chemical biology: pathophysiological roles and detection*. Nitric Oxide, 2013. **35**: p. 5-20.
180. Lin, V.S., et al., *Chemical probes for molecular imaging and detection of hydrogen sulfide and reactive sulfur species in biological systems*. Chem Soc Rev, 2015. **44**(14): p. 4596-618.
181. Beard, R.S., Jr. and S.E. Bearden, *Vascular complications of cystathionine beta-synthase deficiency: future directions for homocysteine-to-hydrogen sulfide research*. Am J Physiol Heart Circ Physiol, 2011. **300**(1): p. H13-26.
182. Watanabe, M., et al., *Mice deficient in cystathionine beta-synthase: animal models for mild and severe homocyst(e)inemia*. Proc Natl Acad Sci U S A, 1995. **92**(5): p. 1585-9.
183. Furne, J., et al., *Oxidation of hydrogen sulfide and methanethiol to thiosulfate by rat tissues: a specialized function of the colonic mucosa*. Biochem Pharmacol, 2001. **62**(2): p. 255-9.
184. Lagoutte, E., et al., *Oxidation of hydrogen sulfide remains a priority in mammalian cells and causes reverse electron transfer in colonocytes*. Biochim Biophys Acta, 2010. **1797**(8): p. 1500-11.
185. Beauchamp, R.O., Jr., et al., *A critical review of the literature on hydrogen sulfide toxicity*. Crit Rev Toxicol, 1984. **13**(1): p. 25-97.
186. Levitt, M.D., et al., *Detoxification of hydrogen sulfide and methanethiol in the cecal mucosa*. J Clin Invest, 1999. **104**(8): p. 1107-14.
187. Burnet, A. and J. Weissenbach, *Valeur des renseignements fournis par la culture en glucose d'un lactate de plomb, pour la différenciation des bacillus typhique, paratyphique A et paratyphique B*. CR SOC Biol Paris, 1915. **78**: p. 565.

188. Kaspar, P., et al., *Evaluation of a simple screening test for the quality of drinking water systems*. Trop Med Parasitol, 1992. **43**(2): p. 124-7.
189. Pathak, S.P. and K. Gopal, *Efficiency of modified H<sub>2</sub>S test for detection of faecal contamination in water*. Environ Monit Assess, 2005. **108**(1-3): p. 59-65.
190. Suarez, F., et al., *Insights into human colonic physiology obtained from the study of flatus composition*. Am J Physiol, 1997. **272**(5 Pt 1): p. G1028-33.
191. Scanlan, P.D., F. Shanahan, and J.R. Marchesi, *Culture-independent analysis of desulfovibrios in the human distal colon of healthy, colorectal cancer and polypectomized individuals*. FEMS Microbiology Ecology, 2009. **69**(2): p. 213-221.
192. Cord-Ruwisch, R., H.-J. Seitz, and R. Conrad, *The capacity of hydrogenotrophic anaerobic bacteria to compete for traces of hydrogen depends on the redox potential of the terminal electron acceptor*. Archives of Microbiology, 1988. **149**(4): p. 350-357.
193. Gibson, G.R., J.H. Cummings, and G.T. Macfarlane, *Growth and activities of sulphate-reducing bacteria in gut contents of healthy subjects and patients with ulcerative colitis*. FEMS Microbiology Ecology, 1991. **9**(2): p. 103-111.
194. Levine, J., et al., *Fecal hydrogen sulfide production in ulcerative colitis*. Am J Gastroenterol, 1998. **93**(1): p. 83-7.
195. Loubinoux, J., et al., *Sulfate-reducing bacteria in human feces and their association with inflammatory bowel diseases*. FEMS Microbiol Ecol, 2002. **40**(2): p. 107-12.
196. Rowan, F.E., et al., *Sulphate-reducing bacteria and hydrogen sulphide in the aetiology of ulcerative colitis*. Br J Surg, 2009. **96**(2): p. 151-8.
197. Pitcher, M.C., E.R. Beatty, and J.H. Cummings, *The contribution of sulphate reducing bacteria and 5-aminosalicylic acid to faecal sulphide in patients with ulcerative colitis*. Gut, 2000. **46**(1): p. 64-72.
198. Wallace, J.L., et al., *Endogenous and exogenous hydrogen sulfide promotes resolution of colitis in rats*. Gastroenterology, 2009. **137**(2): p. 569-78, 578 e1.
199. Blachier, F., et al., *Luminal sulfide and large intestine mucosa: friend or foe?* Amino Acids, 2010. **39**(2): p. 335-47.
200. Flannigan, K.L., K.D. McCoy, and J.L. Wallace, *Eukaryotic and prokaryotic contributions to colonic hydrogen sulfide synthesis*. Am J Physiol Gastrointest Liver Physiol, 2011. **301**(1): p. G188-93.
201. Shen, X., et al., *Microbial regulation of host hydrogen sulfide bioavailability and metabolism*. Free Radic Biol Med, 2013. **60**: p. 195-200.
202. Shen, X., et al., *Measurement of plasma hydrogen sulfide in vivo and in vitro*. Free Radic Biol Med, 2011. **50**(9): p. 1021-31.
203. Shen, X., et al., *Analytical measurement of discrete hydrogen sulfide pools in biological specimens*. Free Radic Biol Med, 2012. **52**(11-12): p. 2276-83.
204. Shen, X., et al., *Measurement of H<sub>2</sub>S in vivo and in vitro by the monobromobimane method*. Methods Enzymol, 2015. **554**: p. 31-45.
205. Shatalin, K., et al., *H<sub>2</sub>S: a universal defense against antibiotics in bacteria*. Science, 2011. **334**(6058): p. 986-90.
206. Zhao, W., et al., *The vasorelaxant effect of H(2)S as a novel endogenous gaseous K(ATP) channel opener*. EMBO J, 2001. **20**(21): p. 6008-16.
207. Abe, K. and H. Kimura, *The possible role of hydrogen sulfide as an endogenous neuromodulator*. J Neurosci, 1996. **16**(3): p. 1066-71.
208. Distrutti, E., et al., *Evidence that hydrogen sulfide exerts antinociceptive effects in the gastrointestinal tract by activating KATP channels*. J Pharmacol Exp Ther, 2006. **316**(1): p. 325-35.
209. Hosoki, R., N. Matsuki, and H. Kimura, *The possible role of hydrogen sulfide as an endogenous smooth muscle relaxant in synergy with nitric oxide*. Biochem Biophys Res Commun, 1997. **237**(3): p. 527-31.
210. Teague, B., S. Asiedu, and P.K. Moore, *The smooth muscle relaxant effect of hydrogen sulphide in vitro: evidence for a physiological role to control intestinal contractility*. Br J Pharmacol, 2002. **137**(2): p. 139-45.
211. Schicho, R., et al., *Hydrogen sulfide is a novel prosecretory neuromodulator in the Guinea-pig and human colon*. Gastroenterology, 2006. **131**(5): p. 1542-52.
212. Wallace, J.L., *Physiological and pathophysiological roles of hydrogen sulfide in the gastrointestinal tract*. Antioxid Redox Signal, 2010. **12**(9): p. 1125-33.
213. Wallace, J.L., et al., *Hydrogen sulfide enhances ulcer healing in rats*. FASEB J, 2007. **21**(14): p. 4070-6.
214. Fiorucci, S., et al., *Inhibition of hydrogen sulfide generation contributes to gastric injury caused by anti-inflammatory nonsteroidal drugs*. Gastroenterology, 2005. **129**(4): p. 1210-24.



215. Fomenko, I., et al., *Effects of conventional and hydrogen sulfide-releasing non-steroidal anti-inflammatory drugs in rats with stress-induced and epinephrine-induced gastric damage*. *Stress*, 2014. **17**(6): p. 528-37.
216. Fiorucci, S. and L. Santucci, *Hydrogen sulfide-based therapies: focus on H<sub>2</sub>S releasing NSAIDs*. *Inflamm Allergy Drug Targets*, 2011. **10**(2): p. 133-40.
217. Linden, D.R., *Hydrogen sulfide signaling in the gastrointestinal tract*. *Antioxid Redox Signal*, 2014. **20**(5): p. 818-30.
218. Edmond, L.M., et al., *The effect of 5-aminosalicylic acid-containing drugs on sulfide production by sulfate-reducing and amino acid-fermenting bacteria*. *Inflamm Bowel Dis*, 2003. **9**(1): p. 10-7.
219. Matsunami, M., et al., *Hydrogen sulfide-induced colonic mucosal cytoprotection involves T-type calcium channel-dependent neuronal excitation in rats*. *J Physiol Pharmacol*, 2012. **63**(1): p. 61-8.
220. Fiorucci, S., et al., *Enhanced activity of a hydrogen sulphide-releasing derivative of mesalamine (ATB-429) in a mouse model of colitis*. *Br J Pharmacol*, 2007. **150**(8): p. 996-1002.
221. Furne, J.K., et al., *Binding of hydrogen sulfide by bismuth does not prevent dextran sulfate-induced colitis in rats*. *Dig Dis Sci*, 2000. **45**(7): p. 1439-43.
222. Conlon, M.A. and A.R. Bird, *The impact of diet and lifestyle on gut microbiota and human health*. *Nutrients*, 2015. **7**(1): p. 17-44.
223. Gerritsen, J., et al., *Intestinal microbiota in human health and disease: the impact of probiotics*. *Genes Nutr*, 2011. **6**(3): p. 209-40.
224. Bajzer, M. and R.J. Seeley, *Physiology: obesity and gut flora*. *Nature*, 2006. **444**(7122): p. 1009-10.
225. Brussow, H. and S.J. Parkinson, *You are what you eat*. *Nat Biotechnol*, 2014. **32**(3): p. 243-5.
226. Suarez, F., et al., *Production and elimination of sulfur-containing gases in the rat colon*. *Am J Physiol*, 1998. **274**(4 Pt 1): p. G727-33.
227. Rey, F.E., et al., *Metabolic niche of a prominent sulfate-reducing human gut bacterium*. *Proc Natl Acad Sci U S A*, 2013. **110**(33): p. 13582-7.
228. Sarna, L., et al., *High fat diet alters homocysteine metabolism and hydrogen sulfide biosynthesis in mice (1116.3)*. *The FASEB Journal*, 2014. **28**(1 Supplement).
229. Marquet, P., et al., *Lactate has the potential to promote hydrogen sulphide formation in the human colon*. *FEMS Microbiol Lett*, 2009. **299**(2): p. 128-34.
230. Magee, E.A., et al., *Contribution of dietary protein to sulfide production in the large intestine: an in vitro and a controlled feeding study in humans*. *The American Journal of Clinical Nutrition*, 2000. **72**(6): p. 1488-1494.
231. Richardson, C.J., E.A. Magee, and J.H. Cummings, *A new method for the determination of sulphide in gastrointestinal contents and whole blood by microdistillation and ion chromatography*. *Clin Chim Acta*, 2000. **293**(1-2): p. 115-25.
232. Hine, C., et al., *Endogenous hydrogen sulfide production is essential for dietary restriction benefits*. *Cell*, 2015. **160**(1-2): p. 132-44.
233. Dorman, D.C., et al., *Cytochrome oxidase inhibition induced by acute hydrogen sulfide inhalation: correlation with tissue sulfide concentrations in the rat brain, liver, lung, and nasal epithelium*. *Toxicol Sci*, 2002. **65**(1): p. 18-25.
234. Oh, G.S., et al., *Hydrogen sulfide inhibits nitric oxide production and nuclear factor-kappaB via heme oxygenase-1 expression in RAW264.7 macrophages stimulated with lipopolysaccharide*. *Free Radic Biol Med*, 2006. **41**(1): p. 106-19.
235. Yang, G., et al., *Cystathionine gamma-lyase overexpression inhibits cell proliferation via a H<sub>2</sub>S-dependent modulation of ERK1/2 phosphorylation and p21Cip/WAK-1*. *J Biol Chem*, 2004. **279**(47): p. 49199-205.
236. Szabo, C., *Hydrogen sulphide and its therapeutic potential*. *Nat Rev Drug Discov*, 2007. **6**(11): p. 917-35.
237. Goodwin, L.R., et al., *Determination of sulfide in brain tissue by gas dialysis/ion chromatography: postmortem studies and two case reports*. *J Anal Toxicol*, 1989. **13**(2): p. 105-9.
238. Mitchell, T.W., J.C. Savage, and D.H. Gould, *High-performance liquid chromatography detection of sulfide in tissues from sulfide-treated mice*. *Journal of Applied Toxicology*, 1993. **13**(6): p. 389-394.
239. Savage, J.C. and D.H. Gould, *Determination of sulfide in brain tissue and rumen fluid by ion-interaction reversed-phase high-performance liquid chromatography*. *Journal of Chromatography B: Biomedical Sciences and Applications*, 1990. **526**: p. 540-545.
240. Warenycia, M.W., et al., *Acute hydrogen sulfide poisoning*. *Biochemical Pharmacology*, 1989. **38**(6): p. 973-981.
241. Ogasawara, Y., S. Isoda, and S. Tanabe, *Tissue and Subcellular Distribution of Bound and Acid-Labile Sulfur, and the Enzymic Capacity for Sulfide Production in the Rat*. *Biological & Pharmaceutical Bulletin*, 1994. **17**(12): p. 1535-1542.

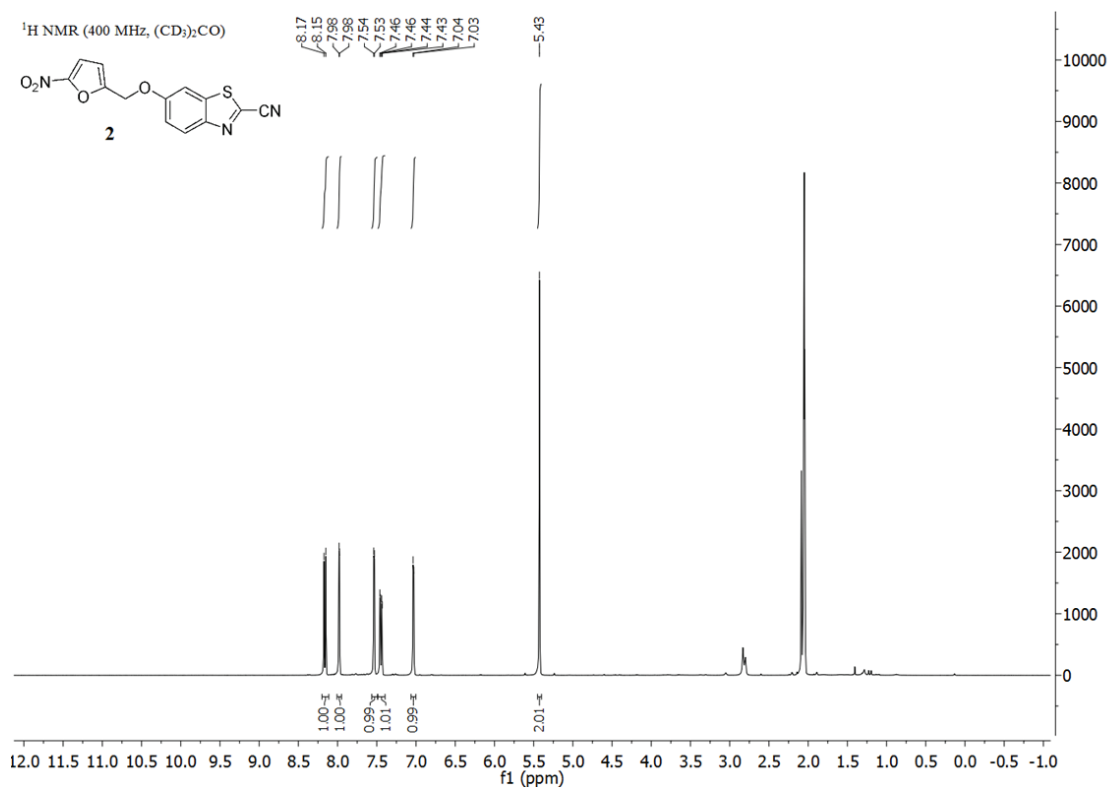
242. Chen, Y.H., et al., *Endogenous hydrogen sulfide in patients with COPD*. Chest, 2005. **128**(5): p. 3205-11.
243. Zhong, G., et al., *The role of hydrogen sulfide generation in the pathogenesis of hypertension in rats induced by inhibition of nitric oxide synthase*. Journal of Hypertension, 2003. **21**(10): p. 1879-1885.
244. Han, Y., et al., *Hydrogen sulfide and carbon monoxide are in synergy with each other in the pathogenesis of recurrent febrile seizures*. Cell Mol Neurobiol, 2006. **26**(1): p. 101-7.
245. Levitt, M.D., et al., *Physiology of sulfide in the rat colon: use of bismuth to assess colonic sulfide production*. J Appl Physiol (1985), 2002. **92**(4): p. 1655-60.
246. Furne, J., A. Saeed, and M.D. Levitt, *Whole tissue hydrogen sulfide concentrations are orders of magnitude lower than presently accepted values*. Am J Physiol Regul Integr Comp Physiol, 2008. **295**(5): p. R1479-85.
247. Whitfield, N.L., et al., *Reappraisal of H<sub>2</sub>S/sulfide concentration in vertebrate blood and its potential significance in ischemic preconditioning and vascular signaling*. Am J Physiol Regul Integr Comp Physiol, 2008. **294**(6): p. R1930-7.
248. Kabil, O. and R. Banerjee, *Redox biochemistry of hydrogen sulfide*. J Biol Chem, 2010. **285**(29): p. 21903-7.
249. Fogo, J.K. and M. Popowsky, *Spectrophotometric Determination of Hydrogen Sulfide*. Analytical Chemistry, 1949. **21**(6): p. 732-734.
250. Olson, K.R., *Is hydrogen sulfide a circulating "gasotransmitter" in vertebrate blood?* Biochim Biophys Acta, 2009. **1787**(7): p. 856-63.
251. Levitt, M.D., M.S. Abdel-Rehim, and J. Furne, *Free and acid-labile hydrogen sulfide concentrations in mouse tissues: anomalously high free hydrogen sulfide in aortic tissue*. Antioxid Redox Signal, 2011. **15**(2): p. 373-8.
252. Varlet, V., et al., *Hydrogen sulfide measurement by headspace-gas chromatography-mass spectrometry (HS-GC-MS): application to gaseous samples and gas dissolved in muscle*. J Anal Toxicol, 2015. **39**(1): p. 52-7.
253. Ida, T., et al., *Reactive cysteine persulfides and S-polythiolation regulate oxidative stress and redox signaling*. Proc Natl Acad Sci U S A, 2014. **111**(21): p. 7606-11.
254. Doeller, J.E., et al., *Polarographic measurement of hydrogen sulfide production and consumption by mammalian tissues*. Anal Biochem, 2005. **341**(1): p. 40-51.
255. Olson, K.R., *A practical look at the chemistry and biology of hydrogen sulfide*. Antioxid Redox Signal, 2012. **17**(1): p. 32-44.
256. Wintner, E.A., et al., *A monobromobimane-based assay to measure the pharmacokinetic profile of reactive sulphide species in blood*. Br J Pharmacol, 2010. **160**(4): p. 941-57.
257. Liu, T., et al., *A lysosome-targetable fluorescent probe for imaging hydrogen sulfide in living cells*. Org Lett, 2013. **15**(9): p. 2310-3.
258. Pak, Y.L., et al., *Mitochondria-Targeted Reaction-Based Fluorescent Probe for Hydrogen Sulfide*. Anal Chem, 2016. **88**(10): p. 5476-81.
259. Yang, S., et al., *Design of a simultaneous target and location-activatable fluorescent probe for visualizing hydrogen sulfide in lysosomes*. Anal Chem, 2014. **86**(15): p. 7508-15.
260. Montoya, L.A. and M.D. Pluth, *Organelle-Targeted H<sub>2</sub>S Probes Enable Visualization of the Subcellular Distribution of H<sub>2</sub>S Donors*. Anal Chem, 2016. **88**(11): p. 5769-74.
261. Chen, S., et al., *Reaction-based genetically encoded fluorescent hydrogen sulfide sensors*. J Am Chem Soc, 2012. **134**(23): p. 9589-92.
262. Lin, V.S., A.R. Lippert, and C.J. Chang, *Cell-trappable fluorescent probes for endogenous hydrogen sulfide signaling and imaging H<sub>2</sub>O<sub>2</sub>-dependent H<sub>2</sub>S production*. Proc Natl Acad Sci U S A, 2013. **110**(18): p. 7131-5.
263. Hartle, M.D. and M.D. Pluth, *A practical guide to working with H<sub>2</sub>S at the interface of chemistry and biology*. Chem Soc Rev, 2016.
264. Lippert, A.R., *Designing reaction-based fluorescent probes for selective hydrogen sulfide detection*. J Inorg Biochem, 2014. **133**: p. 136-42.
265. Prescher, J.A. and C.R. Bertozzi, *Chemistry in living systems*. Nat Chem Biol, 2005. **1**(1): p. 13-21.
266. Prescher, J.A., D.H. Dube, and C.R. Bertozzi, *Chemical remodelling of cell surfaces in living animals*. Nature, 2004. **430**(7002): p. 873-7.
267. Laughlin, S.T., et al., *In vivo imaging of membrane-associated glycans in developing zebrafish*. Science, 2008. **320**(5876): p. 664-7.
268. Agard, N.J., et al., *A Comparative Study of Bioorthogonal Reactions with Azides*. ACS Chemical Biology, 2006. **1**(10): p. 644-648.
269. Lippert, A.R., E.J. New, and C.J. Chang, *Reaction-based fluorescent probes for selective imaging of hydrogen sulfide in living cells*. J Am Chem Soc, 2011. **133**(26): p. 10078-80.
270. Dufton, N., et al., *Hydrogen sulfide and resolution of acute inflammation: A comparative study utilizing a novel fluorescent probe*. Sci Rep, 2012. **2**: p. 499.

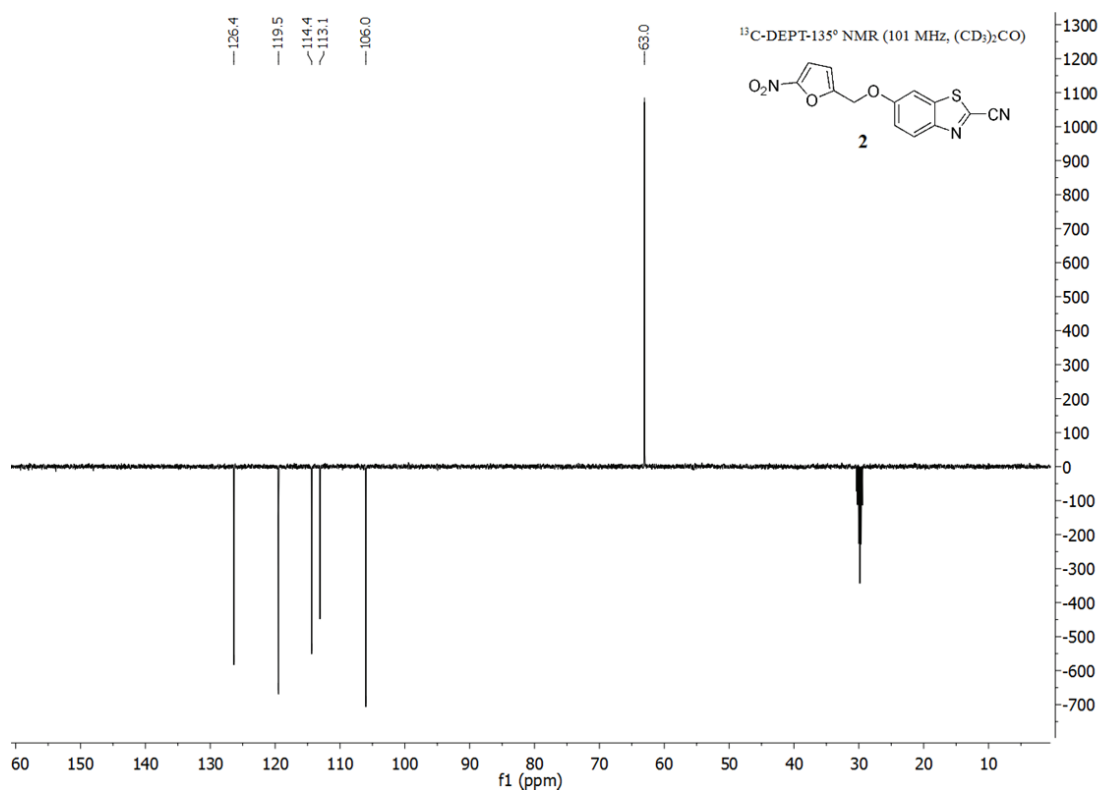
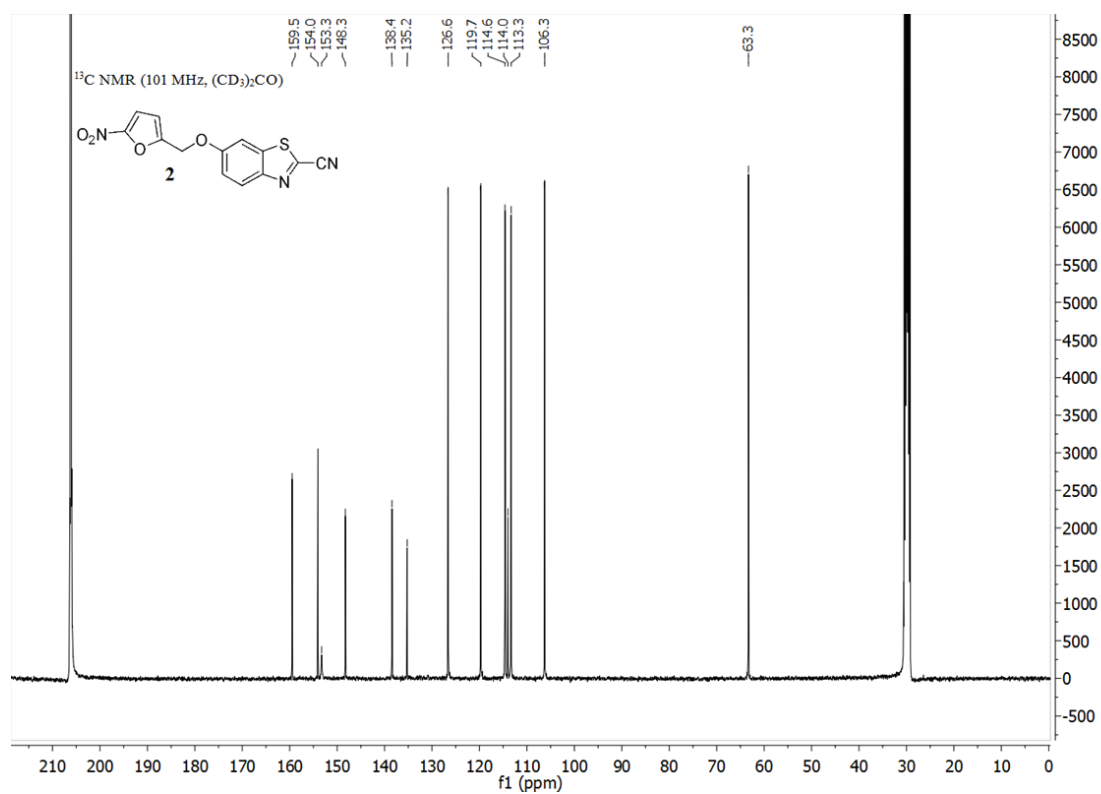
271. Hammers, M.D., et al., *A Bright Fluorescent Probe for H<sub>2</sub>S Enables Analyte-Responsive, 3D Imaging in Live Zebrafish Using Light Sheet Fluorescence Microscopy*. J Am Chem Soc, 2015. **137**(32): p. 10216-23.
272. Zou, X.J., et al., *A lysosome-targeted fluorescent chemodosimeter for monitoring endogenous and exogenous hydrogen sulfide by in vivo imaging*. Chem Commun (Camb), 2014. **50**(89): p. 13833-6.
273. Zhang, L., et al., *A highly selective and sensitive near-infrared fluorescent probe for imaging of hydrogen sulphide in living cells and mice*. Sci Rep, 2016. **6**: p. 18868.
274. Chen, H., et al., *Development of unique xanthene-cyanine fused near-infrared fluorescent fluorophores with superior chemical stability for biological fluorescence imaging*. Chemistry, 2015. **21**(2): p. 733-45.
275. Cao, J., et al., *Chemiluminescent Probes for Imaging H<sub>2</sub>S in Living Animals*. Chem Sci, 2015. **6**(3): p. 1979-1985.
276. Griffin, R.J., *The medicinal chemistry of the azido group*. Prog Med Chem, 1994. **31**: p. 121-232.
277. Bayley, H., D.N. Standring, and J.R. Knowles, *Propane-1,3-dithiol: A selective reagent for the efficient reduction of alkyl and aryl azides to amines*. Tetrahedron Letters, 1978. **19**(39): p. 3633-3634.
278. Henthorn, H.A. and M.D. Pluth, *Mechanistic Insights into the H(2)S-Mediated Reduction of Aryl Azides Commonly Used in H(2)S Detection*. J Am Chem Soc, 2015. **137**(48): p. 15330-6.
279. Brase, S., et al., *Organic azides: an exploding diversity of a unique class of compounds*. Angew Chem Int Ed Engl, 2005. **44**(33): p. 5188-240.
280. Fortman, G.C., B. Captain, and C.D. Hoff, *Thermodynamic investigations of the staudinger reaction of trialkylphosphines with 1-adamantyl azide and the isolation of an unusual s-cis phosphazide*. Inorg Chem, 2009. **48**(5): p. 1808-10.
281. Leffler, J.E. and R.D. Temple, *Staudinger reaction between triarylphosphines and azides. Mechanism*. Journal of the American Chemical Society, 1967. **89**(20): p. 5235-5246.
282. Zhu, Z., et al., *Multi-Fluorinated Azido Coumarins for Rapid and Selective Detection of Biological H<sub>2</sub>S in Living Cells*. Chem Asian J, 2016. **11**(1): p. 68-71.
283. Wei, L., et al., *A highly selective and fast-response fluorescent probe for visualization of enzymatic H<sub>2</sub>S production in vitro and in living cells*. Chem Commun (Camb), 2015. **51**(52): p. 10463-6.
284. Wei, C., et al., *o-Fluorination of aromatic azides yields improved azido-based fluorescent probes for hydrogen sulfide: synthesis, spectra, and bioimaging*. Chem Asian J, 2014. **9**(12): p. 3586-92.
285. Torres-Vega, J.J., et al., *Revisiting Aromaticity and Chemical Bonding of Fluorinated Benzene Derivatives*. ChemistryOpen, 2015. **4**(3): p. 302-7.
286. Pirrung, M.C., et al., *Synthesis and bioluminescence of difluoroluciferin*. Bioorg Med Chem Lett, 2014. **24**(20): p. 4881-3.
287. Steinhardt, R.C., et al., *Design and Synthesis of an Alkynyl Luciferin Analogue for Bioluminescence Imaging*. Chemistry, 2016. **22**(11): p. 3671-5.
288. Tajc, S.G., et al., *Direct determination of thiol pK<sub>a</sub> by isothermal titration microcalorimetry*. J Am Chem Soc, 2004. **126**(34): p. 10508-9.
289. Tang, S.S. and G.G. Chang, *Kinetic characterization of the endogenous glutathione transferase activity of octopus lens S-crystallin*. J Biochem, 1996. **119**(6): p. 1182-8.
290. Bang, S.W., D.S. Clark, and J.D. Keasling, *Engineering hydrogen sulfide production and cadmium removal by expression of the thiosulfate reductase gene (phsABC) from Salmonella enterica serovar typhimurium in Escherichia coli*. Appl Environ Microbiol, 2000. **66**(9): p. 3939-44.
291. Clark, M.A. and E.L. Barrett, *The phs gene and hydrogen sulfide production by Salmonella typhimurium*. J Bacteriol, 1987. **169**(6): p. 2391-7.
292. Awano, N., et al., *Identification and functional analysis of Escherichia coli cysteine desulphydrases*. Appl Environ Microbiol, 2005. **71**(7): p. 4149-52.
293. Peng, B., et al., *Fluorescent probes based on nucleophilic substitution-cyclization for hydrogen sulfide detection and bioimaging*. Chemistry, 2014. **20**(4): p. 1010-6.
294. Deplancke, B., et al., *Gastrointestinal and microbial responses to sulfate-supplemented drinking water in mice*. Exp Biol Med (Maywood), 2003. **228**(4): p. 424-33.
295. McCutcheon, D.C., W.B. Porterfield, and J.A. Prescher, *Rapid and scalable assembly of firefly luciferase substrates*. Org Biomol Chem, 2015. **13**(7): p. 2117-21.
296. Belkheira, M., et al., *Organocatalytic synthesis of 1,2,3-triazoles from unactivated ketones and arylazides*. Chemistry, 2011. **17**(46): p. 12917-21.
297. Keana, J.F.W. and S.X. Cai, *New reagents for photoaffinity labeling: synthesis and photolysis of functionalized perfluorophenyl azides*. The Journal of Organic Chemistry, 1990. **55**(11): p. 3640-3647.

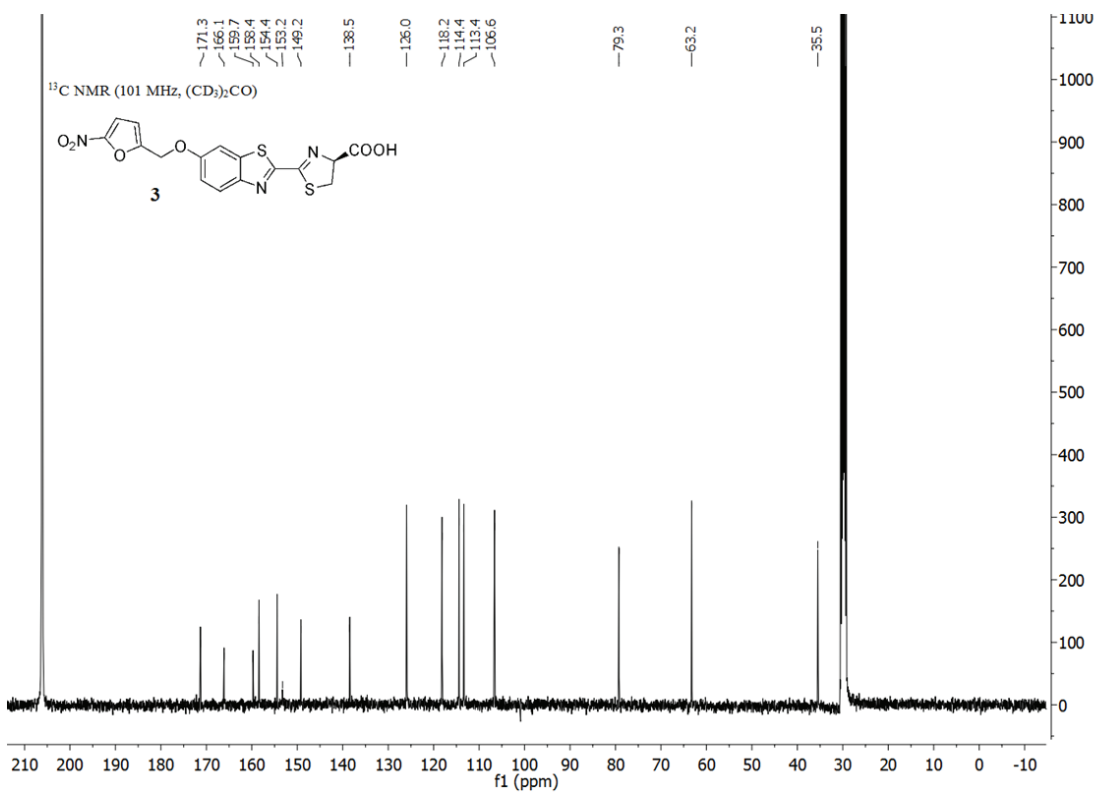
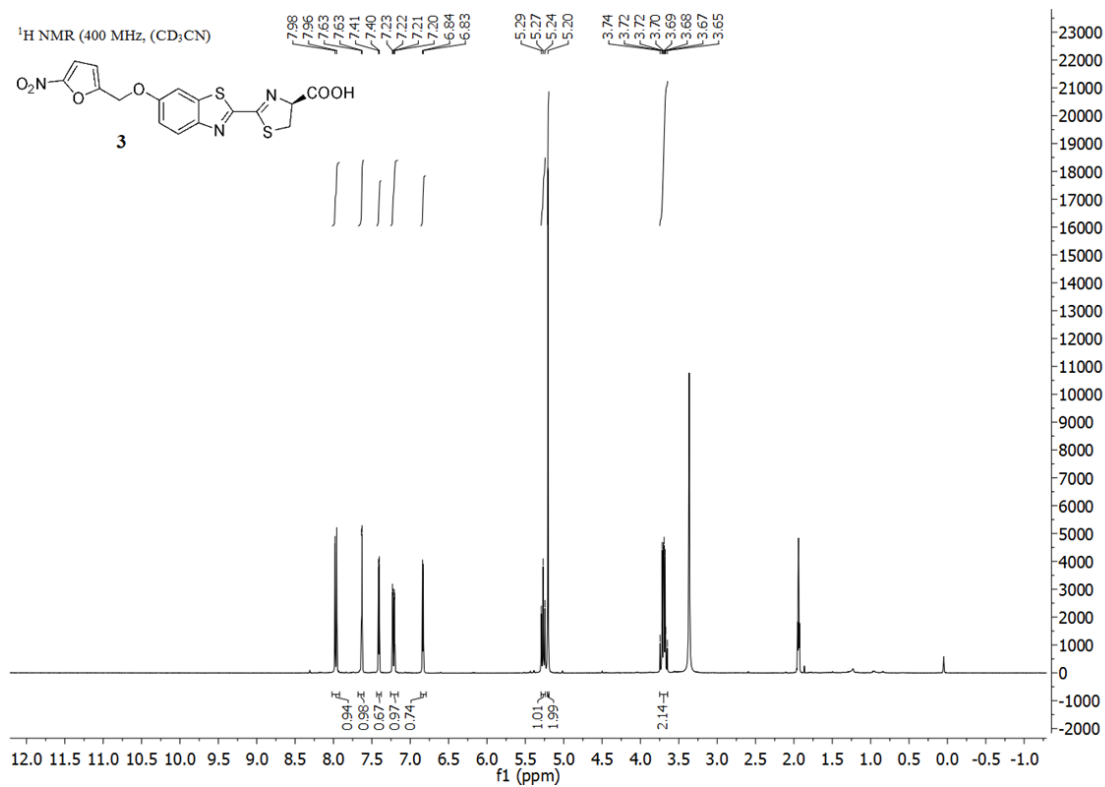
298. Besson, T., Dozias M.-J., Guillard J., Rees W. C., *New route to 2-cyanobenzothiazoles via N-arylimino-1,2,3-dithiazoles*. J. Chem. Soc., Perkin Trans. 1, 1998: p. 3925-3926.
299. Bellamy, F.D., Ou K., *Selective reduction of aromatic nitro compounds with stannous chloride in non acidic and non aqueous medium*. Tetrahedron Letters, 1984. **25**(8): p. 839-842.

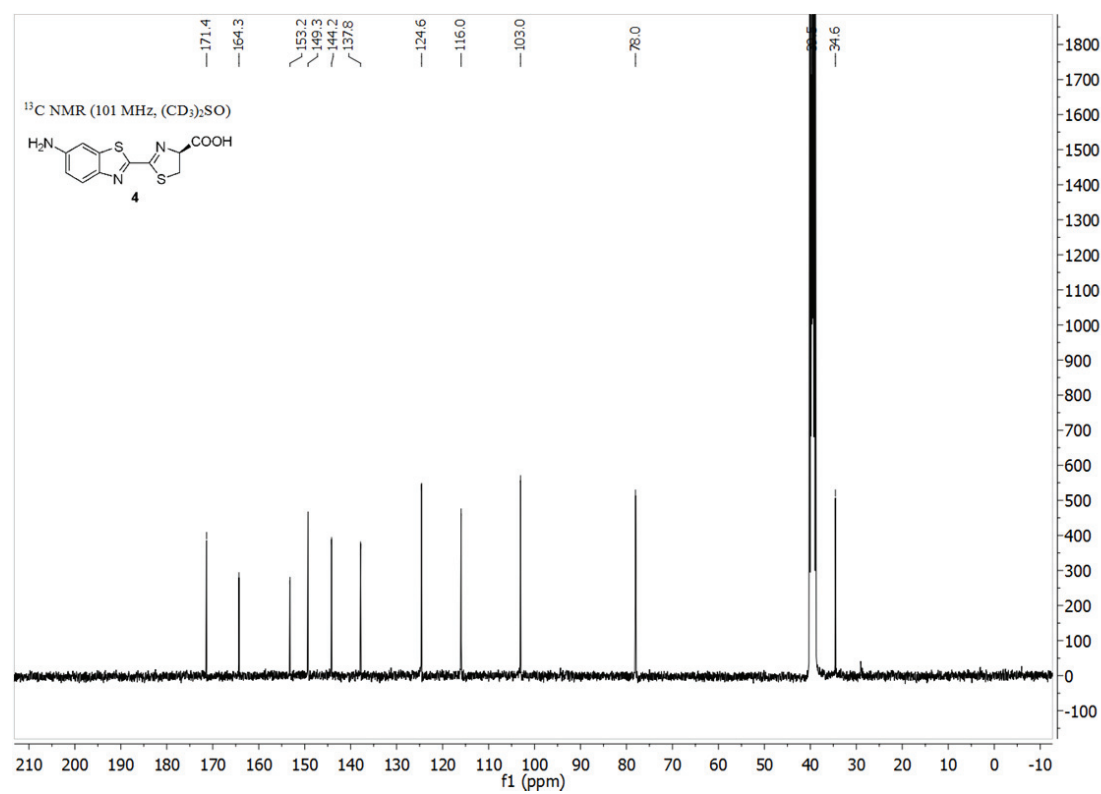
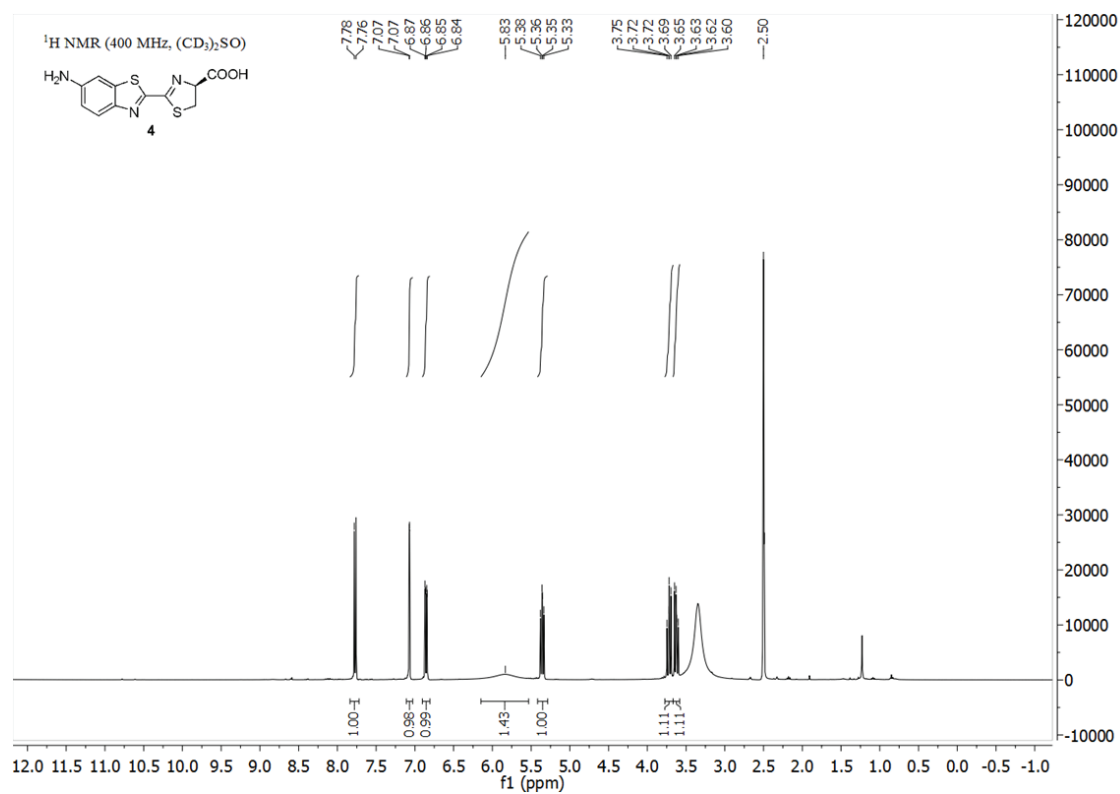
## Chapter 6 Annexes

### 6.1 NMR spectra

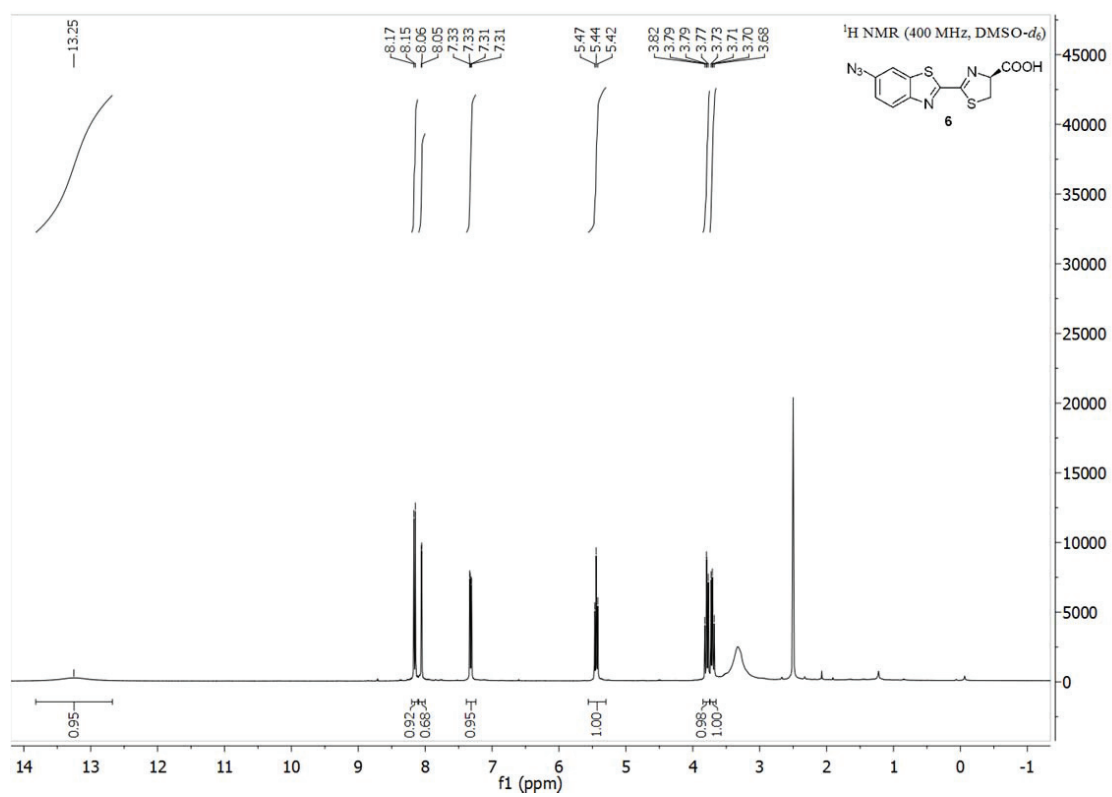
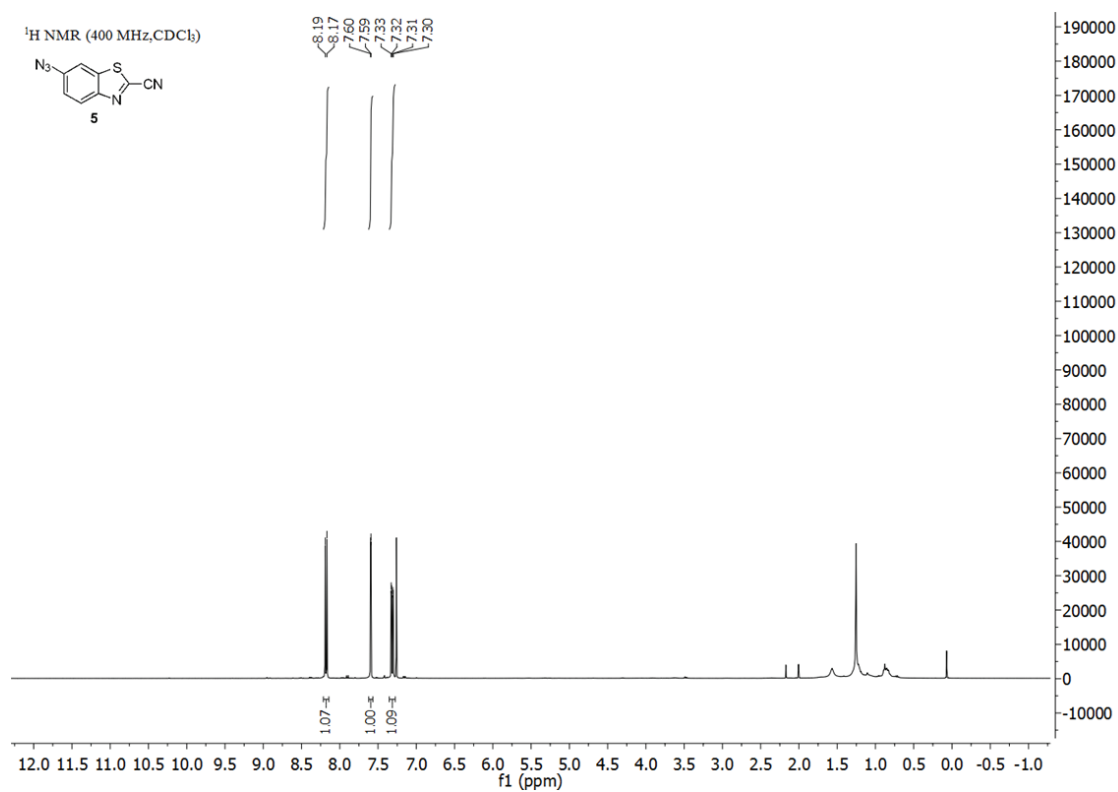


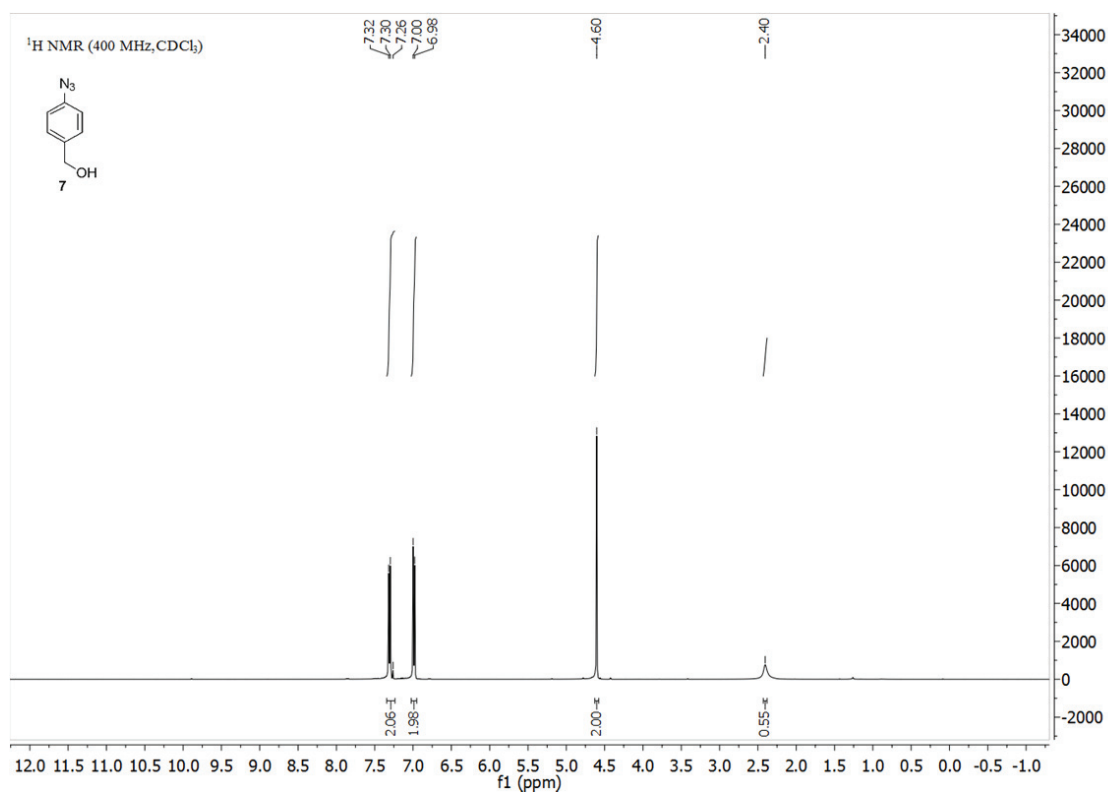
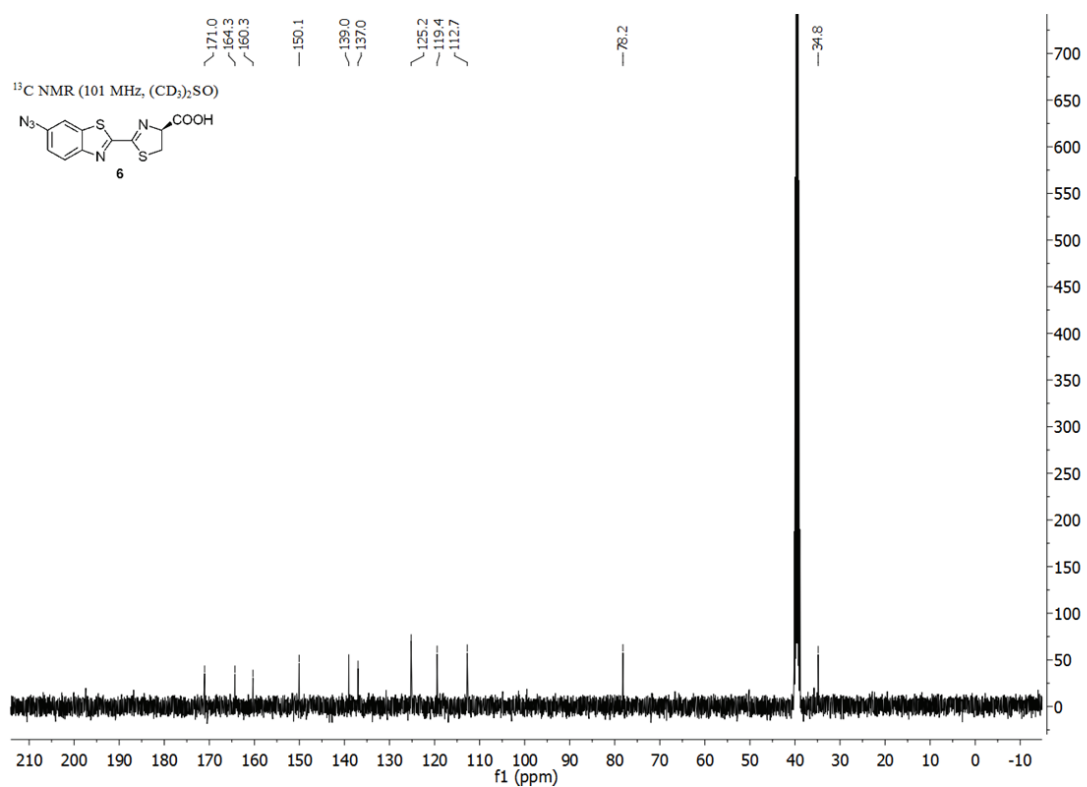


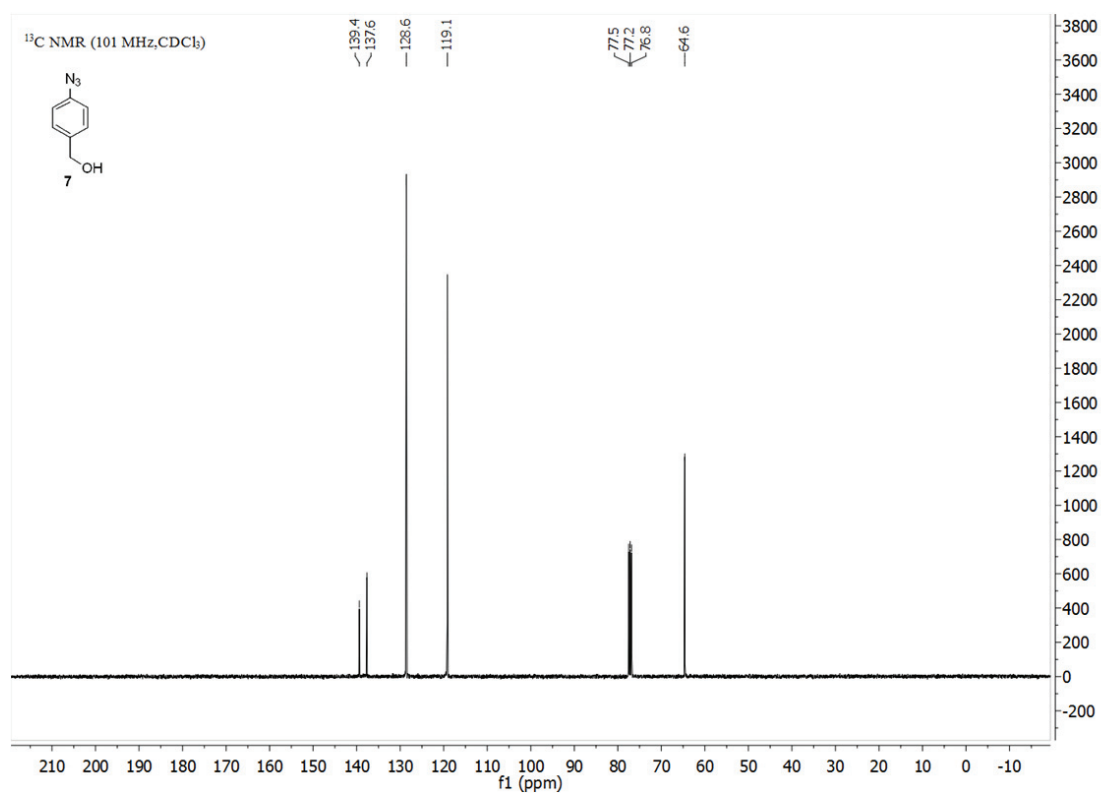


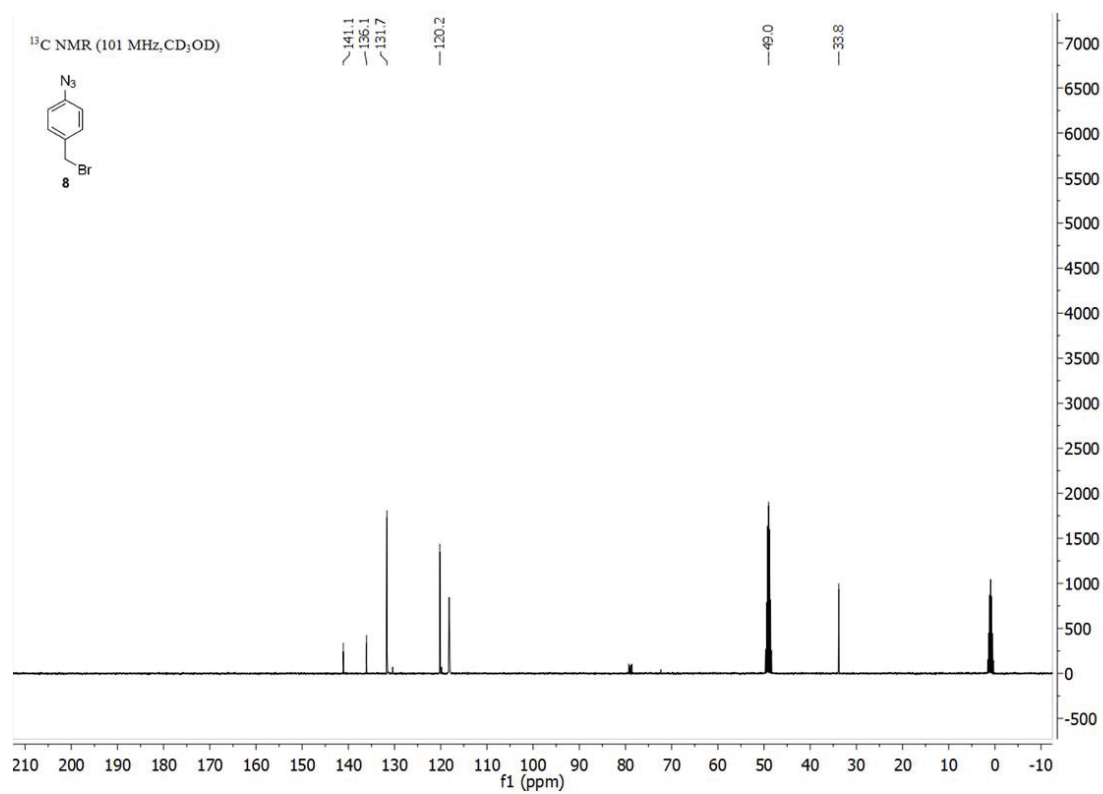
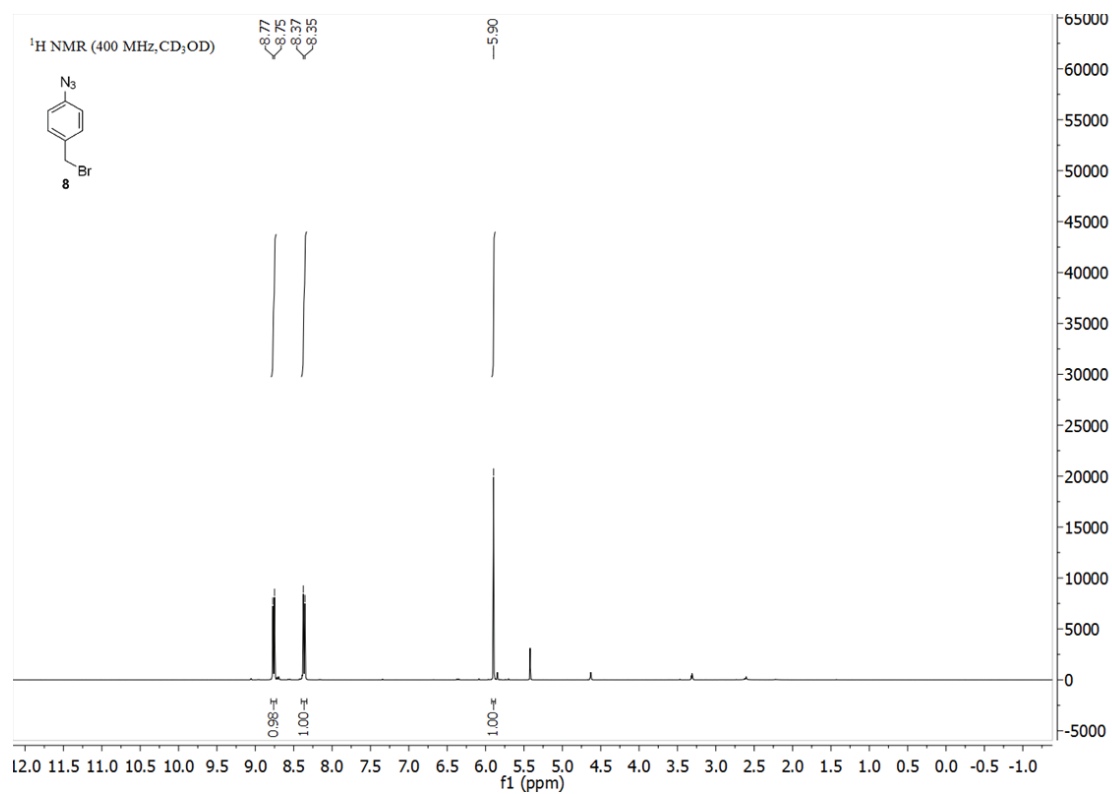


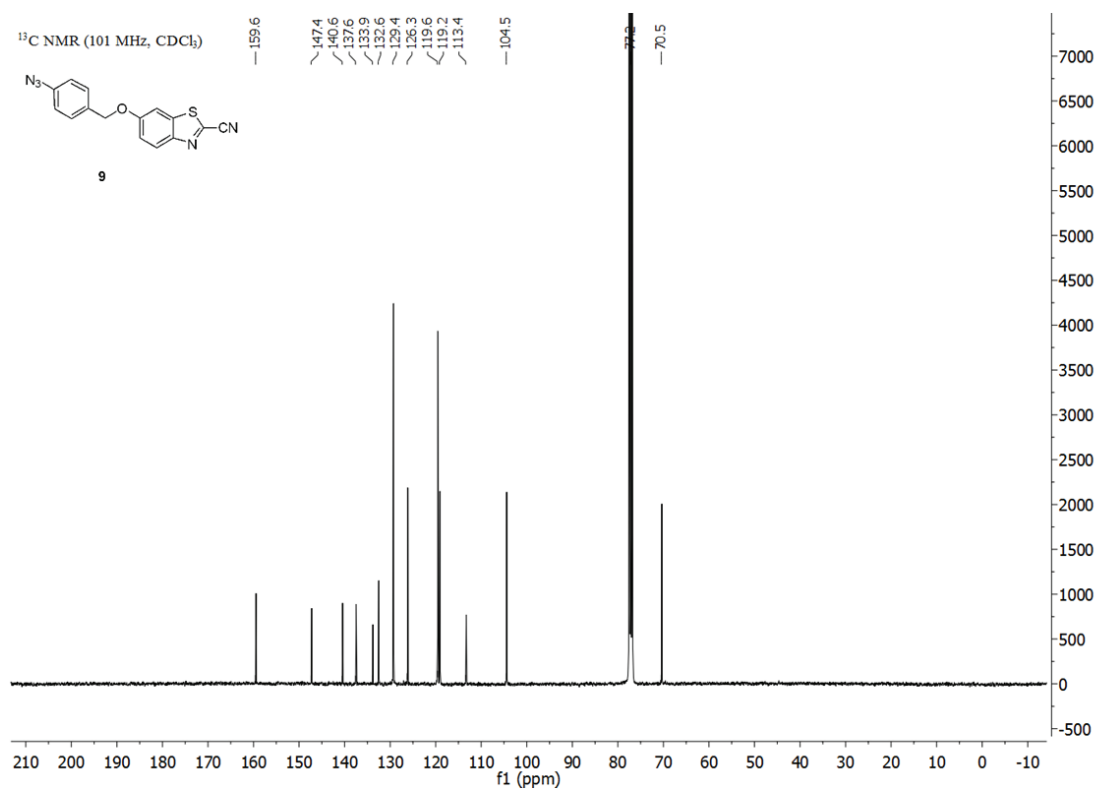
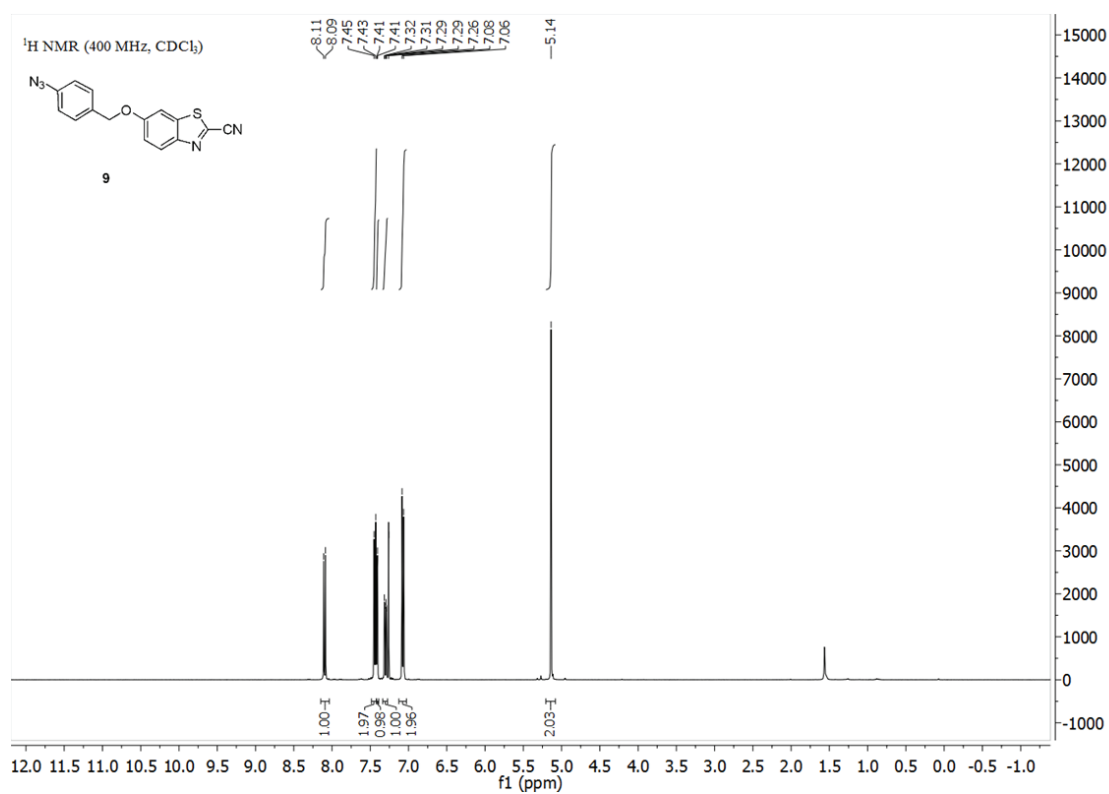


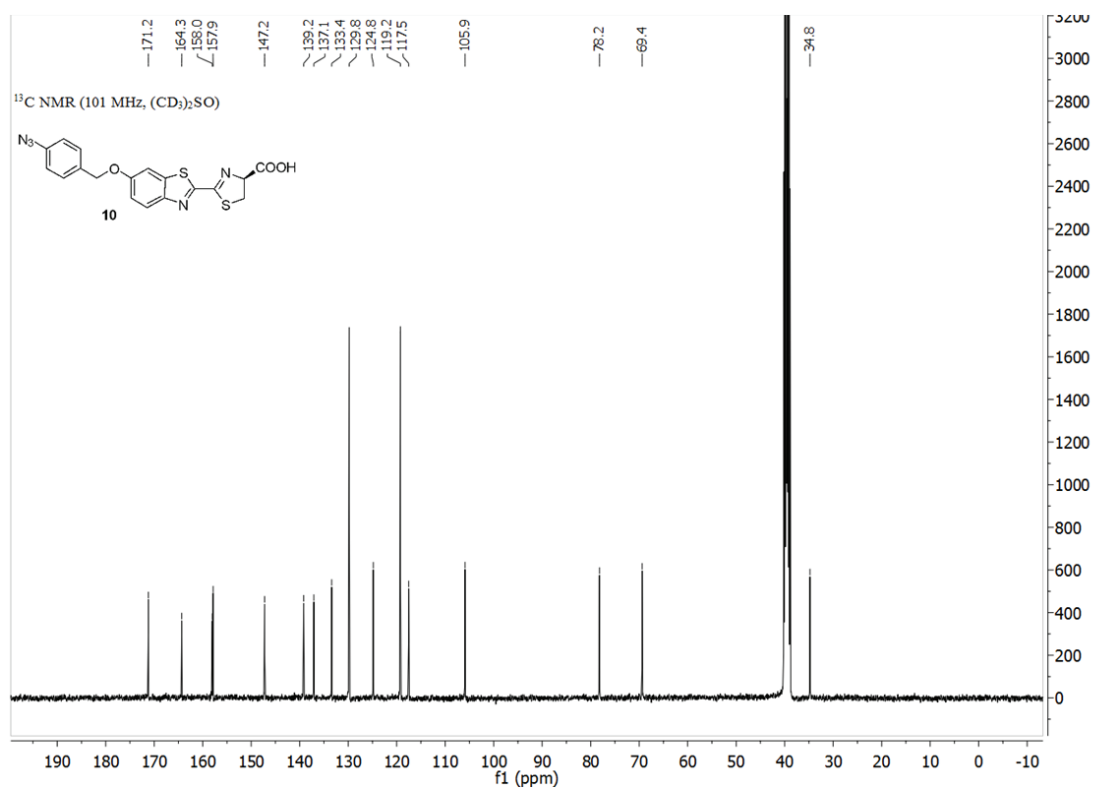
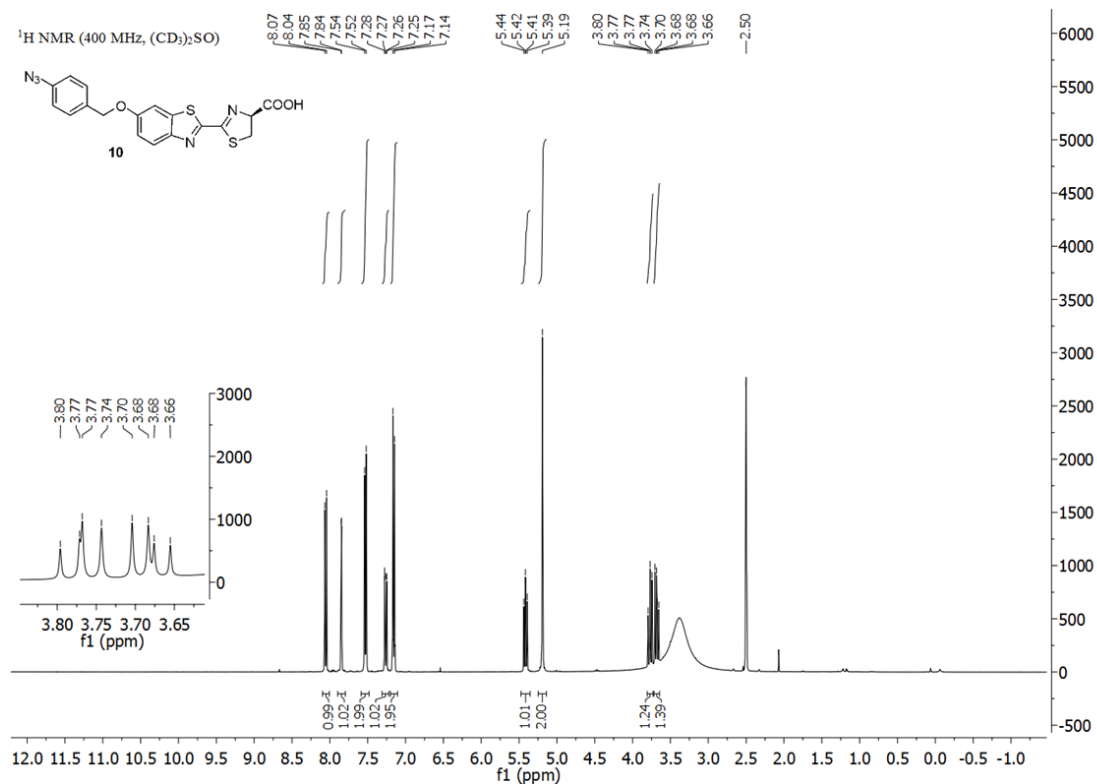


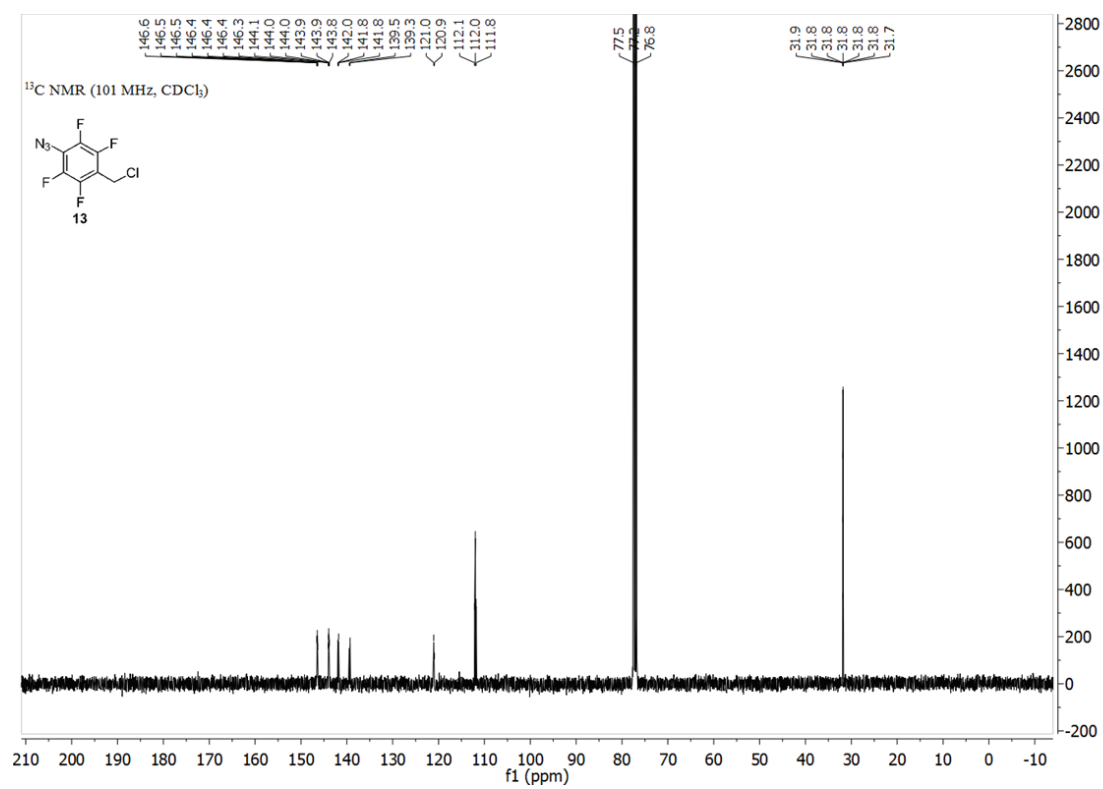
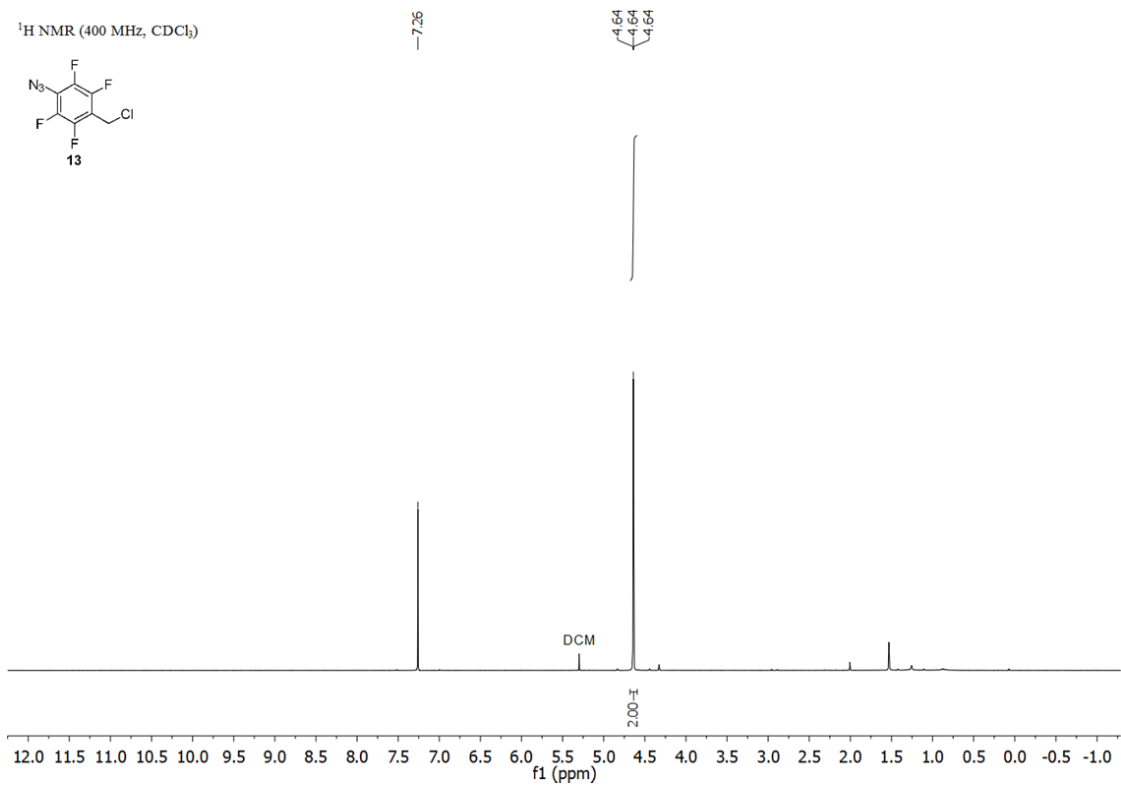


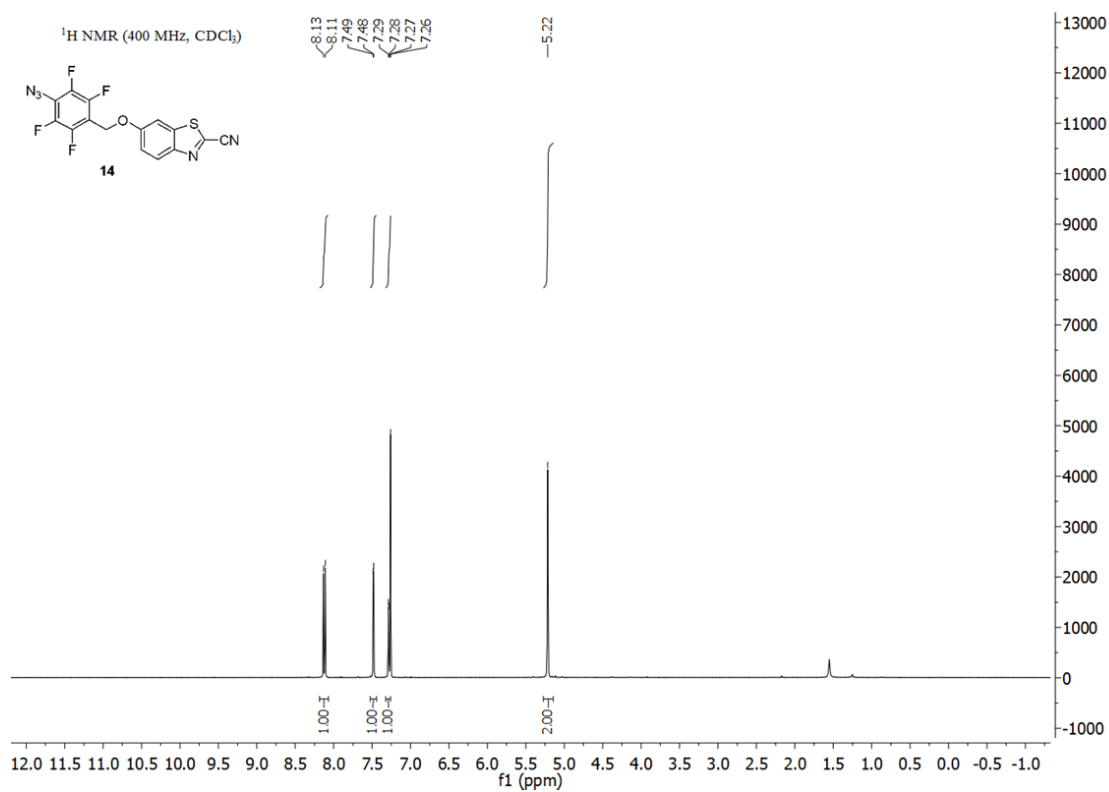
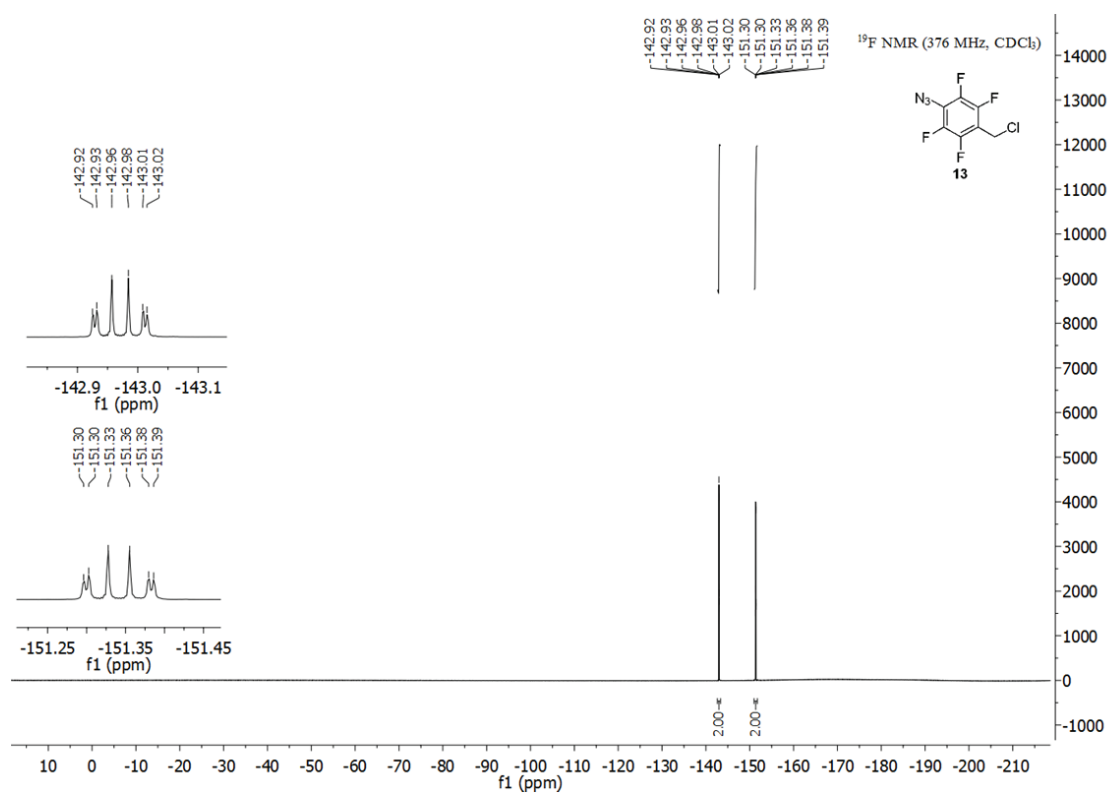




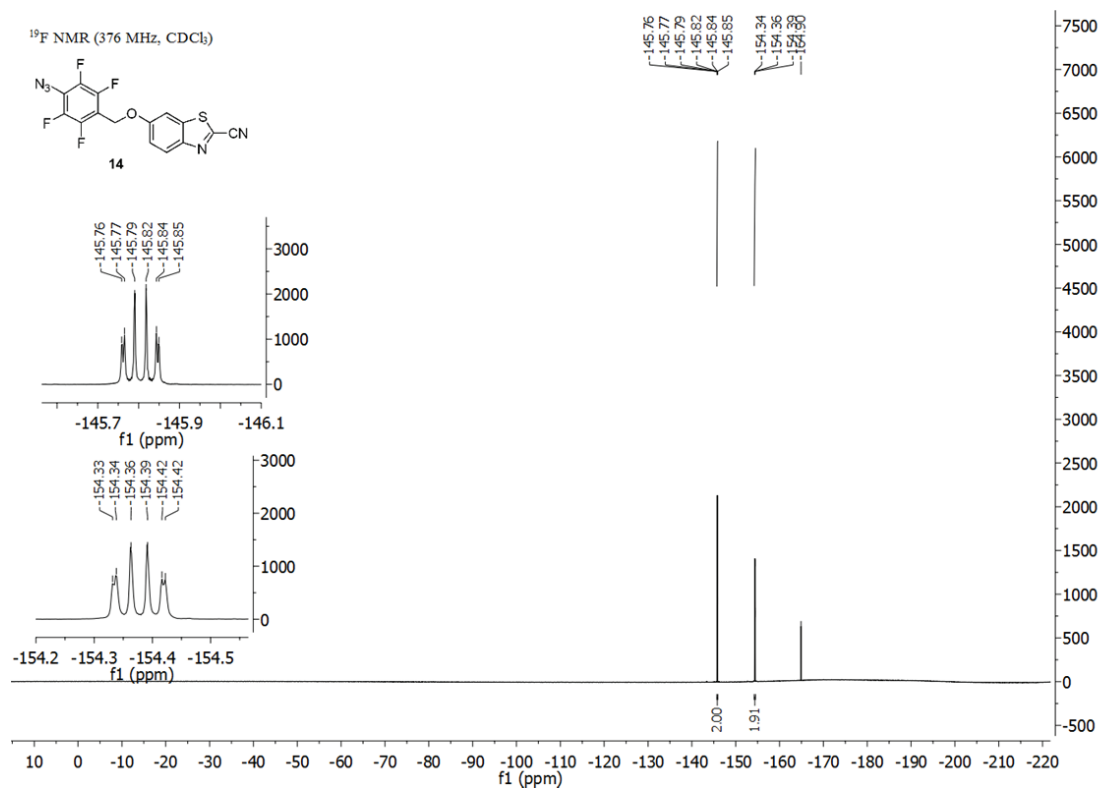
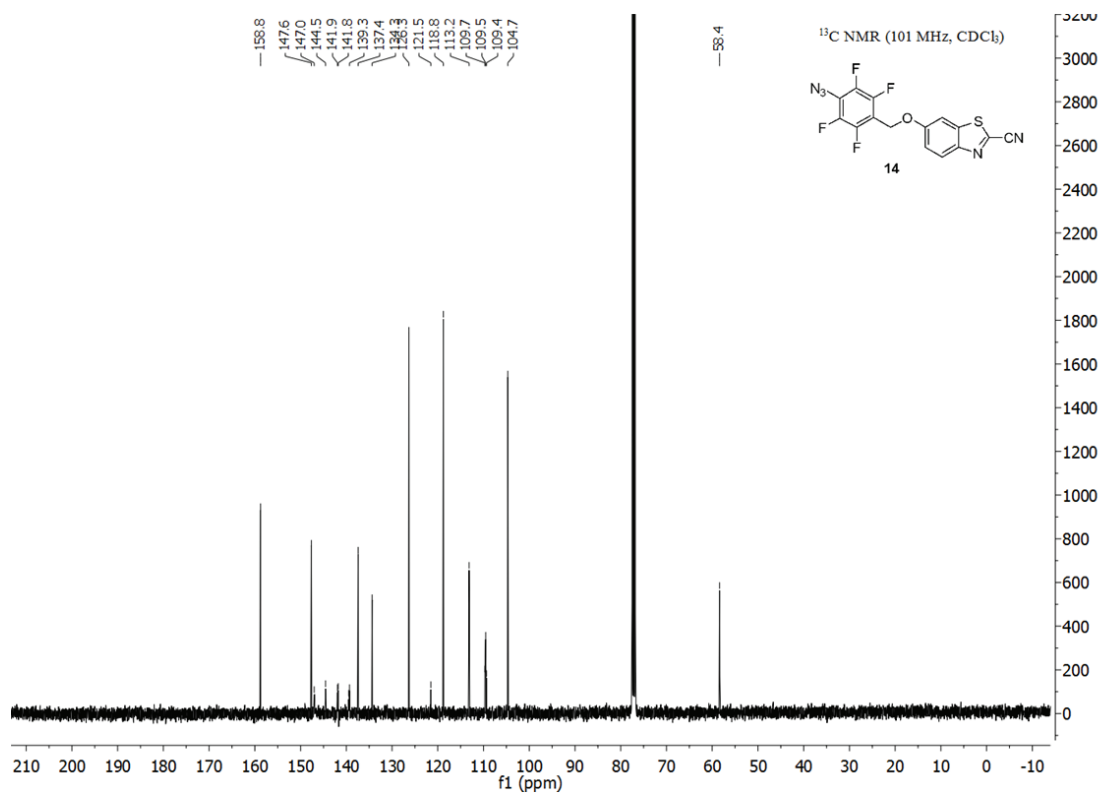


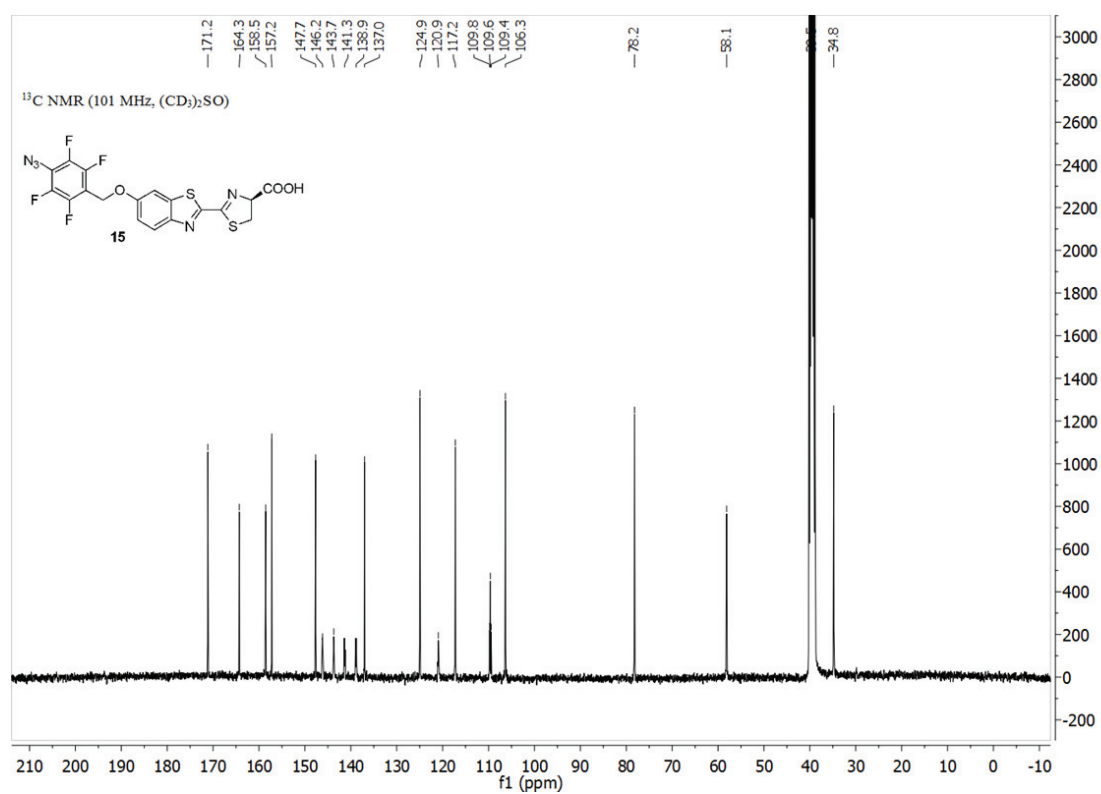
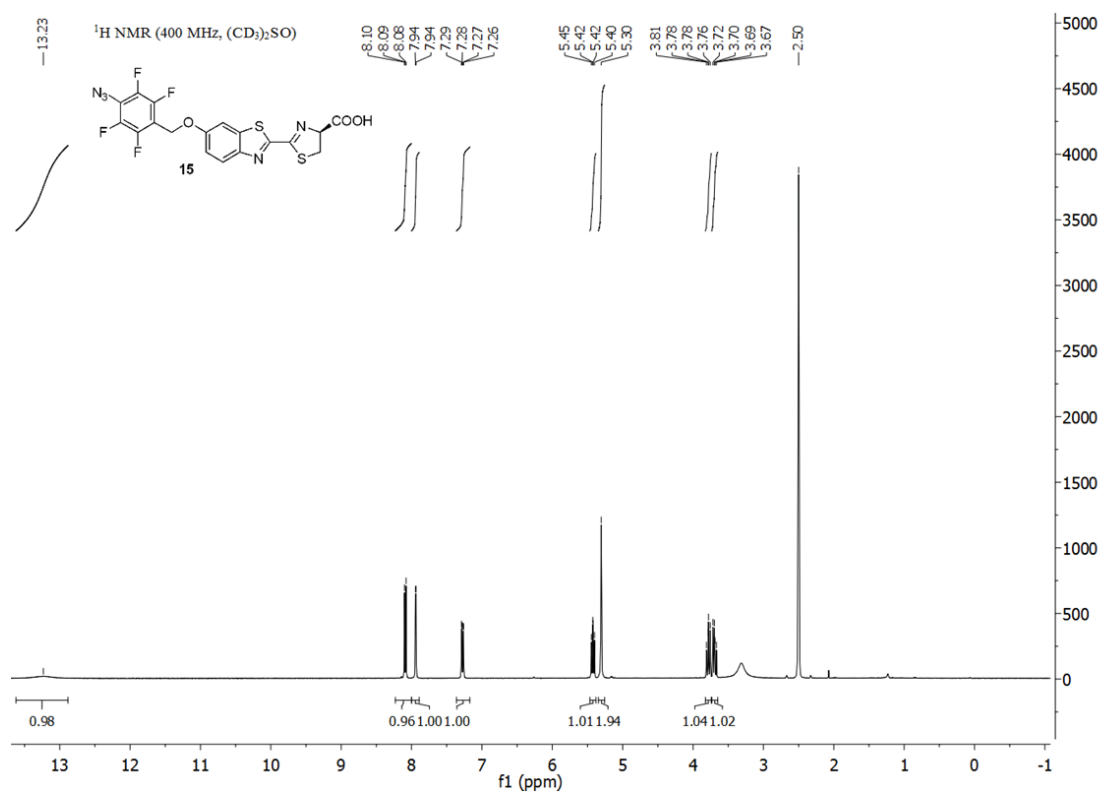


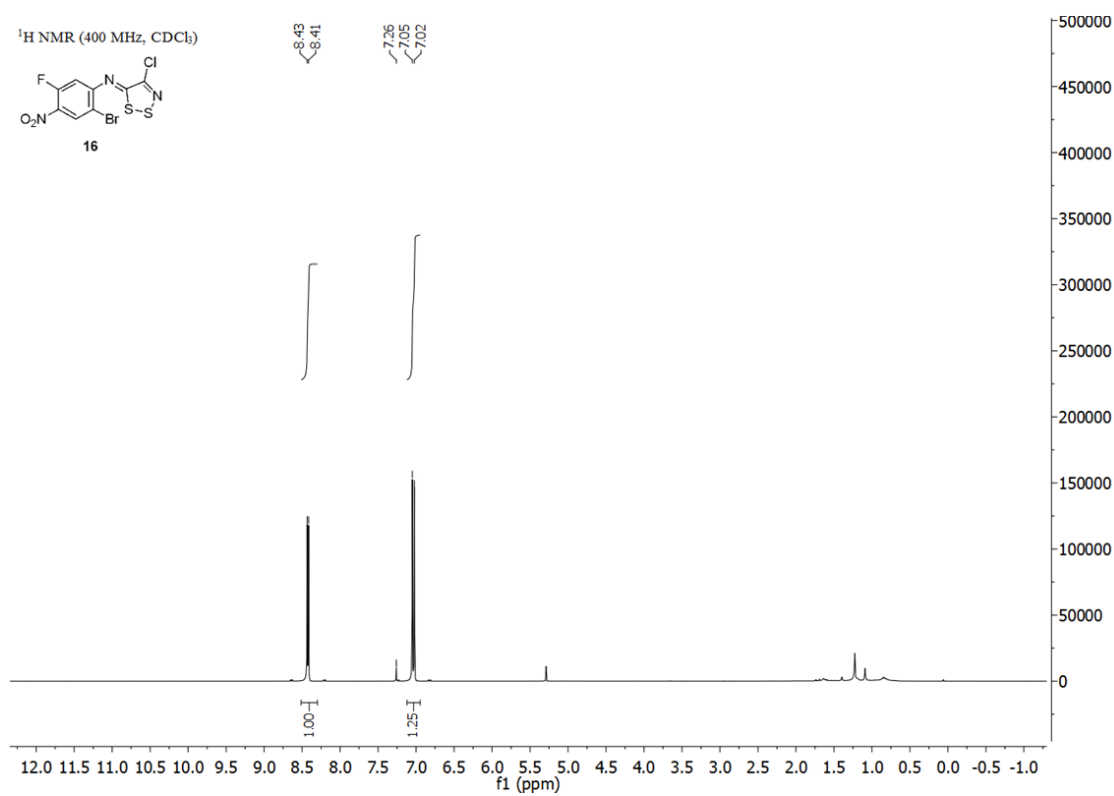
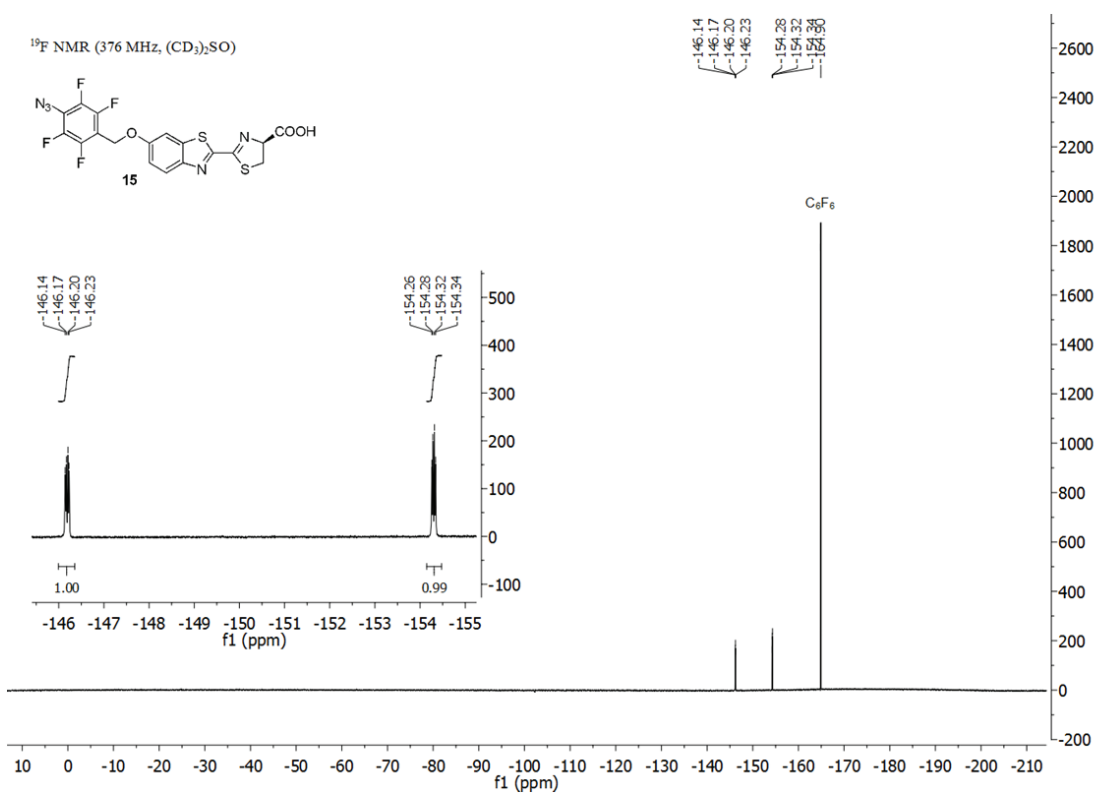


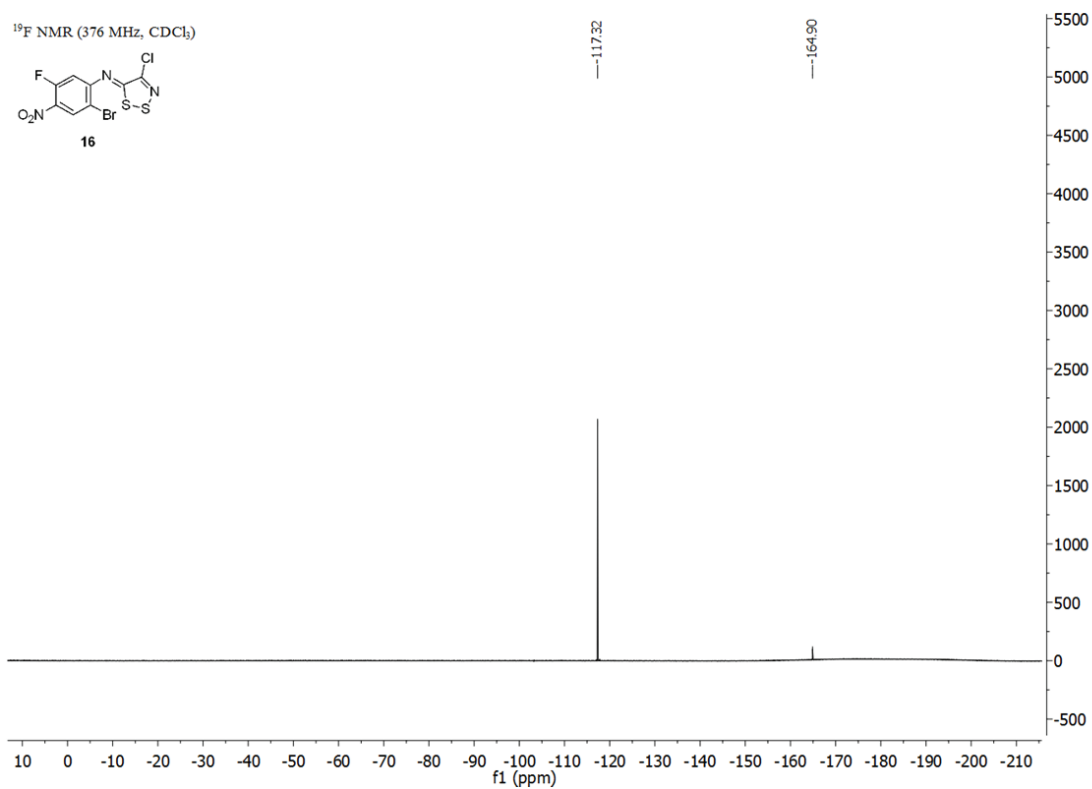
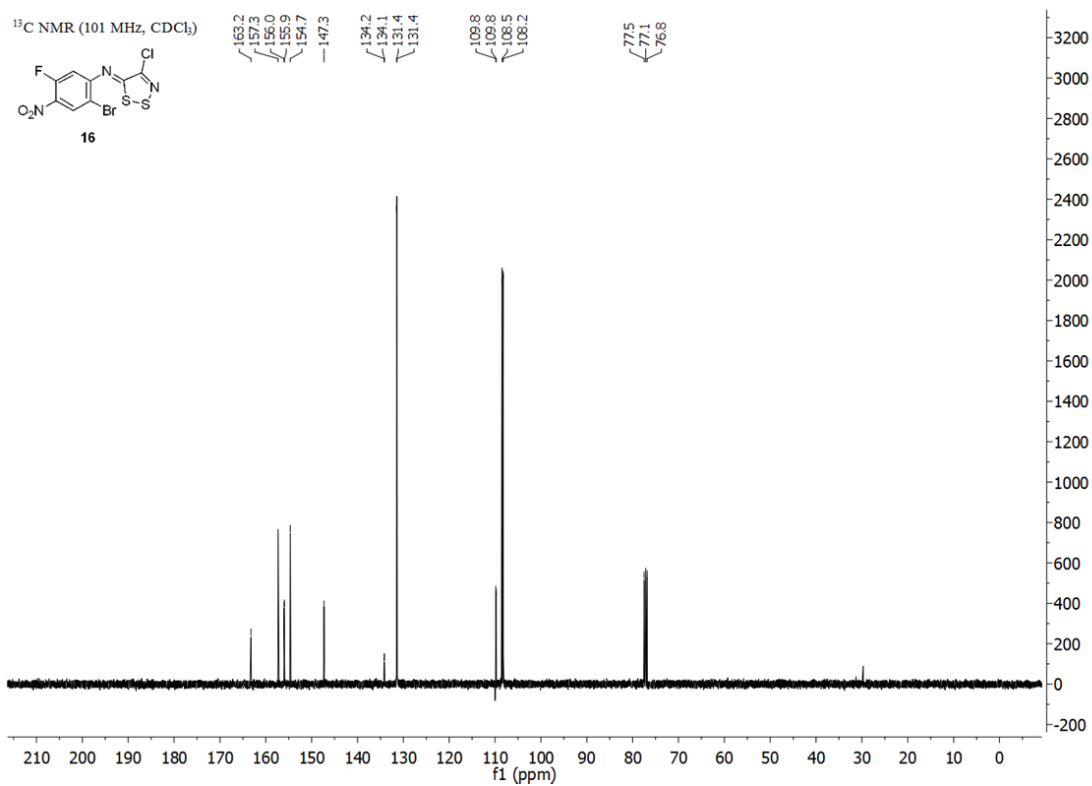


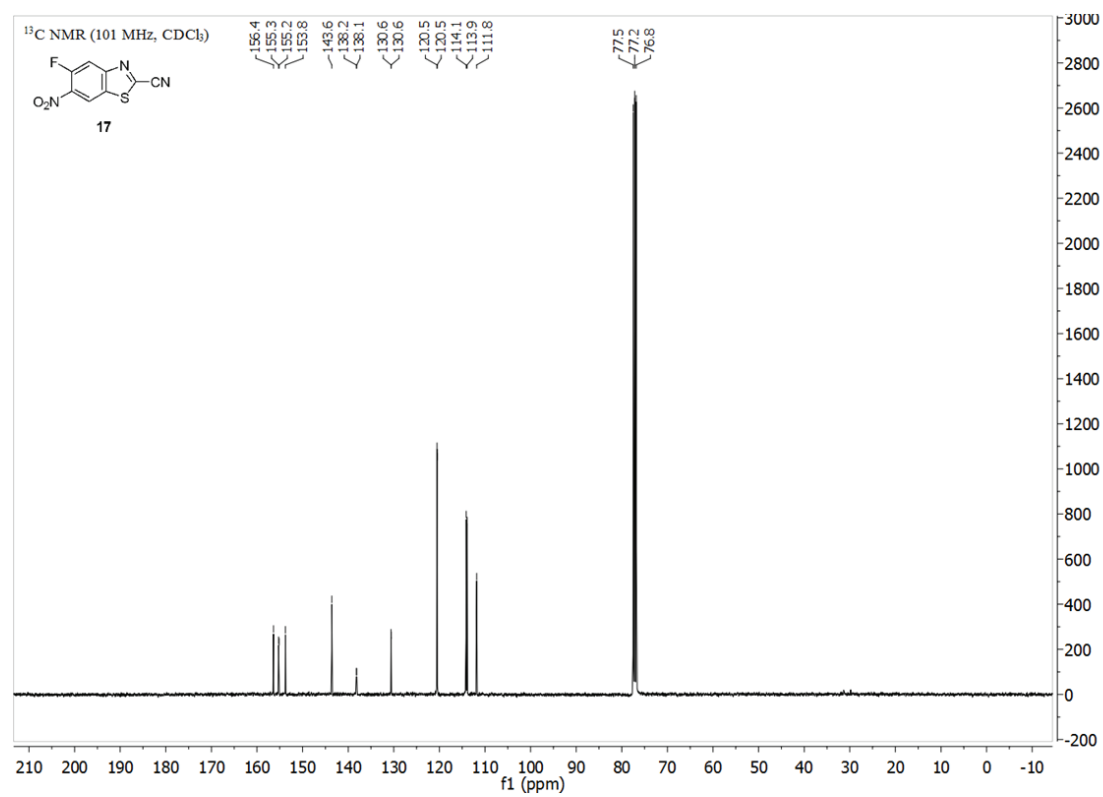
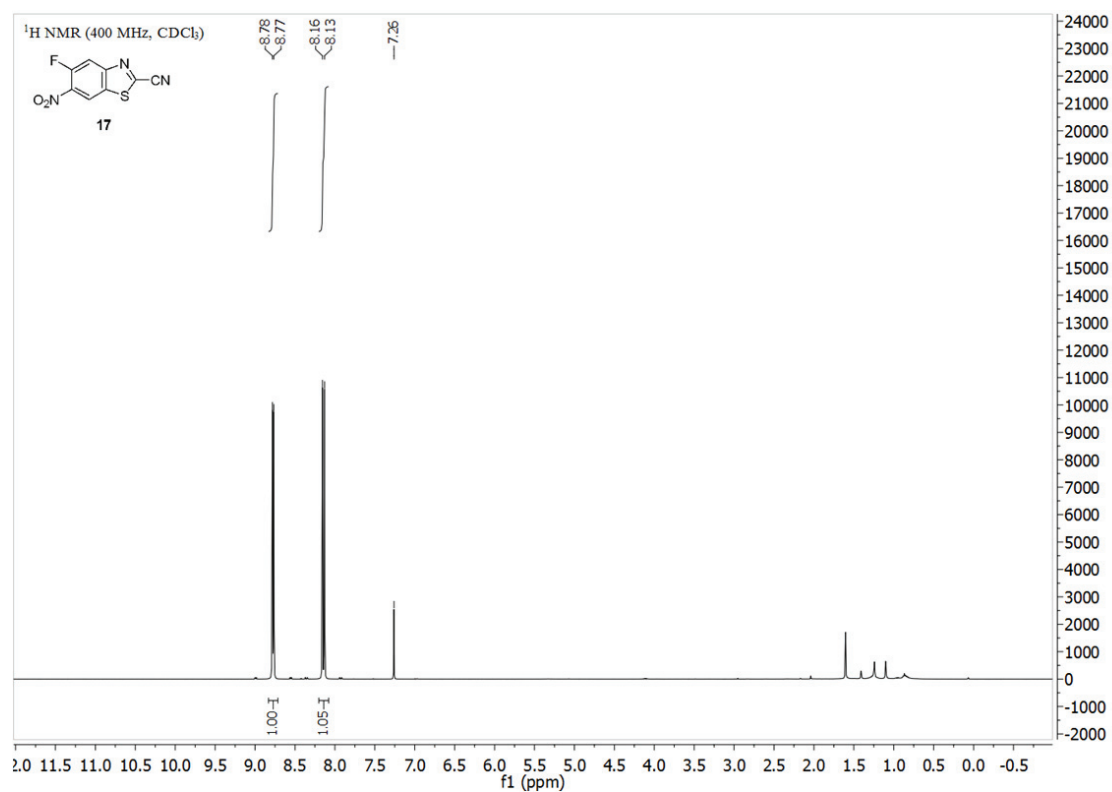


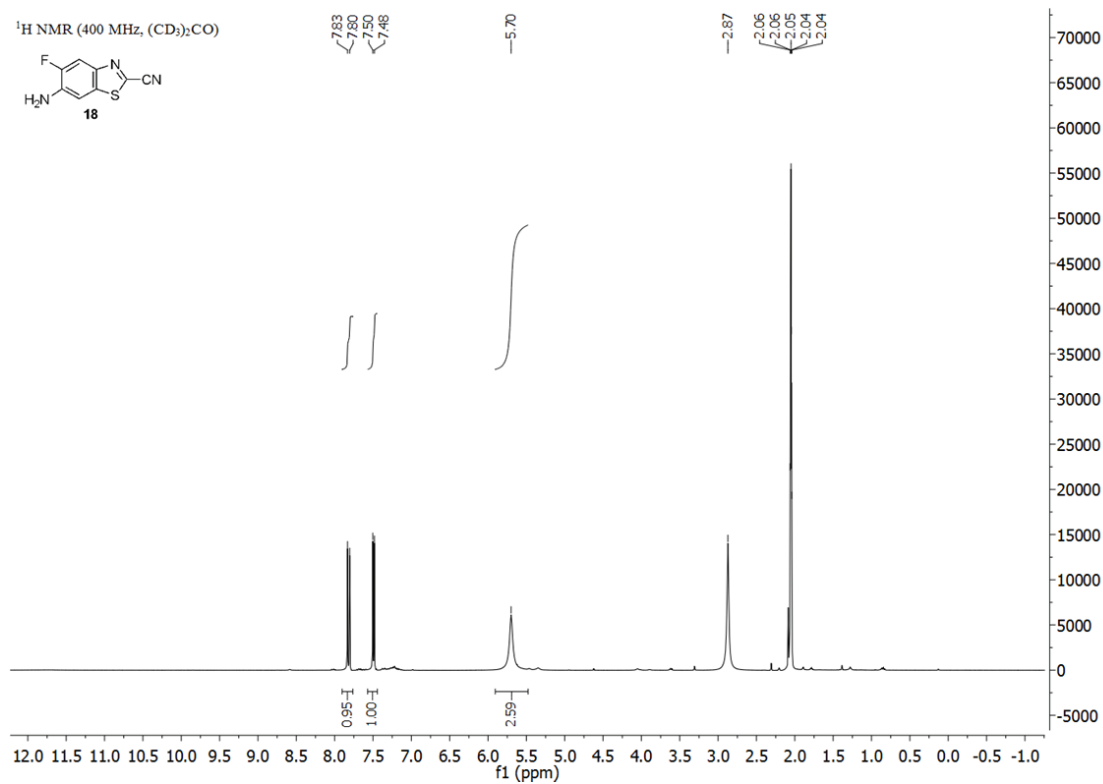
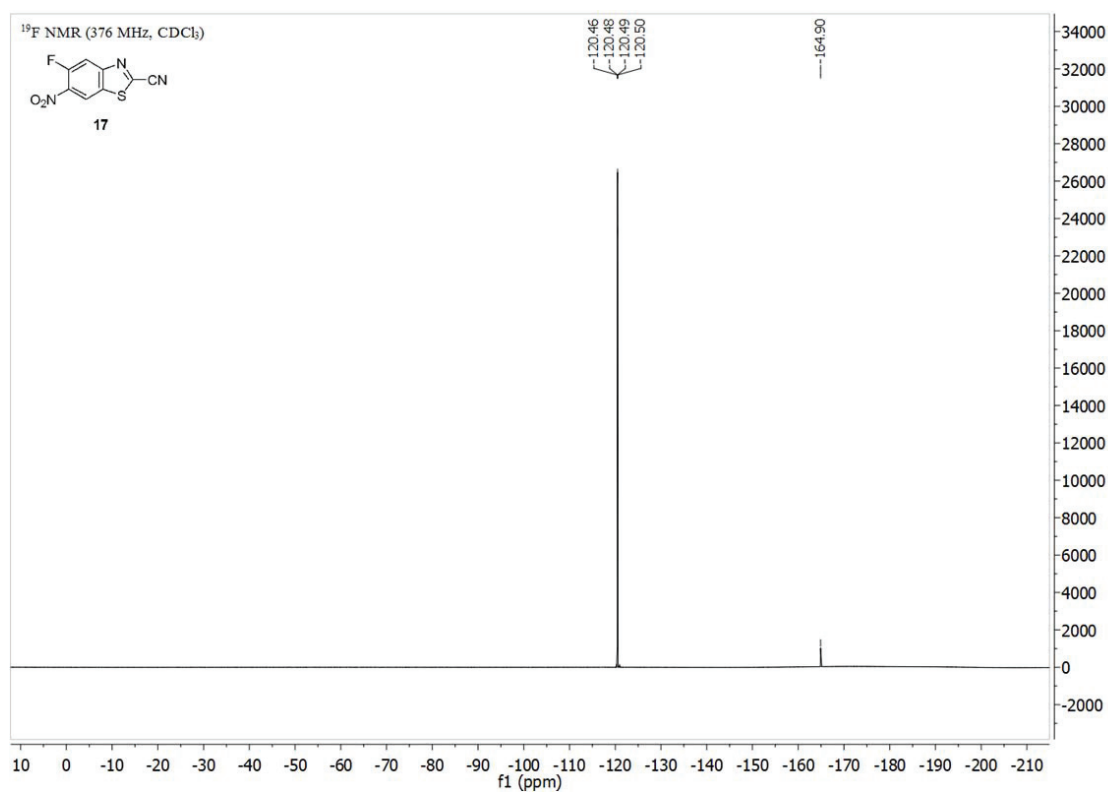


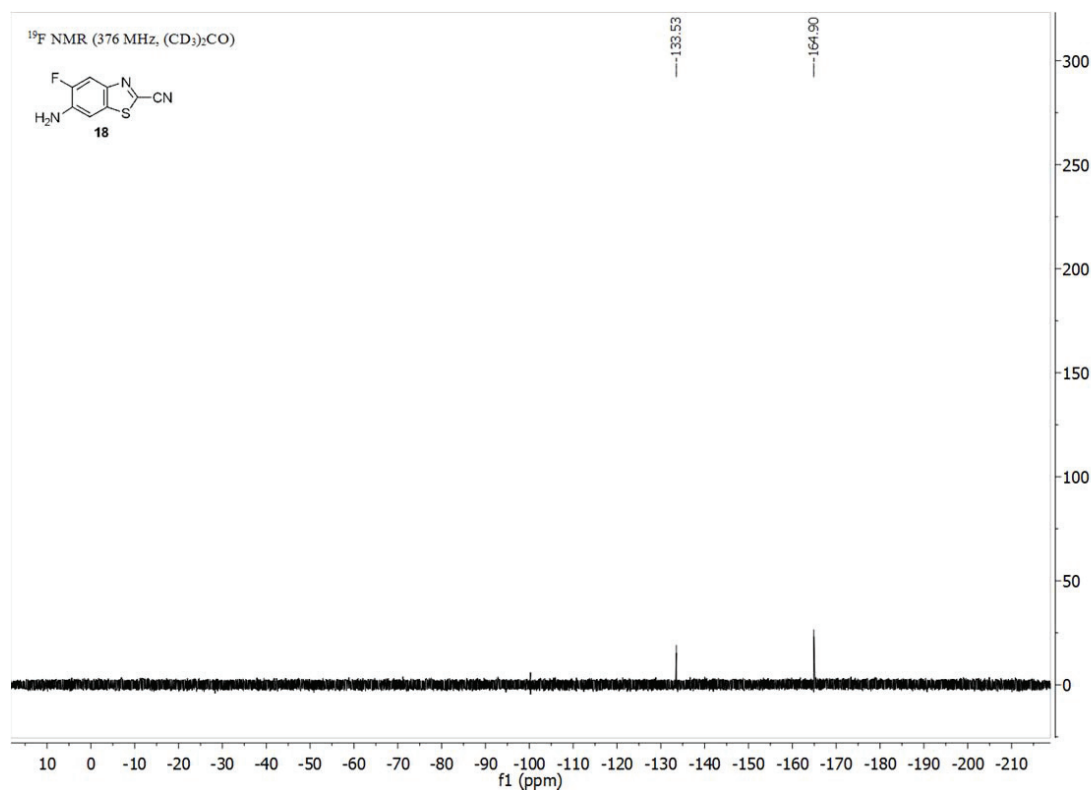
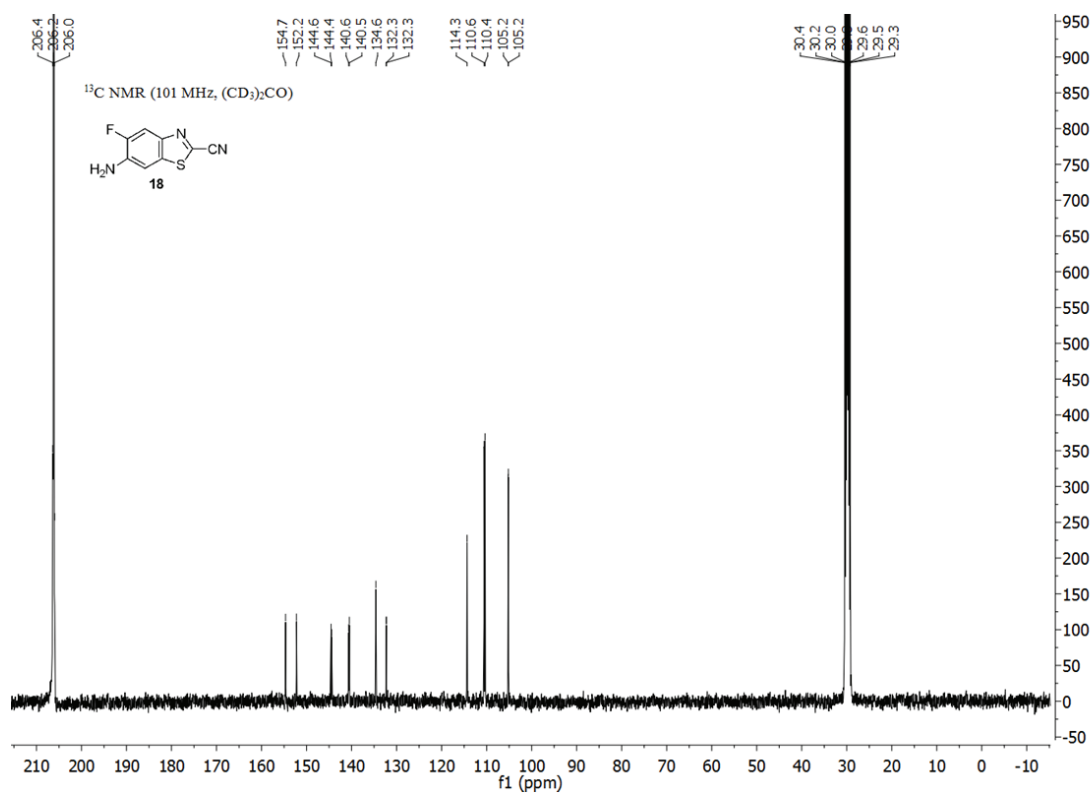


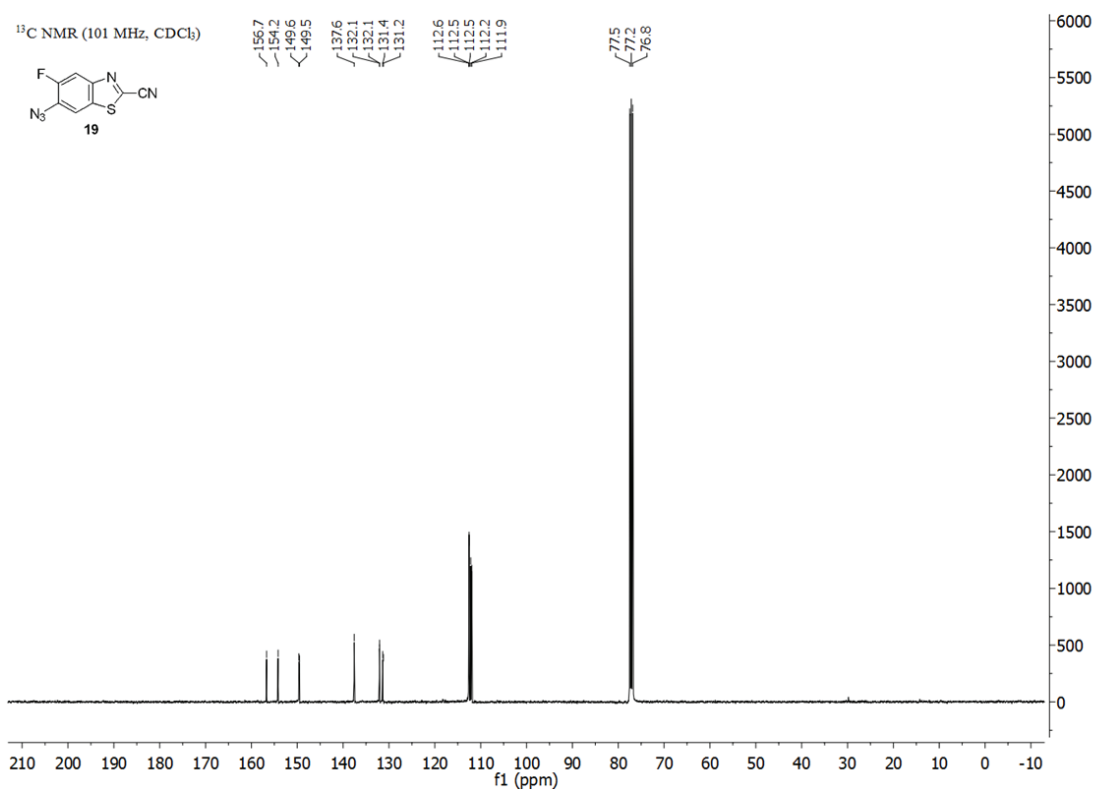
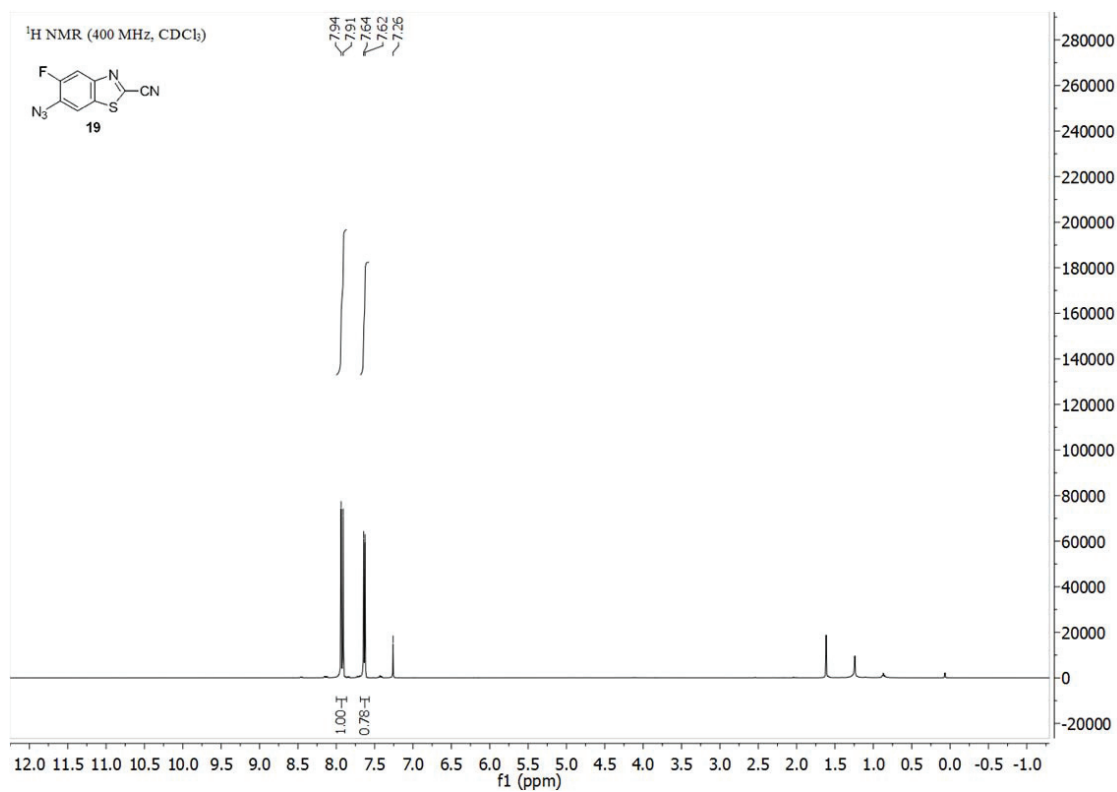




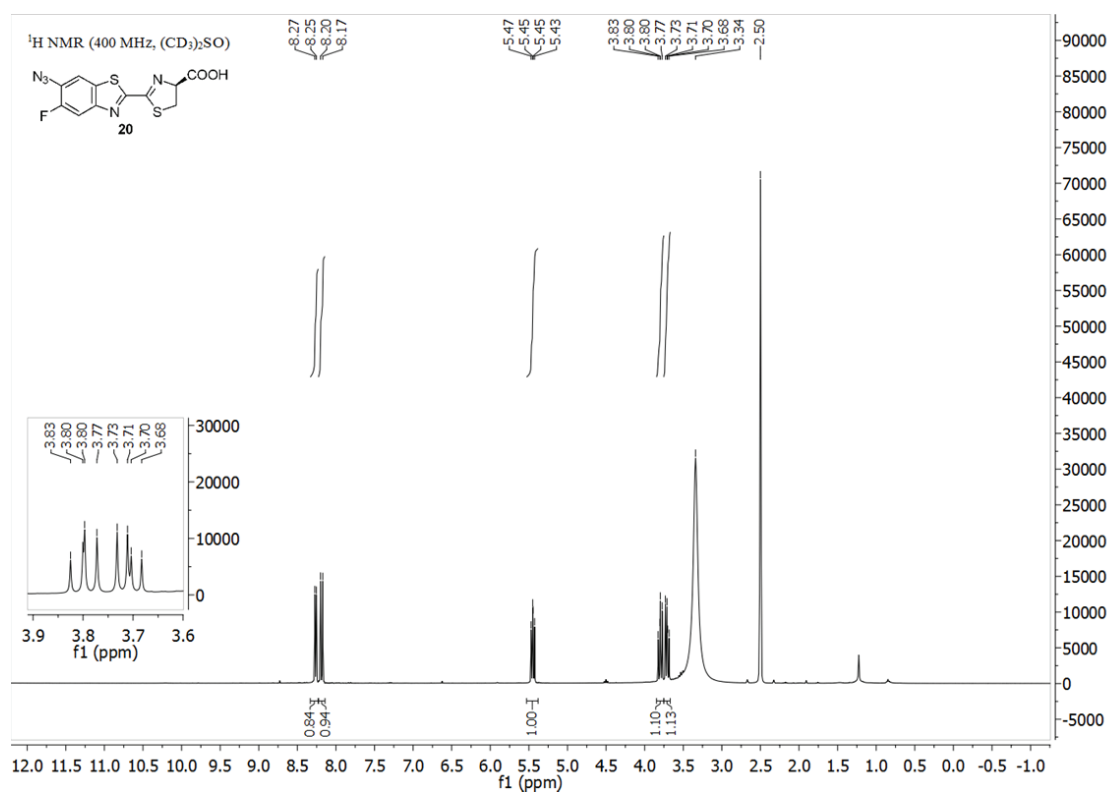
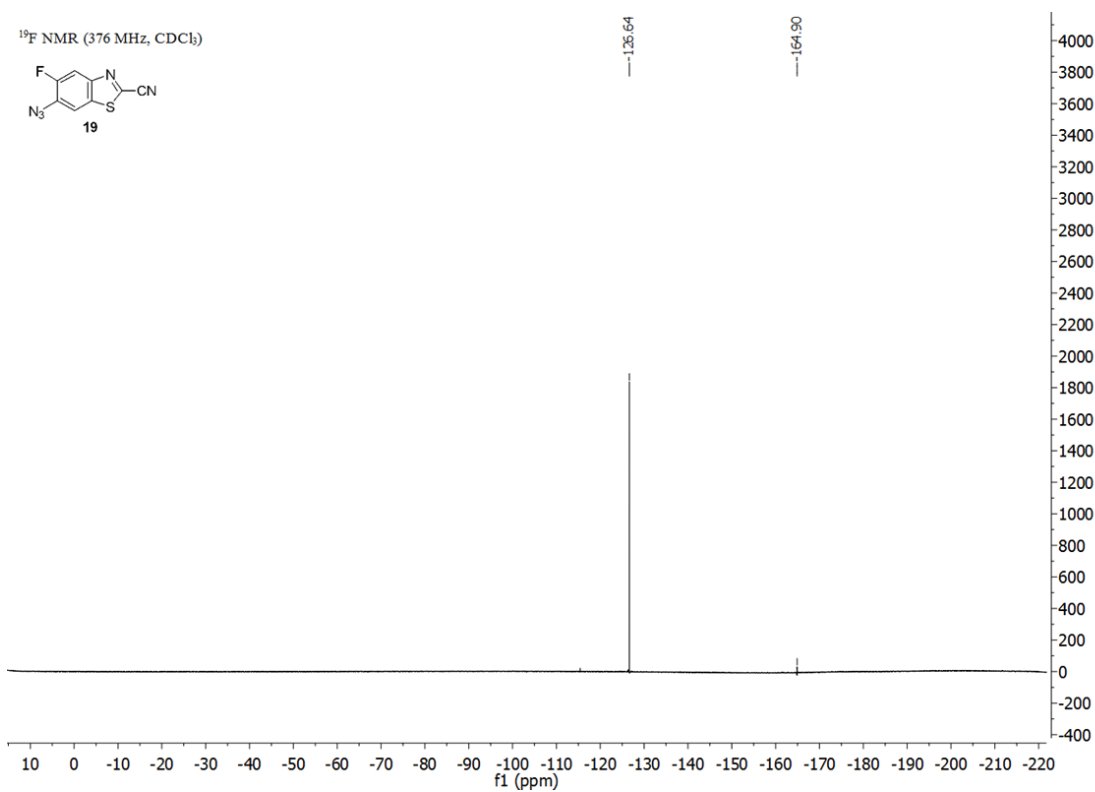


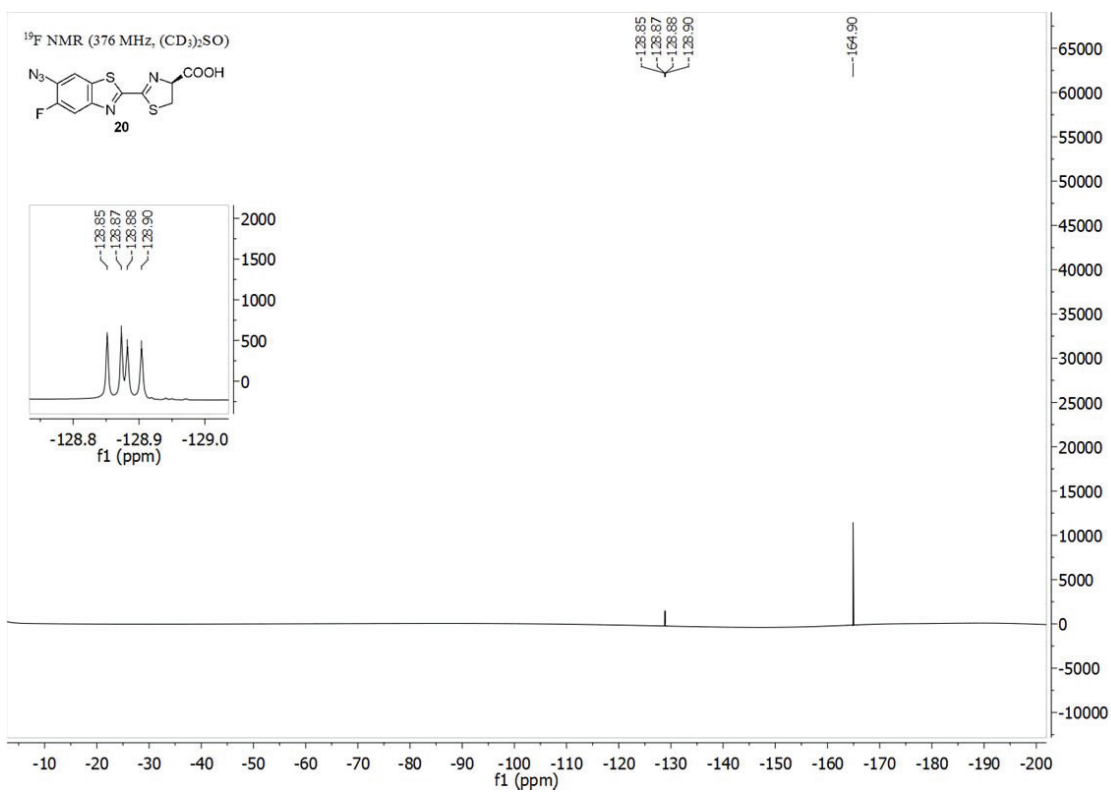
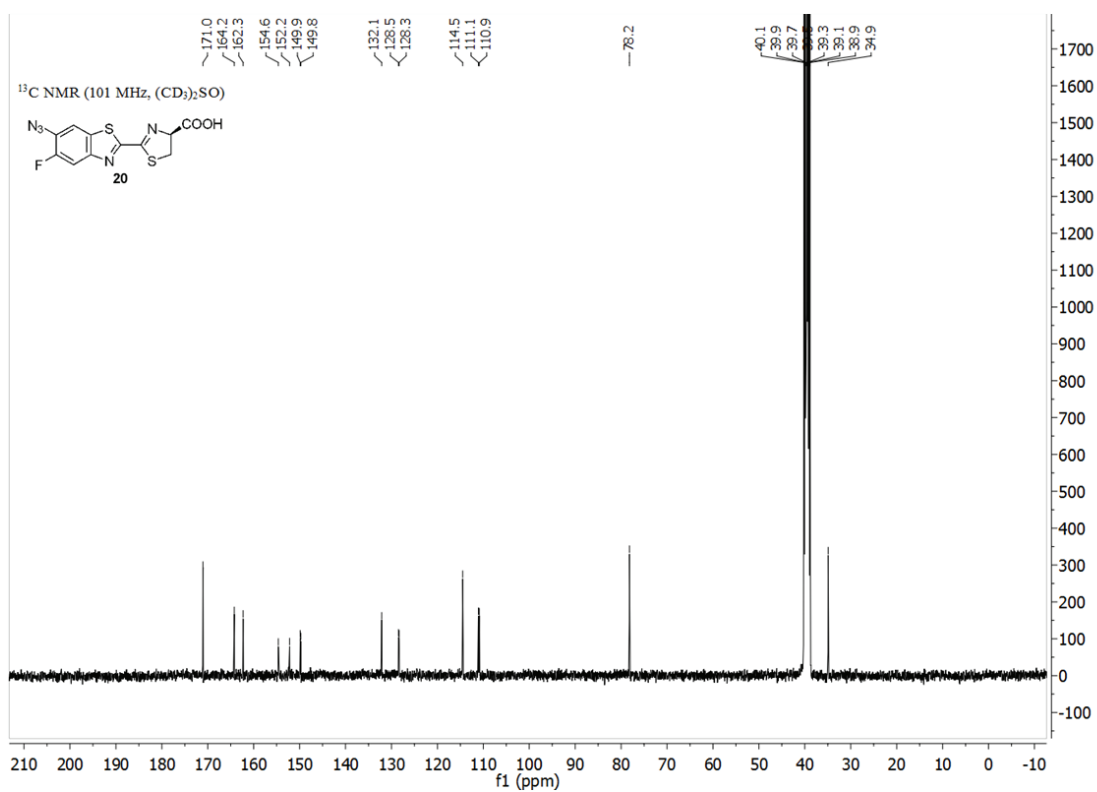


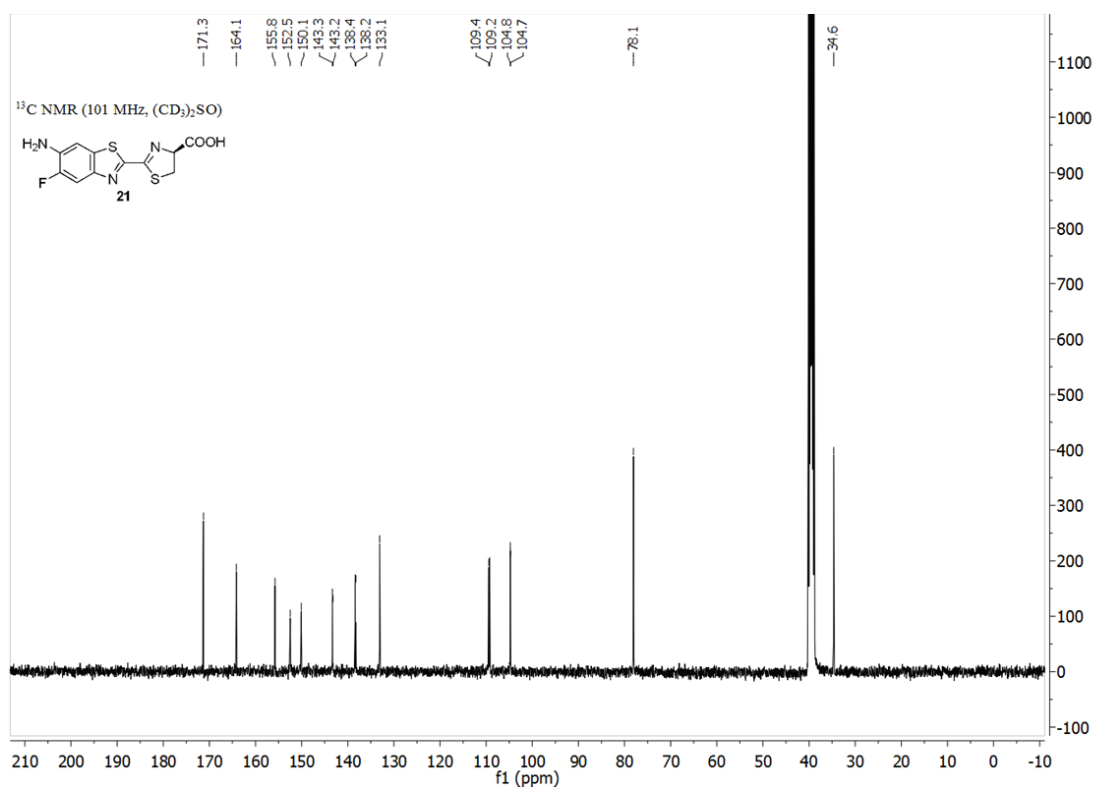
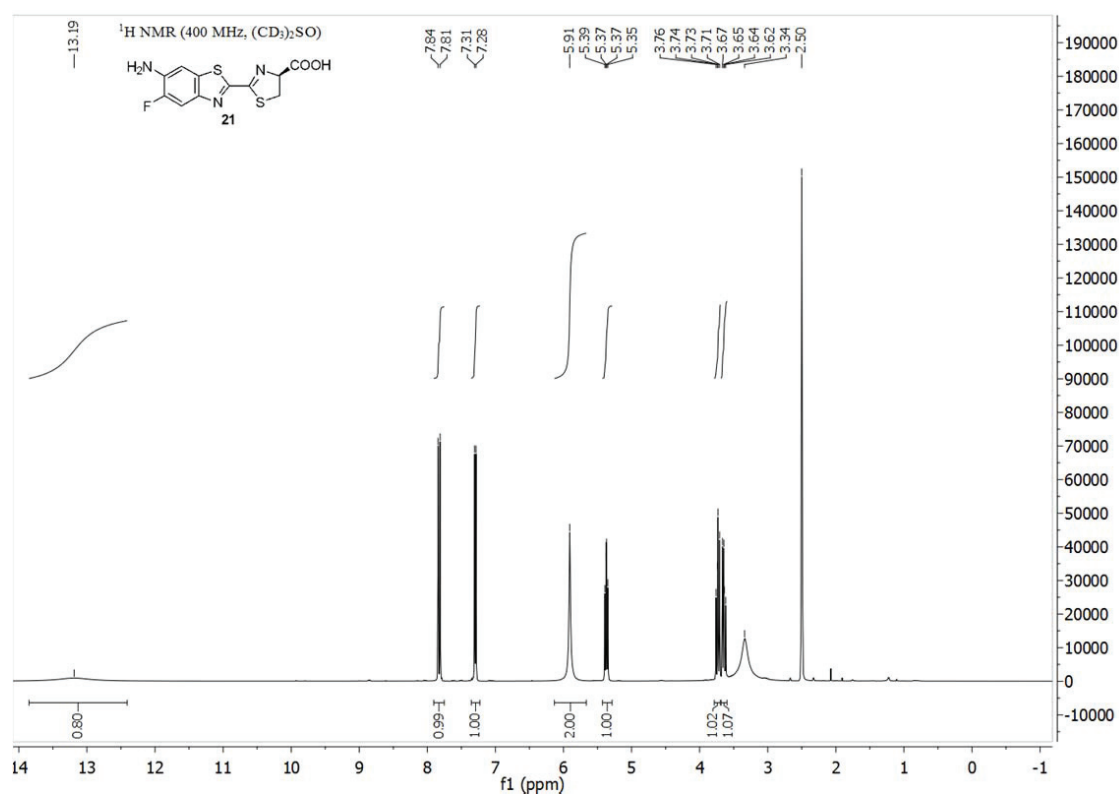


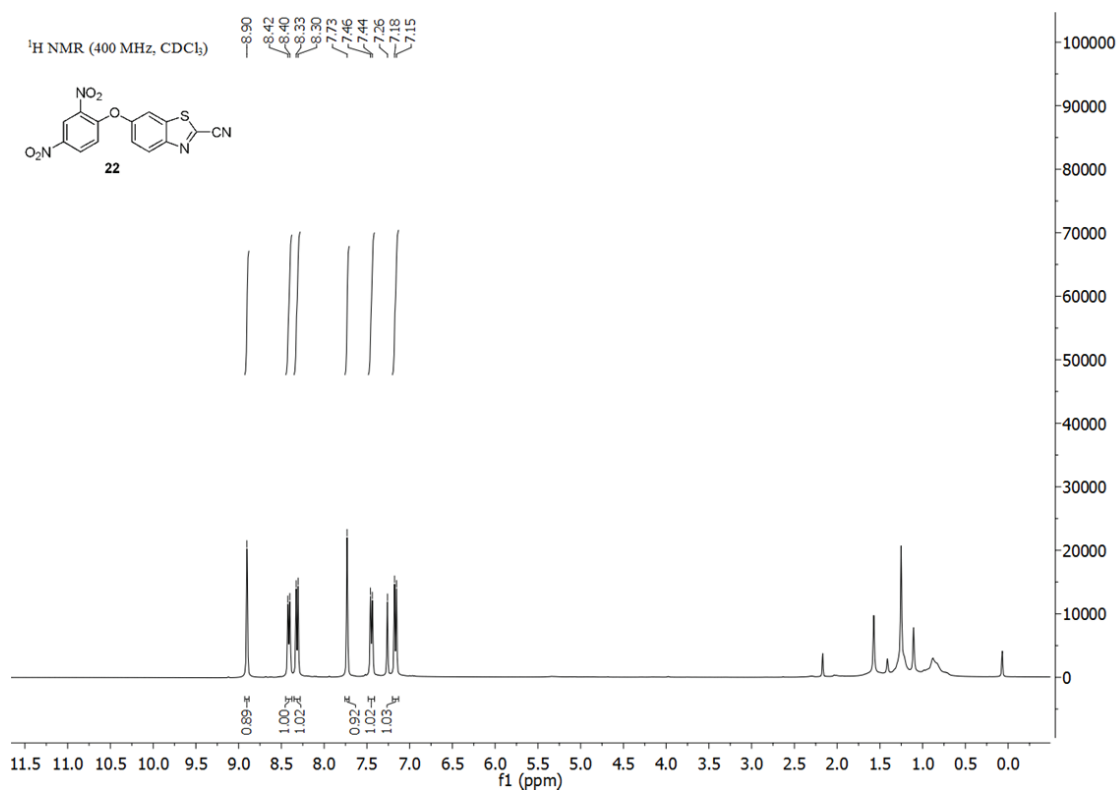
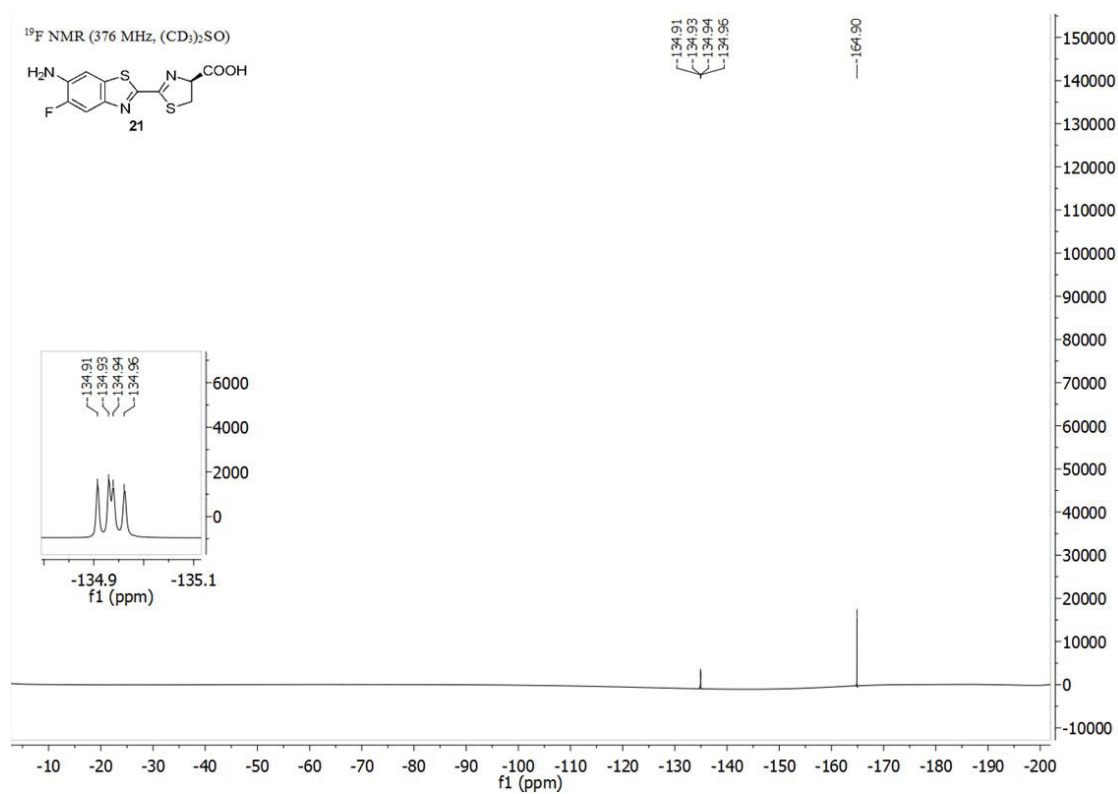


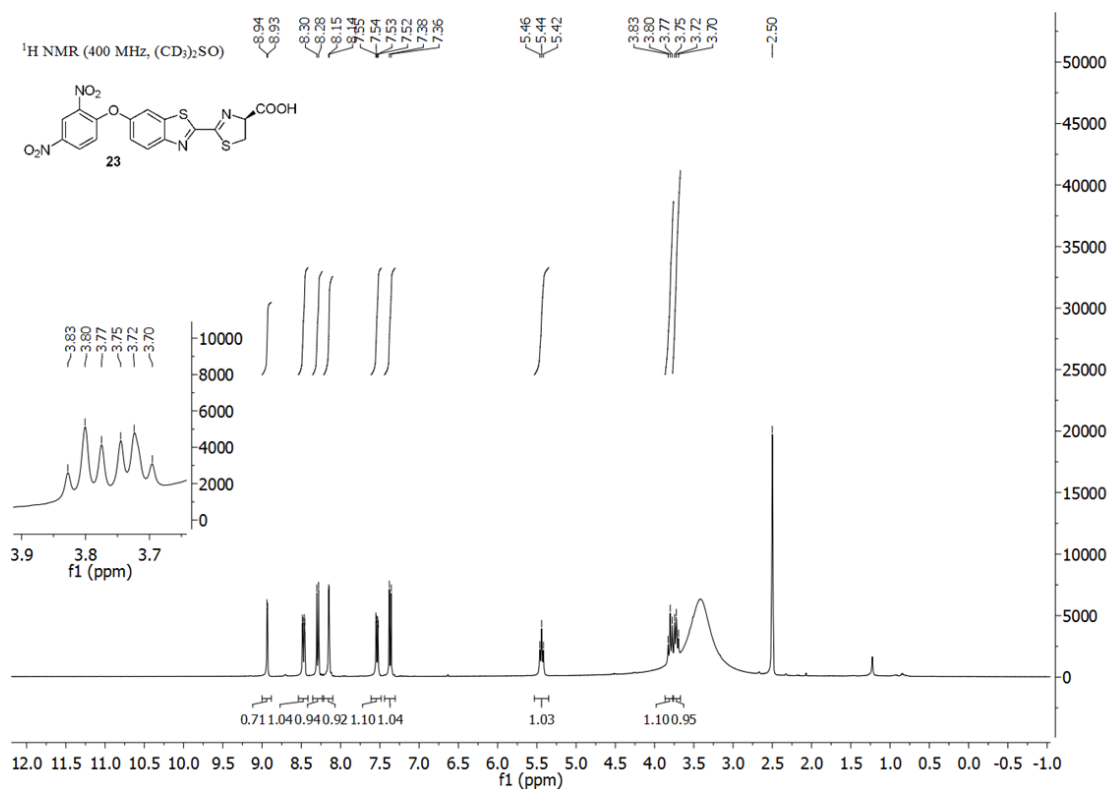
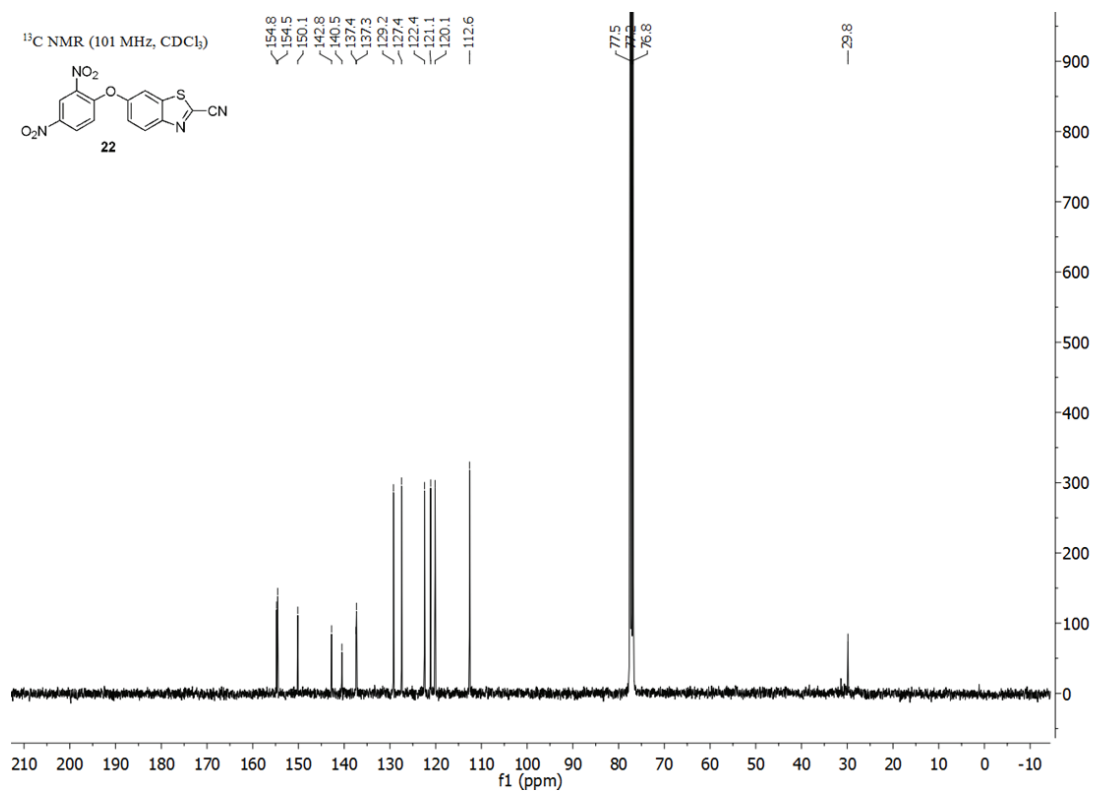


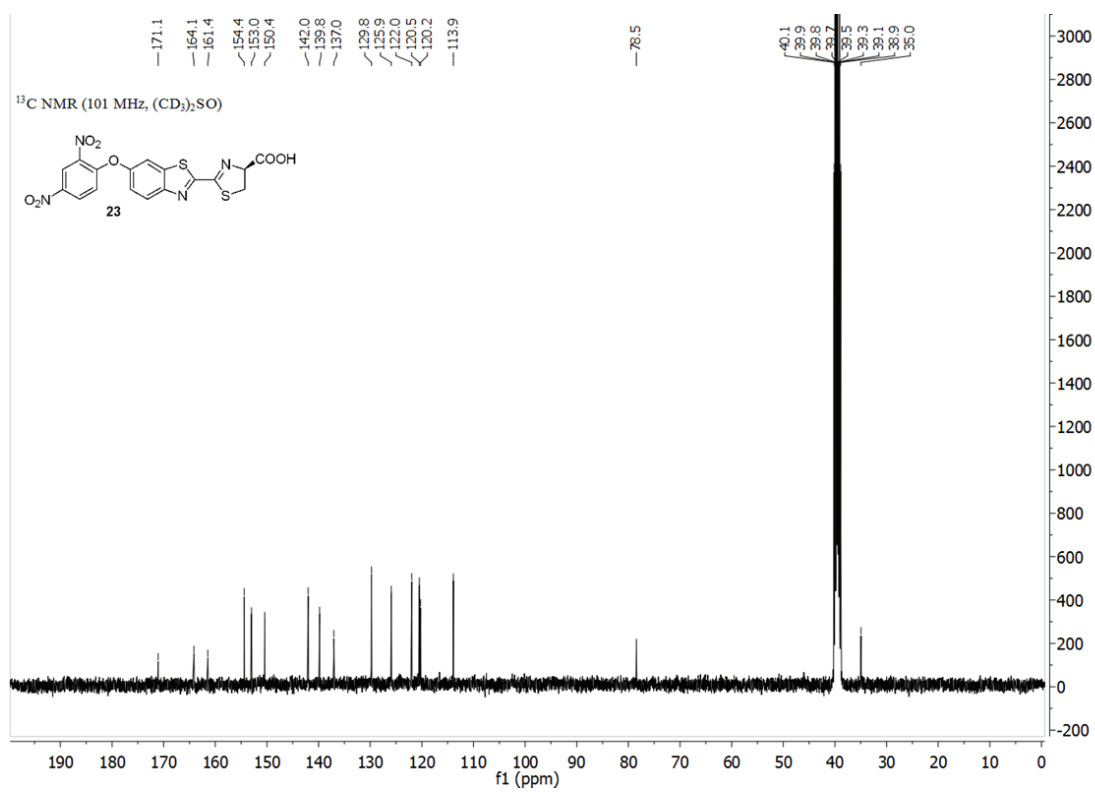












## 6.2 Curriculum Vitae

### Anzhelika G. Vorobyeva

E-mail: anzhelika.vorobyeva@epfl.ch, angel.vorob@gmail.com

Date of birth: 01. 10. 1990

Citizenship: Russian

#### Education

- 09.2012-09.2016      Ph.D. studies in Chemistry and Chemical Engineering  
under the supervision of Prof. Elena A. Dubikovskaya  
Laboratory of bioorganic chemistry and molecular imaging (LCBIM)  
Swiss Federal Institute of Technology (EPFL), Lausanne, Switzerland
- 09.2007-06.2012      Diploma in Pharmacy  
"Synthesis and evaluation of biological activity of water soluble derivatives of arylpyruvic acids"  
under the supervision of Prof. N. A. Pulina, co-supervisors Dr. F. V. Sobin and Dr. S. V. Chaschina  
Perm State Pharmaceutical Academy (PSPA), Perm, Russian Federation

#### Publications

- Vorobyeva AG, Stanton M, Godinat A, Lund KB, Karateev GG, et al. (2015) Development of a Bioluminescent Nitroreductase Probe for Preclinical Imaging. PLoS ONE 10(6): e0131037. doi: 10.1371/journal.pone.0131037.
- Burkina YA, Vorobyeva AG, Sobin FV. (2012) Evaluation of wound healing activity of ointments based on new arylpyruvic acid derivatives. Herald of Russian State Medical University (RSMU), Materials of VII International Pirogov Scientific Medical Conference of Students and Young Scientists. - Moscow. - №1. – p. 465- 466.
- Burkina YA, Vorobyeva AG, Sobin FV. (2012) Synthesis and biological activity of new naphthalene derivatives. Herald of Perm State Pharmaceutical Academy. - №9. – p. 104 – 106 (in russian).
- Vorobyeva AG, Plishkina MS, Chaschina SV, Igidov NM, Borodin AY. (2010) Evaluation of biological activity of new pharmaceutical forms of local anesthetics. Herald of Perm State Pharmaceutical Academy. - №6. – p. 71- 72 (in russian).

#### Conferences and awards

**June 2015** Swiss National Centre of Competence in Research (NCCR) Chemical Biology Retreat. "Development of a Bioluminescent Nitroreductase Probe for Preclinical Imaging", Villars-sur-Ollon, Switzerland. Oral presentation.

**June 2014** European Society for Molecular Imaging (ESMI) meeting. "Real-time Noninvasive Imaging of Nitroreductase Activity In Live Animals", Antwerp, Belgium. Poster award (winner).

**April 2012** Student's Annual Conference of Perm State Pharmaceutical Academy. "Synthesis and biological activity of water soluble derivatives of arylpyruvic acids". 1st place at the Department of Physiology and Pathology, PSPA, Russia.

**2011** Scholarship of Russian Federation Government.

**2011** Scholarship of Rector of PSPA.



